The sophisticated architecture of the rat atrioventricular node

Shin Yoo

Submitted in accordance with the requirements for the degree of Doctor of Philosophy

The University of Leeds

School of Biomedical Sciences

August 2005

The candidate confirms that the work submitted is his own and that appropriate credit has been given where reference has been made to the work of others

Abstract

In the mammalian heart, the action potential spontaneously generated in the sinoatrial (SA) node propagates through the atria to reach the atrioventricular (AV) node. As the only conduction pathway between the atria and ventricles, the AV node functions to delay and regulate action potential conduction between the atria and ventricles. Since Tawara described the anatomical and morphological characteristics of the AV node in 1906, it has been difficult to correlate electrophysiological recordings with distinct cell types and the three dimensional structure of the AV node due to the exceptional functional and architectural complexity of this region. The cardiac voltage-gated Na^+ channel isoform ($Na_v1.5$) is known to play a major role in the generation and conduction of the action potential in the heart. Recently, various mutations of $Na_v1.5$ responsible for AV conduction block and $Na_v1.5^{+/-}$ mice with impaired AV conduction have been reported. Various neuronal Na^+ channel isoforms have also been shown to be expressed in the heart (mouse ventricular myocytes and rat and mouse SA node) and to be functionally important. The distribution of neuronal Na^+ channel isoforms in the AV node is unknown. The aim of this study was to investigate the distribution of cardiac and neuronal Na^+ channel isoforms in and around the AV node.

The nodal cell region was identified by Masson's trichrome staining and confocal microscopy with immunohistochemical markers, such as connexin43 (Cx43), desmoplakin (DP), atrial natriuretic peptide (ANP) and the type 4 hyperpolarization-activated cyclic nucleotide-gated cation (HCN) channel. The unique pattern of expression in the nodal cell region (DP-positive/Cx43-negative/ANP-negative/HCN4-positive) allowed it to be distinguished from the surrounding working myocardium (DP-positive/Cx43-positive/HCN4-negative).

I have investigated the expression of $Na_v1.5$ and other Na^+ channel isoforms in rat AV node. $Na_v1.1$ was distributed in a similar manner to $Na_v1.5$. $Na_v1.2$ was not detected. $Na_v1.3$ labelling was restricted to nerve fibres and nerve cell bodies and was not detected in myocytes. $Na_v1.3$ labelling was abundant in the enclosed node and the common bundle, but much less abundant in other regions. $Na_v1.4$, the skeletal isoform, was not studied. $Na_v1.5$ labelling was present in atrial and ventricular myocardium and the left bundle branch (right not studied). However, $Na_v1.5$ labelling was absent in the open node, the enclosed node and the common bundle, but present at a reduced level in the posterior nodal extension, transitional cells and AV ring bundle. $Na_v1.6$ was not detected.

The study has revealed a complex organisation of three different myocyte types at the AV junction (including the tricuspid annulus). Impaired AV conduction as a result of mutations in or loss of $Na_v1.5$ must be the result of impaired conduction in the AV node inputs (posterior nodal extension and transitional cells) or output (bundle branch) rather than the AV node itself (open and enclosed nodes).

Contents

Chapter 3

Histology of the AV node

Chapter 4

Immunohistochemical markers of the AV node

Chapter 5

HCN4 expression in the AV node

Chapter 6

Expression of Na^+ channel isoforms in isolated atrial and ventricular myocytes and tissue sections

Chapter 7

Na^+ channel expression in the AV node

Chapter 8

Cx40 expression in the AV node

Chapter 9

Expansion to AV junction (around tricuspid annulus)

Chapter 10

The different architecture of the SA node

Chapter 11

Summary

Figures

Chapter 1

Chapter 2

Chapter 3

Chapter 4

Chapter 5

Chapter 6

Chapter 7

Chapter 8

Chapter 9

Chapter 10

Chapter 11

Tables

Abbreviations

SA	Sinoatrial
AV	Atrioventricular
Cx43	Connexin43
DP	Desmoplakin
ANP	Atrial natriuretic peptide
HCN	Hyperpolarization-activated cyclic nucleotide-gated cation
AN	Atrionodal
N	Nodal
NH	Nodal-His
AVNRT	AV nodal reentrant tachycardia
Cx40	Connexin40
Cx45	Connexin45
I_{Na}	Voltage-dependent Na^+ current
I_{to}	Transient outward K^+ current
TTX	Tetrodotoxin
I_f	Hyperpolarization-activated inward current
$I_{Ca,L}$	L-type Ca^{2+} current
$I_{Ca,T}$	T-type Ca^{2+} current
I_{Kr}	Rapidly activating delayed rectifier K^+ current
I_{Ks}	Slowly activating delayed rectifier K^+ current
Kir	Inwardly rectifying K^+ channel
I_{K1}	Inward rectifier K^+ current
$I_{K,ACh}$	ACh-sensitive K^+ current
cAMP	Cyclic adenosine monophosphate
$I_{Na\text{-}Ca}$	Na^+/Ca^{2+} exchange current
HEPES	4-(2-Hydroxyethyl)piperazine-1-ethanesulfonic acid
EGTA	Ethylene glycol-bis(2-aminoethylether)-*N,N,N',N'*-tetraacetic acid
BSA	Bovine serum albumin
KB	Kraft-Brühe
PBS	Phosphate buffered saline
CCD	Charge coupled device
FITC	Fluorescein isothiocyanate
TRITC	Tetramethyl rhodamine
PMT	Photomultiplier tube
cGMP	Cyclic guanosine monophosphate
CNBD	Cyclic nucleotide binding domain
NF160	Neurofilament160

Acknowledgements

I am grateful to a large number of key individuals without whose help and support this Ph.D. thesis would not be a reality. My special and enormous thanks must go first and foremost to my principle supervisor Professor Mark R. Boyett for his expertise, advice, help, patience and understanding throughout my Ph.D. course. My gratitude also goes to my other supervisor Dr. Simon Harrison for advice and help he provided. I am grateful to the head of the School of Biomedical Sciences, Dr Mike Yates, for his support.

I would like to thank all those people in the Cellular Cardiology group with whom during my Ph.D. course I have worked: Halina, Mitsuru, Tomoko, Zhigang, Sandra, Matthew, Jue, Shin I., James, Ian, Rudy, Samy, Binbin, Tom and Zoe. Their contribution, expertise, help, advice, support and friendship is appreciated. Especially, I would like to thank Halina for teaching me immunohistochemistry.

Also, without the financial support from the British Heart Foundation, I would not have finished this degree course.

I would like to thank many people in the School of Biomedical Sciences, technicians, office staff and many other colleagues whom I have been acquainted: Hanny, Mark G., Sarah, Rachael, Steve, Amber, Moza, Vic, Fabien, Mark F., and Holy. Their assistance, support and friendship is appreciated.

I am indebted to many Korean friends here: Jangjin, Yoonhee, Juhyun, Kisup, Seunghee, Jinha, Dongil, Eunja, Bokim, Namjun and so on. They encouraged me and prayed for me constantly.

I need to thank my father, mother, sister, brother and late grand mom for financial support, encouragement and understanding. They have prayed for me all the time since I left Korea.

I wish to dedicate this Ph.D. thesis my wife, Soojung, due to her constant love, support, advice and understanding. I cannot express too much delight with my little ones, Eun and Min, and my nephews, Wonseok and Wonjun.

Finally, I would like to give thanks to Father in heaven. Thanks Almighty God, particularly, for making me realize that I am more than qualified when armed with your help. Without you, my entire life is meaningless. You know everything including this Ph.D. thesis. What I can and must do is to glorify you as much as I can.

Chapter 1

General Introduction

1.1. AV node: structure and function

The cardiac impulse is generated in the SA node from where it traverses and activates the atria before arriving at the AV node. From the AV node, the impulse is distributed to the ventricular myocardium via a specialised conduction system consisting of the His bundle, the bundle branches to each ventricle and the ramifying Purkinje fibre network (Fig. 1.1A) (Anderson & Ho, 2000; Schram *et al.*, 2002).

Tawara (2000) was the first to describe the morphology of the AV node in the hearts of several species. His major achievement was to show that the AV conduction axis is a continuous system of histologically distinctive cells from the atrial septum to the ventricular Purkinje cells.

The AV nodal area is within the boundaries of the so-called triangle of Koch (Koch, 1909). This is the region demarcated by the attachment of the septal leaflet of the tricuspid valve, the ostium of the coronary sinus and the tendon of Todaro. Precise borders for the AV

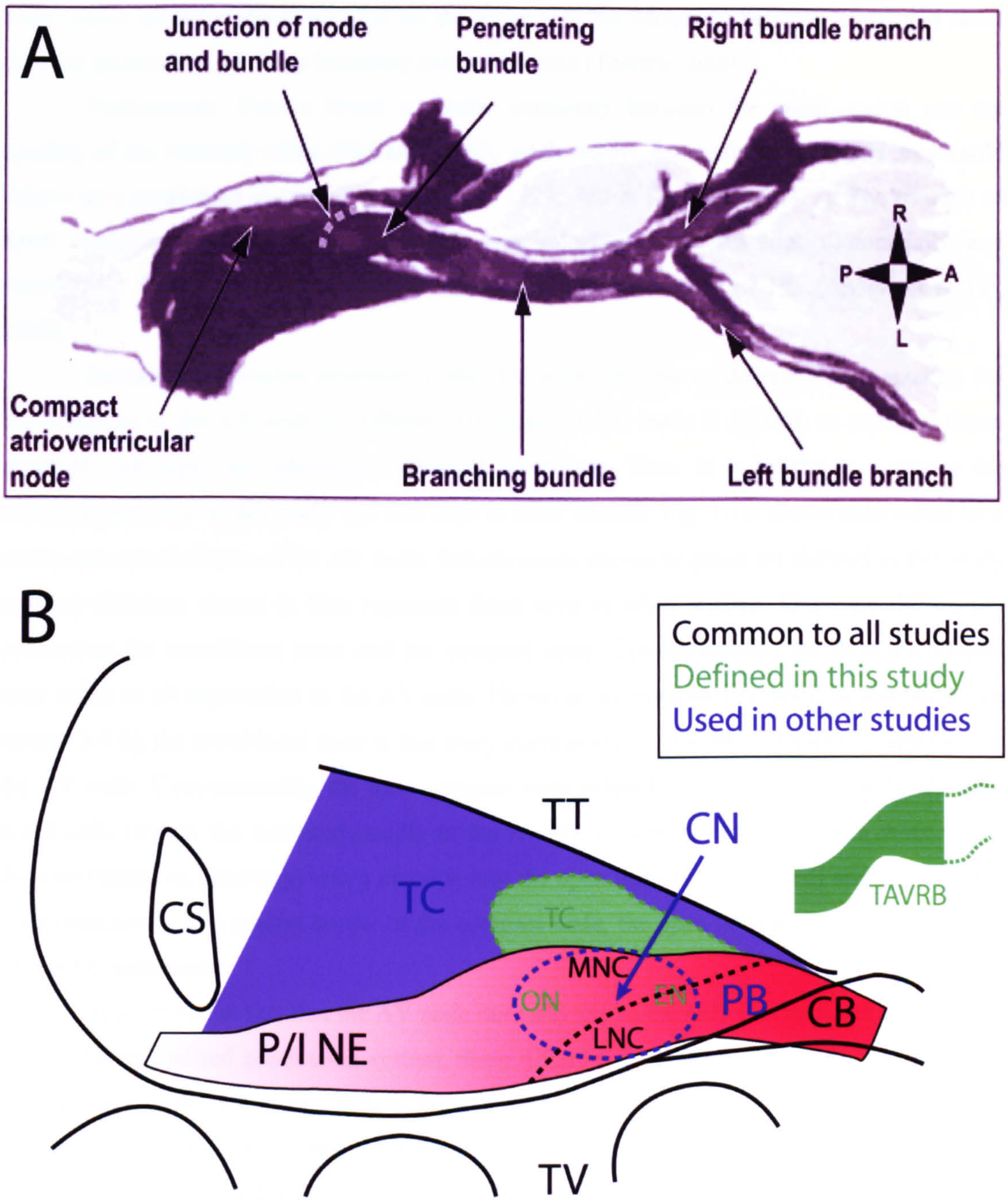

Figure 1.1 Sub-divisions in the AV conduction axis

A, Tawara's initial description of AV conduction axis. This figure originally drawn by Tawara (2000) shows the various sub-divisions of the AV conduction axis. A, anterior; L, left; P, posterior; R, right. From Mazgalev *et al*. (2001). B, AV node landmarks and sub-divisions. CB, common bundle; CN, compact node; CS, coronary sinus; EN, enclosed node; LNC, lower nodal cells; MNC, mid-nodal cells; ON, open node; PB, penetrating bundle; P/I NE, posterior/inferior nodal extension; TAVRB, termination of the AV ring bundle; TC, transitional cells; TT, tendon of Todaro; TV, tricuspid valve. Modified from Medkour *et al*. (1998).

node cannot be determined, because on the atrial side the transition between nodal and atrial tissue is gradual and no sharp boundary can be detected (Tawara, 2000).

Furthermore, Tawara found a similar continuity between the nodal region and the opening of the coronary sinus (Tawara, 2000), while others demonstrated that this area could behave as a pacemaker in special cases (Koch, 1909; Wit & Cranefield, 1977). The triangle of Koch contains multilayered and complex morphological structures that anatomically and functionally form a continuum between the atrium and the bundle of His (Anderson & Ho, 2000).

Besides the complex structure of the AV node, the use of different nomenclature for sub-divisions of the AV node by different investigators has made it difficult to correlate tissue structure, cell types and electrophysiological recordings. Thus, it is helpful to compare the nomenclature used in this study and that used in other studies. Fig. 1.1B shows anatomical land marks and sub-divisions of the AV node. Sub-divisions shown in green are defined in this study and sub-divisions shown in blue represent those used in other studies. There are differences concerning the transitional zone and the compact node. Conventionally, the term transitional zone refers to all approaches to the AV node. However, as explained in detail in chapter 3 (see section 3.4.4), the transitional zone in this study corresponds to the anterior/superior approach to the AV node. Conventionally, the term compact node refers to a group of compactly arranged nodal cells (within the insulated bundle in the rabbit). However, in this study, a more useful division (based on histology) was a division into the open node (not insulated) and the enclosed node (insulated). The precise border of the compact node, the open node and the enclosed node cannot be made easily.

Apart from the fact that the AV node normally forms the only link between the atria and ventricular specialised conduction system, three different functional characteristics distinguish the AV node: 1) the AV node conducts the impulse slowly, thereby causing a delay between the activation of the atria and ventricles. Because of this so-called AV nodal delay, the contractions of the atria and ventricles are coordinated (Tawara, 2000). 2) The AV node is capable of blocking impulses on their way from the atria to ventricles, when these occur prematurely or at a rapid rate, thus protecting the ventricles from too rapid rhythms and to a certain extent from irregularities in rhythm (Lewis, 1925). 3) The AV node may serve as a pacemaker to the ventricles when the SA node fails or when conduction block between the atria and AV node develops (Watanabe & Dreifus, 1968; James *et al.*, 1979; Janse & Tranum-Jensen, 1981; Dobrzynski *et al.*, 2003).

The relative importance of the functions of the AV node differs in large and small mammalian hearts. In small mammals, synchronisation of atrial and ventricular contractions is the major function of the AV node, whereas protection from rapid atrial arrhythmias may be its most important function in large mammals. For example, it is clear that in small mammals, where conduction time in the ventricular conduction system may take no more than 2-5 ms, an

AV nodal delay is necessary to ensure that ventricular contraction does not begin before atrial contraction has ended (Altman & Dittmer, 1971; Meijler, 1985).

1.2. Electrophysiology of the AV node

1.2.1. The difficulties in correlating morphological cell types with electrophysiological recordings

Although different authors usually use different nomenclature, the AV nodal region is most frequently described as encompassing transitional cells, mid-nodal cells, and lower nodal cells (Fig. 1.2) (Janse *et al.*, 1978; Billette & Amellal, 2000). Early microelectrode studies showed that based on activation times and the action potential characteristics, the cells of the AV node are frequently described as atrionodal (AN), nodal (N), and nodal-His (NH) (Fig. 1.2) (de Carvalho & de Almeida, 1960).

As noticed by Tawara (2000), on the atrial side, the transition between nodal and atrial tissue is gradual and the boundaries of the compact node are not sharply defined. Furthermore, Tawara (2000) found similar continuity between the nodal region and the opening of the coronary sinus. Similarly, the electrical responses of the nodal cells are not unique. Thus, action potentials with low resting potentials, a slow upstroke and small amplitudes can be recorded from "nodal-like" cells that are found in the nodal approaches (Billette, 1987).

AN cells are transitional cells. These cells are morphologically different from the working atrial cells and are widely spread within the nodal approaches and are intermingled with the even smaller nodal cells in the compact region (de Carvalho & de Almeida, 1960; Billette, 1987). There is no correlation between action potential types and the specific areas from which the responses are recorded. Paradoxically, the most *typical* nodal action potential has not yet been linked to the most *typical* nodal cell (Meijler & Janse, 1988). Although AV nodal cells now can be enzymatically dissociated and the electrical properties of cells isolated from the AV node have been studied, the precise region from which they were isolated is unknown (Munk *et al.*, 1996; Workman *et al.*, 2000). The difficulties in providing precise morphological electrophysiological descriptions are in part the result of the lack of appropriate techniques for simultaneous examination of the electrical responses and the structure of the same cells (Meijler & Janse, 1988).

1.2.2. Dual pathway electrophysiology and AV nodal reentry

The AV node is activated by atrial wavefronts travelling via the terminal part of the crista terminalis and interatrial septum (Amellal & Billette, 1996). Although the specialised components of the AV node communicate with the atrial myocardium through connections running in virtually all directions (Sanchez-Quintana *et al.*, 1997), the dual pathways refer to posterior/inferior and anterior/superior sites. These two major inputs have been specifically

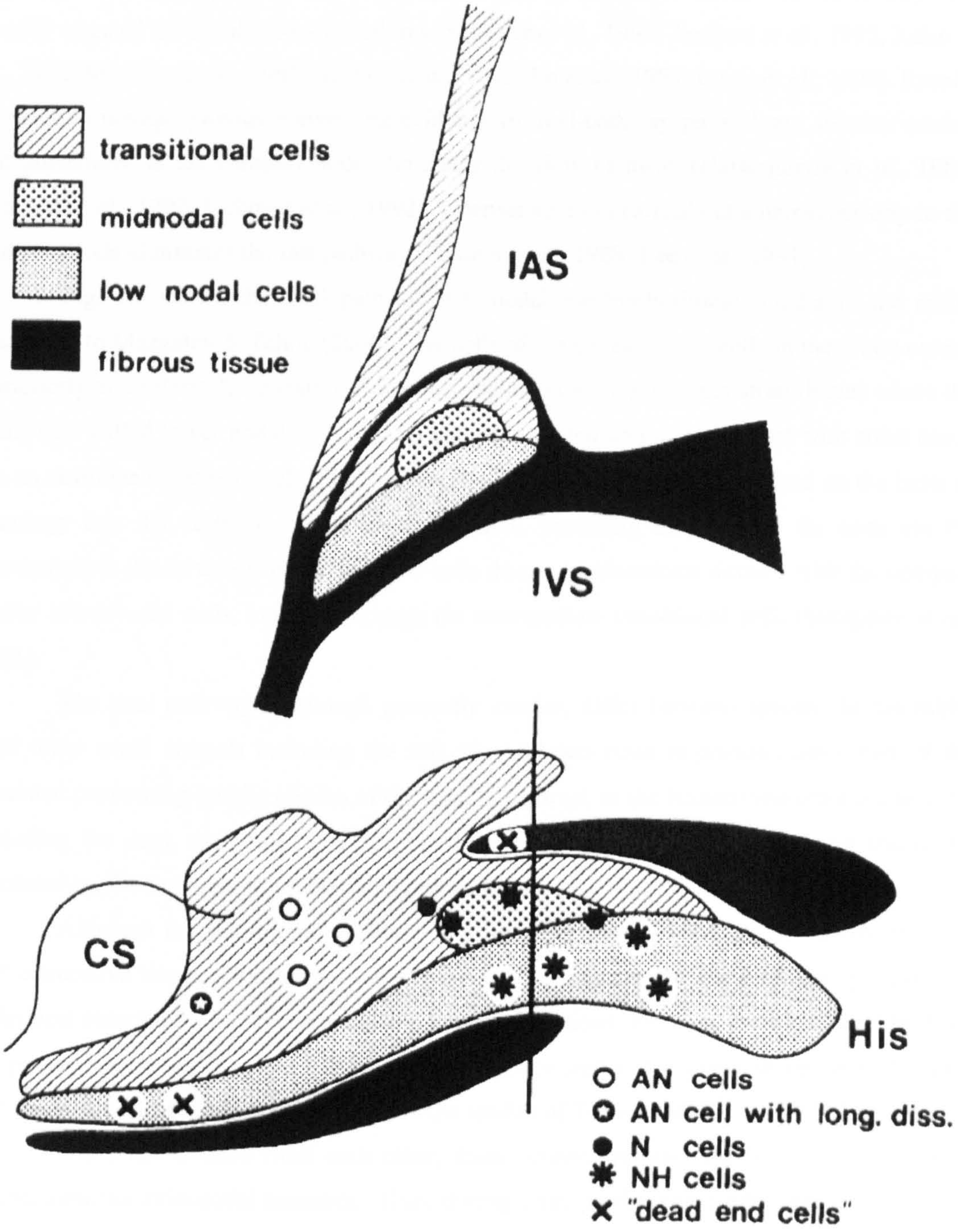

Figure 1.2 The morphological divisions of the AV node of the rabbit

Diagrams show distribution of morphologically different cell types in rabbit AV node. *Top*: transverse section showing trilaminar appearance in the enclosed node. The position of this section is demarcated by a bar in the bottom panel. *Bottom*: diagram indicates sites where typical transmembrane potentials were recorded. CS, coronary sinus; IAS, interatrial septum; IVS, interventricular septum; His, His bundle. From Janse *et al.* (1978).

regarded as having special functional importance: the substrate for AV nodal reentry and usually targeted during ablation procedures (Schluter *et al.*, 1991; Jazayeri *et al.*, 1992; Keim *et al.*, 1992; McGuire *et al.*, 1993; Mitrani *et al.*, 1993; Lo *et al.*, 1995; Inoue *et al.*, 1999). Results of ablation therapy provide convincing evidence of dual-pathway physiology; ablation carried out posteriorly to the compact node eliminates the slow pathway (Haissaguerre *et al.*, 1989; Jazayeri *et al.*, 1992; Jackman *et al.*, 1992), whereas ablation carried out anterosuperiorly to the compact node eliminates the fast pathway (Epstein *et al.*, 1989; Lee *et al.*, 1991).

Fig. 1.3 shows the dual pathway AV nodal electrophysiology model in the rabbit according to Mazgalev & Tchou (2000). The cells of the penetrating bundle in the rabbit extend posteriorly and inferiorly beneath the compact region, emerging into the atrial tissues where the cells, now called lower nodal cells, are no longer insulated and make contact with atrial tissue via an envelope of transitional cells. The inferior nodal extensions can be traced on the basis of histology into the vestibule of the tricuspid valve, providing the input to the node via the terminal crest (crista terminalis). The atrial cells do not communicate directly with the compact and/or lower nodal cells, but only through the intermediate transitional cells (Mazgalev *et al.*, 2001).

The dual pathways, although generally similar, differ between species. In the rabbit (and other small animals including the rat), the compact node is predominantly part of the insulated penetrating bundle portion of the axis. In contrast, in the human (and other big animals including the dog), the compact node is part of the atrial component of the axis and is not insulated by fibrous tissue from the atrial myocardium.

Although the transitional envelope and the lower nodal tracts are intermixed with fat and connective tissue, they are not electrically insulated (as in the His-Purkinje system). The atrial beat enters the AV node proper from several directions, the most prominent of which are the posterior approaches (crista terminalis), the superior septal approaches along the fosa ovalis, and the broad mid-septal approaches across the tendon of Todaro (Mazgalev *et al.*, 2001).

While not isolated from each other, these connections result in a functionally highly inhomogeneous atrio-nodal transition. Thus, during sinus rhythm (with relatively long coupling intervals between beats) predominant is the wavefront formed along the anterior septal nodal input(s). It reaches the bundle of His first, generating the relatively brief basic conduction delay. In contrast, premature stimuli (with short coupling intervals) are blocked in these anterior approaches allegedly due to the relatively long refractoriness of the tissue and/or due to specific passive properties of the conducting fibers and their interconnections. Therefore, the short-coupled beats proceed along the posterior input approaches and, in general, require longer time to reach the bundle of His. Based on these properties and following a very simplified (and therefore approximate) morphological model, the posterior approaches are regarded as a domain of the so-called slow pathway, while the anterior septal input region hosts the fast pathway.

RABBIT AV NODAL AXIS (anterograde propagation)

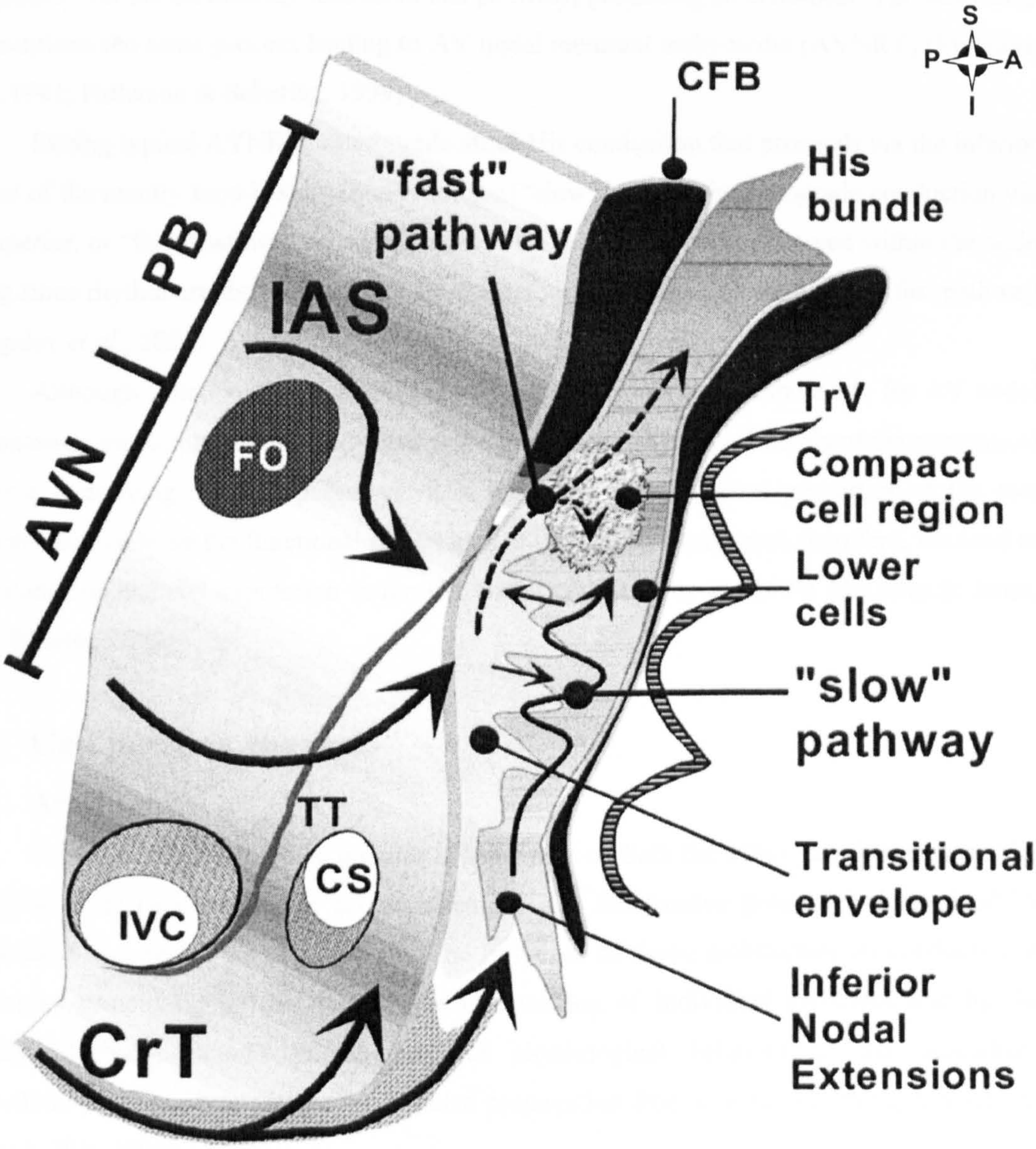

Figure 1.3 Schematic illustration of dual pathway AV nodal electrophysiology in the rabbit

Dashed arrow, fast pathway; wavy arrow, slow pathway. AVN, AV node; CFB, central fibrous body; CrT, crista terminalis; CS, coronary sinus, FO, fossa ovalis; IAS, interatrial septum; IVC, inferior vena cava; PB, penetrating bundle; TrV, tricuspid valve; TT, tendon of Todaro. Orientation is shown by the "compass" (A, anterior; I, inferior; P, posterior; S, superior). Modified from Mazgalev & Tchou (2000a).

In summary, a short-coupled atrial stimulus may be blocked in the fast pathway (anterior septal input) while successfully propagating via the slow pathway (posterior input) toward the bundle of His. If this propagation is slow enough, the impulse may reenter the atrium retrogradely via the sufficiently recovered fast pathway, producing an echo-beat. The latter may then continue the same process leading to AV nodal reentrant tachycardia (AVNRT) (McGuire *et al.*, 1991; Patterson & Scherlag, 1999).

During typical AVNRT, anterograde atrial-His conduction that proceeds via the inferior portion of the reentry loop is substantially longer ("slow") than is the retrograde conduction via the superior, or "fast," pathway. In addition, the relatively short delays observed within the node during sinus rhythm are thought to result from anterograde conduction through the fast pathway (Mazgalev *et al.*, 2001).

Although functionally we know the fast and slow pathways responsible for AV nodal dual pathway electrophysiology and reentry are important, we know little about the anatomical substrate underlying the two pathways. It is the electrophysiological properties of the two pathways that underlie the functional importance of the two pathways and, therefore, we need to understand ion channel expression in the two pathways (Sung *et al.*, 1994; McGuire & Janse, 1995; Billette, 2002).

1.3. Gap junction channels

1.3.1. Architecture

Conduction of the cardiac impulse is dependent on both the active membrane properties of cardiac cells (generating the action potential) and the passive properties determined by architectural features of the myocardium. The influence of tissue architecture on conduction is determined principally by the size, shape and packing of individual myocytes and by the quantity, three-dimensional distribution and physiological behavior of the specialised intercellular junctions responsible for impulse propagation from cell to cell, the gap junctions (Peters & Wit, 1998).

It has been reported that conduction is more rapid in the direction parallel to the myocardial cell axis than in the transverse direction, because of the lower resistivity of the myocardium in the longitudinal than the transverse direction. Gap-junctional channels create continuity between the cytoplasmic compartments of abutting myocytes, but act as resistive discontinuities to the cytoplasmic current flow between the intracellular compartments of the cells (the "intracellular" conduction pathway). Longitudinal resistivity is lower than transverse resistivity because intracellular pathway encounters fewer cell boundaries per unit distance in the longitudinal than the transverse direction and the resistivity of the gap-junctional membrane is several orders of magnitude higher than the cytoplasmic intracellular resistivity (Peters & Wit, 1998). In the myocardium, approximately half of all connections are side to side and half

are end to end (Hoyt *et al.*, 1989; Luke & Saffitz, 1991). This means that there is a greater density of connections end-to-end than side-to side.

The archetypal working myocytes of the ventricles and atria are elongated, branching, contractile cells, extensively interconnected by clusters of gap junctions organized in intercalated disks (Page, 1992; Peters *et al.*, 1993; Peters *et al.*, 1994; Severs *et al.*, 2001). The myocytes in the atrial myocardium are slender and have less extensive intercalated disks and more lateral junctional contacts than their ventricular counterparts (Severs *et al.*, 2001). The intercalated disks also contain two types of anchoring junction, the fascia adherens and desmosome, which mediate cell-to-cell linkage of the contractile filaments and the intermediate filament cytoskeleton, respectively. These anchoring junctions act in concert with the gap junctions to integrate cardiac mechanical, metabolic and electrical function (Sjöstrand & Andersson-Cedergren, 1960; Severs, 1990; Severs *et al.*, 2001).

Gap junctions are specialised regions of the intercalated disk (Sjöstrand & Andersson-Cedergren, 1960; Severs, 1990; Beyer, 1993; Bruzzone *et al.*, 1996) in which integral proteins, connexins (Fig. 1.4), exist in hexameric units called connexons (Beyer, 1993), each of which possesses a 1.5- to 2-nm central pore (Flagg-Newton *et al.*, 1979). The connexons in the abutting myocyte membranes (Fig. 1.4) align, and the pair forms a complete channel linking the cytoplasmic compartments, providing a relatively low-resistance pathway for the passage of ions and small molecules (up to $\approx$ 1 kD) (Imanaga *et al.*, 1987) and for electrical propagation (Spray & Burt, 1990).

In the mammalian heart, a connexin composed of 342 amino acid residues (Beyer *et al.*, 1987) with a molecular weight of 43,000 (connexin43 or Cx43) is the most abundant connexin and is abundant in the working ventricle and atrium. Two further isotypes, connexin40 (with a molecular weight of 40,000; Cx40) and connexin45 (with a molecular weight of 45,000; Cx45), are also expressed in a myocyte subtype and chamber-specific manner.

In cells expressing more than one connexin type, however, a multiplicity of different arrangements involving heterotypic channels (those in which the connexin makeup of the component connexons differs), homotypic channels (in which the connexin makeup of the component connexons is identical) or heteromeric channels (in which the component connexons contain mixtures of connexins) is possible, the functional correlates of which are yet to be fully clarified (Severs *et al.*, 2001).

1.3.2. Gating and unitary conductance

Gap-junctional channels can exist in open or closed states. The proportion of channels that are in an open state and the physiological properties of the channel, such as selective ion permeability, unitary conductance and voltage sensitivity, are determined by the characteristics of the connexin isoforms composing the channel (Veenstra *et al.*, 1994; Moreno *et al.*, 1994; Beblo *et al.*, 1995; Veenstra, 1996).

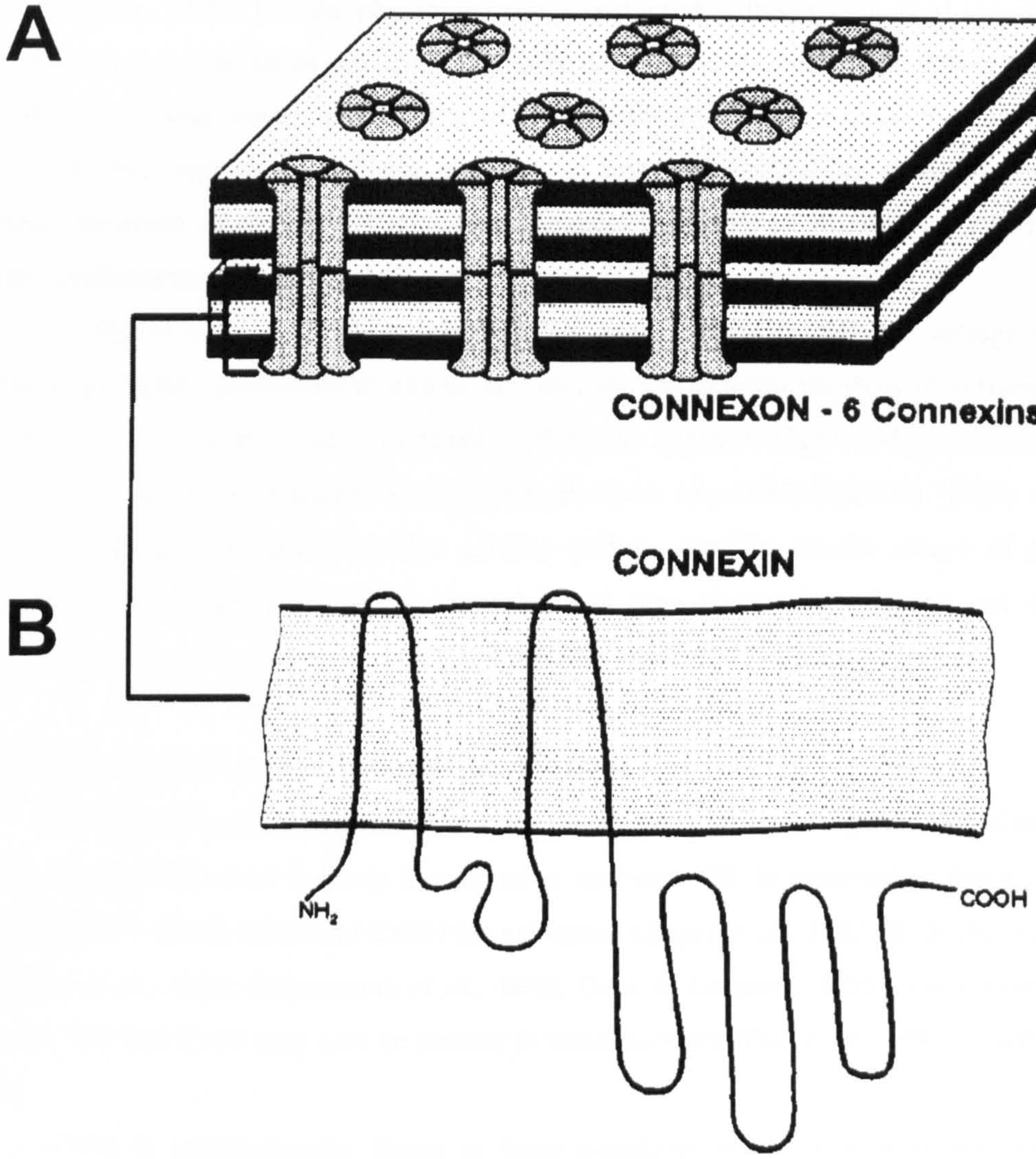

Figure 1.4 Model of a gap junction

A, model of a gap junction. A gap junction consists of a cluster of channels. Each channel consists of a pair of connexons, one contributed from each plasma membrane. A connexon consists of six connexin molecules (connexin40, 43 or 45 in the heart). B, molecular structure of one connexin. A connexin molecule consists of four transmembrane regions and amino and carboxy termini situated on the cytoplasmic side of the membrane. From Peters & Wit (1998).

The conductance of a single Cx43 channel in its main conductance state is 40 to 60 pS (Burt & Spray, 1988), but the physiological and potential pathophysiological significance of two other minor conductance states remains to be determined (Moreno *et al.*, 1994; Bruzzone *et al.*, 1996). The main unitary conductance of Cx40 is 150 to 200 pS, a value higher than that of Cx43. Selective expression of Cx40 in the atrial myocardium and His-Purkinje tissues may therefore facilitate rapid conduction in these tissues (Bruzzone *et al.*, 1996). Cx45 has a low unitary conductance (22 and 36pS; Bruzzone *et al.*, 1996).

Gating of Cx43 channels is relatively insensitive to transmembrane voltage and Cx43 channels are highly permeable to anions and cations and fluorescent dyes of different charge densities and molecular weights (Veenstra, 1996). In contrast, Cx40 and Cx45 channels are highly cation selective (Veenstra *et al.*, 1994; Beblo *et al.*, 1995; Veenstra, 1996) and Cx45 gating is voltage-dependent. The dye Lucifer yellow, used in classic assays of junctional coupling, passes much more freely through Cx43 than Cx40 channels and not detectably through Cx45 channels (Veenstra *et al.*, 1994; Beblo *et al.*, 1995; Veenstra, 1996).

1.3.3. Distribution in and around the AV node

19 different connexin genes have been identified in the mouse genome (Willecke *et al.*, 2002) and the final count is likely to take us to well over 20. In mammalian heart, four main isotypes (Cx37, Cx40, Cx43 and Cx45) are expressed (Beyer *et al.*, 1987; Willecke *et al.*, 1991; Haefliger *et al.*, 1992; Hennemann *et al.*, 1992; Gros & Jongsma, 1996) and further isotypes such as Cx46 and Cx57 may also be present in trace amounts (Paul *et al.*, 1991; Manthey *et al.*, 1999).

Cx43 is predominantly found in large quantities in the ventricles and atria of all mammalian species (Gros & Jongsma, 1996; Severs *et al.*, 1996). Cx40 is abundant in the atrial myocytes of most species, co-organized with Cx43 in the same junctional plaques, though working ventricular myocytes characteristically lack this connexin (Van Kempen *et al.*, 1995; Vozzi *et al.*, 1999). Cx40 is also abundant in the AV conduction system, i.e. the His bundle, bundle branches and Purkinje fibres, where it is implicated in facilitating fast conduction (Gourdie *et al.*, 1993; Kanter *et al.*, 1993; Bastide *et al.*, 1993; Davis *et al.*, 1994; Gros *et al.*, 1994). Cx45 is present only in very low quantities; this connexin is typically undetectable or barely detectable by immunocytochemistry in working ventricular myocytes, though slightly higher levels are present in the atrium (Coppen *et al.*, 1998; Vozzi *et al.*, 1999). Cx45 is preferentially expressed in the SA node and the AV conduction system (Coppen *et al.*, 1998; Coppen *et al.*, 1999; Severs *et al.*, 2001).

1.4. Ionic currents in the AV node

Although the action potentials recorded from isolated cells can also be classified into AN, N and NH subgroups (Munk *et al.*, 1996), direct juxtaposition of these groups to the groups

described in the intact heart (see section 1.2.1) is only approximate, because the isolation procedures are blind and do not permit the identification of the specific regions from which the isolated cells originate. Instead, isolated cells have been described based on their shape after isolation (ovoid or rod-shaped) (Munk *et al.*, 1996). Ovoid cells have N- or NH-like action potentials showing post-repolarization refractoriness and no action potential abbreviation with increased frequency, less negative maximum diastolic potentials, faster diastolic-depolarization, and lower upstroke velocity than those in rod shaped cells. Rod-shaped cells display action potentials intermediate between ovoid cells and atrial cells (AN type) (Munk *et al.*, 1996). Fig. 1.5 shows action potentials recorded from single cells isolated from rabbit AV node.

Several studies have reported ionic currents recorded during voltage clamp of isolated AV nodal cells (Taniguchi *et al.*, 1981; Nakayama *et al.*, 1984; Nakayama & Irisawa, 1985) or small preparations of AV nodal tissue (Nishimura *et al.*, 1989). While voltage clamp studies have identified the presence of various ionic currents, there is still relatively little known about the distribution, nature and function of these currents in the various AV nodal cell types. However, something is known as described below.

1.4.1. Na^+ current

A number of studies have attempted to resolve the nature of the ionic currents responsible for the action potential upstroke, a key determinant of AV nodal cell excitability. In the working myocarium, it has long been known that a voltage-dependent Na^+ current (I_{Na}) is responsible for the action potential upstroke (Weidmann, 1955). However, it has been suggested that I_{Na} is either absent or reduced in the mid-nodal region (N cells). This hypothesis is supported by the observations that application of hyperpolarizing current to N cells did not result in an increase in the maximum upstroke velocity (Hoffman, 1961; Anderson *et al.*, 1974) and that verapamil, D600 and Mn^{2+} suppressed action potentials in the N region whereas TTX was without effect (Zipes & Mendez, 1973; Watanabe, 1981). In contrast, other groups have reported that application of a hyperpolarizing current resulted in an increase in the amplitude and maximum upstroke velocity of N cell action potentials (Shigeto & Irisawa, 1974) and the availability of the Na^+ channel (Kokubun *et al.*, 1982; Nakayama *et al.*, 1984). Moreover, it was also reported that the action potential upstroke of AV nodal cells can be biphasic, with one component being TTX-sensitive (Ruiz-Ceretti & Zumino, 1976). However, it is still unclear as to the origin of the cells studied and which cell types, if any, lack Na^+ channels. In order to address these issues, patch clamp studies were undertaken by Munk *et al.* (1996) in different AV node cell types. I_{Na} appears to be absent in ovoid cells (Munk *et al.*, 1996). In rod-shaped cells, I_{Na} is present, but it is much reduced compared with the levels in the working myocardium (Munk *et al.*, 1996). Cells that lacked a significant I_{Na} also appeared to lack a significant transient outward K^+ current (I_{to}), but had a prominent I_f (hyperpolarization-activated inward current) (Munk *et al.*, 1996).

Figure 1.5 Action potentials recorded from isolated AV nodal myocytes

A-C, whole cell patch electrode recordings of AN-, N- and NH-like action potentials from isolated AV nodal myocytes of the rabbit. Calibration values in A apply to all panels. Modified from Munk *et al.* (1996).

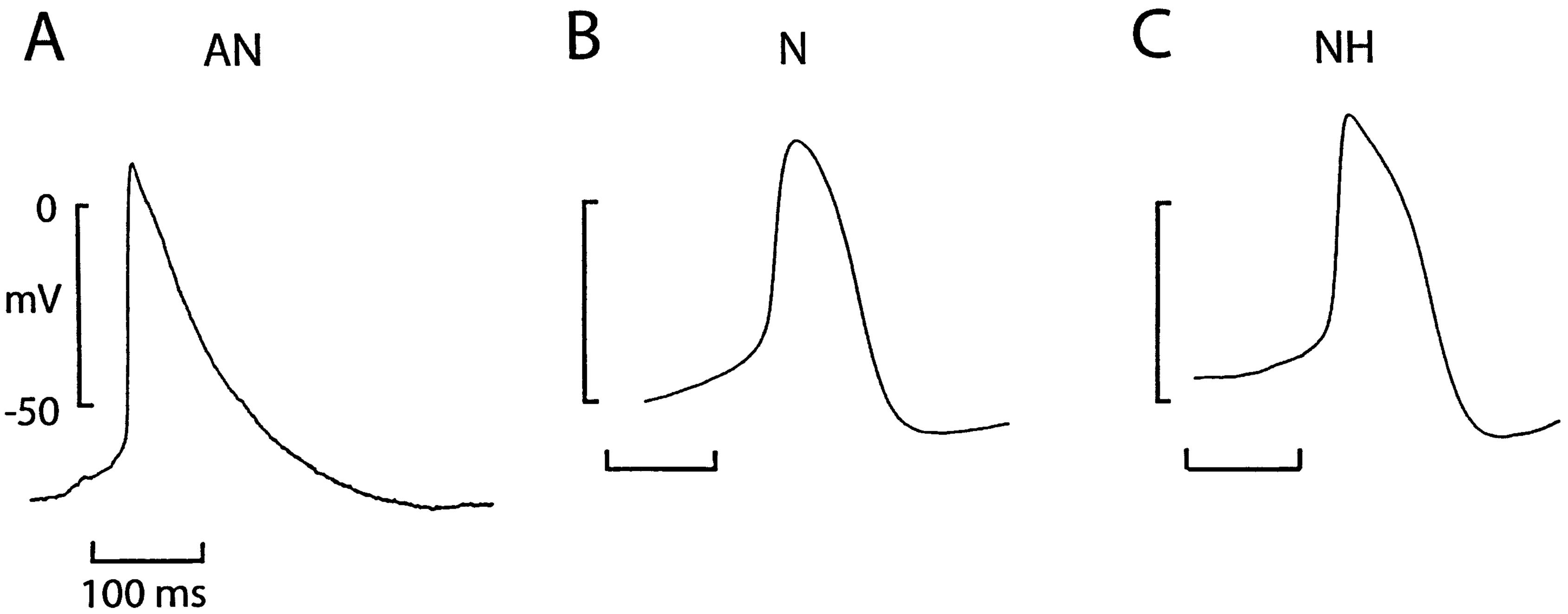
A
AN
0
mV
-50
100 ms
B
N
C
NH

1.4.2. Ca^{2+} current

Early studies on the intact AV node using various ion channel blocking agents such Mn^{2+}, tetrodotoxin (TTX) and verapamil revealed that a slow inward current was present in AV nodal myocytes (Zipes & Mendez, 1973; Noma *et al.*, 1980; Kokubun *et al.*, 1982). This TTX-resistant slow inward current is consistent with the L-type Ca^{2+} current ($I_{Ca,L}$) originally described in atrial cells (Bean, 1985). Importantly, $I_{Ca,L}$ was found to be present in single cells isolated from all nodal regions (Hancox & Levi, 1994; Munk *et al.*, 1996).

To date, little data exist concerning the role of T-type Ca^{2+} current ($I_{Ca,T}$) in the AV node. The threshold of T-type Ca^{2+} channels is more negative than that of L-type Ca^{2+} channels, making it well suited for participation in pacemaker activity in the SA node (Hagiwara *et al.*, 1988; Lipsius *et al.*, 2001).

1.4.3. Transient outward K^+ current

Using the whole cell voltage clamp technique, I_{to} was observed in cells isolated from the AV nodal region (Nakayama & Irisawa, 1985); however, the nodal region from which the cells were isolated was not determined. More recently, I_{to} has been reported to be variably expressed in AV nodal cells (Munk *et al.*, 1996). I_{to} was observed in combination with I_{Na} in 93 % of rod-shaped cells, presumably isolated from the transitional cell region, but in only 24 % of ovoid-shaped cells, presumably isolated from the mid-nodal cell region. I_{to} alone was found in ~40 % of ovoid-shaped cells. Taken together, this indicates that the majority of I_{to}, similar to I_{Na}, is relegated to the AN region and to a certain population of cells in the N region.

4-aminopyridine, a blocker of I_{to}, inhibits spontaneous AV node action potentials, which is consistent with a role for I_{to} in AV node pacemaking (Mitcheson & Hancox, 1999). I_{to} elimination in transgenic mice causes AV block (Guo *et al.*, 2000).

1.4.4. Delayed rectifier K^+ current

A major repolarizing current in AV nodal myocytes is the delayed rectifier K^+ current, I_K (Noma *et al.*, 1980). Contrary to the SA node, where both I_{Kr} and I_{Ks} (the rapidly and slowly, respectively, activating delayed rectifier K^+ currents) are important, the inward rectifier properties and relatively negative activation range of this current are consistent with I_{Kr} alone (Sanguinetti & Jurkiewicz, 1991). I_{Kr} activation contributes to AV node repolarization and I_{Kr} deactivation to diastolic depolarization (Hancox & Mitcheson, 1997).

1.4.5. Inward rectifier K^+ currents

Inwardly rectifying K^+ current channels are critical for establishing the resting membrane potential of cardiomyocytes and thus are independently critical in determing the upstroke velocity of the action potential and hence conduction velocity. Furthermore, they carry

a small but significant outward current during the late stages of the action potential, thus contributing to final repolarization (Nichols & Lopatin, 1997).

A family of genes encoding inwardly rectifying K^+ channels (Kir) has been identified. There are at least six Kir subfamilies (Kir1-6), classified according to similarities in amino acid sequence. To date, only Kir2 (IRK-type) (Kubo *et al.*, 1993) and Kir3 (GIRK-type) (Krapivinsky *et al.*, 1995a) transcripts have been found in the heart. Heterologously expressed Kir2 channels exhibit time- and voltage-dependent rectification almost indistinguishable from that of native inward rectifier K^+ current (I_{K1}), which is abundant in atria and ventricles, but largely absent from the AV node. The absence of I_{K1} in the AV node is consistent with the relatively positive maximum diastolic potential in the AV node.

Conversely, the ACh-sensitive K^+ current ($I_{K,ACh}$; GIRK-type) is known to be a critical modulator of atrial, SA and AV nodal excitability (Wickman & Clapham, 1995). In the heart, the channel for $I_{K,ACh}$ is a heteromultimer of two subunits, Kir3.1 (GIRK1) and Kir3.4 (GIRK4). $I_{K,ACh}$ depresses heart rate by hyperpolarizing pacemaker cells in the SA and AV nodes by binding to type 2 muscarinic receptors activating pertussis toxin-sensitive G proteins (Clapham & Neer, 1997). The active $G_{\beta\gamma}$ subunits (released from the G protein) directly bind and activate the $I_{K,ACh}$ channel (Krapivinsky *et al.*, 1995b). Importantly, $I_{K,ACh}$ also mediates the effects of adenosine (Belardinelli *et al.*, 1995). Adenosine binds to type 1 purinergic receptors, in turn catalyzing the G protein complex dissociation enabling $G_{\beta\gamma}$ subunits to directly activate $I_{K,ACh}$.

Adenosine administration results in a concentration-dependent decrease in the duration and amplitude of action potentials of AN and N cells (Clemo & Belardinelli, 1986). In N, but not in AN cells, adenosine also depresses the upstroke velocity of the action potential (Clemo & Belardinelli, 1986). At high concentrations, adenosine completely abolishes N cell action potentials (Clemo & Belardinelli, 1986). In contrast, adenosine has no effect on NH cell action potentials (Clemo & Belardinelli, 1986). The mechanism by which adenosine depresses action potentials of AN and N cells is most likely its effect on $I_{K,ACh}$, and/or inhibition of cyclic adenosine monophosphate (cAMP) production, which results in a decrease in $I_{Ca,L}$ and I_f (Belardinelli *et al.*, 1995; Martynyuk *et al.*, 1995).

1.4.6. Pacemaker current

Noma *et al.* (1980) first demonstrated the presence of I_f in the AV node. Kokubun *et al.* (1982) observed this current in 20 % of their AV nodal specimens. Similarly, Hancox & Levi (1994) reported the absence of this current in 80 - 90 % of the isolated AV nodal cells they analyzed. Conversely, Habuchi *et al.* (1995) reported that I_f was present in 90 % of the AV nodal cells they studied. In the study of Munk *et al.* (1996), approximately 90 % of the ovoid-shaped cells displayed a relatively large I_f that was activated at relatively positive potentials in a range that could affect excitability and pacemaker activity, whereas I_f was present in 10 % of rod-shaped cells. I_f density in ovoid cells was also 25-fold larger than that in rod-shaped cells.

This is consistent with the much greater ovoid cell pacemaker activity (Munk *et al.*, 1996). Thus, it would appear that there is a heterogeneous regional distribution of I_f in the AV nodal region.

1.4.7. Na^+/Ca^{2+} exchanger

Studies in working myocardial cells indicate that the Na^+/Ca^{2+} exchange current ($I_{Na\text{-}Ca}$) is significant in the repolarizing phase of the action potential (Hryshko, 2004). Hilgemann (1989) demonstrated that $I_{Na\text{-}Ca}$ is an important inward current in the negative potential range of the cardiac action potential. Modelling studies of the SA node suggest that $I_{Na\text{-}Ca}$ contributes to the action potential configuration and pacemaker activity (Wilders *et al.*, 1991). Bodganov *et al.* (2001) have more recently shown experimentally a role of $I_{Na\text{-}Ca}$ in pacemaker activity in the SA node. A recent report has indicated that $I_{Na\text{-}Ca}$ is present in AV nodal cells and exhibits a similar profile to that in ventricular cells (Convery & Hancox, 2000).

1.5. Na^+ channel expression in the AV node

1.5.1. Voltage-gated Na^+ channel isoforms

Voltage-gated Na^+ channels are responsible for action potential initiation and propagation in excitable cells, including nerve, muscle, and neuroendocrine cell types. They are also expressed at low levels in non-excitable cells, where their physiological role is unclear. Na^+ channels consist of an α subunit, which is approximately 260 kDa, and auxiliary β subunits (Catterall, 2000). The pore-forming α subunit is sufficient for functional expression, but the kinetics and voltage-dependence of channel gating are modified by the β subunits, and these auxiliary subunits are involved in channel localization and interaction with cell adhesion molecules, the extracellular matrix, and the intracellular cytoskeleton. The α subunits are organized in four homologous domains (I–IV), each of which contain six transmembrane α helices (S1–S6) and an additional pore loop located between the S5 and S6 segments (Fig. 1.6). The pore loops line the outer, narrow entry to the pore, whereas the S5 and S6 segments line the inner, wider exit from the pore. The S4 segments in each domain contain positively charged amino acid residues at every third position. These residues serve as gating charges and move across the membrane to initiate channel activation in response to depolarization of the membrane. The short intracellular loop connecting homologous domains III and IV serves as the inactivation gate, folding into the channel structure and blocking the pore from the inside during sustained depolarization of the membrane.

A variety of different Na^+ channels has been identified by electrophysiological recording, biochemical purification, and cloning (Goldin, 2001). The functional properties of the known Na^+ channels are similar. Despite their similarity of function, the Na^+ channels were originally named in many different ways, with no consistent nomenclature for the various

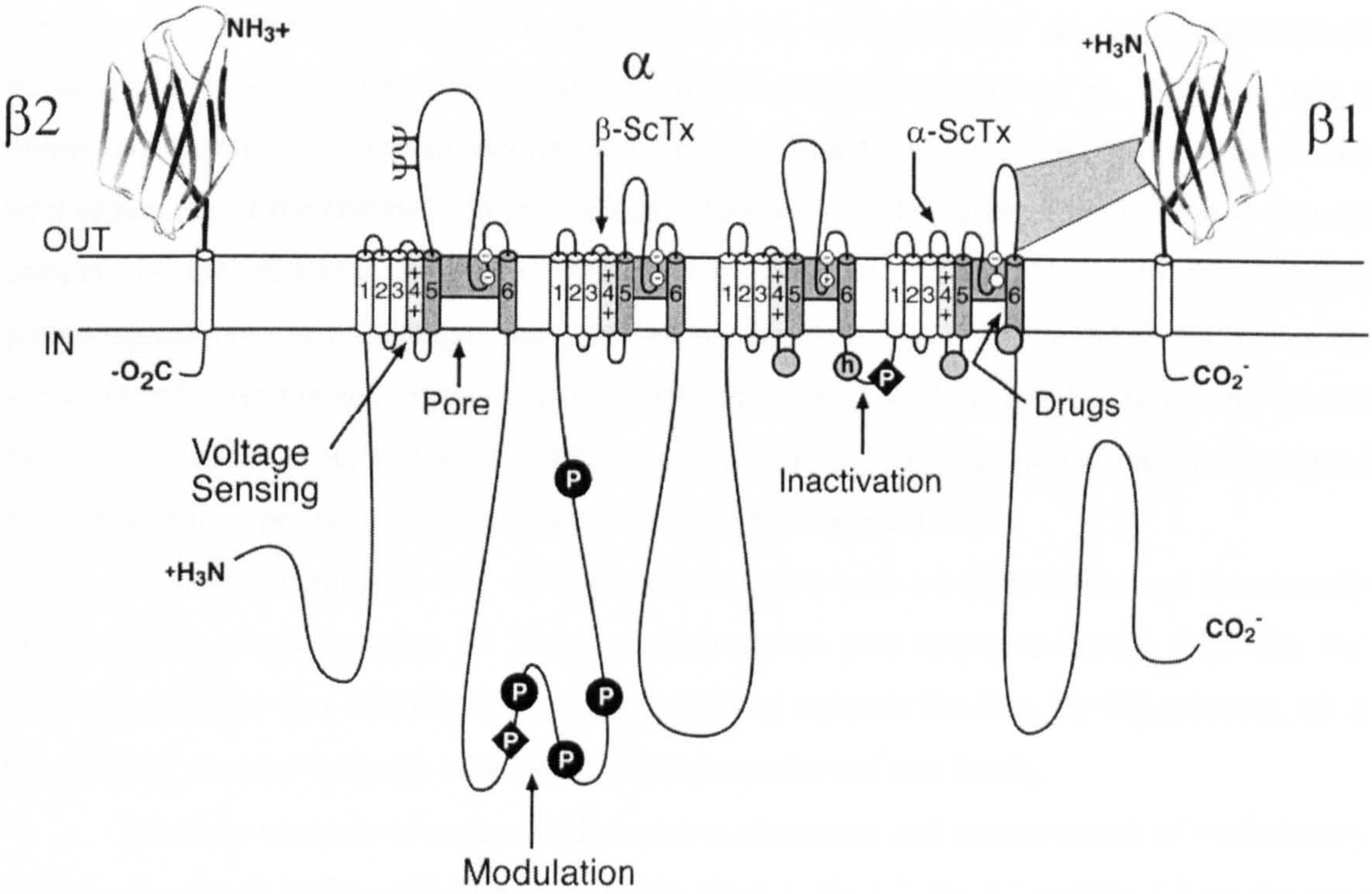

Figure 1.6. Transmembrane organization of Na^+ channel subunits

The primary structures of the subunits of the voltage-gated Na^+ channel are illustrated as transmembrane-folding diagrams. Cylinders represent probable α-helical segments. Bold lines represent the polypeptide chains of each subunit, with length approximately proportional to the number of amino acid residues in the brain sodium channel subtypes. The extracellular domains of the β1 and β2 subunits are shown as immunoglobulin-like folds. Ψ, sites of probable N-linked glycosylation; P, sites of demonstrated protein phosphorylation by protein kinase A (circles) and protein kinase C (diamonds); shaded, pore-lining S5-P-S6 segments; white circles, the outer (EEDD) and inner (DEKA) rings of amino residues that form the ion selectivity filter and tetrodotoxin binding site; + +, S4 voltage sensors; h in shaded circle, inactivation particle in the inactivation gate loop; open shaded circles, sites implicated in forming the inactivation gate receptor. Sites of binding of α- and β-scorpion toxins and a site of interaction between α and β1 subunits are also shown. From Catterall (2000).

isoforms. To eliminate confusion resulting from the multiplicity of names, a standardized nomenclature was developed for voltage-gated Na^+ channels (Goldin et al., 2000). It uses a numerical system to define subfamilies and subtypes based on similarities between the amino acid sequences of the channels. In this nomenclature system, the name of an individual channel consists of the chemical symbol of the principal permeating ion (Na) with the principal physiological regulator (voltage) indicated as a subscript (Na_V). The number following the subscript indicates the gene subfamily (currently only Na_V1), and the number following the full point identifies the specific channel isoform (e.g., $Na_V1.1$). This last number has been assigned according to the approximate order in which each gene was identified.

The nine mammalian Na^+ channel isoforms that have been identified and functionally expressed are all greater than 50 % identical in amino acid sequence (Table 1.1). The Na^+ channel sequences vary continuously, without defining separate families. By this criterion, all of the nine Na^+ channel isoforms may be considered members of one family.

Based on analysis of amino acid sequence alignment and measurement of evolutionary distance from each isoform (Goldin *et al*, 2000), $Na_v1.1$, $Na_v1.2$, $Na_v1.3$ and $Na_v1.7$ are the most closely related because their genes are all located on human chromosome 2q23-24 (Table 1.1). All four of these Na^+ channels are highly TTX-sensitive and are broadly expressed in the central nervous system. $Na_v1.5$, $Na_v1.8$ and $Na_v1.9$ have a common evolutionary origin because of the location of their genes on human chromosome 3p21-24 (Table 1.1). These Na^+ channels are TTX-resistant to varying degrees, due to changes in amino acid sequence at a single position in the pore region of domain I (in case of $Na_v1.5$, there is a cysteine instead of an aromatic residue, Fozzard & Hanck, 1996), and they are expressed in heart and dorsal root ganglion neurons. $Na_v1.4$, expressed primarily in skeletal muscle, and $Na_v1.6$, expressed primarily in the central nervous system, are different from the other two closely related groups of Na^+ channel genes. The location of the genes encoding these two Na^+ channels on chromosomes 17q23-25 and 12q13 can be the result of distant evolutionary origin (Table 1.1).

1.5.2. The identification of Na^+ channel isoforms in the heart

Relatively TTX-insensitive $Na_v1.5$ is known to the predominant Na^+ channel isoform in the heart. However, a neuronal Na^+ channel ($Na_v1.1$) has been reported in the SA node in the newborn rabbit (Baruscotti *et al.*, 1997). Neuronal Na^+ channels are also present in the adult heart: multiple neuronal Na^+ channel isoforms ($Na_v1.1$, $Na_v1.3$ and $Na_v1.6$), as well as $Na_v1.5$, are expressed in adult mouse ventricular myocytes and are involved in excitation-contraction coupling (Maier *et al.*, 2002). In addition, TTX-sensitive neuronal Na^+ channel isoforms have been shown to be expressed in the adult mouse and adult rat SA node and block of the channels has been shown to lead to a slowing of the heart rate in the isolated mouse heart (Maier *et al.*, 2003). Recently, Lei *et al.* (2004) showed that in the mouse SA node $Na_v1.1$ and $Na_v1.5$ are

Table 1.1 The Na^+ channel protein family

Protein name (synonyms)	Sequence identity (percent)	Chromosome location (human)	Primary site of expression	Primary accession number (UniProtKB)	Entry name (UniProtKB)
$Na_v1.1$ (type I)	87	2q23-24	Brain	P35498	SCN1A_HUMAN
$Na_v1.2$ (type II)	100	2q23-24	Brain	Q99250	SCN2A_HUMAN
$Na_v1.3$ (type III)	87	2q23-24	Brain	Q9NY46	SCN3A_HUMAN
$Na_v1.4$ (SkM1)	74	17q23-25	Skeletal muscle	P35499	SCN4A_HUMAN
$Na_v1.5$ (HH1)	62	3p21-24	Heart	Q14524	SCN5A_HUMAN
$Na_v1.6$ (type VI)	75	12q13	Brain	Q9UQD0	SCN8A_HUMAN
$Na_v1.7$ (PN1)	77	2q23-24	Dorsal root ganglion	Q15858	SCN9A_HUMAN
$Na_v1.8$ (PN3)	56	3p21-24	Dorsal root ganglion	Q9Y5Y9	SC10A_HUMAN
$Na_v1.9$ (PN5)	53	3p21-24	Dorsal root ganglion	Q9UI33	SC11A_HUMAN

The Na^+ channel proteins are listed according to standardized nomenclature. The common names given to each Na^+ channel α subunits are also listed in brackets. Sequence identity against $Na_v1.2$ is for human Na^+ channel isoforms determined by NCBI-blastp program (version 2.2.2) and information in the universal protein knowledgebase (www.ebi.uniprot.org).

involved in pacemaking, but only $Na_v1.5$ is involved in action potential propagation. The distribution of neuronal Na^+ channel isoforms in the AV node is unknown.

1.5.3. AV conduction block associated with SCN5A mutations

Alterations in Na^+ channel expression and function are known to have severe effects on excitability. In the nervous system, mutations in Na^+ channel α and β subunits cause epilepsy and febrile seizures (Wallace *et al.*, 1998; Wallace *et al.*, 2001). In the heart, mutations in the gene encoding $Na_v1.5$ cause inherited hyperexcitability syndromes, including long QT syndrome type III and Brugada syndrome, which can lead to sudden cardiac death (Keating & Sanguinetti, 2001). Recently, various naturally occurring mutations of $Na_v1.5$ have been associated with familial cases of AV conduction block (Schott *et al.*, 1999; Lupoglazoff *et al.*, 2001; Kyndt *et al.*, 2001) or slowing of AV conduction (Tan *et al.*, 2001; Wang *et al.*, 2002). In addition, heterozygous mutant mice lacking one copy of the $Na_v1.5$ gene have impaired AV conduction (as well as other cardiac conduction defects) (Papadatos *et al.*, 2002).

1.6. Aim of thesis

Although there is abundant histological and electrophysiological data concerning AV node (Mazgalev & Tchou, 2000a), it has been difficult to correlate electrophysiological recordings and distinct cell types (Anderson, 1972; Anderson *et al.*, 1974; Tranum-Jensen & Janse, 1982; McGuire *et al.*, 1996). AV nodal cells can now be enzymatically dissociated and studied individually. However, the tracking of a cell from its original anatomic location to the experimental bath has not yet been possible and, therefore, the cell origin has still to be postulated from its shape and ionic characteristics (Munk *et al.*, 1996; Workman *et al.*, 2000). It may be possible to solve this problem using immunohistochemistry to show the expression of different ion channels in the different cell types of the AV node. The aim of the thesis is to investigate by immunohistochemistry the distribution of cardiac and neuronal Na^+ channel isoforms in and around the AV node of the rat. In addition, the histology of the rat AV node and the distribution of other marker proteins (including Cx43 and the channel responsible pacemaker current, I_f,) were studied in parallel.

Chapter 2

Materials and methods

A number of different techniques were used in the present study; these included preparation of AV and SA node tissue, atrial and ventricular myocyte isolation, electrophysiology, histological staining, immunocyto- or immunohisto-chemistry and confocal microscopy. Immunocyto- or immunohisto-chemistry and confocal microscopy were the principal techniques used and this chapter describes in detail these techniques. This chapter also outlines the other techniques. More details are given in the corresponding chapters.

2.1. Preparation of AV and SA node of the rat

2.1.1. Solutions

Carbonate buffered Tyrode solution contained (mM): NaCl 93; $NaHCO_3$ 20; Na_2HPO_4 1; KCl 5; $CaCl_2$ 2; $MgSO_4$ 1; sodium acetate 20; glucose 10; insulin 5 units/ml; equilibrated with 95 % O_2 and 5 % CO_2 to give pH 7.4.

2.1.2. Dissection of tissue

Wistar rats weighing 250-300 g were killed humanely by Dr. M. Yamamoto according to the United Kingdom Animals (Scientific Procedures) Act, 1986 and the heart was quickly removed and pinned onto a dissection chamber containing oxygenated bicarbonate-buffered Tyrode solution at 37°C. The right atrium and the AV septum were cut away from the ventricles. Then, the right atrium was opened by a longitudinal incision through the tricuspid valve and into the superior vana cava. The SA and AV nodes were identified from their anatomical landmarks (Fig. 2.1). The opened right atrium was divided into the intercaval region for the SA node and the atrioventricular junction for the AV node (Fig. 2.1)

2.2. Preparation of atrial and ventricular myocytes of the rat

2.2.1. Solutions

Isolation solution contained (mM): NaCl 130; KCl 5.4; $MgCl_2$ 1.4; NaH_2PO_4 0.4; 4-(2-hydroxyethyl)piperazine-1-ethanesulfonic acid (HEPES) 5; glucose 10; taurine 20; creatine 10; titrated to pH 7.3 with NaOH

2.2.2. Isolation procedure

Cells were isolated as described by Shui *et al.* (1997) with a few minor modifications. Adult male Wistar rats weighing 250-300 g were killed by cervical dislocation by Dr. Z. Shui according to the United Kingdom Animals (Scientific Procedures) Act, 1986. The heart was removed and was washed in isolation solution and then retrogradely perfused via the aorta at a flow rate of 10 ml min^{-1} on a Langendorff apparatus. All perfusates were at 37°C. Initially the heart was perfused with isolation solution containing 0.5 mM Ca^{2+} for 2-3 min to clear the heart of blood. The heart was then perfused with Ca^{2+} free isolation solution containg 100 μM ethylene glycol-bis(2-aminoethylether)-*N,N,N',N'*-tetraacetic acid (EGTA) for 4 min. Finally, the heart was perfused with enzyme solution for 6-10 min. Enzyme solution consisted of isolation solution with 1 mg ml^{-1} collagenase (Worthington Biochemical, Lakewood, NJ, USA, Type II) and 0.1 mg ml^{-1} protease (Type XIV, Sigma Chemical Co.). Enzyme solution was recirculated through the heart. After perfusion with enzyme solution, the atria and ventricles were separated, finely chopped and added to an aliquot of enzyme solution to which was added 1 % (w/v) bovine serum albumin (BSA). Both atria and ventricles were separately digested with this solution (at 37°C) for several 15 min or 5 min periods, respectively. At the end of each period, the mixture was filtered through nylon gauze. The dissociated cells were then sedimented by centrifugation at 400 r.p.m. for 3 min. The supernatant was removed and the cells were resuspended in isolation solution. Both atrial and ventricular cells were kept at 4°C until use.

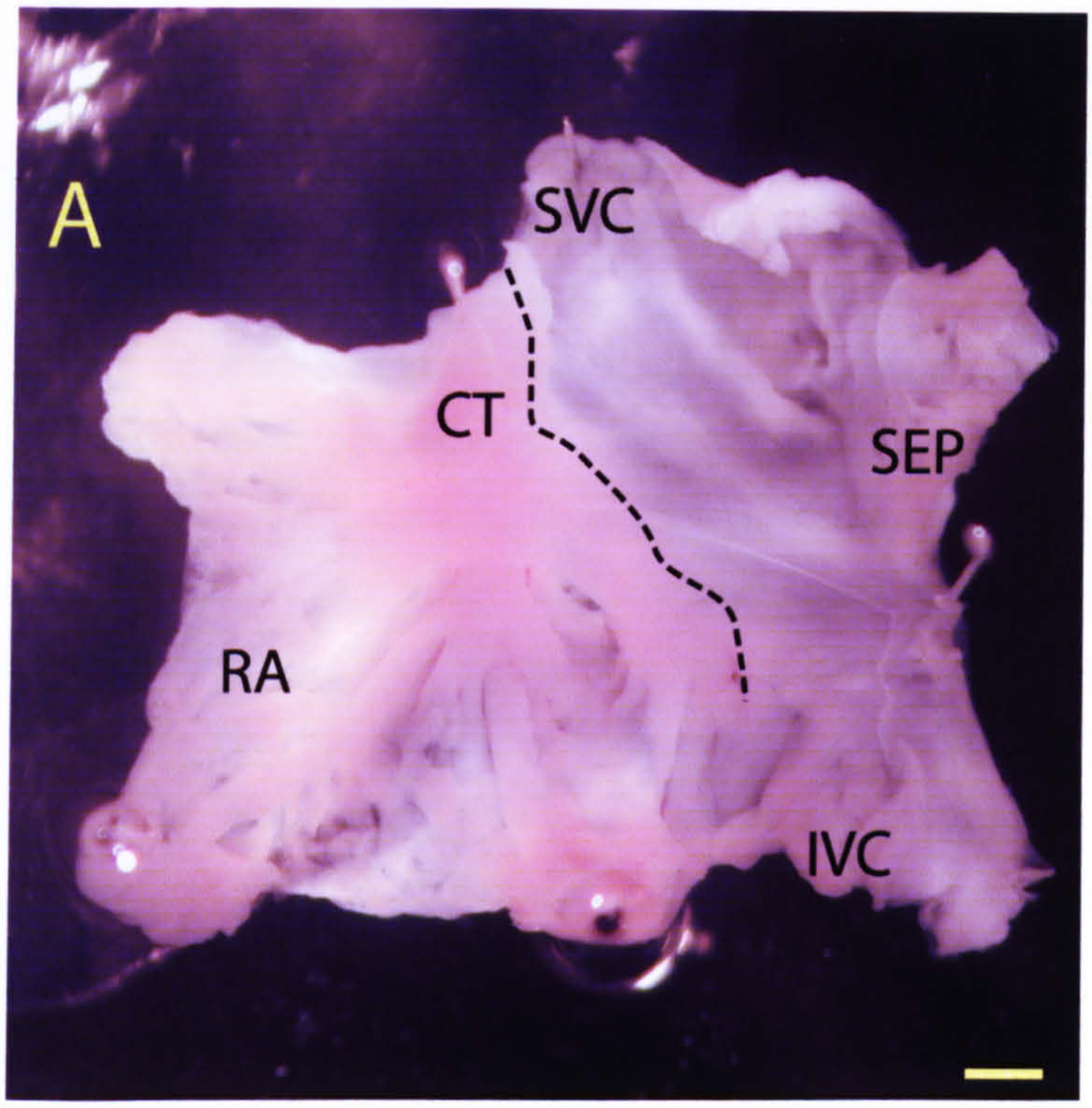

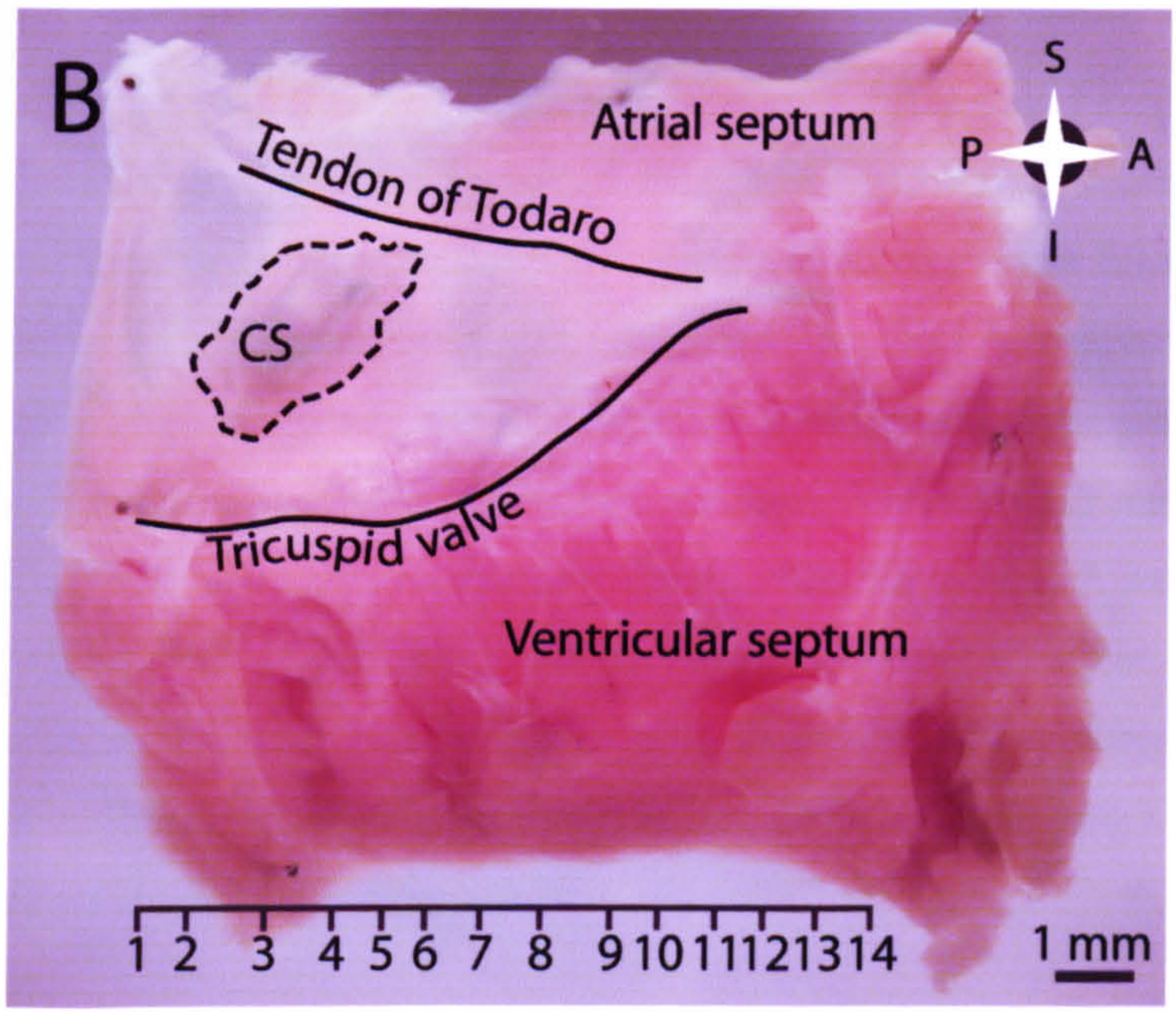

Figure 2.1 Dissected rat SA and AV nodes

A, dissected rat SA node preparation. CT, crista terminalis; IVC, inferior vena cava; RA, right atrium free wall; SEP, septum; SVC, superior vena cava. B, dissected rat AV node preparation. For Masson's trichrome and immunohistochemical staining, the AV node preparations was cryosectioned and divided into several levels at ~500 μm intervals. Numbers indicate position of each level. Labels show conventional orientation (for more information, see chapter 3, section 3.4.5). CS, coronary sinus; A, anterior; I, inferior; P, posterior; S, superior. Scale bars, 1 mm.

2.3. Freezing and cryosectioning of dissected AV and SA node of the rat

Dissected AV or SA node preparations, still pinned to a silicon rubber base, were frozen with Jung tissue freezing medium (Leica instruments GmbH, Heidelberg, Germany) or 10 % gelatin (Porcine type A, Sigma, Poole, UK) in isopentane cooled by liquid N_2. Frozen tissues were secured on a cryostat chuck using Jung tissue freezing medium. The AV node preparation was serially sectioned perpendicular to the endocardium along the AV axis from the common bundle to the coronary sinus and the SA node tissue was serially sectioned perpendicular to the crista terminalis through the intercaval region at 10 μm thickness using a cryostat (CM1850; Leica Microsystems, Heidelberg, Germany) at -15°C. Among seven AV node preparations, three preparations were mainly used in this study. 300 to 500 tissue sections cryosectioned were divided at 525 ± 7.31 (one case shown in Fig. 2.1B) or 500 (two cases) μm intervals. Sets of sections were used for Masson's trichrome and immunohistochemical staining. After cryosectioning, the sections were mounted on Superfrost Plus slides (BDH, Poole, UK) and stored at -80 °C until use.

2.4. Summary of AV node preparation studied

As a major subject of this thesis, sets of 10 μm sections were cut perpendicular to the AV junction at ~500 μm intervals from three AV node preparations. Data for Cx43 (chapter 4), desmoplakin (chapter 4), ANP (chapter 4), HCN4 (chapter 5), $Na_v1.1$ (chapter 6 and 7), $Na_v1.3$ (chapter 6 and 7) and $Na_v1.5$ (chapter 6 and 7) were obtained from all three preparations (except desmoplakin was studied in one preparation only and $Na_v1.1$ and $Na_v1.3$ were studied in two preparations only). In addition, similar data for Cx43, $Na_v1.1$ and $Na_v1.3$ were obtained from three other preparations and similar data for $Na_v1.5$ were obtained from one other preparation (level of the enclosed node only). Cx40 was studied in two preparations (chapter 8). $Na_v1.2$ and $Na_v1.6$ were studied in three preparations (level of the enclosed node only). Sagittal sections were cut from one preparation only (chapter 9).

2.5. Histology

In order to characterize the anatomy of the AV node, Masson's trichrome staining was used. Histological stains are made of compounds which absorb visible light differently and bind to different tissues to produce coloured tissue sections and thus increase the visibility of the sections (Sanderson, 1994).

2.5.1. Solutions

Bouin's fluid contained: saturated aqueous picric acid, 75 ml; 40 % formaldehyde, 25 ml; glacial acetic acid, 5 ml. Celestine blue B contained: Celestine blue B, 2.5 g; ferric

ammonium sulphate, 25 g; glycerine, 70 ml; distilled water, 500 ml. The ferric ammonium sulphate was dissolved in the cold distilled water by stirring. The Celestine blue B was added to this solution and the mixture was boiled for a few minutes. After cooling, the stain was filtered and glycerine was added. The final stain should be usable for over 5 months. It had to be filtered before use. Cole's alum hematoxylin contained: hematoxylin, 1.5 g; saturated aqueous potassium alum, 700 ml; 1 % iodine in 95 % alcohol, 50 ml; distilled water, 250 ml. The hematoxylin was dissolved in the distilled water (warmed) and mixed with the iodine solution. The alum solution was added, and the mixture brought to the boil and then cooled quickly and filtered. The solution was ready for immediate use. The solution may need filtering after storage. The quality of the nuclear staining begins to deteriorate after a few months. This deterioration is marked by the formation of a precipitate in the stored stain. At this stage, the stain should be filtered before use, and the staining time may need to be increased. The solution was filtered before use. Acid alcohol: 1 % HCl in 70 % ethanol. Acid fuchsin contained: acid fuchsin, 0.5 g; glacial acetic acid, 0.5 ml; distilled water, 100 ml. Phosphomolybdic acid contained: phosphomolybdic acid, 1.0 g; distilled water, 100 ml. Methyl blue contained: methyl blue, 2.0 g; glacial acetic acid, 2.5 ml; distilled water, 100 ml.

2.5.2. Masson's trichrome staining

The sections were taken from -80 °C storage and were dried at room temperature for 5 min. After Embedding medium was removed (Table 2.1), the sections were fixed in Bouin's fluid for 15 min and were washed in 70 % ethanol three times (10 min each) to remove yellow fixatives. Then the sections were stained in Celestine blue B for 5 min and were rinsed in distilled water two to three times until colourless. The sections were stained in Cole's alum hemotoxylin for 5 min and were washed in running tap water for 15 min. At this stage, nuclear staining was checked at low power using a light microscope. If nuclear staining was too light, steps from Celestine blue B to Cole's alum hematoxylin staining were carried out again. If nuclear staining was too dark, the sections were differentiated in Acid alcohol for 5 s. The sections were washed in tap water and re-checked. Then the sections were washed in tap water for 2 min and stained in Acid fuchsin for 10 min. The sections were rinsed in distilled water and treated with phosphomolybdic acid for 5 min. The sections were drained and were stained with Methyl blue for 1.5 min. The sections were rinsed in distilled water and treated with 1 % acetic acid for 2 min. The sections were then dehydrated in 70 % alcohol for 20 s, 90 % alcohol for 20 s, and absolute alcohol for 2 min two times and were cleared in clear solvent two times (5 min each). Then, the sections were mounted with XAM mounting medium (BDH) (Bancroft & Gamble, 2002).

2.5.3. Light microscopy

Table 2.1 Removal of embedding medium

Medium	OCT	Gelatin
Removing procedure	10 min in phosphate buffered saline (PBS) at room temperature	30 min in PBS at 37°C

Histological images were taken using a Leica Materials Workstation System, comprising a high performance personal computer, charge coupled device (CCD) camera and image acquisition board. Mosaic images of whole sections or regions of interest were constructed by an automatic facility of the system.

2.6. Immunocytochemistry and immunohistochemistry

The principle of immunocyto- or immunohisto-chemistry is to use specific primary antibodies to determine the sub-cellular location of proteins of interest in tissue sections or single cells (Fig. 2.2). To locate a protein of interest, the antibody binds to the protein's antibody-binding site, known as the epitope. The antibody bound to its binding site can be then detected by a selected secondary antibody conjugated, for example, to a fluorochrome (Fig. 2.2), which can be visualized by confocal microscopy. Polyclonal or monoclonal primary antibodies can be used. A polyclonal antibody is produced by injecting, into a host laboratory animal, a selected protein molecule and collecting serum samples. The collected serum samples contain antibodies to several regions of the molecule and also other antibodies produced by plasma cells, hence the name polyclonal. Because the serum samples also contain other antibodies produced by the animal, the antibody needs to be purified from other proteins in the serum samples in order to avoid non-specific labelling (Harlow & Lane, 1998). A monoclonal antibody is produced by hybridoma cells. Hybridoma cells are "immortal cells of the B-cell lineage" fused with isolated precursors of the plasma cells which only produce an antibody to one region of the molecule, hence the term monoclonal (Harlow & Lane, 1998). The great advantage of monoclonal antibodies is their absolute specificity for a single sequence (or epitope) on the antigen molecule. The problems associated with the multiple antibodies contained in a polyclonal antibody thus do not arise and immunolabelled preparations are usually very clean and labelling is specific. A possible disadvantage of a monoclonal antibody derives from its monospecificity. A polyclonal antibody is probably multivalent, consisting of antibodies to several regions of the antigen molecule, providing a strong detecting capacity. On the contrary, a monoclonal antibody, reactive with only one site on the molecule, may result in fewer antibody molecules being bound to the antigen and subsequently detected by the labelling method, resulting in weaker staining (Polak & Noorden, 2002).

2.6.1. Primary antibodies used

Use of primary antibodies raised from different host species makes it possible to undertake multiple immunolabelling by using sets of species-specific secondary antibody-detection systems, thereby permitting simultaneous visualization of the expression patterns of different combinations of proteins of interest. All primary monoclonal and polyclonal antibodies used during the course of the present study are summarised in Table 2.2 and are also referred to in relevant chapters. Among primary antibodies, the most important ones are Na^+ channel

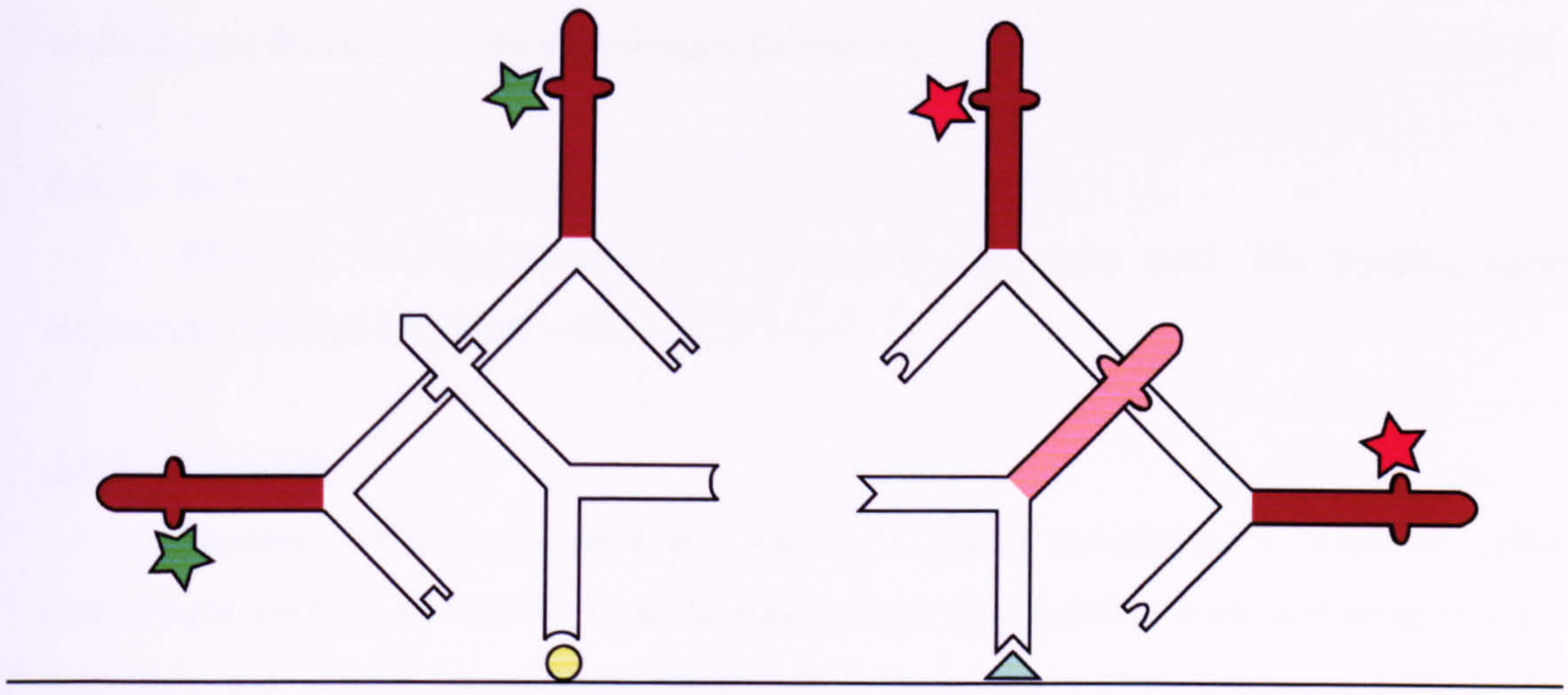

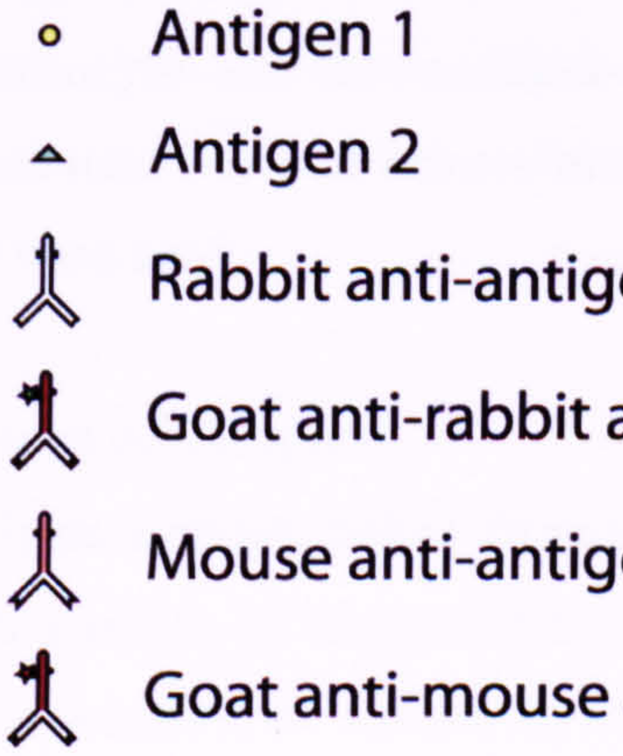

Antigen 1

Antigen 2

Rabbit anti-antigen 1 antibody

Goat anti-rabbit antibody conjugated to FITC

Mouse anti-antigen 2 antibody

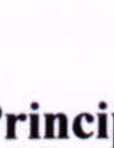

Goat anti-mouse antibody conjugated to TRITC

Figure 2.2 Principles of immunocytochemistry

Simultaneous or sequential double labelling by the double immunofluorescence labelling method is illustrated. Rabbit anti-antigen 1 antibody binds to antigen 1 and mouse anti-antigen 2 antibody binds to antigen 2. The anti-antigen 1 antibody is then detected by goat anti-rabbit antibody conjugated to fluorescein isothiocyanate (FITC), whereas the anti-antigen 2 antibody is detected by goat anti-mouse antibody conjugated to tetramethyl rhodamine (TRITC). FITC and TRITC are fluorochromes. From Polak & Noorden (2002).

antibodies. The reason of use of rat as an experimental animal in this thesis is the availability of antibody only raised from rabbit. The antibodies were stored at – 20°C in small aliquots and were used approximately within a year from the date of delivery. Working solutions of antibodies were stored at 4°C and were used for one to several months depending on the type of antibody and frequency of the experiments carried out.

2.6.2. Solutions

PBS (pH 7.4, Sigma) and 10 % gelatin in PBS were used. The freezing agents, isopentane and liquid N_2 were used.

2.6.3. Fixatives

Fixative is commonly used to preserve biological specimens. It preserves cellular components such as proteins by cross-linking end-groups of amino acids and coagulating the secondary and tertiary structures of proteins to form insoluble gels (Sanderson, 1994). 10 % neutral buffered formalin (Sigma) was used as a fixative.

2.6.4. Immunocyto- and immunohisto-chemical agents

For immunocyto- and immunohistochemistry, BSA (Sigma), normal donkey serum and Triton X-100 were used.

2.6.5. Fixation of samples

For tissue sections, before fixation, the sections were dried at room temperature for 5 min and were fixed in 10 % neutral buffered formalin at room temperature for 30 min. For single cardiac myocytes, the cardiac myocytes were placed on pieces of coverslips coated with carbon (coverslips were placed in a flame) for 30 min, washed in PBS for 10 min and then fixed in 10 % neutral buffered formalin at room temperature for 15 min. To remove excess of fixative, both sections and myocytes were washed three times in PBS over 30 min.

2.6.6. Treatment by Triton X-100

The samples were treated with 0.1 % Triton X-100 in PBS at room temperature for 10 min. In the case of $Na_v1.5$, 0.3 % Triton X-100 was used. The purpose of treatment with Triton X-100 was to permeablise the cell membrane, thus allowing the penetration of the primary and secondary antibodies and other immunocyto- or immunohisto-chemical reagents to access the epitopes located on the cytoplasmic side.

2.6.7. Blocking of non-specific sites

To block non-specific sites and reduce background 'noise', the samples were incubated with 10 % normal serum and 1 % BSA in PBS. The incubation was carried out either overnight

at 4°C or for 1 h at room temperature. The samples that were incubated with blocking solution were washed in PBS to prevent contamination of the primary antibody.

2.6.8. Labelling with primary antibodies

Primary antibodies were diluted in 1 % BSA in PBS with (in case of $Na_v1.5$) or without (in all other cases) 10 % normal donkey serum. The samples were incubated with a suitable concentration of each primary antibody (see Table 2.2) in a humid box at -4°C overnight.

2.6.9. Labelling with secondary antibodies

To detect the primary antibody binding, the samples were then incubated with species-specific secondary antibody conjugated to a fluorochrome. In the case of multiple labelling experiments, a mixture of appropriate secondary antibodies was applied. Table 2.3 summarises the secondary antibodies used in this study. The secondary antibodies were diluted in 1 % BSA in PBS with (in case of Nav1.5) or without (in all other cases) 10 % normal donkey serum. The secondary antibody was applied for 1 h at room temperature in the dark. For multiple labelling experiments, appropriate combinations of secondary antibodies were used.

2.6.10. Washing and mounting of samples

After application of the primary and secondary antibodies, the samples were thoroughly washed in PBS three times for 30 min. The samples were mounted under coverslips with the anti-fade reagent, Vectashield (#H-1000, Vector Laboratories, Peterborough, UK).

2.6.11. Variations in the immunolabelling procedure

In view of the many variables such as sample used, fixation, membrane permeabilisation, blocking, type of labelling, combination of primary and secondary antibodies, incubation time and temperature, the specific procedures for a particular investigation are described in the relevant chapters.

2.6.12. Control experiments

When either single or double labelling experiments with a particular primary antibody was carried out for the first time, the primary antibody in question was omitted or preincubated with the antigenic peptide. In immunocyto- and immunohisto-chemistry, an experiment without the primary antibody is a standard control experiment. This is done to ascertain the background labelling by the secondary antibody in the absence of the primary antibody and to confirm that the secondary antibody does not crossreact between species. For example, no signal was detected in atrial myocytes and myocardium on omission of primary antibody against $Na_v1.1$ (Figs. 2.3B and 2.4C). Preincubation of the primary antibody with the antigenic peptide (to which the antibody was raised) is also a standard control experiment. This is done to confirm

Table 2.2 Summary of primary antibodies used

Primary antibody	Host	Recognition peptide (epitope) and location of epitope	Supplier	Dilution
$Na_v1.1$	Rabbit polyclonal	Residues 465-481 of rat $Na_v1.1$	1	1:100
$Na_v1.2$	Rabbit polyclonal	Residues 467-485 of rat $Na_v1.2$	1	1:100
$Na_v1.3$	Rabbit polyclonal	Residues 511-524 of rat $Na_v1.3$	1	1:100
$Na_v1.5$	Rabbit polyclonal	Residues 493-511 of rat $Na_v1.5$; intracellular loop domains between I and II	2	1:30
$Na_v1.6$	Rabbit polyclonal	Residues 1042-1061 of rat $Na_v1.6$; intracellular loop between domains II and III	2	1:100
HCN4	Rabbit polyclonal	Residues 119-155 of human HCN4; intracellular N-terminus	2	1:20 and 1:100
Cx40	Rabbit polyclonal	19 Residues of mouse Cx40 C-terminal cytoplasmic domain	1	1:2000 and 1:5000
Cx43	Mouse monoclonal	Residues 252-270 of rat Cx43	1	1:100
Cx43	Rabbit polyclonal	Residues 363-382 of human Cx43 with an N-terminal added lysine	3	1:100
NF160	Mouse monoclonal	Purified neurofilament polypepti-des.	1	1:1000
ANP	Mouse monoclonal	Residues 1-28 of human ANP (conjugated to KLH; carrier protein)	4	1:100
DP 1/II	Mouse monoclonal	Bovine DP 1 and 2	5	Ready to use

1: Chemicon International Ltd., Harrow, UK

2: Alomone labs, Jerusalem, Israel

3: Sigma, Poole, UK

4: Biogenesis Ltd., Poole, UK

5: Progen (Biotechnik GmbH), Heidelberg, Germany

Table 2.3 Summary of secondary antibodies used

Secondary antibody	Host	Supplier	Dilution
Anti-rabbit conjugated FITC	Donkey	1, 2	1:100
Anti-mouse conjugated FITC	Donkey	1	1:100
Anti-mouse conjugated TRITC	Donkey	2	1:100
Anti-mouse conjugated Cy3	Donkey	2	1:400

1: Jackson Immuno Research Laboratories Inc.

2: Chemicon International, Ltd.

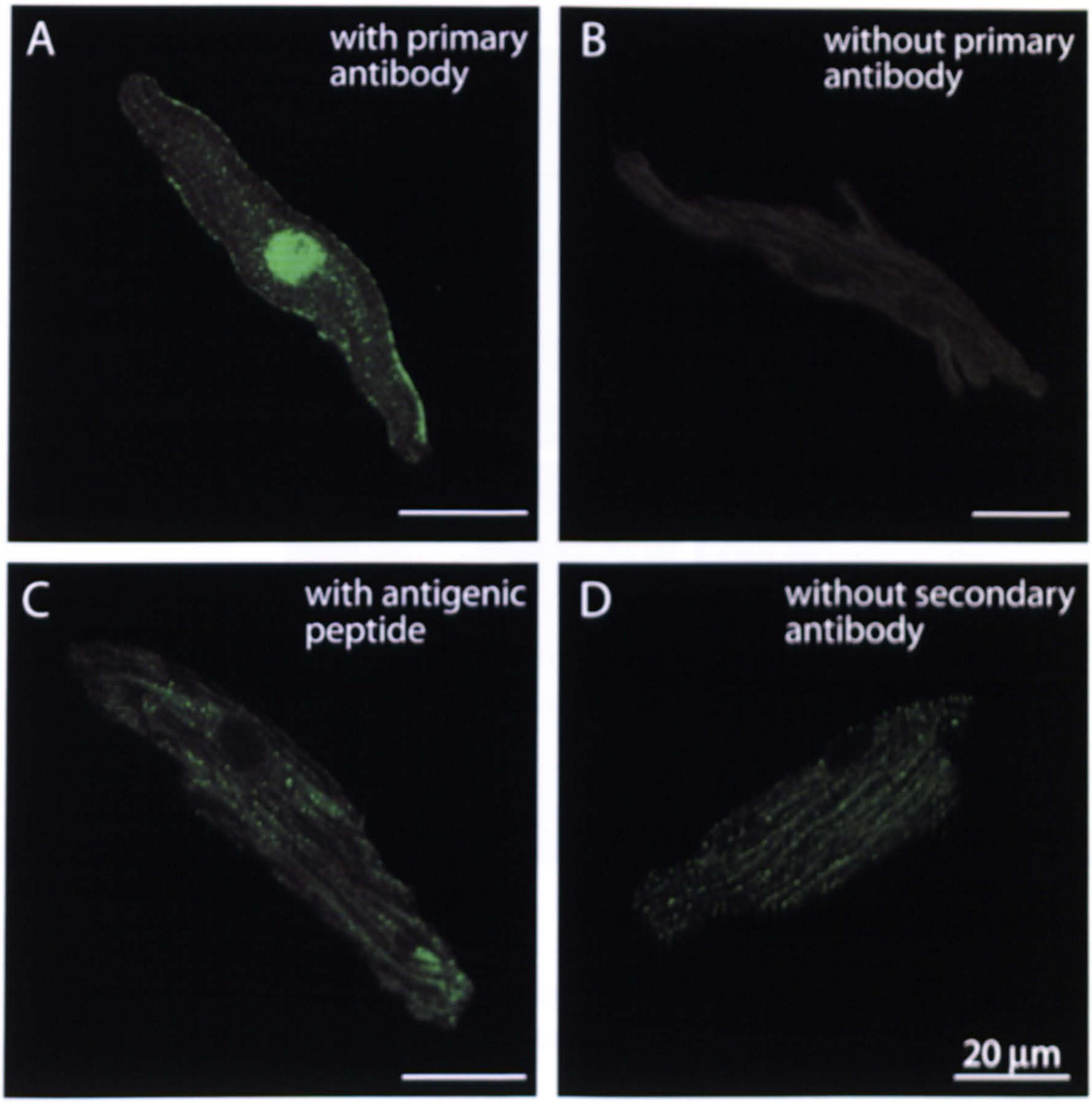

Figure 2.3 Control experiment 1

A, $Na_v1.1$ labelling in an atrial myocyte (with primary antibody and no antigen preincubation). B, no labelling without the primary antibody to $Na_v1.1$. C, no labelling on preincubation of the primary antibody to $Na_v1.1$ with the antigen peptide. D, no labelling of $Na_v1.1$ without the secondary antibody. Scale bars, 20 µm.

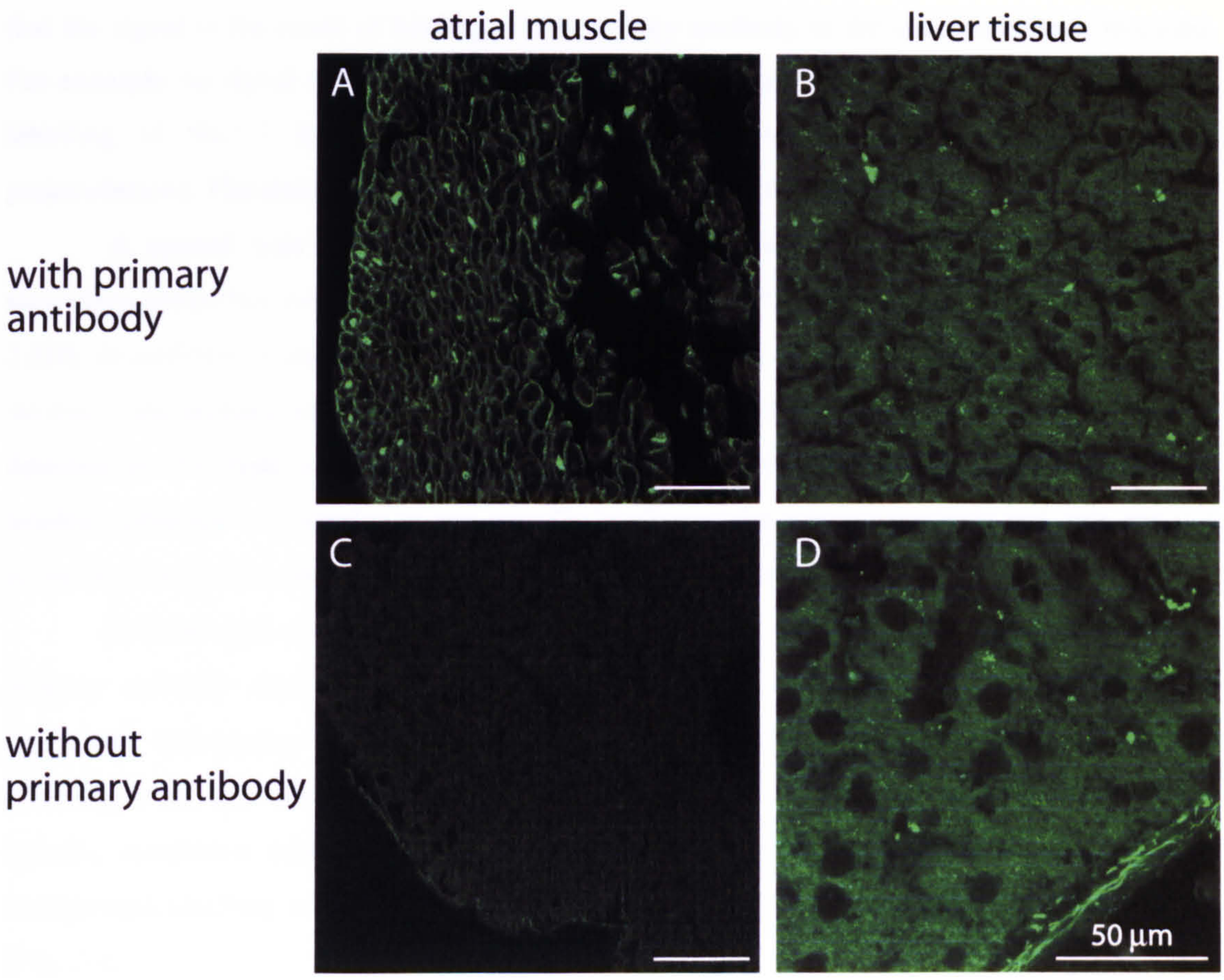

Figure 2.4 Control experiment 2

A, C, sections from atrial myocardium. B, D, sections from liver. A and B were labelled with primary antibody to $Na_v1.1$. C and D were labelled without primary antibody. Scale bars, 50 µm.

that the signal is the result of binding of the primary antibody to the specific epitope intended. For example, no signal was detected in Fig. 2.3C. As a comparison, Fig. 2.3A shows membrane labelling of $Na_v1.1$ in an atrial myocyte (with the primary antibody and no antigen preincubation). The staining in the nucleus is assumed to be non-specific.

A second type of control experiment was performed: an experiment in which the secondary antibodies were omitted while the primary antibodies were applied (for example, Fig. 2.3D). In addition, a control experiment was carried out in which wrong secondary antibodies (to detect the primary antibody) were applied. No example of this is shown, but no labeling was detected in this type of control experiment. These control experiments confirmed that the labelling obtained was not due to non-specific binding of the primary antibody and only suitable secondary antibodies could detect the primary antibodies used.

A third type of control experiment was to process sections from tissues in which the primary antibody should not bind, because the protein of interest is not expected to be expressed. Comparing labelling patterns from different tissue sections confirmed that the labelling of sections from a tissue of interest was specific. For example, anti-$Na_v1.1$ produced specific membrane labelling of $Na_v1.1$ in atrial tissue sections, whereas it produced only background labelling in liver tissue sections in which $Na_v1.1$ is not expected to be expressed (Fig. 2.4).

2.7. Confocal laser scanning microscopy

The single or multiple immunolabelled tissue sections and cardiac myocytes were viewed by conventional epi-fluorescence and confocal laser scanning microscopy (CLSM). The principles of the CLSM are illustrated in Fig. 2.5. Labelling in tissue sections and cardiac myocytes was visualised using a laser scanning confocal microscope (TCS SP, Leica Microsystems or LSM 5 Pascal, Carl Zeiss, NY, USA).

2.7.1. Image formation

Through x10, x20, x40 and x63 objectives lenses, the immunofluorescent signal was recorded via a photomultiplier tube (PMT). In the confocal system, in order to produce a whole image, the point of light from a laser is moved over the entire specimen in the objective's field of view line by line (in the x-y axis) by means of a scanning mirror (see Fig. 2.5). The arrangement of the illumination and detection pinholes assures that only signal from the focal plane reaches the detector and, unlike standard epi-fluorescence microscopy, in CLSM, out-of-focus rays coming from above and below the focal plane (see dashed lines in Fig. 2.5) are rejected and the produced image is clear with improved resolution of fine details (Sheppard & Shotton, 1997).

The acquired images were digitized and displayed on computer monitors as 1024 x 1024 pixels frames. To construct montages of an immunolabelled section, six to twelve single

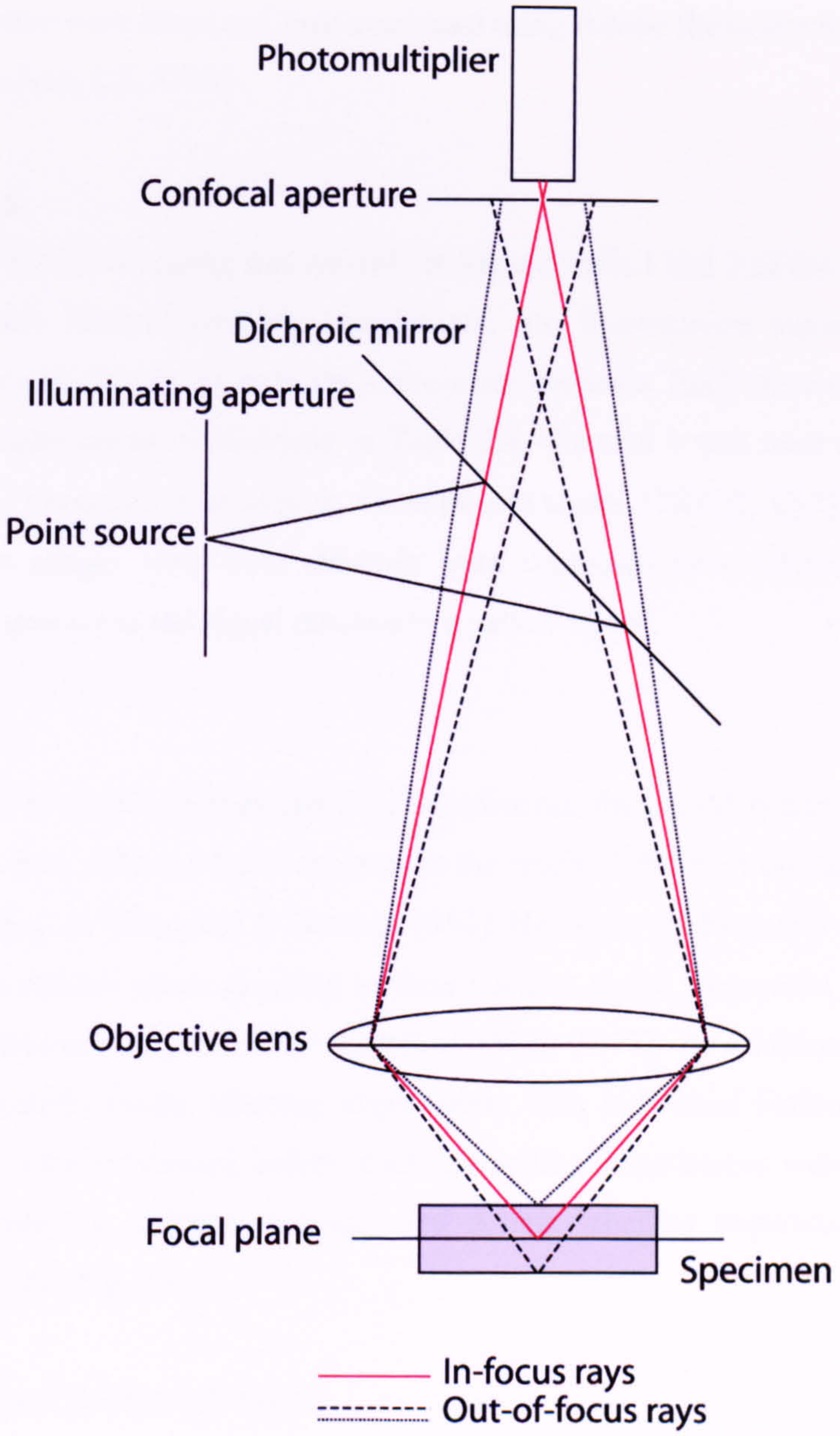

Figure 2.5 Principles of confocal microscopy

The excitation light (black solid line) from the point source passes through the illumination aperture and an excitation filter (not shown). The excitation light is then reflected by the dichroic mirror and is focused by the objective lens to a diffraction-limited spot illuminated in the focal plane of the specimen. The spot of light is scanned in the x- and y-axis, line by line, in the field of view of the focal plane of the specimen by the scanning mirror. Emitted fluorescence (red solid line) from the focal plane, as well out-of-focus planes, from the specimen passes through the objective lens, dichroic mirror and emission filter (not shown). Only emitted fluorescence from the focal plane passes through the confocal aperture, and is collected by the detector (photomultiplier). Emission light from below and above the focal plane (dashed black lines) cannot pass through the confocal aperture, because these regions have different focal planes and are 'attenuated' by the confocal aperture. From Sheppard & Shotton (1997)

images of the section were taken and then combined using Adobe Illustrator 9.0 (Adobe System Incorporated, San Jose, CA, USA).

2.7.2. Scanning

Single or double scanning was carried out via channels 1 and 2 of the CLSM system. In the case of double immunolabelling experiments, the fluorescence signals were scanned simultaneously or sequentially through the appropriate channels. Each channel was assigned to a particular fluorochrome as summarised in Table 2.4. Channel 1 was used to visualise green signal (FITC) and channel 2 was used to visualise red signal (TRITC, Cy3) on the computer screen. When the images from both channels were combined new colours were produced; co-localisation of green and red signal resulted in a yellow signal.

2.7.3. Crosstalk

In the case of double immunolabelling experiments, the CLSM system should be able to distinguish signal from different fluorochromes as the result of different excitation and emission wavelengths (Table 2.4) (Sheppard & Shotton, 1997). However, to check that crosstalk between different channels did not occur resulting in false-positive signal, sequential scanning of each channel was performed as previously described (Yeh, 1997). In addition, to exclude the possibility of crosstalk, single labelling experiments with individual antibodies on different types of samples were performed before double labelling experiments were carried out and compared. The labelling patterns in single and double labelling experiments were always identical (for example, Fig. 2.6).

2.7.4. Storing and analysing images

Images were taken as soon as possible after an experiment was finished (normally within one week). The images were stored on optical discs in TIFF format and were analysed and processed using graphics software, such as Corel Draw 10 (Corel Corporation, Ottawa, Ontario, Canada), Adobe Photoshop 7.0 (Adobe System Incorporated) and Adobe Illustrator 9.0 (Adobe System Incorporated). Scion image release 4.0.3.2 (Scion Corporation, Frederick, USA) was used to quantify immunofluorescence.

Table 2.4 Excitation and emission wavelengths for detection of fluorochromes used

Fluorochrome	Excitation wavelength (nm)	Emission wavelength (nm)	Laser	Channel
FITC	496	518	Argon	1
TRITC, Cy3	554/556	576/574	Krypton	2

From Sheppard & Shotton (1997).

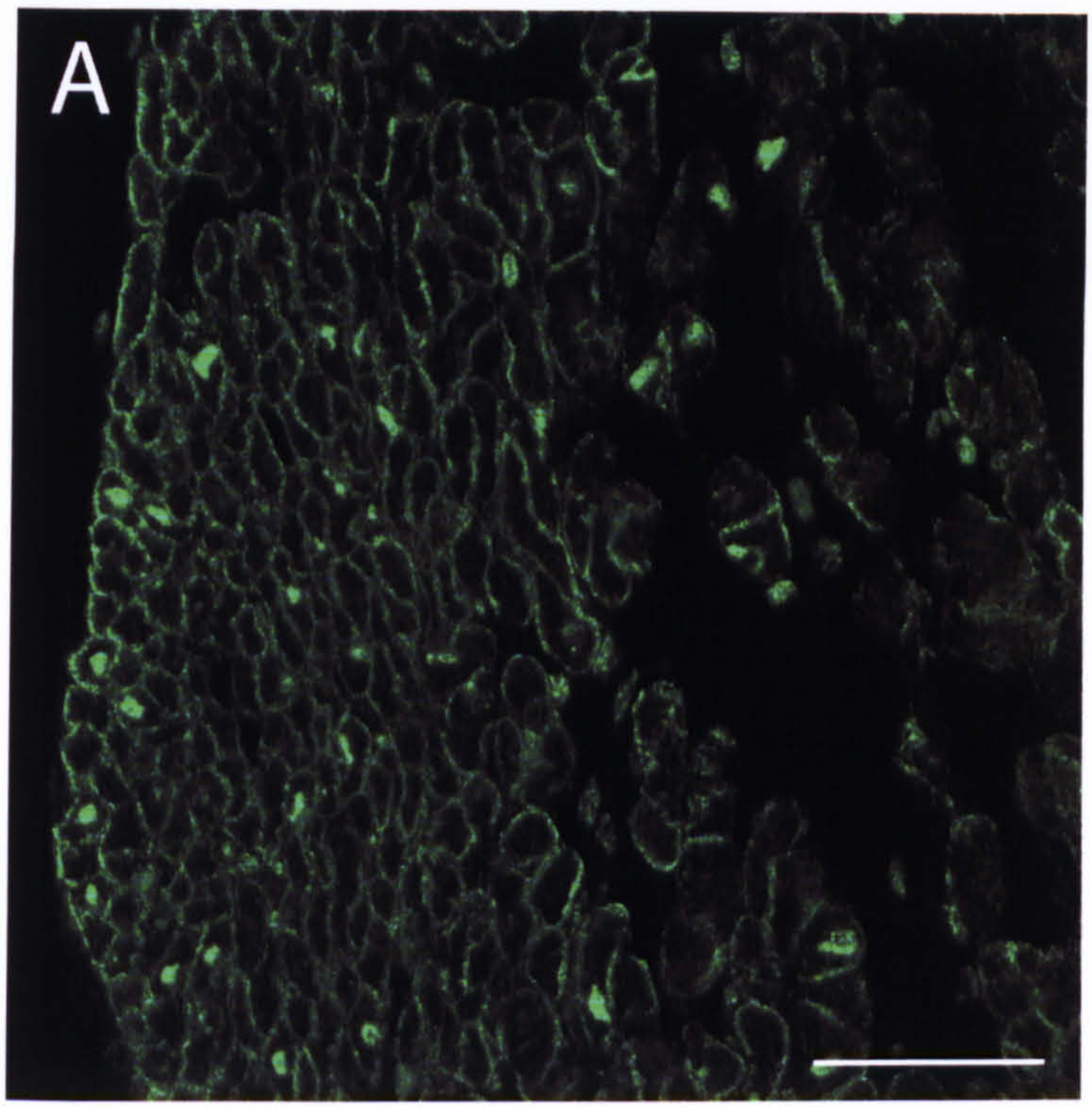

Figure 2.6 Crosstalk

A, single labelling of $Na_v1.1$(green signal from FITC) in rat atrium myocardium. B, double labelling of $Na_v1.1$ (green signal from FITC) and Cx43 (red signal from TRITC) in rat atrial myocardium. Scale bars, 50 μm.

Chapter 3

Histology of the AV node

3.1. Introduction

In the mammalian heart, the AV node is located in a triangular region, the triangle of Koch (Koch, 1909), with the apex being the membranous septum, the inferior border the attachment of the septal tricuspid leaflet, and the superior border a strand of fibrous tissue extending from the central fibrous body to the sinus septum above the ostium of the coronary sinus, known as the tendon of Todaro.

As shown by Tawara in 1906 (Tawara, 2000), the AV conduction axis is a continuous system of histologically discrete cells. The achievement of Tawara was to show that the bundle of His commenced in a well-demarcated collection of histologically discrete atrial cells, which he christened the "knoten." He also described transitional cells as approaching the compact AV node from all sides. These transitional cells interpose between the compact nodal cells and the atrial myocardium. In 1910, Aschoff (1910) and Monckeberg (1910) proposed criteria for discrete tracts of conducting cells in the hearts: the tracts should be insulated from the

neighboring myocardium, should be composed of cells discrete histologically from the adjacent myocardium, and should be traceable as continuous structures through serial sections. The descriptions of Tawara (2000) and the application of the criteria proposed by Aschoff (1910) and Monckeberg (1910) provide the basis for understanding the structure of the AV node.

Histologically, in general, the AV node consists of a meshwork of cells that are approximately the size of atrial cells, but are smaller than ventricular cells (Bharati, 2000). The cytoplasm of the cells stains lightly, i.e. not as intensely as the surrounding atrial and ventricular cells (Bharati, 2000). There are spaces and mesothelial-like cells between the nodal cells (Bharati, 2000). The collagen and elastic content intermingling with the nodal cells is more copious than that of the atria and the ventricles (Bharati, 2000). There is some fat and a moderate to large amount of nerve fibres (Bharati, 2000). In essence, the AV conduction axis consists of histologically distinct cell types: 1) transitional cells between atrial myocardium and enclosed nodal cells; 2) enclosed node (possibly divided into midnodal cells and lower nodal cells); 3) cells of the penetrating AV bundle embedded within the central fibrous body (also called the bundle of His); and 4) the cells of the ventricular bundle branches. However, there is no sharp transition from one cell type to another type (Meijler & Janse, 1988).

The transitional cells (cell type 1), whilst satisfying two of the criteria (Racker & Kadish, 2000; Mazgalev *et al.*, 2001), are not insulated by fibrous tissue from the remainder of the atrial myocardium (unlike cell types 2 - 4). Thus, the transitional cells do not constitute an anatomically discrete conducting tract, but they do constitute a functionally recognisable component of AV conduction. Thus, for example, they form the substrate for AV nodal reentry.

3.2. Methods

In order to characterise the anatomy of the AV node, Masson's trichrome staining was carried out on sections from throughout the the rat AV. The procedures involved in preparation of the tissue for histological examination are described in chapter 2 (section 2.1). The tissue sections were stained with Masson's trichrome as described in chapter 2 (section 2.5.2) and observed by light microscopy as described in chapter 2 (section 2.5.3).

3.3. Results

Among seven preparations, Masson's trichrome staining was carried out on three serially-sectioned preparations. Tissue sections were cut perpendicular to the tricuspid annulus. The number of 10 μm thick sections obtained was 300 to 500 from 10 mm of tissue. The main preparation was divided into 14 levels at ~500 μm intervals (Fig. 2.1B). Low magnification montages of 14 Masson's trichrome stained sections from 14 levels of the main preparation are shown in Fig. 3.1. Fig. 3.1 shows the various divisions of the AV node: the posterior/inferior nodal extension, open node, enclosed node, common bundle and AV ring bundle. High

Figure 3.1 Low power images of 14 Masson's trichrome stained sections through the rat AV node

Micrographs were taken using a x10 objective lens and montages of each section were constructed. The position of each section in the original AV node preparation is shown in Fig. 2.1B. AM, atrial myocardium; Ao, aorta; AoV, aortic valve; MV, mitral valve; TV, tricuspid valve; VM, ventricular myocardium. Scale bars, 0.5 mm.

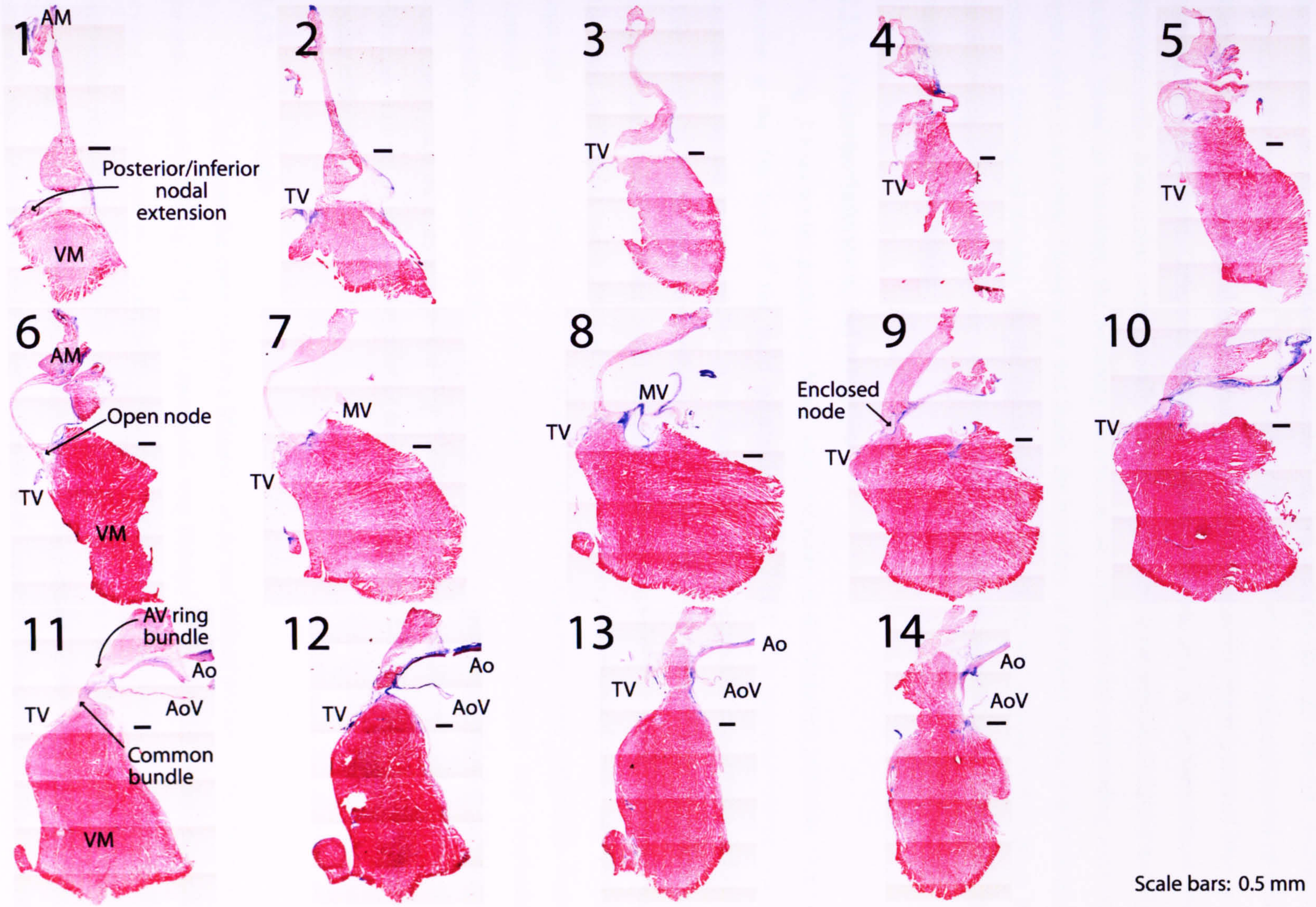
1
AM
Posterior/inferior nodal extension
VM
2
TV
3
TV
4
TV
5
TV
6
AM
Open node
TV
VM
7
MV
TV
8
MV
TV
9
Enclosed node
TV
10
TV
11
AV ring bundle
Ao
AoV
TV
Common bundle
VM
12
Ao
AoV
TV
13
Ao
TV
AoV
14
Ao
AoV
Scale bars: 0.5 mm

magnification montages of Masson's trichrome stained sections through the AV junctional region are shown in Figs 3.2 and 3.3. The various divisions of the AV node are demarked with black solid or dotted lines. In Masson's trichrome staining, connective tissue is stained blue and myocytes are stained red. Compared to the surrounding atrial and ventricular myocardium, the myocytes in the nodal tissue were generally stained a lighter red, were smaller, and were loosely packed. Based on histology, the boundary between nodal tissue and the surrounding working myocardium is not clear. However in this thesis, the boundary of the nodal tissue was not solely based on histological staining. The definition and boundary of the nodal tissue will be given in the following chapters, which are concerned with ion channel expression as determined by immunohistochemical staining.

3.3.1. Posterior/inferior nodal extension

Fig. 3.4 shows the posterior/inferior nodal extension in the Masson's trichrome stained section at the 4th level of the main preparation (Fig. 2.1B). The posterior/inferior nodal extension is located on the right (left in the figure) side of the ventricular myocardium and is in close proximity to the atrial myocardium (Fig. 3.4A). Fig. 3.4B shows a high magnification image of the posterior/inferior nodal extension. The posterior/inferior nodal extension was demarked with black solid line and was located on the root of tricuspid valve and it was separated from the ventricular myocardium by fat cells (adipocytes) and connective tissue (centrial fibrous body) (Fig. 3.4B). Compared to the surrounding atrial and ventricular myocardium, the myocytes in the posterior/inferior nodal extension were stained a lighter red, were smaller, and were loosely packed (Fig. 3.4B). Fig 3.5 shows another example of Masson's trichrome staining of the posterior/inferior nodal extension in a different preparation and shows similar architecture.

3.3.2. Open node

Fig. 3.6 shows the open node in a Masson's trichrome stained section at the 7th level of the main preparation (Fig. 2.1B). The open node was situated on the summit of the ventricular myocardium and was in contact with the atrial myocardium (Fig. 3.6A). Compared to the ventricular myocardium, the width of atrial myocardium was very narrow at the junctional region (Fig. 3.6A). Fig. 3.6B shows a high magnification image of the open node. The open node was separated from the ventricular myocardium by connective tissue (Fig. 3.6B). The open node was in contact with the root of the tricuspid valve and atrial myocardium (Fig. 3.6B). The myocytes in the open node were generally stained a lighter red than the ventricular muscle and were more loosely packed than the surrounding atrial and ventricular myocardium (Fig. 3.6B). In addition to the myocytes of the open node, there was another group of nodal-like myocytes above the tricuspid valve (Fig. 3.6B). These myocytes will be referred to as transitional cells and together with the posterior/inferior nodal extension are part of a continuous structure (the

Figure 3.2 High magnification images of Masson's trichrome stained sections (at levels 1 to 7) through the AV junctional region

Micrographs were taken at high magnification of the AV junctional region. Every section is the same as in Fig. 3.1. AM, atrial myocardium; ON, open node; P/I NE, posterior/inferior nodal extension; TC, transitional cells; TV, tricuspid valve; VM, ventricular myocardium. Scale bars, 200 μm.

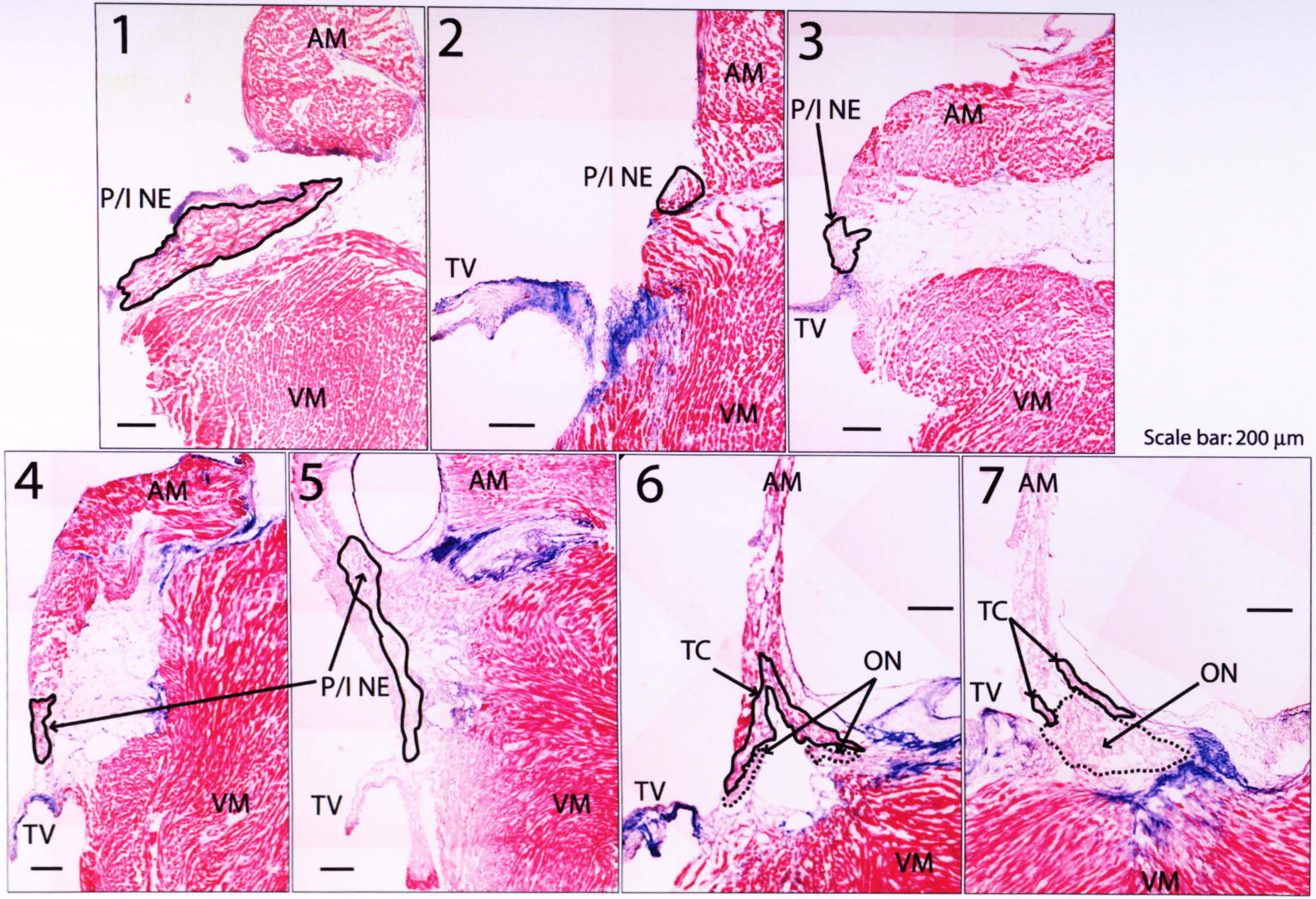
1
AM
P/I NE
VM
2
AM
P/I NE
TV
VM
3
P/I NE
AM
TV
VM
Scale bar: 200 µm
4
AM
P/I NE
VM
TV
5
AM
P/I NE
TV
VM
6
AM
TC
ON
TV
VM
7
AM
TC
TV
ON
VM

Figure 3.3 High magnification images of Masson's trichrome stained sections (at levels 8 to 14) through the AV junctional region

Micrographs were taken at high magnification of the AV junctional region. Every section is the same as in Fig. 3.1. AM, atrial myocardium; Ao, aorta; AoV, aortic valve; CB, common bundle; EN, enclosed node; ON, open node; P, posterior; P/I NE, posterior/inferior nodal extension; TAVRB, termination of the AV ring bundle; TV, tricuspid valve; VM, ventricular myocardium. Scale bars, 200 μm.

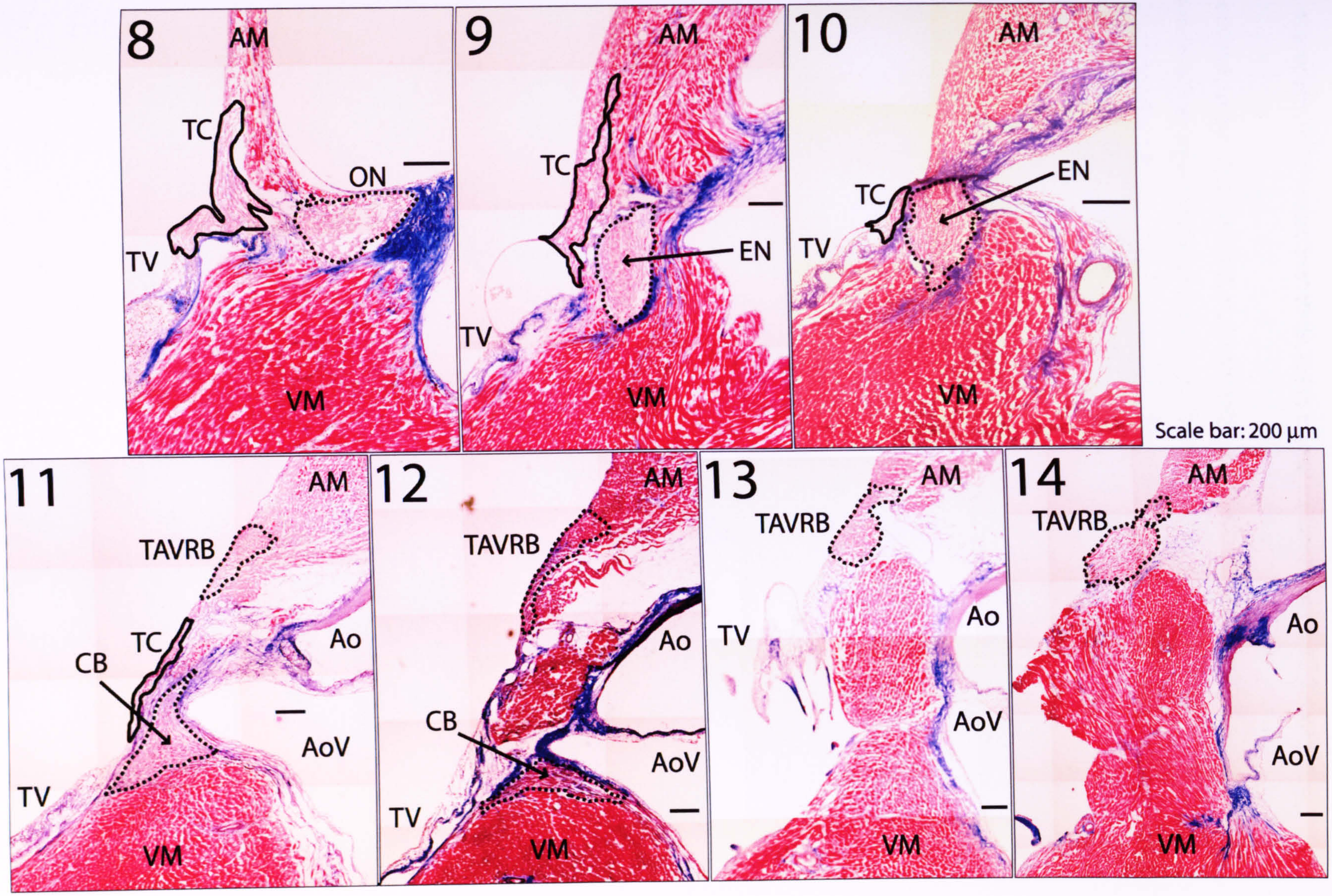
8
AM
TC
ON
TV
VM
9
AM
TC
EN
TV
VM
10
AM
EN
TC
TV
VM
Scale bar: 200 µm
11
AM
TAVRB
TC
CB
Ao
AoV
TV
VM
12
AM
TAVRB
Ao
CB
AoV
TV
VM
13
AM
TAVRB
Ao
TV
AoV
VM
14
AM
TAVRB
Ao
AoV
VM

Figure 3.4 Masson's trichrome staining of the posterior/inferior nodal extension

A, low-magnification montage of Masson's trichrome stained section at level 4 (see Figs. 3.1 and 3.2). Scale bar, 0.5 mm. B, high-magnification micrograph of Masson's trichrome staining of the posterior/inferior nodal extension. B corresponds to the framed area in A. Scale bar, 200 μm. AM, atrial myocardium; VM, ventricular myocardium.

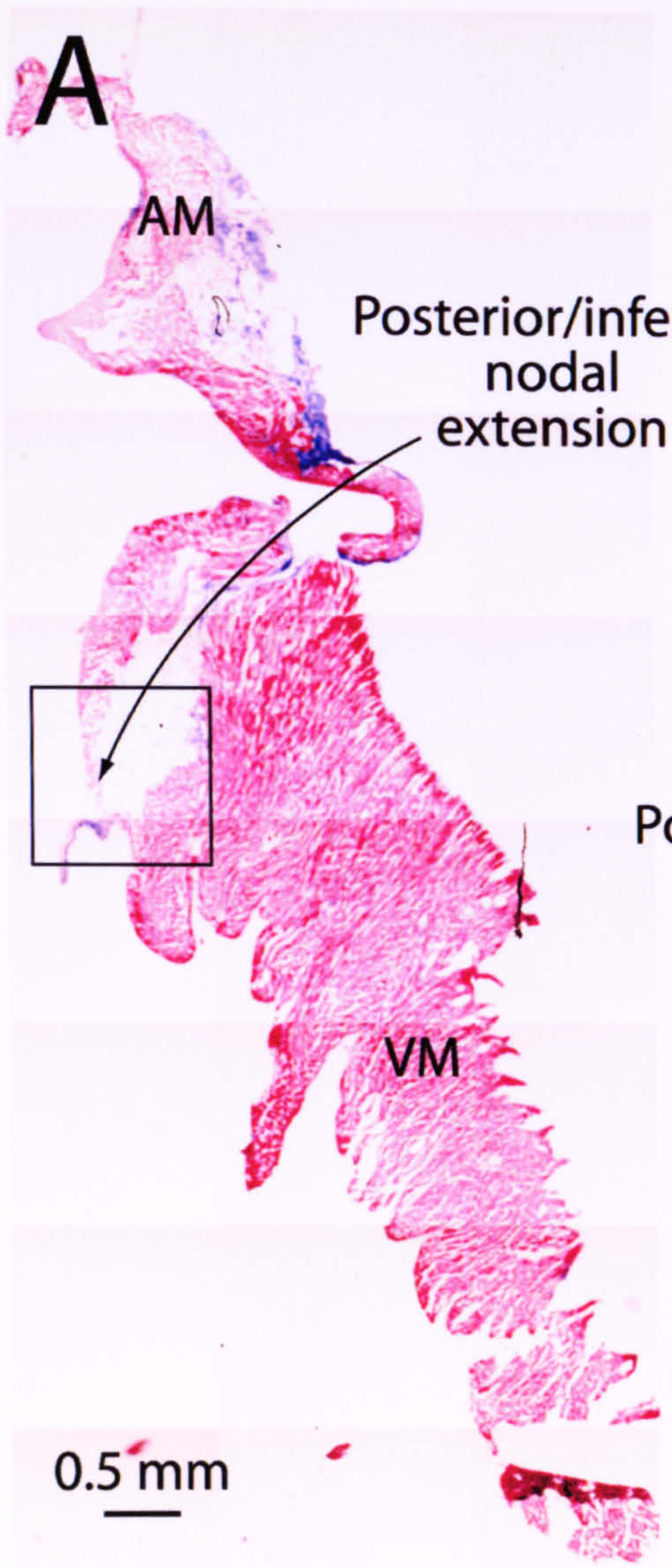
A
AM
Posterior/inferior
nodal
extension
VM
0.5 mm

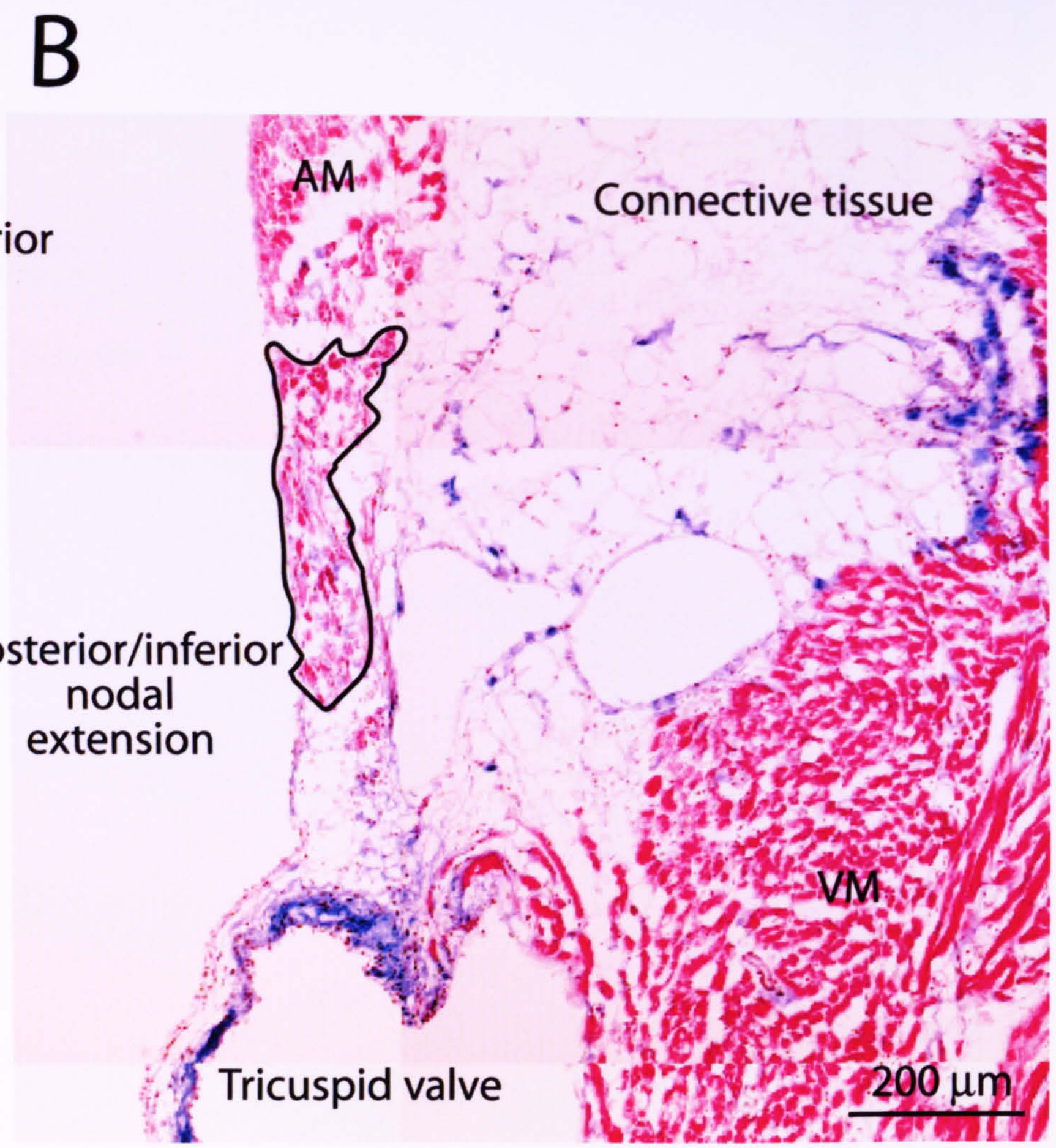
B
AM
Connective tissue
Posterior/inferior
nodal
extension
VM
Tricuspid valve
200 µm

Figure 3.5 Another example of Masson's trichrome staining of the posterior/inferior nodal extension

A, low-magnification montage of Masson's trichrome staining. Scale bar, 1 mm. B, high-magnification micrograph of Masson's trichrome staining. B corresponds to the framed area in A. Scale bar, 200 μm. AM, atrial myocardium; VM, ventricular myocardium.

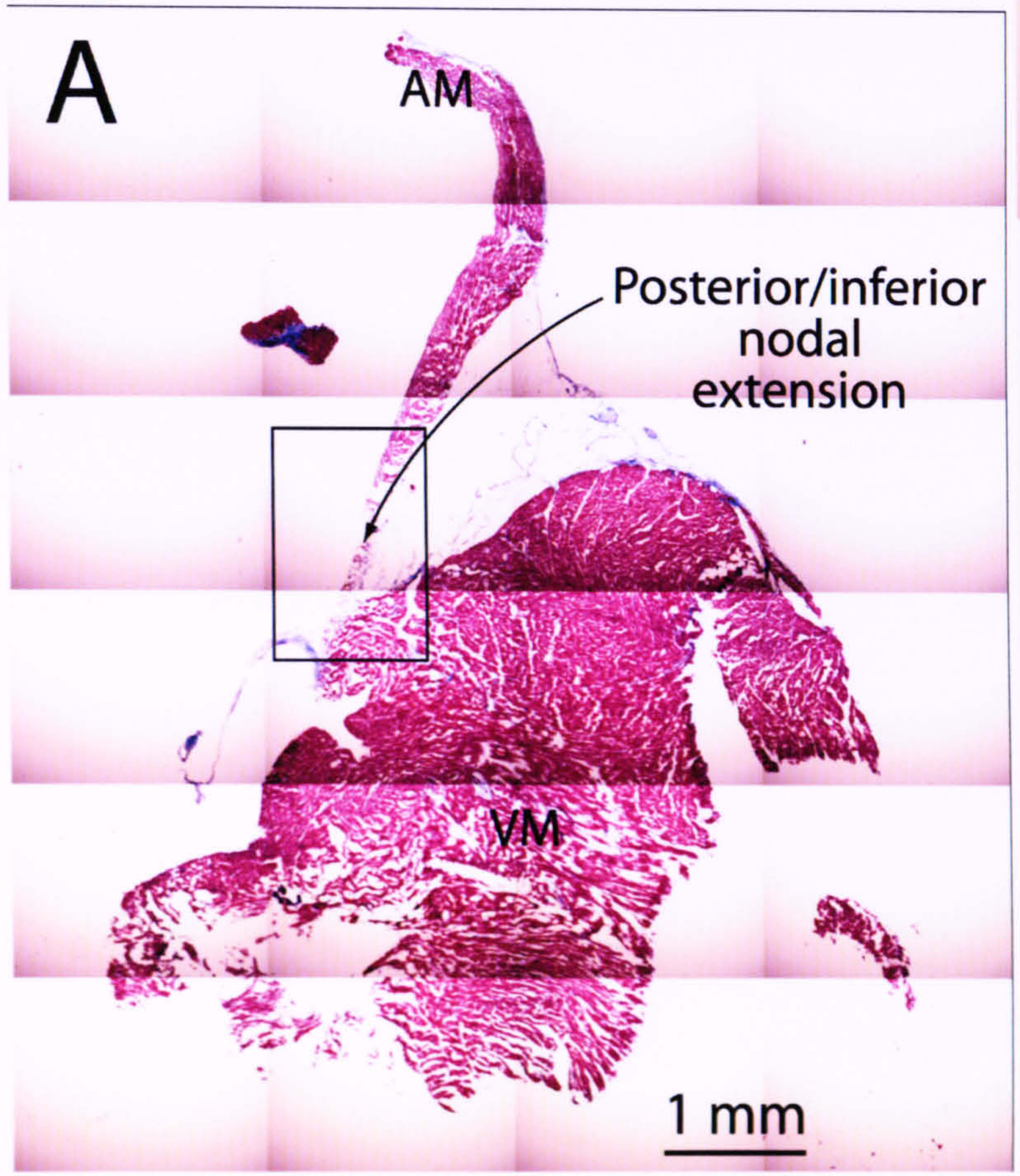
A
AM
Posterior/inferior
nodal
extension
VM
1 mm

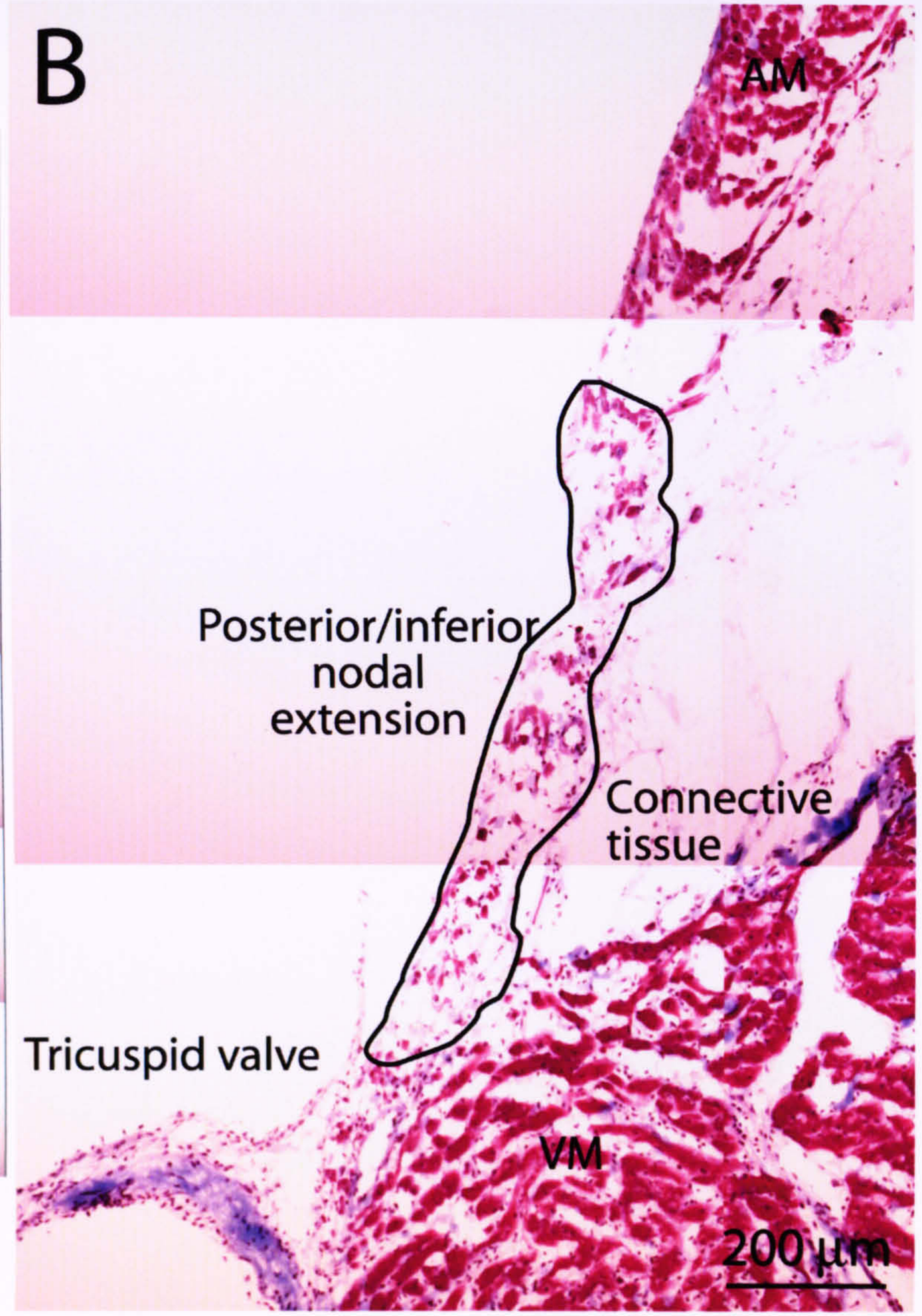
B
AM
Posterior/inferior
nodal
extension
Connective
tissue
Tricuspid valve
VM
200 µm

Figure 3.6 Masson's trichrome staining of the open node

A, low-magnification montage of Masson's trichrome stained section at level 7 (see Figs. 3.1 and 3.2). Scale bar, 0.5 mm. B, high-magnification micrograph of Masson's trichrome staining of the open node. B corresponds to the framed area in A. Scale bar, 200 μm. AM, atrial myocardium; VM, ventricular myocardium.

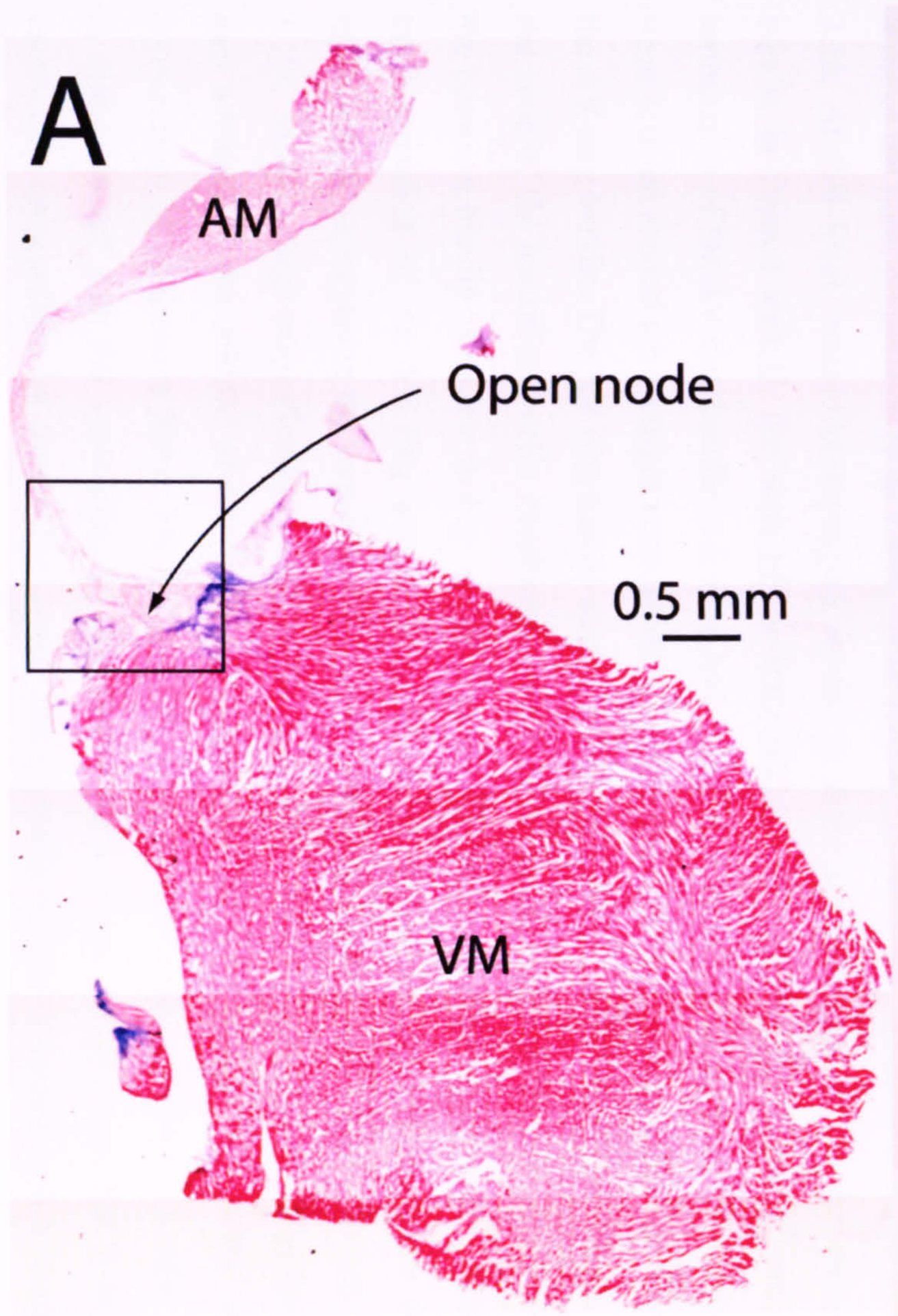
A
AM
Open node
0.5 mm
VM

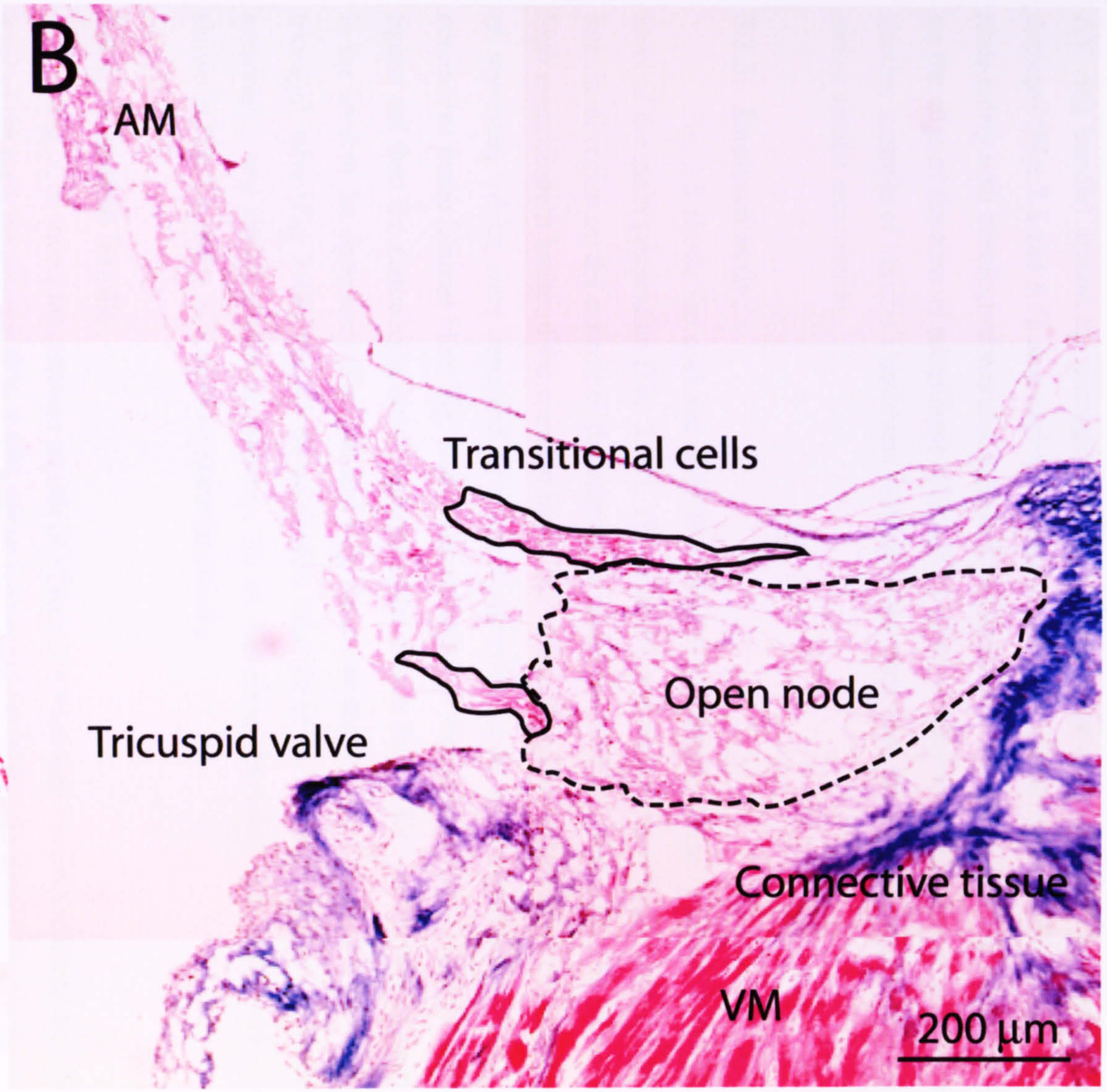
B
AM
Transitional cells
Open node
Tricuspid valve
Connective tissue
VM
200 µm

AV ring bundle) around the tricuspid annulus. Although the zone of transitional cells was depicted (Figs 3.6 and 3.7), it is hard to distinguish the zone of transitional cells and the open node solely with histological staining, especially at the level of the open node. The explanation on the edge of the zone of transitional cells will be given in the following chapters. Fig. 3.7 is another example of Masson's trichrome staining of the open node in a different preparation and shows similar architecture.

3.3.3. Enclosed node

Fig. 3.8 shows the enclosed node in a Masson's trichrome stained section at the 9th level of the main preparation (Fig. 2.1B). The enclosed node was situated at the centre of the junctional region on the summit of the ventricular myocardium (Fig. 3.8A). Fig. 3.8B shows a high magnification image of the enclosed node. The enclosed node consisted of an ovoid group of myocytes, which were separated from the surrounding atrial and ventricular muscle by connective tissue (stained blue; Fig. 3.8B). The myocytes in the enclosed node were stained a lighter red than the surrounding atrial and ventricular muscle (Fig. 3.8B). As already appeared in the level of the open node (Figs 3.6 and 3.7), there was zone of transitional cells above the tricuspid valve (Fig. 3.8B). Fig 3.9 shows another example of the enclosed node in a different preparation and shows similar architecture. As an anatomical landmark, the mitral valve is shown in Fig. 3.9, along with other common landmarks.

3.3.4. Common bundle

Fig. 3.10 shows the common bundle in a Masson's trichrome stained section at the 11th level of the main preparation (Fig. 2.1B). As an anatomical landmark, the aorta is shown in Fig. 3.10. At this level, nodal-like myocytes existed in three separate regions, i.e. the common bundle in framed area C, the zone of the transitional cells also in framed area C and the termination of the AV ring bundle in framed area B in Fig. 3.10A. In this study, nodal myocytes were situated around the tricuspid annulus and as stated above the ring structure is referred to as the AV ring bundle. The AV ring bundle started with the common bundle/the enclosed node and the zone of the transitional cells, continued around the tricuspid annulus and terminated above the common bundle as shown in Fig. 3.10A. Fig. 3.10B shows a high magnification image of the termination of the AV ring bundle above the common bundle. Compared to the atrial myocardium, myocytes in the termination of the AV ring bundle were stained a lighter red. Fig. 3.10C shows a high magnification image of the common bundle region. The common bundle was situated in the middle of the junctional region and it was separated from the atrial myocardium by connective tissue. From Fig. 3.10C it is uncertain that the common bundle was in direct contact with the ventricular myocardium - again it was perhaps separated from the ventricular myocardium by connective tissue. The common bundle consisted of a triangle of pale red-staining myocytes. In this region, the zone of transitional myocytes was again present

Figure 3.7 Another example of Masson's trichrome staining of the open node

A, low-magnification montage of Masson's trichrome staining. Scale bar, 1 mm. B, high-magnification micrograph of Masson's trichrome staining. B corresponds to the framed area in A. Scale bar, 200 μm. AM, atrial myocardium; VM, ventricular myocardium.

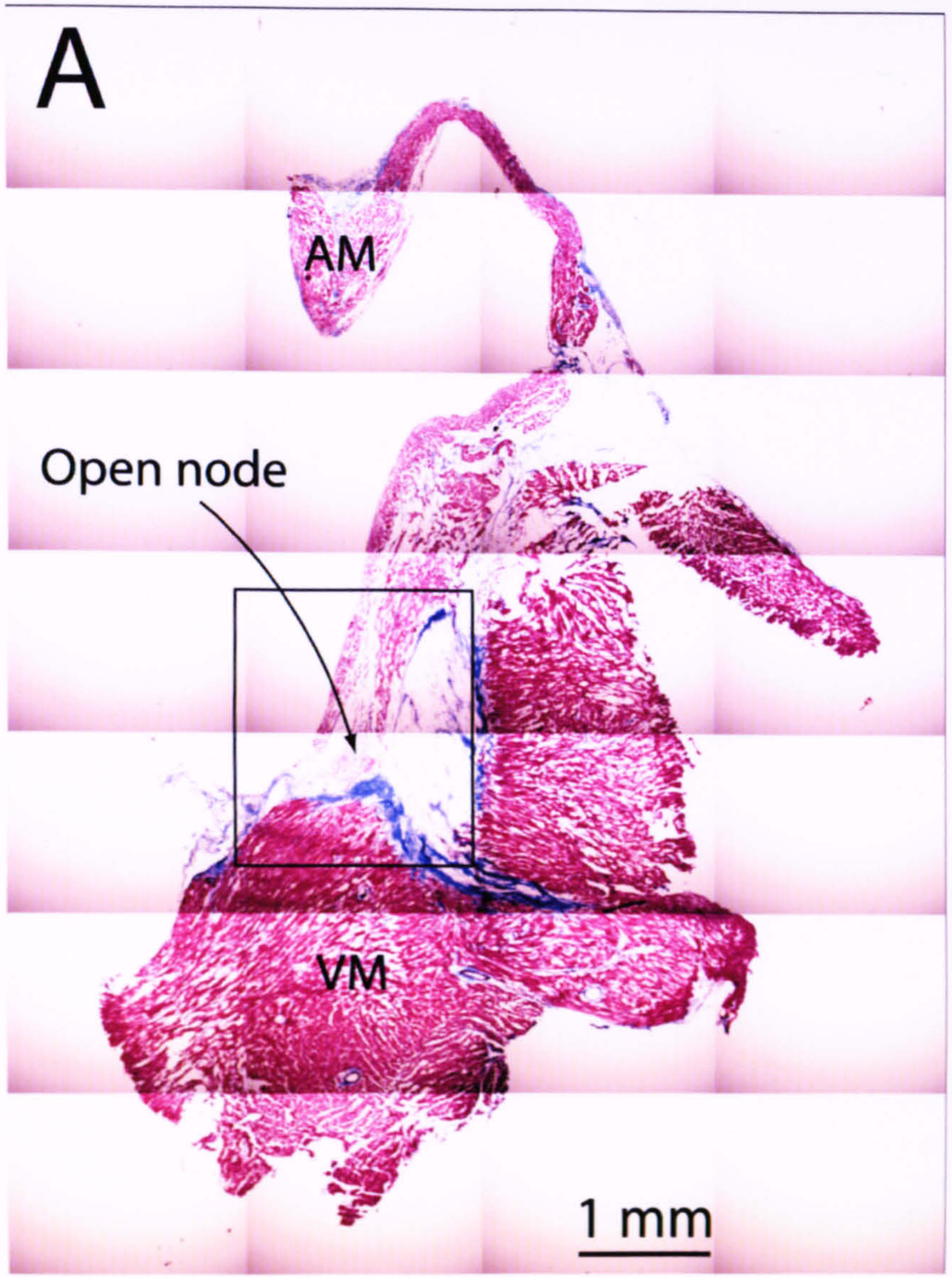
A
AM
Open node
VM
1 mm

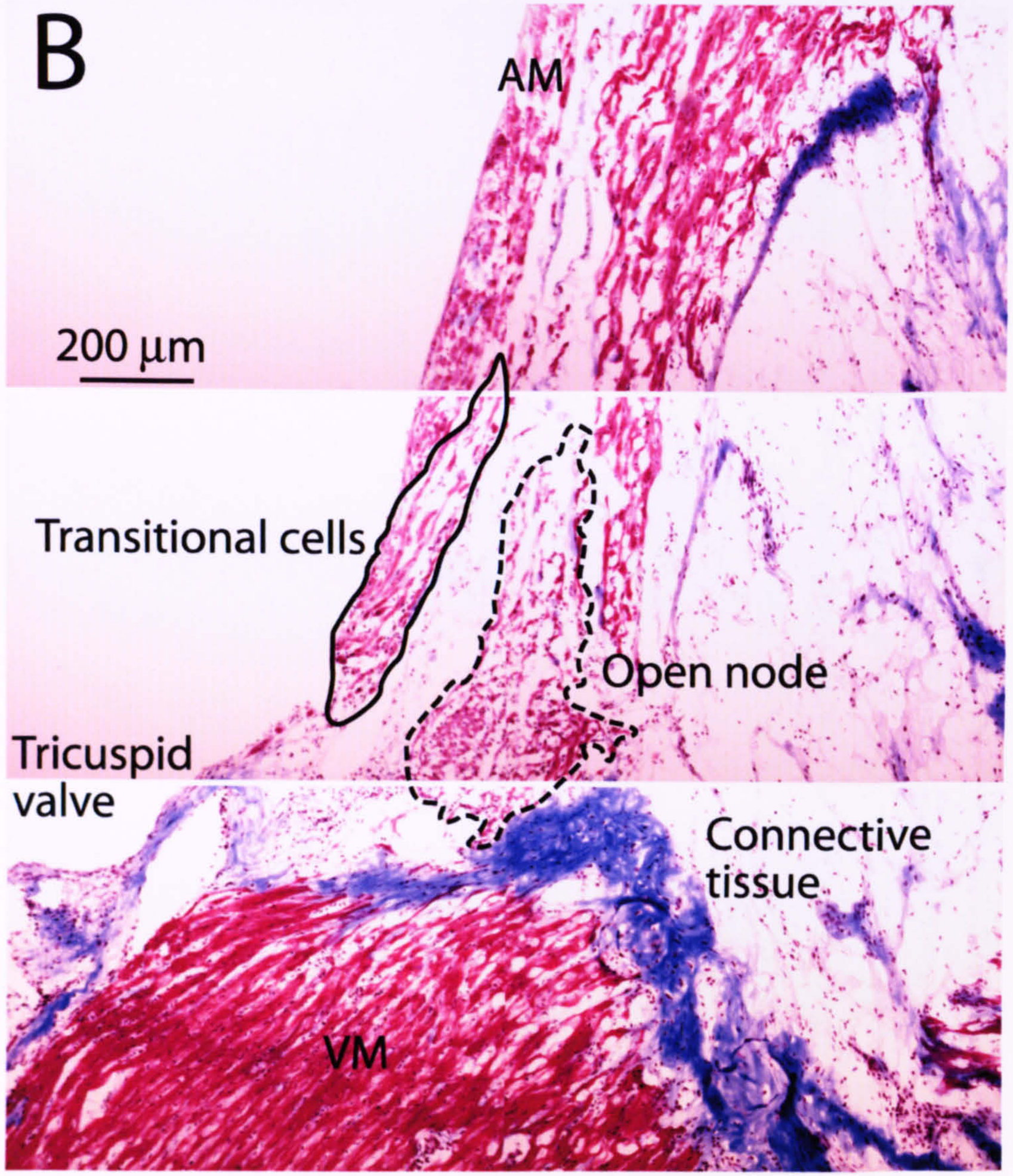
B
AM
200 µm
Transitional cells
Open node
Tricuspid valve
Connective tissue
VM

Figure 3.8 Masson's trichrome staining of the enclosed node

A, low-magnification montage of Masson's trichrome stained section at level 9 (see Figs. 3.1 and 3.3). Scale bar, 0.5 mm. B, high-magnification micrograph of Masson's trichrome staining of the enclosed node. B corresponds to the framed area in A. Scale bar, 200 μm. AM atrial myocardium; VM, ventricular myocardium.

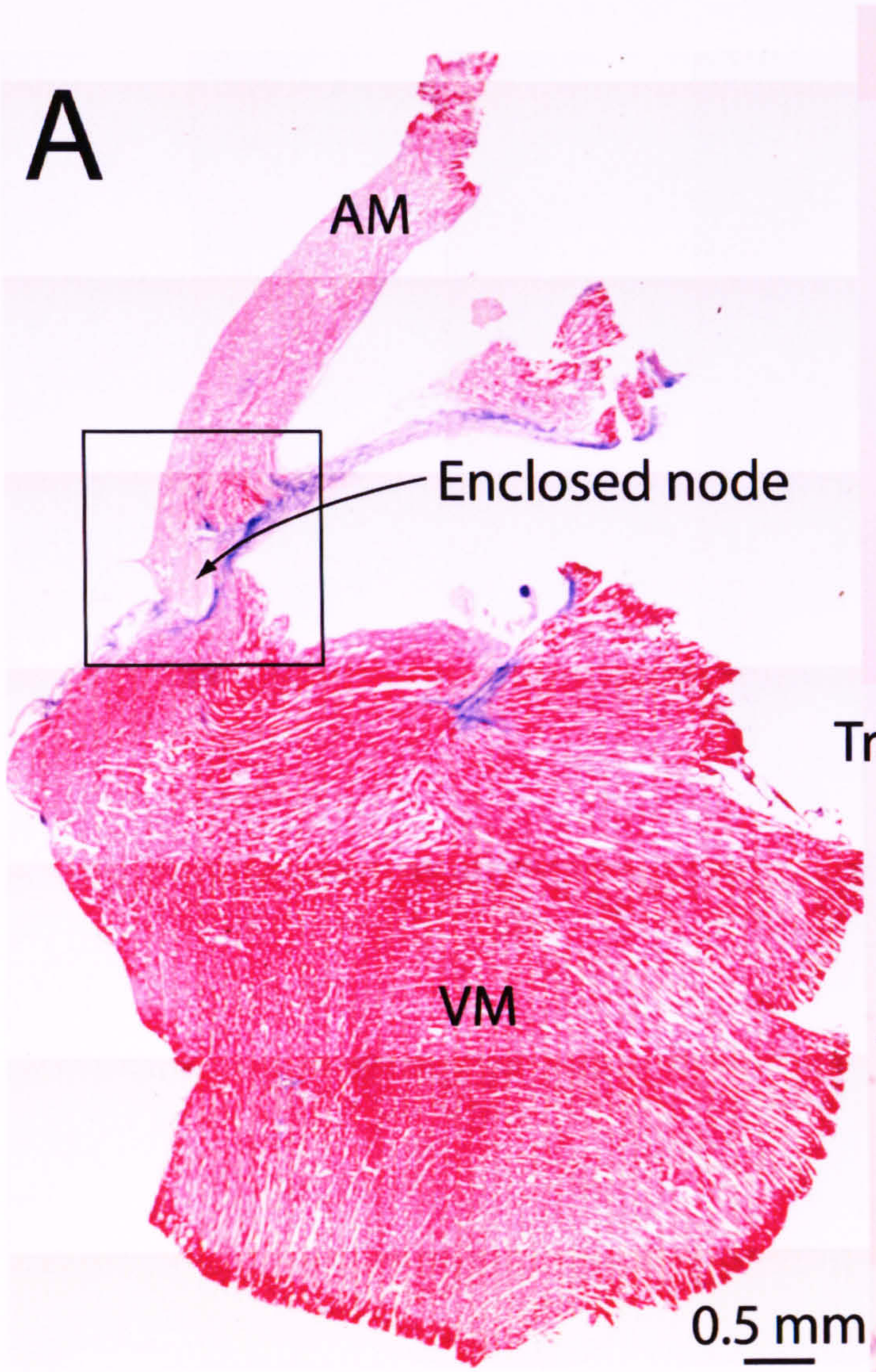
A
AM
Enclosed node
VM
0.5 mm

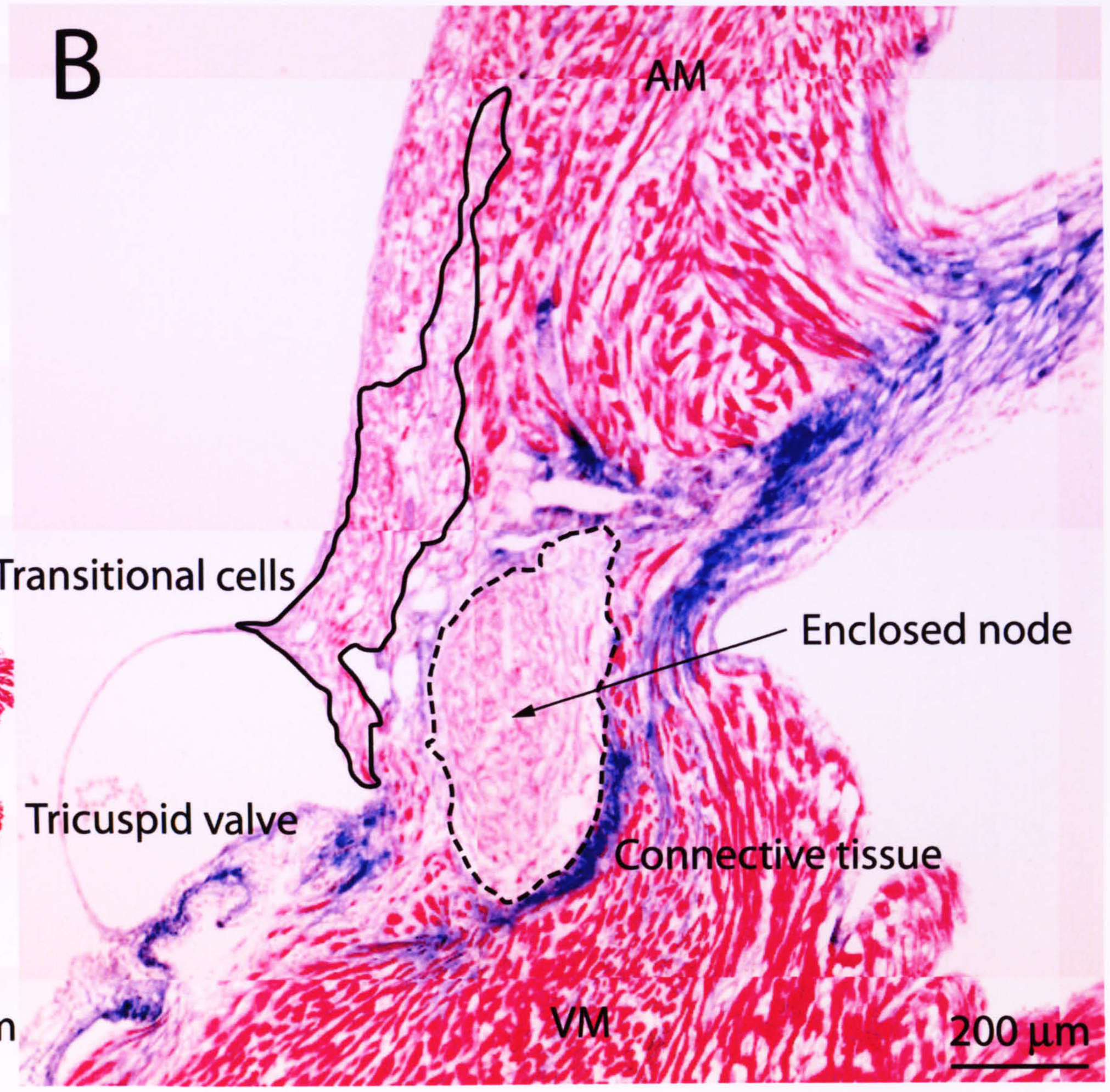
B
AM
Transitional cells
Enclosed node
Tricuspid valve
Connective tissue
VM
200 µm

Figure 3.9 Another example of Masson's trichrome staining of the enclosed node

A, low-magnification montage of Masson's trichrome staining. Scale bar, 1 mm. B, high-magnification micrograph of Masson's trichrome staining. B corresponds to the framed area in A. Scale bar, 200 μm. AM, atrial myocardium; VM, ventricular myocardium.

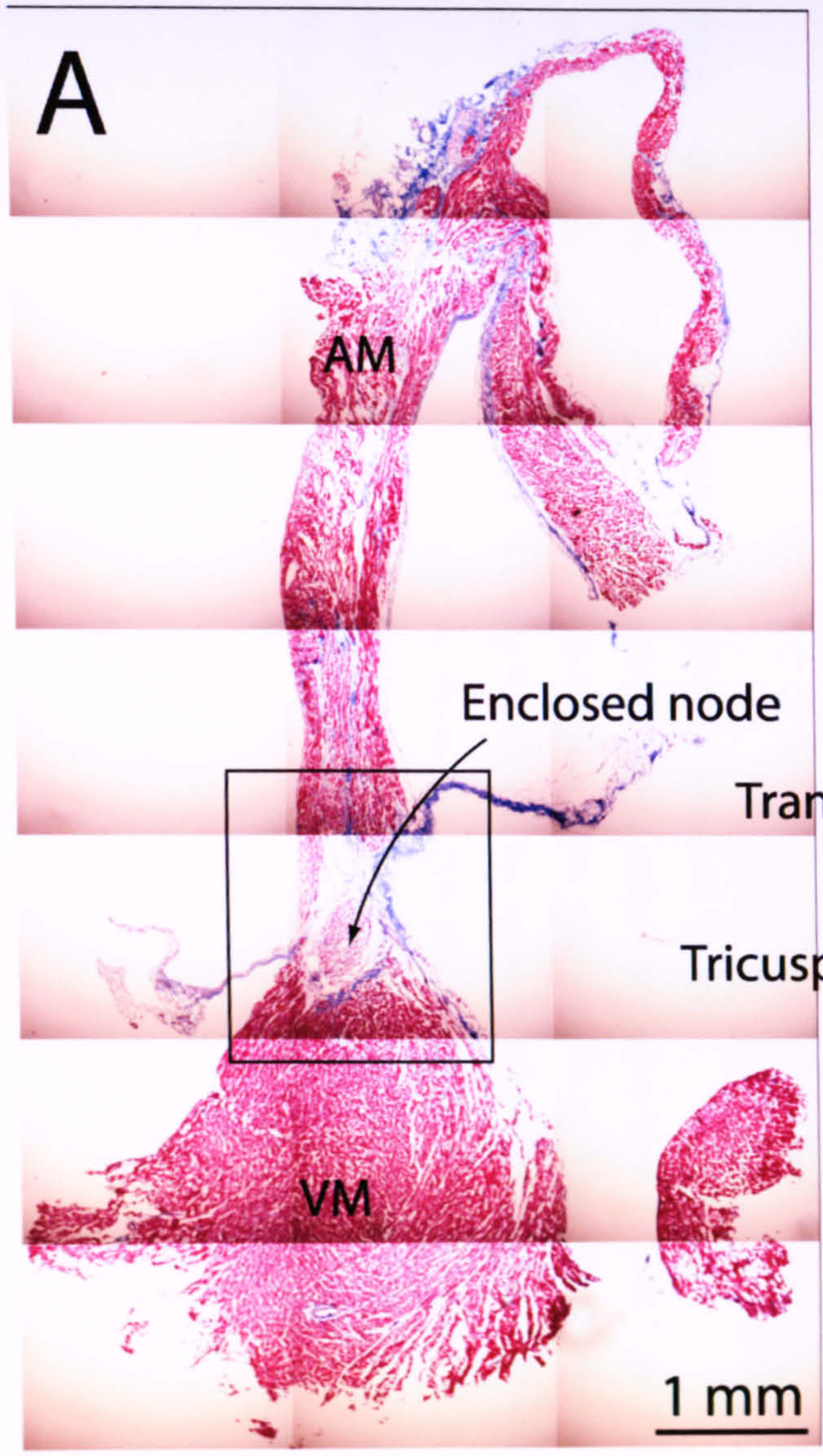
A
AM
Enclosed node
Tricuspid valve
VM
1 mm

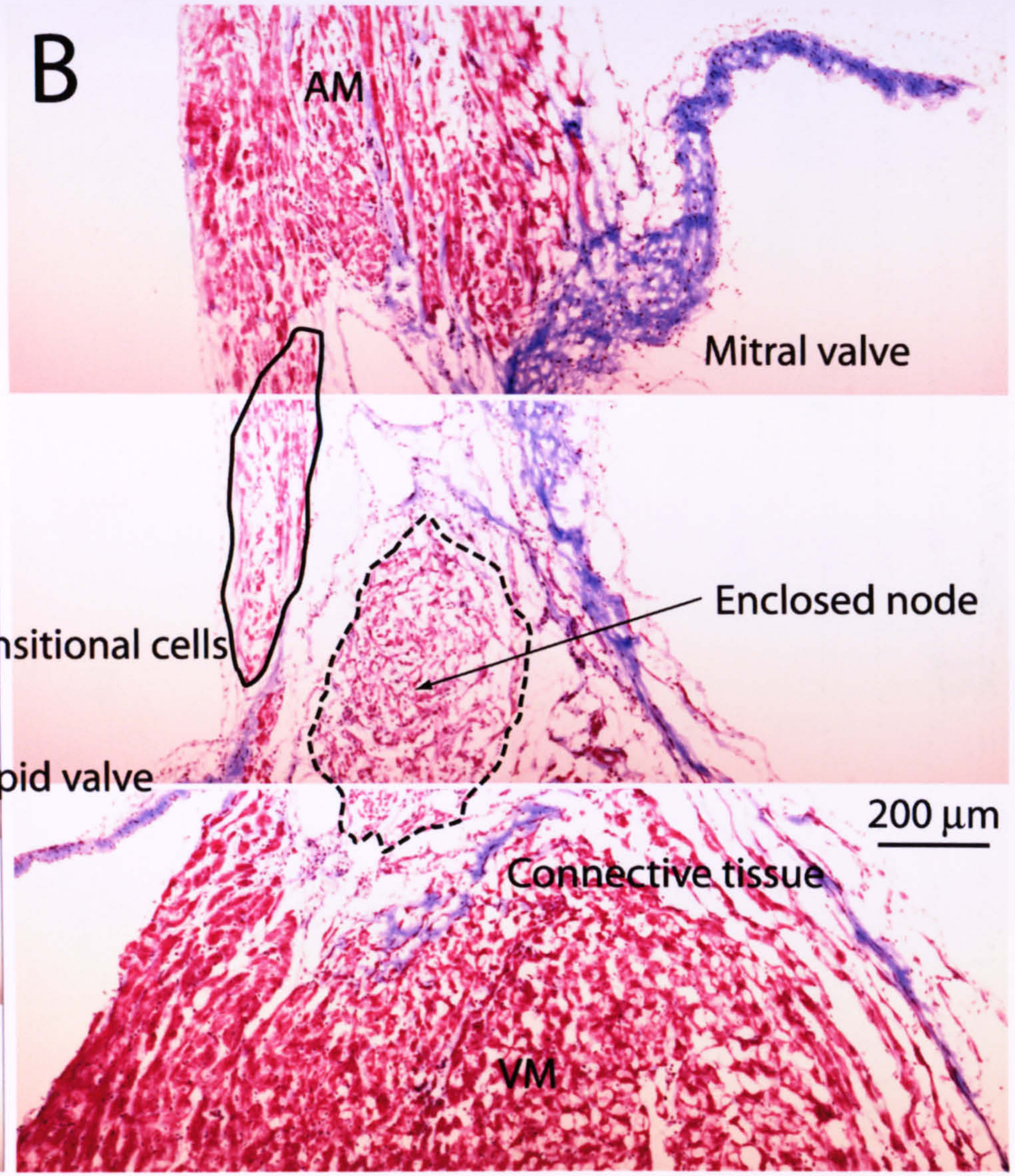
B
AM
Mitral valve
Transitional cells
Enclosed node
200 µm
Connective tissue
VM

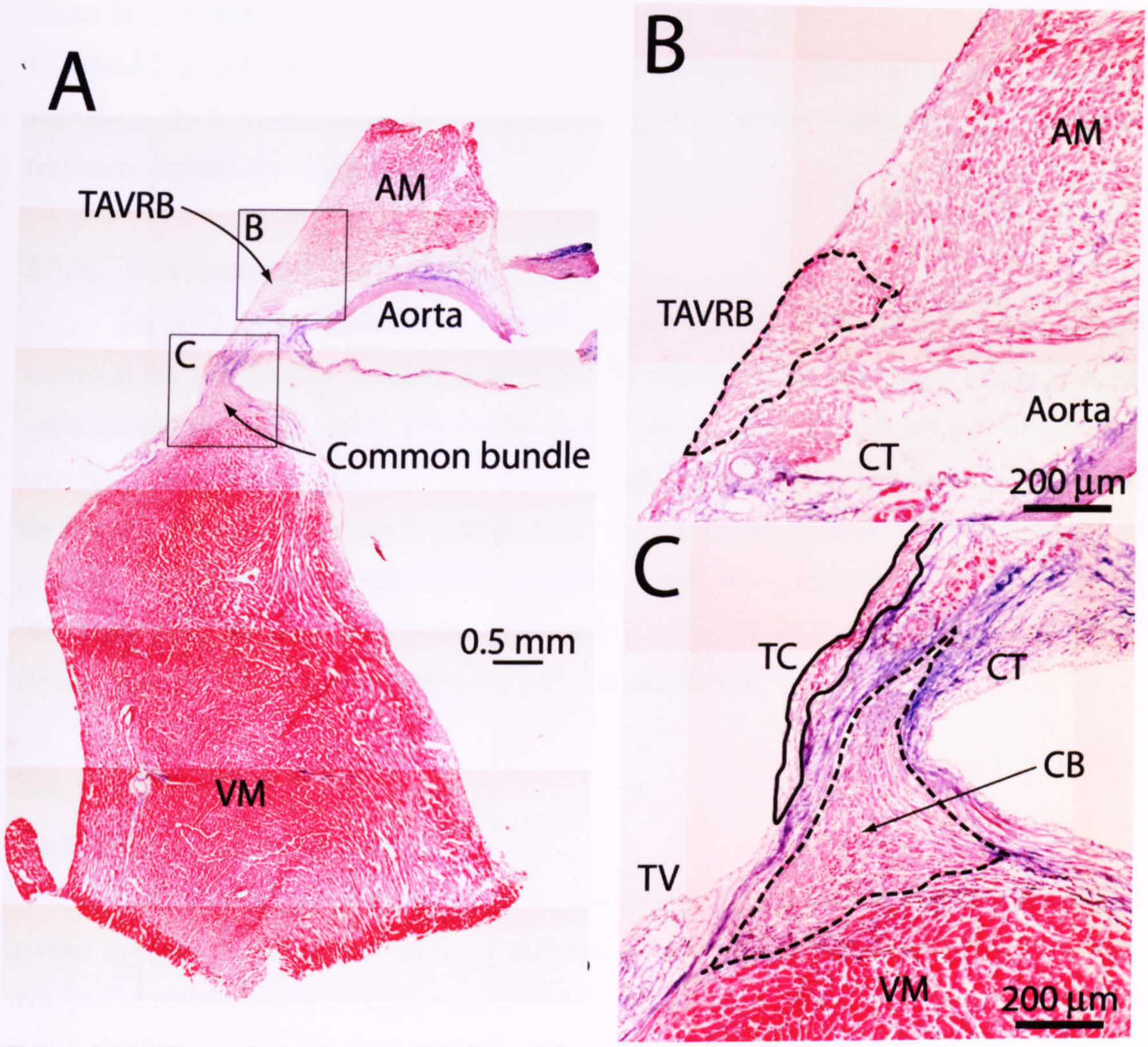

Figure 3.10 Masson's trichrome staining of the common bundle

A, low-magnification montage of Masson's trichrome stained section at level 11 (see Figs. 3.1 and 3.3). Scale bar, 0.5 mm. B, C, high-magnification micrographs of Masson's trichrome staining of the termination of the AV ring bundle and the common bundle, respectively. B and C correspond to the framed areas in A. Scale bar, 200 µm. AM, atrial myocardium; CB, common bundle; CT, connective tissue; TAVRB, termination of AV ring bundle; TC, transitional cells; VM, ventricular myocardium.

above the tricuspid valve (Fig. 3.10C), but it was smaller than at the level of the enclosed node (compare Figs 3.8B and 3.10C). Fig. 3.11 shows another example of Masson's trichrome staining in the common bundle in a different preparation, but the section does not include the termination of the AV ring bundle.

3.3.5. Termination of the AV ring bundle

Fig. 3.12 shows the termination of the AV ring bundle in a Masson's trichrome stained section at the 14th level of the main preparation. As anatomical landmarks, the aorta and aortic valve are shown in Fig. 3.12A. The termination of the AV ring bundle is situated in the atrio-ventricular junctional region. Fig. 3.12B shows a high magnification image of the termination of the AV ring bundle. As discussed in the previous section, the termination of the AV ring bundle consisted of lighter red stained nodal myocytes, which were separated from neighbouring ventricular myocardium by connective tissue and fat cells. Fig 3.13 shows another example of the termination of the AV ring bundle in a different preparation.

3.4. Discussion

3.4.1. Rat AV node histology

Tawara (2000) was the first to describe the morphology of the AV node in the hearts of several species. Rather than describing differences, he emphasized the similarities of this structure in various hearts to support his main hypothesis that the AV node is the only electrical connection between the atria and ventricles. Now, it is well established that the contractions of the adult mammalian heart begin in the SA node, spread over the right and left atria, reach the AV node, and then spread by way of the His-Purkinje fibre to the ventricles (Meijler & Janse, 1988).

Tawara (2000) examined the hearts of the dove, rat, guinea-pig, rabbit, cat, dog, sheep, calf and human and found in all these species essentially the same structure in the anterior part of the base of the interatrial septum. He described a spindle-shaped compact network of small cells. It must be emphasized that in addition to this compact node, Tawara (2000) also described what we now call "transitional cells". Transitional cells are distinguished from atrial cells by their smaller size, their pale staining reaction, and by the fact that they are separated from each other by connective tissue septa.

The architecture of the rat AV node is similar to that of other species. The endocardial conduction elements of the ventricles of animals can be well differentiated or poorly differentiated. Small mammals including rat and rabbit have poor differentiation (Truex & Smythe, 1965). Copenhaver (1981) reported that the special conduction tissue in the rat is not as easily demonstrated as that of the pig and dog and that no continuous pathways of cholinesterease-expressing cardiac muscle fibres from the SA node to the AV node can be identified (Copenhaver, 1981).

Figure 3.11 Another example of Masson's trichrome staining of the common bundle

A, low-magnification montage of Masson's trichrome staining. Scale bar, 0.5 mm. B, high-magnification micrograph of Masson's trichrome staining. B corresponds to the framed area in A. Scale bar, 200 μm. AM, atrial myocardium; VM, ventricular myocardium.

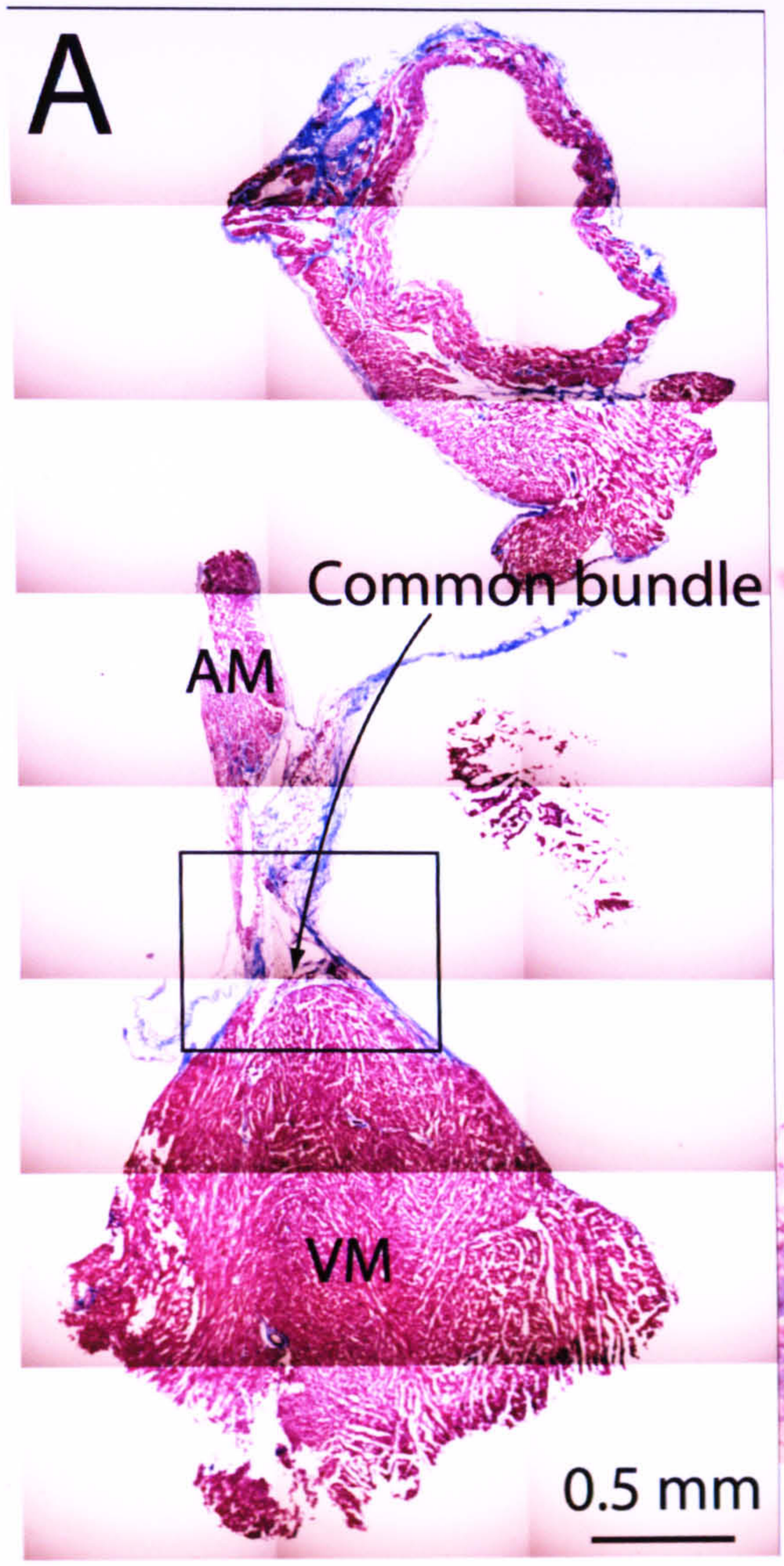
A
Common bundle
AM
VM
0.5 mm

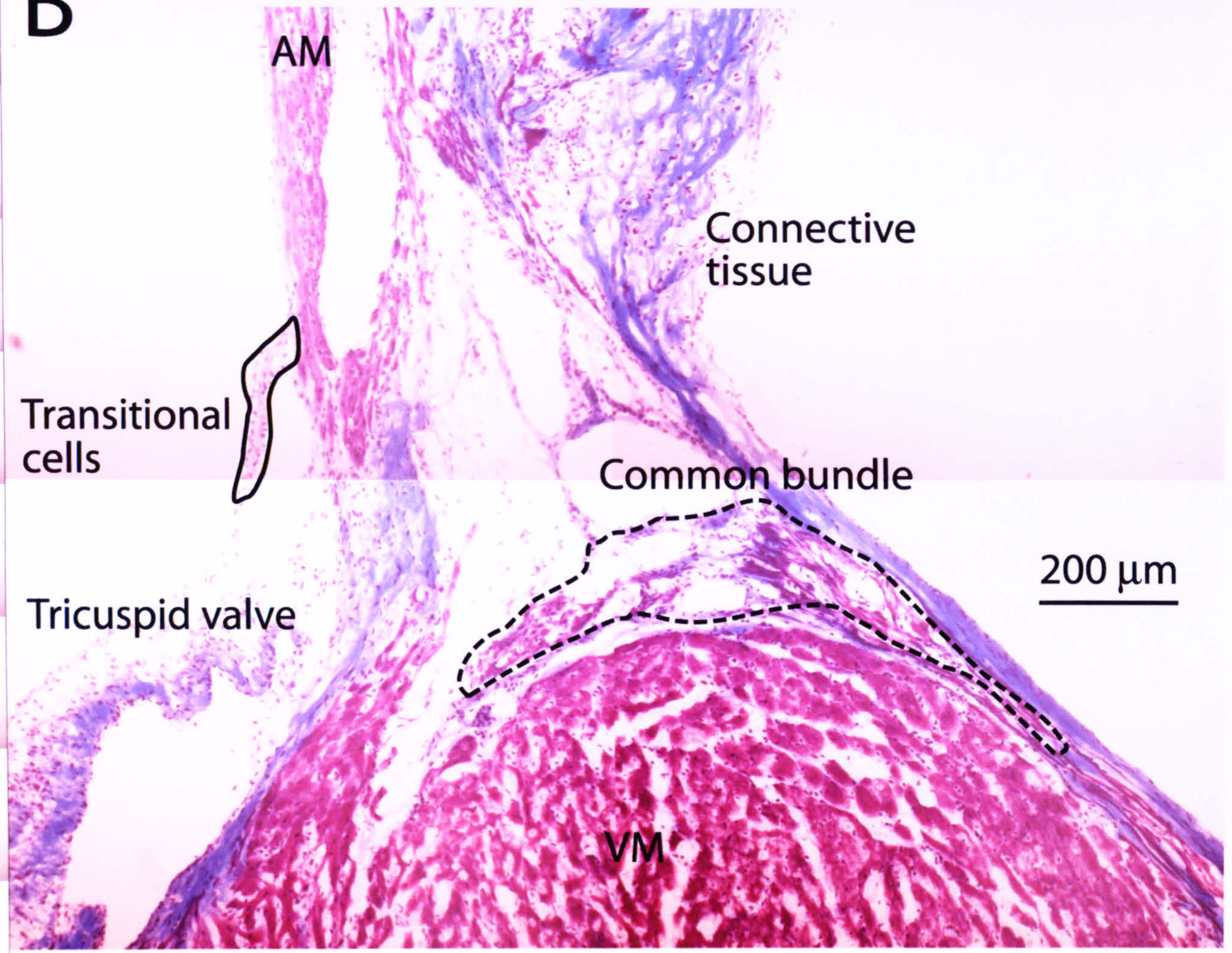
B
AM
Connective tissue
Transitional cells
Common bundle
200 µm
Tricuspid valve
VM

Figure 3.12 Masson's trichrome staining of the termination of the AV ring bundle

A, low-magnification montage of Masson's trichrome stained section at level 14 (see Figs. 3.1 and 3.3). Scale bar, 0.5 mm. B, high-magnification micrograph of Masson's trichrome staining of the termination of the AV ring bundle. Scale bar, 200 μm. AM, atrial myocardium; Ao, aorta; AoV, aortic valve; TAVRB, termination of AV ring bundle; VM, ventricular myocardium.

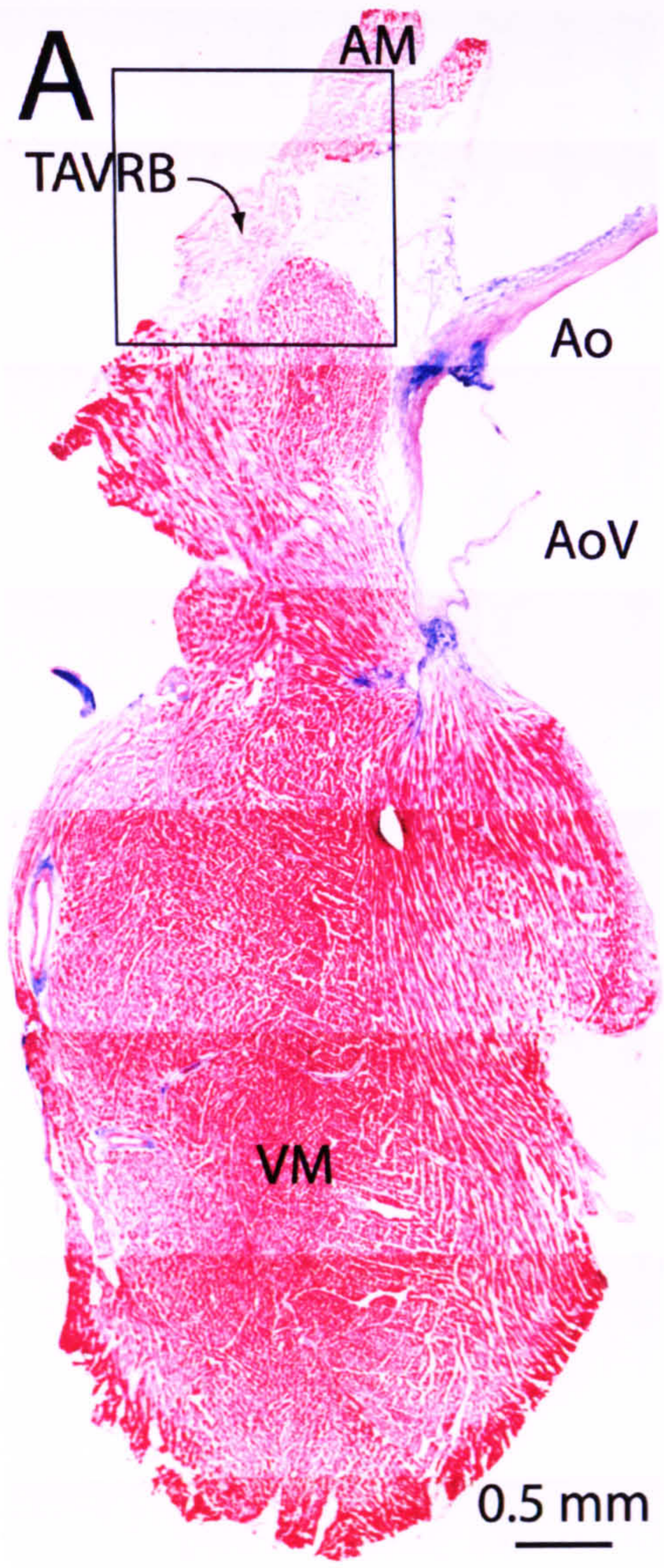
A
AM
TAVRB
Ao
AoV
VM
0.5 mm

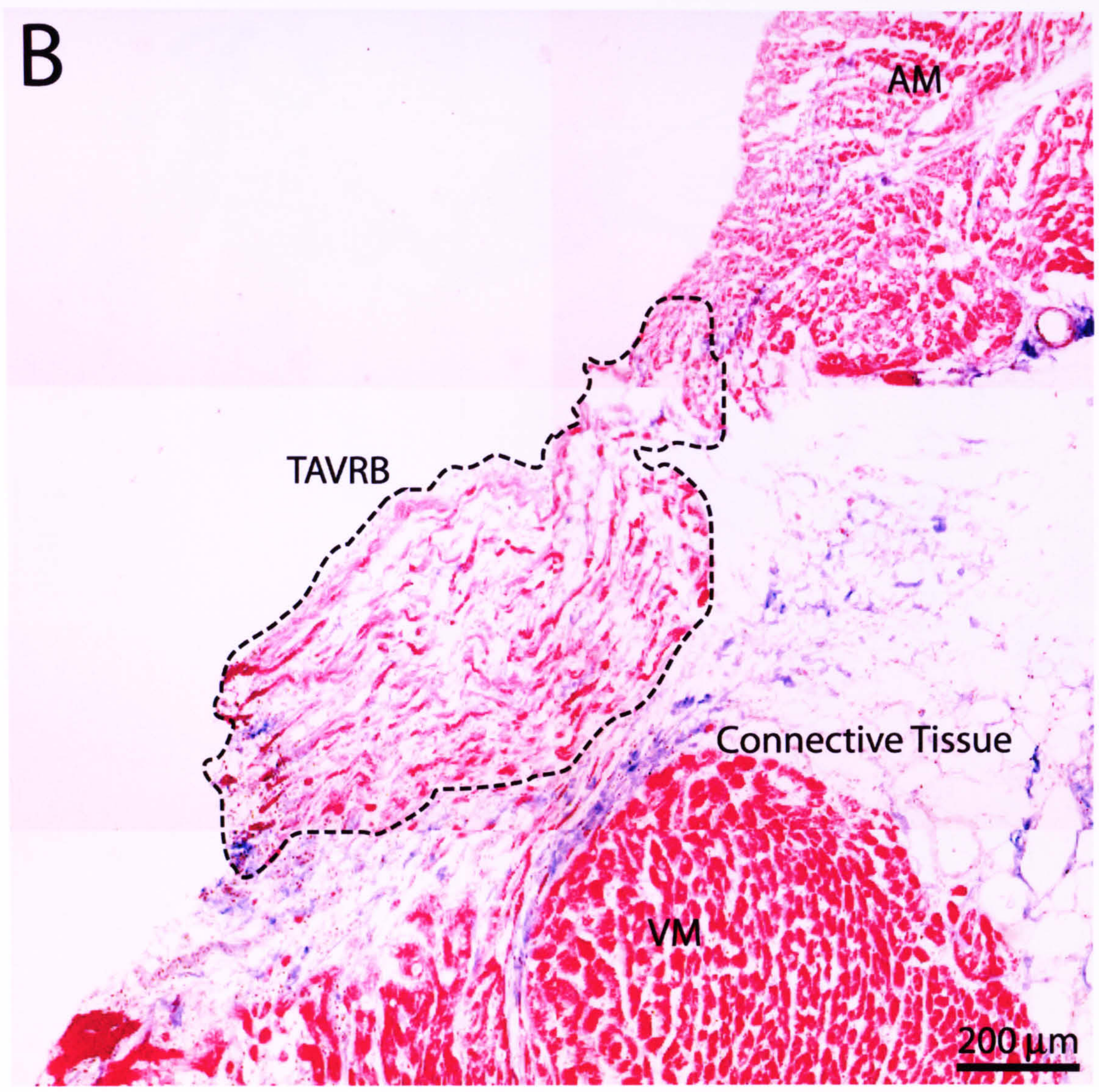
B
AM
TAVRB
Connective Tissue
VM
200 µm

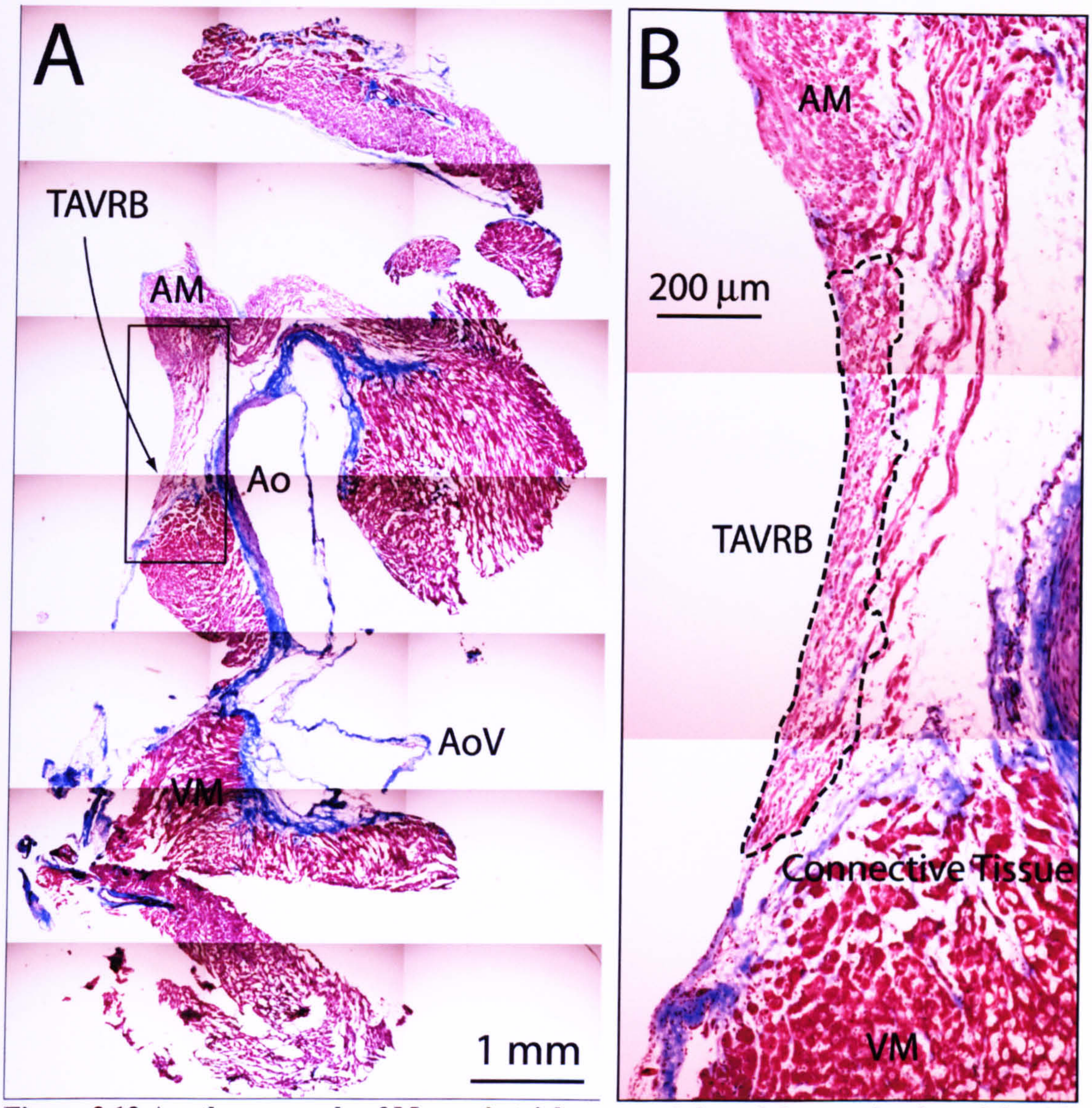

Figure 3.13 Another example of Masson's trichrome staining of the termination of the AV ring bundle

A, low-magnification montage of Masson's trichrome staining. Scale bar, 1 mm. B, high-magnification micrograph of Masson's trichrome staining. Scale bar, 200 µm. AM, atrial myocardium; Ao, aorta; AoV, aortic valve; TAVRB, termination of AV ring bundle; VM, ventricular myocardium.

3.4.2. Comparison with previous histological investigations of the rat AV node

There have been previous histological investigations of the rat AV node (Truex & Smythe, 1965; Copenhaver, 1981). My data agree with previous investigations in several aspects: first, the AV nodal cells shows the same histological characteristics (size, colour, shape, arrangement of cells). Second, the AV node consists of histologically different regions: 1) posterior/inferior nodal extension consisting of nodal cells and surrounded by connective tissue or fat tissue (Figs. 3.4 and 3.5); 2) open node consisting of nodal cells receiving atrial inputs along its upper and posterior margins (Figs. 3.6 and 3.7); 3) enclosed node consisting of nodal cells surrounded by a collar of fibrous tissue formed by the fibrous annulus and an extension from the central fibrous body (Figs. 3.8 and 3.9). Fibres overlying this fibrous collar end in the base of the septal tricuspid valve leaflet and do not make contact with the underlying cells of the enclosed node (Figs. 3.8 and 3.9); 4) the zone of transitional cells separated by connective tissue from the enclosed node and common bundle (Figs. 3.8-3.11); and 5) common bundle consisting of nodal cells surrounded by connective tissue (Figs. 3.10 and 3.11). Finally, the conduction axis outside of the enclosed node is not clear (Truex & Smythe, 1965; Copenhaver, 1981).

However, the AV ring bundle above the common bundle was not observed in earlier studies (Truex & Smythe, 1965; Copenhaver, 1981). The AV ring bundle observed in the present study consisted of nodal (or nodal-like) cells (Figs. 3.12 and 3.13).

3.4.3. What is the AV node?

It is surprising that despite extensive and accurate description (Tawara, 2000), confusion has arisen subsequently concerning the definition of the AV node as given by morphologists and electrophysiologists. The latter tend to define the AV node as the "area where the functional delay between atria and ventricles occurs" and the former as the knot of densely packed small cells, described by Tawara as knoten (Hoffman, 1971).

The need of electrophysiologists for a broadened definition of the AV node arose from the fact that significant events in atrial-His conduction occur outside of the enclosed node. Furthermore, a posterior/inferior extension, which is made of nodal tissue, lies just above the insertion of the tricuspid valve beneath the coronary sinus ostium and likely plays a critical role in the slow AV nodal pathway and acts as the junctional pacemaker. Furthermore, the AV ring bundle along the tricuspid annulus, investigated in this study, also lies outside of the enclosed node.

3.4.4. The definition of transitional cells

As discussed so far, the AV junctional area including the triangle of Koch contains multilayered and complex morphological structures that anatomically and functionally form a continuum between the atrium and the bundle of His. A major source of confusion in delineating the sub-regions of the nodal area is related to the smooth transitions between regions

and the lack of clear morphological/histological features that would easily distinguish between transitional mid-nodal, and lower nodal cells for example. The result is that different investigators have used different nomenclature for the same structures. According to the most common nomenclature used, the AV junctional area can be described as encompassing transitional cells, specialsed nodal cells (AV node), lower nodal cells, and the penetrating AV bundle (bundle of His) (de Carvalho & de Almeida, 1960; Meijler & Janse, 1988). The term "transitional cells" is used broadly to describe the approaches from the working atrial myocardium to the AV node. Most frequently recognized are the posterior (inferior) and anterior (superior) approaches (Bharati, 2000). The posterior approaches serve as a bridge with the atrial myocardium at the coronary sinus ostium, while the anterior approaches merge with the AV node closer to the apex of the triangle of Koch. A third, middle group of transitional cells has also been identified (Anderson *et al.*, 1974; Antz *et al.*, 1998). They account for the nodal connections with the septum and the left atrium.

In the present study, I also use the terms, "transitional cells" and "posterior/inferior nodal extension". Although electrophysiological recordings have not been carried out in this study, the former may correspond to the anterior (superior) approach and the latter may correspond to the posterior (inferior) approach. In this study, unlike in previous studies, I have used immunolabelling of markers, gap junctions and ion channels to identify these different structures (see chapters 4-5 and 7-9). The AV node is a specialsed conducting tissue and, therefore, it is right that the expression of ion channels should be used to define it.

3.4.5. Posterior/inferior nodal extension?

In the classic AV nodal topographic approach, the His bundle has an anterior location, the coronary sinus is posterior, towards the heart base is considered superior, and towards the heart apex is considered inferior. However, this simple practical terminology is inaccurate with respect to AV node orientation within orthogonal axes of the human thorax (Cosio *et al.*, 1999). When the heart is opened through the right atrium and viewed in an attitudinally correct position, then the part of the right atrium containing the AV node (the triangle of Koch) has its apex pointing upwards. In classic conventional descriptions, however, the triangle of Koch is usually illustrated with its apex pointing to the right. Although this provides a realistic orientation of the AV junction within the thorax, some investigators find it complicates AV nodal description (Billette, 2002). The term 'posterior/inferior nodal extension' is used in the present study.

Chapter 4

Immunohistochemical markers of the AV node

4.1. Introduction

The aim of the work described in this chapter was to localise the nodal cell region in serial AV node sections from rat using confocal microscopy with immunohistochemical 'markers': Cx43, DP, and ANP.

4.1.1. Cx43

The predominant connexin of the heart, found in abundance in the adult working ventricle and atrium in all mammalian species, is Cx43 (Severs *et al.*, 2001). In addition, two other major connexins expressed are in the heart, Cx40 and Cx45 (Gros & Jongsma, 1996; Severs *et al.*, 2001). These connexins are constituents of gap junction channels and the primary function of gap junction channels is to provide electrical coupling between heart cells (Kumar &

Gilula, 1996; Bruzzone *et al.*, 1996a; Bruzzone *et al.*, 1996b). The architecture, gating and distribution of the gap junction channels are described in detail in chapter 1 (section 1.3).

Nodal myocytes (both in the SA and AV nodes) are typically small, with a dearth of contractile elements and small, sparse, dispersed gap junctions (Severs *et al.*, 2001). Furthermore, the medium conductance Cx43 is not expressed in the nodal myocytes and the small conductance Cx45 is expressed instead (Coppen *et al.*, 1998; Coppen *et al.*, 1999; Verheijck *et al.*, 2001). These gap junction features correlate with poor electrical coupling, which, in the SA node, is linked to the ability of the SA node to drive the large mass of surrounding atrial tissue while remaining protected from its hyperpolarizing influence, and, in the AV node, to a slowing of conduction, which ensures sequential contraction of the atria and ventricles (Severs *et al.*, 2001). Cx43 can be considered to be a marker for the SA and AV nodes: the absence of Cx43 in the SA and AV nodes enables the SA and AV nodal tissues to be easily distinguished from the surrounding atrial and ventricular myocardium.

4.1.2. DP

It is well known that the adherens junctions and desmosomes, which are responsible for mechanical coupling of cardiac myocytes, are closely juxtaposed to the gap junctions at the intercalated discs (Peters *et al.*, 1994; Angst *et al.*, 1997). DP is a desmosomal plaque protein and is present in all cardiac myocytes (Gutstein *et al.*, 2003; Cheng & Koch, 2004).

4.1.3. ANP

A 28 amino acid peptide hormone (Flynn *et al.*, 1983), ANP is one of a family of natriuretic peptides that play an important homeostatic role in preserving cardiovascular function and body fluid balance (Antunes-Rodrigues *et al.*, 2004). Specific heart granules that comprise the storage site for ANP have been detected in the atria of numerous mammals (Cantin & Huet, 1975; de Bold *et al.*, 1981). ANP released from atrial myocytes circulates to the kidneys and causes diuresis and natriuresis (Forssmann *et al.*, 1998; DiBona, 2000). The natriuretic peptides act at the cell membrane through three types of receptors (NPR-A, NPR-B and NPR-C) (Maack, 1992). NPR-A and NPR-B, but not NPR-C, have an intracellular guanylate cyclase domain that generates cyclic guanosine monophosphate (cGMP) from GTP; cGMP activates protein kinase G in the brain and the periphery (Akamatsu *et al.*, 1993; Favaretto *et al.*, 1997; Jankowski *et al.*, 1998; Soares *et al.*, 1999; Jankowski *et al.*, 2000; Jankowski *et al.*, 2001). In contrast, NPR-C performs a clearance receptor function by binding the peptides (Maack *et al.*, 1987; Maack, 1992). ANP is well known to be abundantly expressed in atrial myocardium and not in the conduction tissue (Benvenuti *et al.*, 1997). ANP is absent in the SA and AV nodes and ventricular myocardium. Because of this distribution, it can be used as a marker for nodal myocytes.

4.2. Methods

4.2.1. Dissection of AV node tissue

Wistar rats weighing 250-300 g were sacrificed and the hearts were collected as described in chapter 2 (section 2.1.2). The AV node was dissected as described in chapter 2 (section 2.1.2 and shown in Fig. 2.1).

4.2.2. Immunohistochemistry

The general immunohistochemistry procedures are described in chapter 2 (section 2.6). Details of procedures (tissue fixation, membrane permeabilisation, blocking of non-specific sites, type of labelling, type of primary and secondary antibodies used, incubation time and temperature during incubation with antibodies, washing and mounting of tissue) are described here. The AV node tissue was prepared and cryosectioned as described in chapter 2 (section 2.1 and 2.4). Prior to immunofluoresecnce labelling, sections were fixed in 10 % neutral buffered formalin at room temperature and washed three times in PBS over 30 min to remove excess fixative. Tissue sections were treated with 0.1 % Triton X-100 in PBS for 10 min at room temperature. Tissue sections were incubated with 10 % normal donkey serum and 1 % BSA in PBS for 60 min at room temperature. Primary antibodies were diluted in 1 % BSA in PBS. The tissue sections were incubated with a suitable concentration of each primary antibody in a humid box at -4°C overnight. Information on primary antibodies can be obtained from chapter 2 (section 2.6.1 and Table 2.1). The secondary antibodies were diluted in 1 % BSA in PBS. The secondary antibodies were applied for 1 h at room temperature in the dark. For multiple labelling experiments, combinations of secondary antibodies were used. Information regarding the incubation time and antibody concentration with the secondary antibodies can be obtained from chapter 2 (section 2.6.9 and Table 2.3). After application of the primary and secondary antibodies, the samples were thoroughly washed in PBS three times for 30 min. Then, the samples were mounted under coverslips with the anti-fade reagent, Vectashield. The immunolabelled tissue sections were viewed by confocal laser scanning microscopy and montages were constructed as described in chapter 2 (section 2.7).

4.3. Results

In this chapter, Cx43, DP and ANP labelling are used as immunohistochemical markers of the AV node. Immunolabelling of Cx43 was observed in three complete AV node preparations and data from two preparations are shown here. In addition, similar data for Cx43 were obtained from three other preparations (region of the enclosed node only). Immunolabelling of ANP was observed in two complete AV node preparations and the data from both preparations are shown here. The DP immunolabelling shown here was obtained from one complete AV node preparation and similar data were obtained from another

preparation (enclosed node region only). Photographs of the two preparations used for the figures in this chapter and also chapters 5 and 7 are shown in Figs 2.1B and 4.6A. In the preparation shown in Fig. 2.1B (the main preparation studied), 14 levels at 525 ± 7.31 μm intervals were studied. In the preparation shown in Fig. 4.6A, five levels at 500 μm intervals were studied. The position of each level is marked in Figs. 2.1B and 4.6A.

Typically, Cx43 labelling was localised at intercalated disks in working myocardium. As desmosomes are juxtaposed to gap junctions, DP labelling was co-localised with Cx43 at intercalated disks. ANP labelling was detected in the cytoplasm of atrial myocytes.

4.3.1. Posterior/inferior nodal extension

Figs. 4.1 to 4.5 show immunolabelling of immunohistochemical markers in the posterior/inferior nodal extension in the 1st to 5th levels of the main preparation studied shown in Fig. 2.1B. The posterior/inferior nodal extension, ringed in yellow, is located above the ventricular myocardium and fibrous annulus (or tricuspid valve), outlined in white, and beneath the atrial myocardium (Figs. 4.1 to 4.5). The atrial myocardium showed co-localisation of Cx43 and DP at intercalated disks and intracellular ANP labelling (Figs. 4.1 to 4.5). The posterior/inferior nodal extension showed DP labelling only at intercalated disks (Figs. 4.1 to 4.5). The fibrous annulus did not show fluorescence above background (Figs. 4.1 to 4.5). The ventricular myocardium showed co-localisation of Cx43 and DP at intercalated disks as in the atrial myocardium (Figs. 4.1 to 4.5). In summary, the posterior/inferior nodal extension is Cx43-negative, DP-positive and ANP-negative and can be distinguished from surrounding atrial myocardium, fibrous annulus and ventricular myocardium.

Fig. 4.6A shows the second AV node preparation and the anatomical landmarks (tendon of Todaro, coronary sinus and tricuspid valve). Fig. 4.6B shows a Masson's trichrome stained section at level 1 in the second preparation. Although the posterior/inferior nodal extension was located above the tricuspid valve, the shape of the section is different from sections from other preparations (Figs. 3.4 and 3.5) when freezing a preparation, tissue sometimes underwent folding. Fig. 4.6C shows a neighbouring section double labelled for Cx43 and ANP and the labelling pattern is similar to that from the main preparation (panel B in Figs. 4.1 to 4.5). Fig. 4.7 shows a Masson's trichrome stained section and a neighbouring section double labelled for Cx43 and ANP at level 2 (posterior/inferior nodal extension) in the second preparation and the tissue architecture and the labelling pattern are similar as shown in Fig. 4.6.

4.3.2. Open node

Figs. 4.8 to 4.10 show immunolabelling of immunohistochemical markers in the open node in sections at levels 6 to 8 of the main preparation (Fig. 2.1B). The open node, ringed in yellow, is located above the ventricular myocardium and fibrous annulus (or tricuspid valve), outlined in white, and beneath the atrial myocardium (Figs. 4.8 to 4.10). The atrial myocardium

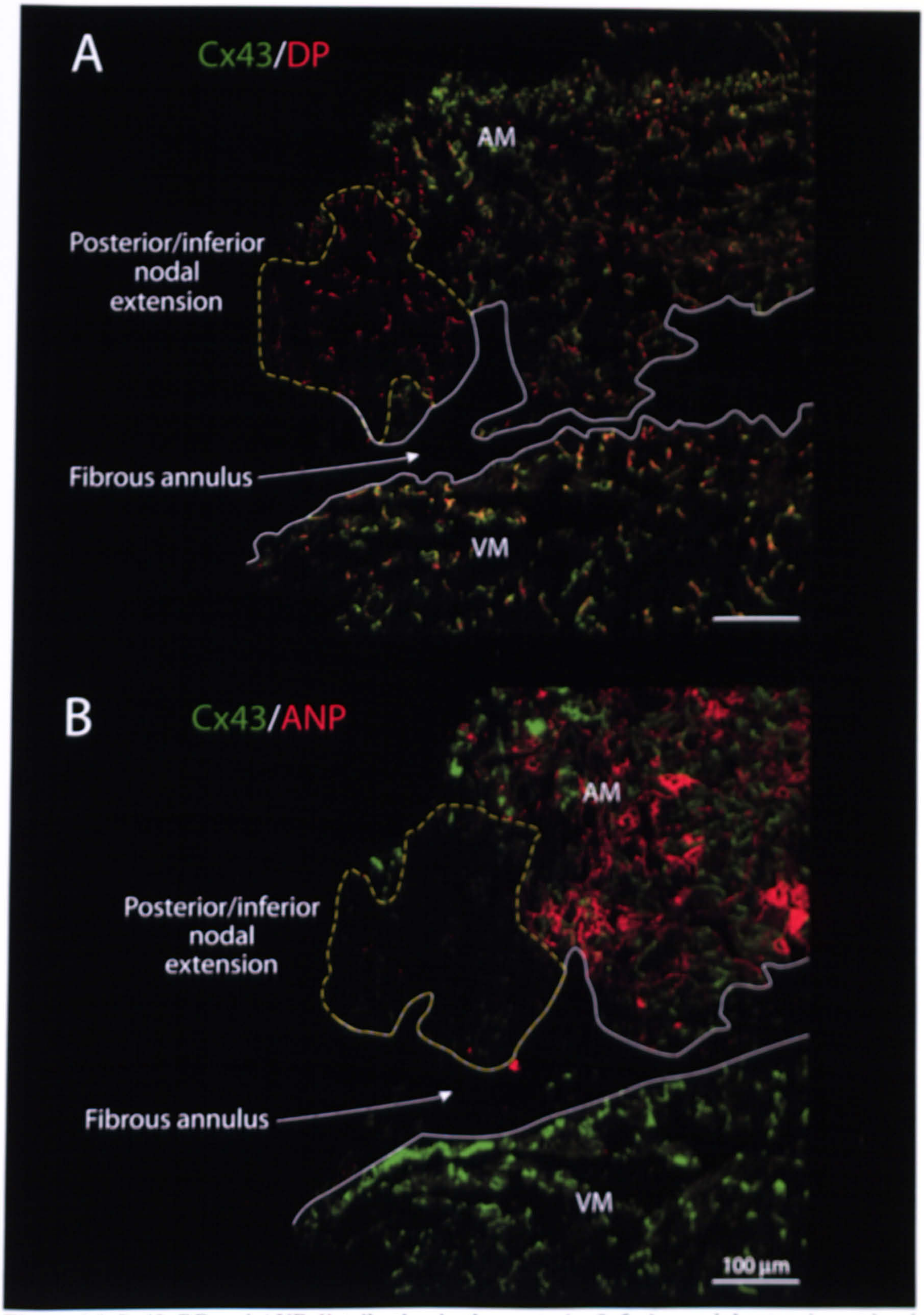

Figure 4.1 Cx43, DP and ANP distribution in the posterior/inferior nodal extension at level 1 in the main preparation studied (Fig. 2.1B)

A, montage of section double labelled for Cx43 (green) and DP (red). B, montage of adjacent section double labelled for Cx43 (green) and ANP (red). AM, atrial myocardium; VM, ventricular myocardium. Scale bars, 100 µm.

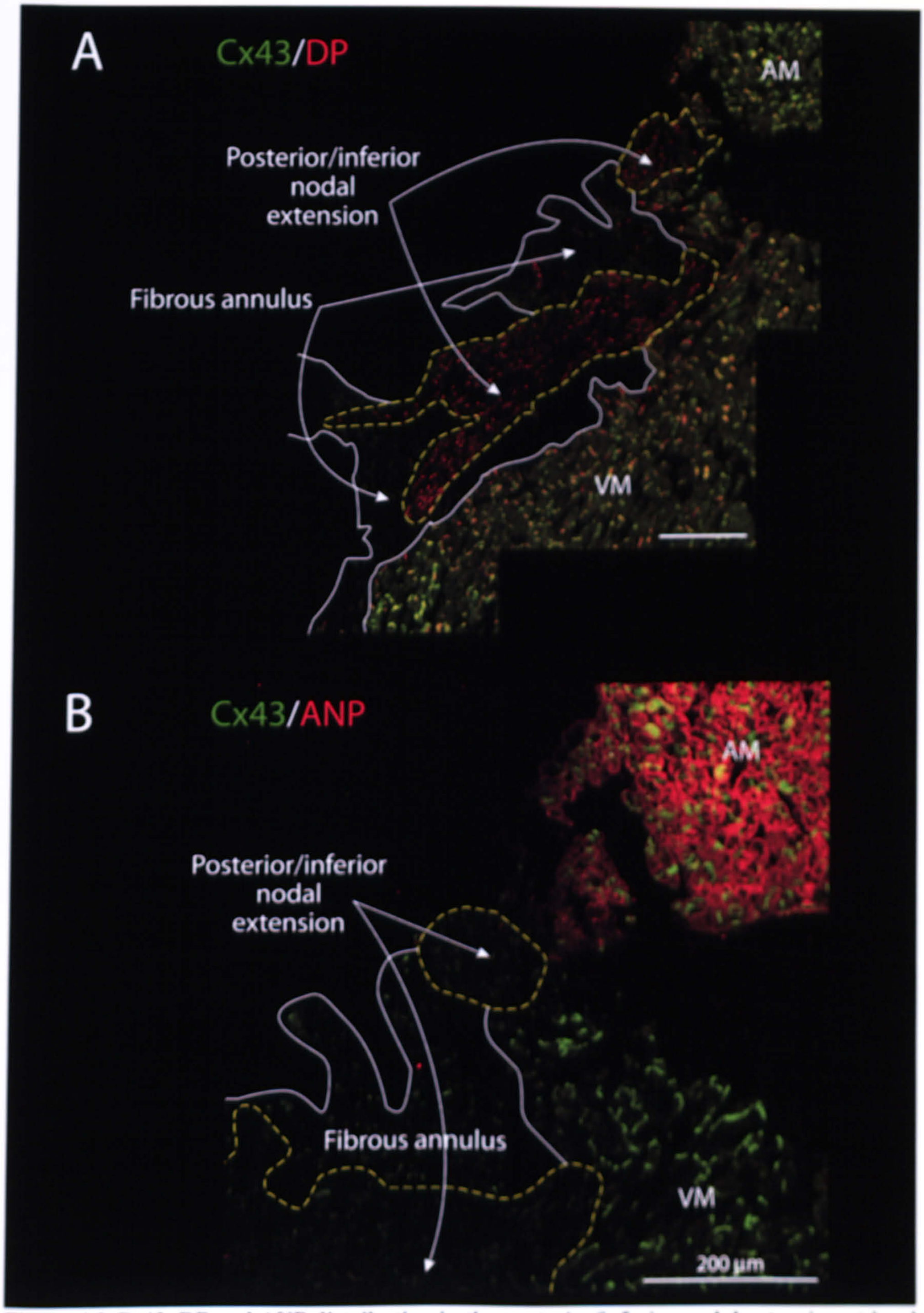

Figure 4.2 Cx43, DP and ANP distribution in the posterior/inferior nodal extension at level 2 in the main preparation studied (Fig. 2.1B)

A, montage of section double labelled for Cx43 (green) and DP (red). B, montage of adjacent section double labelled for Cx43 (green) and ANP (red). The posterior/inferior nodal extension was divided into two at this level. AM, atrial myocardium; VM, ventricular myocardium. Scale bars, 200 µm.

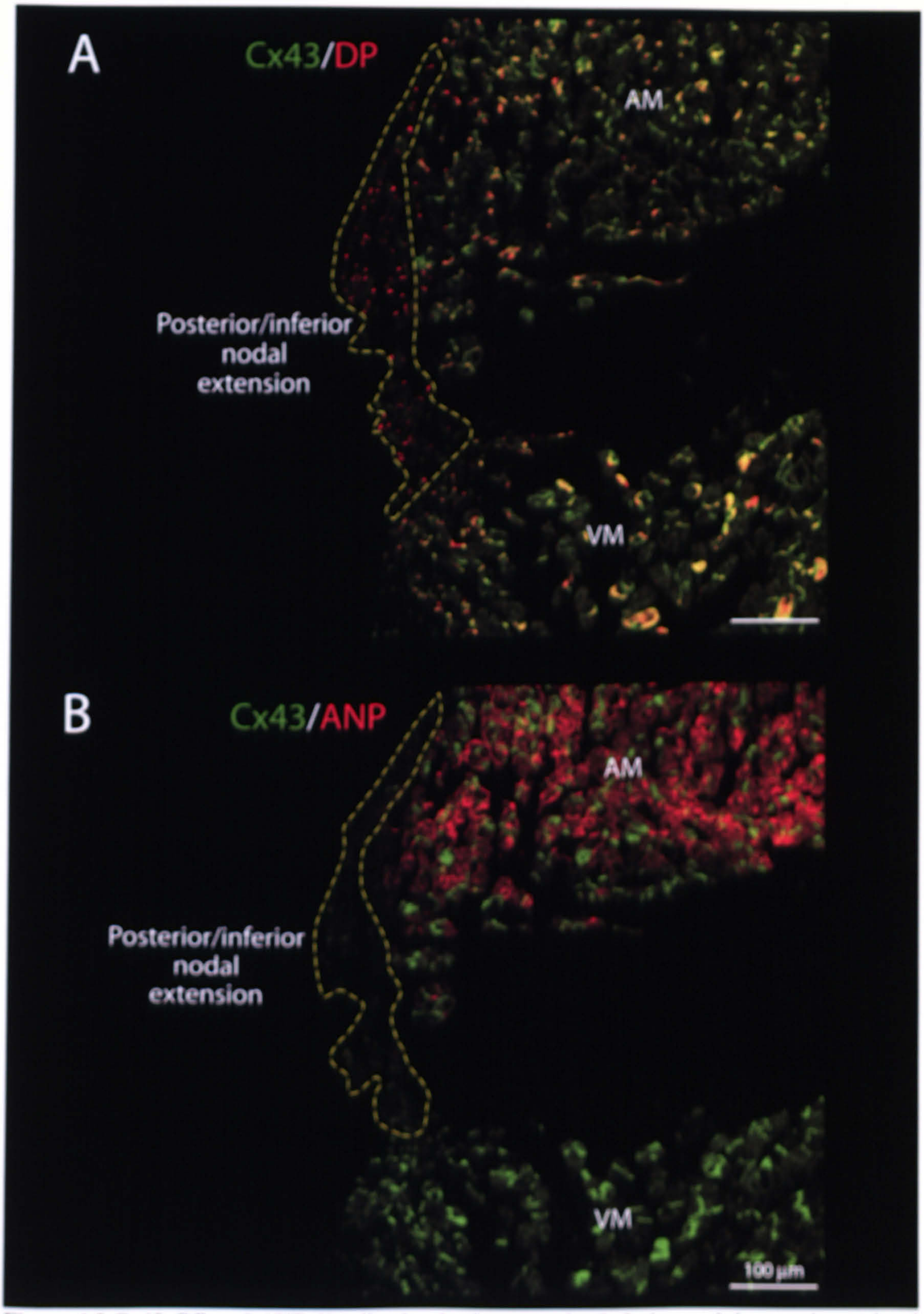

Figure 4.3 Cx43, DP and ANP distribution in the posterior/inferior nodal extension at level 3 in the main preparation studied (Fig. 2.1B)

A, montage of section double labelled for Cx43 (green) and DP (red). B, montage of adjacent section double labelled for Cx43 (green) and ANP (red). AM, atrial myocardium; VM, ventricular myocardium. Scale bars, 100 µm.

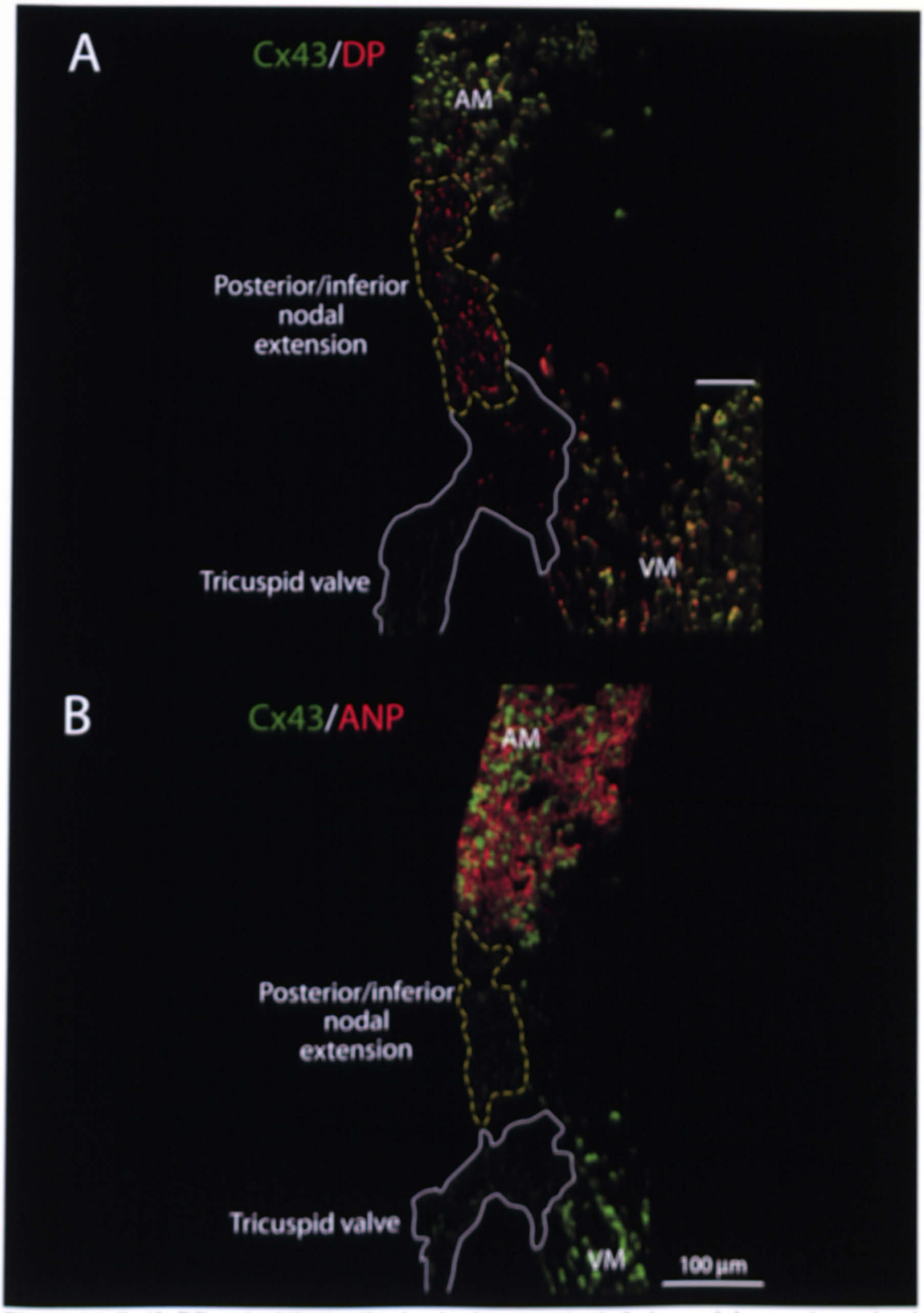

Figure 4.4 Cx43, DP and ANP distribution in the posterior/inferior nodal extension at level 4 in the main preparation studied (Fig. 2.1B)

A, montage of section double labelled for Cx43 (green) and DP (red). B, montage of adjacent section double labelled for Cx43 (green) and ANP (red). AM, atrial myocardium; VM, ventricular myocardium. Scale bars, 100 µm.

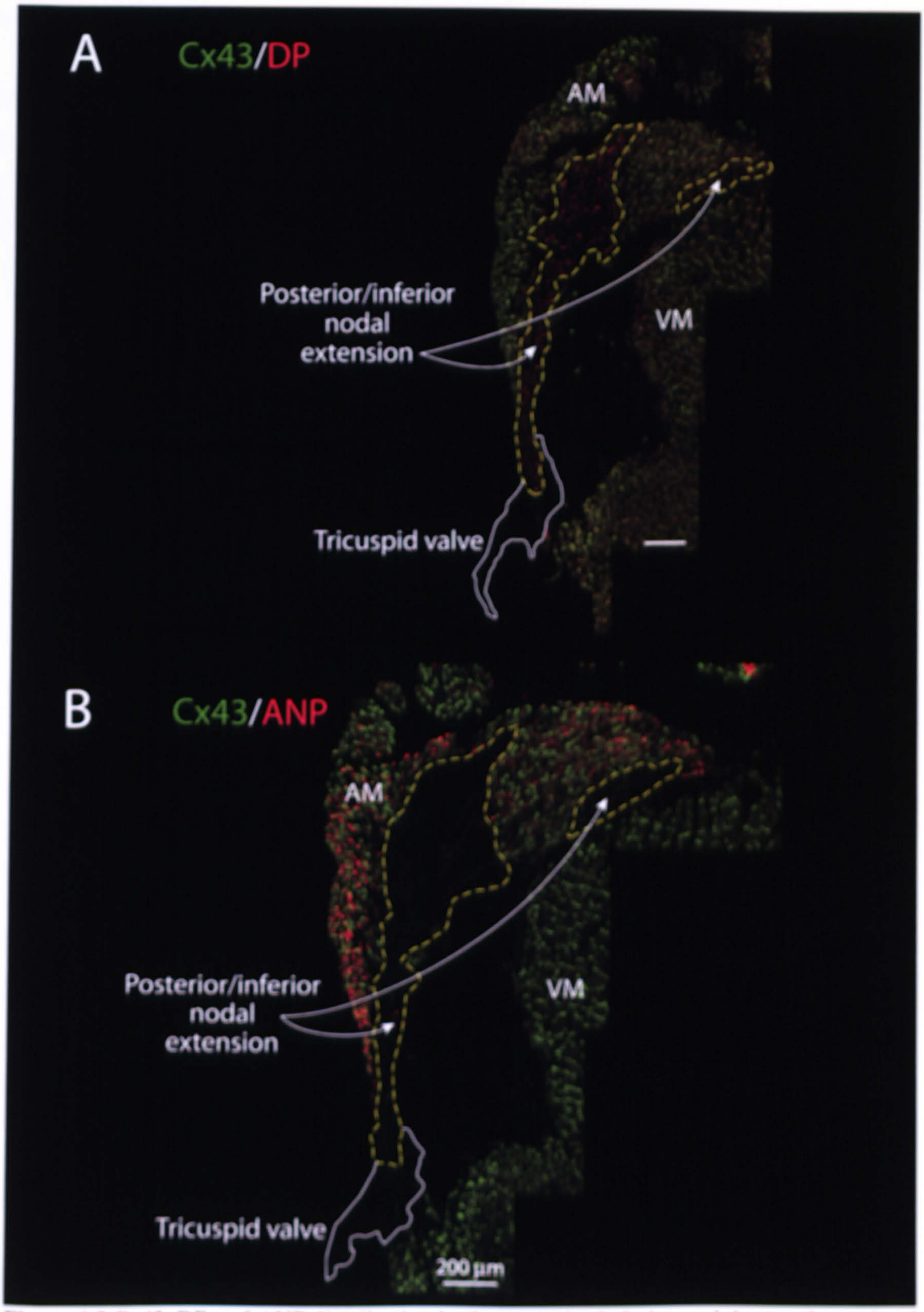

Figure 4.5 Cx43, DP and ANP distribution in the posterior/inferior nodal extension at level 5 in the main preparation studied (Fig. 2.1B)

A, montage of section double labelled for Cx43 (green) and DP (red). B, montage of adjacent section double labelled for Cx43 (green) and ANP (red). The posterior/inferior nodal extension was again divided into two at this level. AM, atrial myocardium; VM, ventricular myocardium. Scale bars, 200 µm.

Figure 4.6 Cx43 and ANP distribution in the posterior/inferior nodal extension at level 1 in the second preparation

A, AV node preparation. Numbers indicate the position of each level. Labels show landmarks. B, Masson's trichrome staining of section at level 1. C, adjacent section double labelled for Cx43 (green) and ANP (red); field of view corresponds to framed area shown in A. A, anterior; AM, atrial myocardium; CS, coronary sinus; I, inferior; P, posterior; S, superior; VM, ventricular myocardium. Scale bars, 1 mm (A and B) and 100 μm (C).

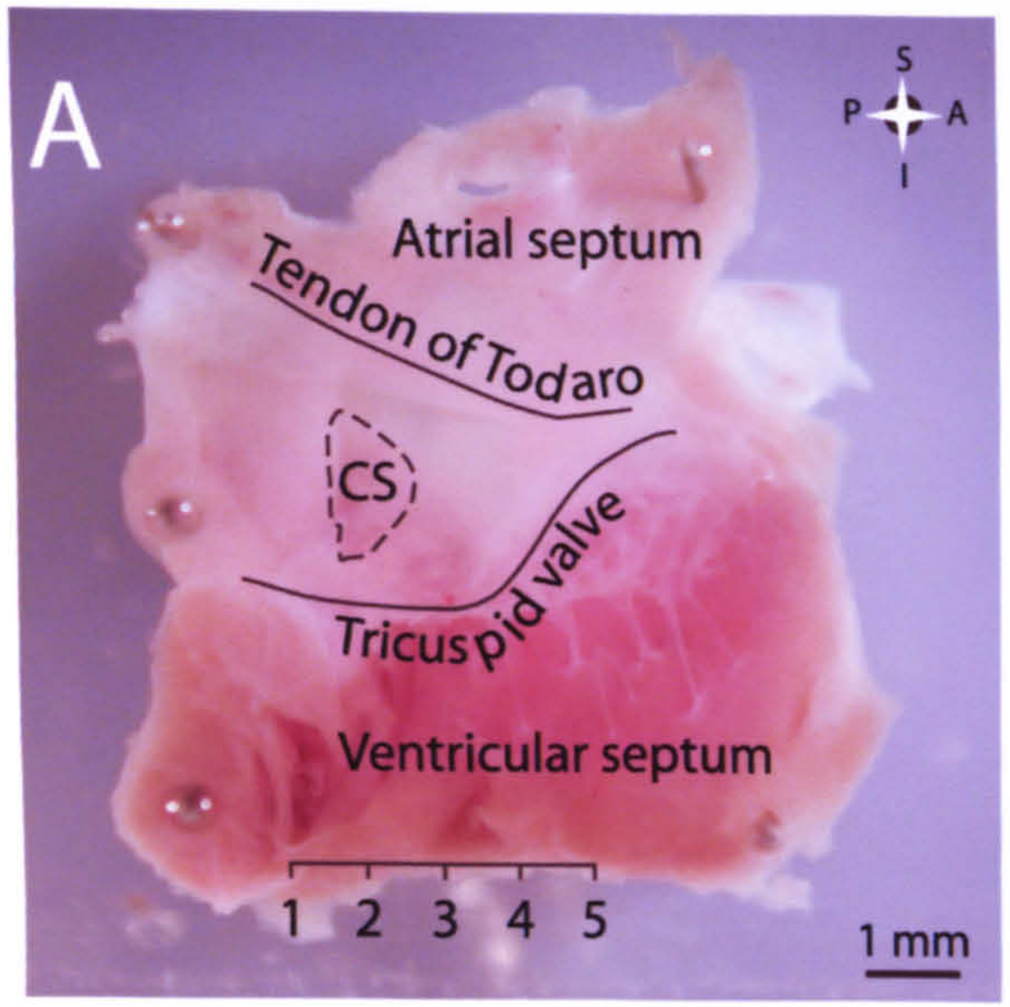
A
S
P
A
I
Atrial septum
Tendon of Todaro
CS
Tricuspid valve
Ventricular septum
1 2 3 4 5
1 mm

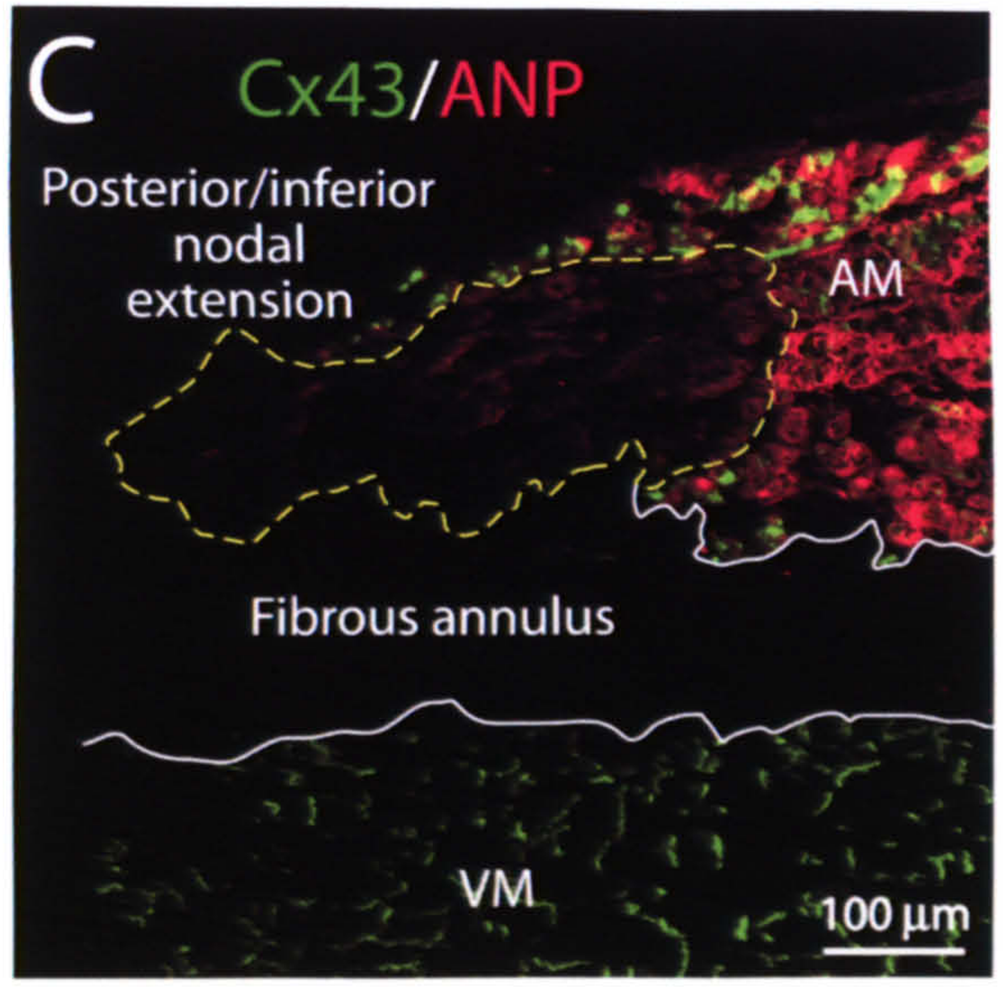
C
Cx43/ANP
Posterior/inferior
nodal
extension
AM
Fibrous annulus
VM
100 µm

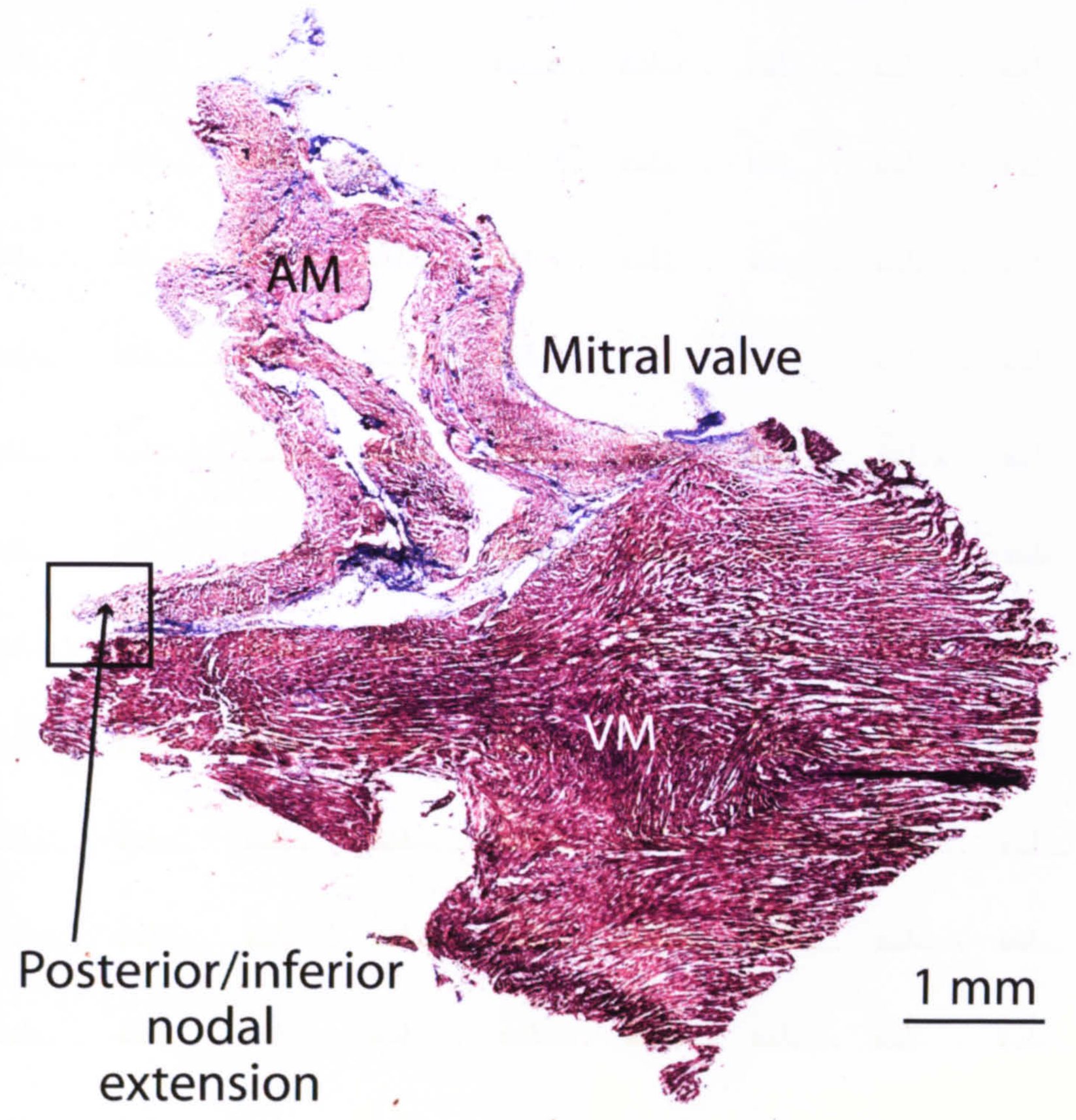
B
AM
Mitral valve
VM
Posterior/inferior
nodal
extension
1 mm

Figure 4.7 Cx43 and ANP distribution in the posterior/inferior nodal extension at level 2 in the second preparation (Fig. 4.6A)

A, Masson's trichrome staining of section at level 2. B, adjacent section double labelled for Cx43 (green) and ANP (red); field of view corresponds to framed area shown in A. AM, atrial myocardium; VM, ventricular myocardium. Scale bars, 1 mm (A) and 100 μm (B).

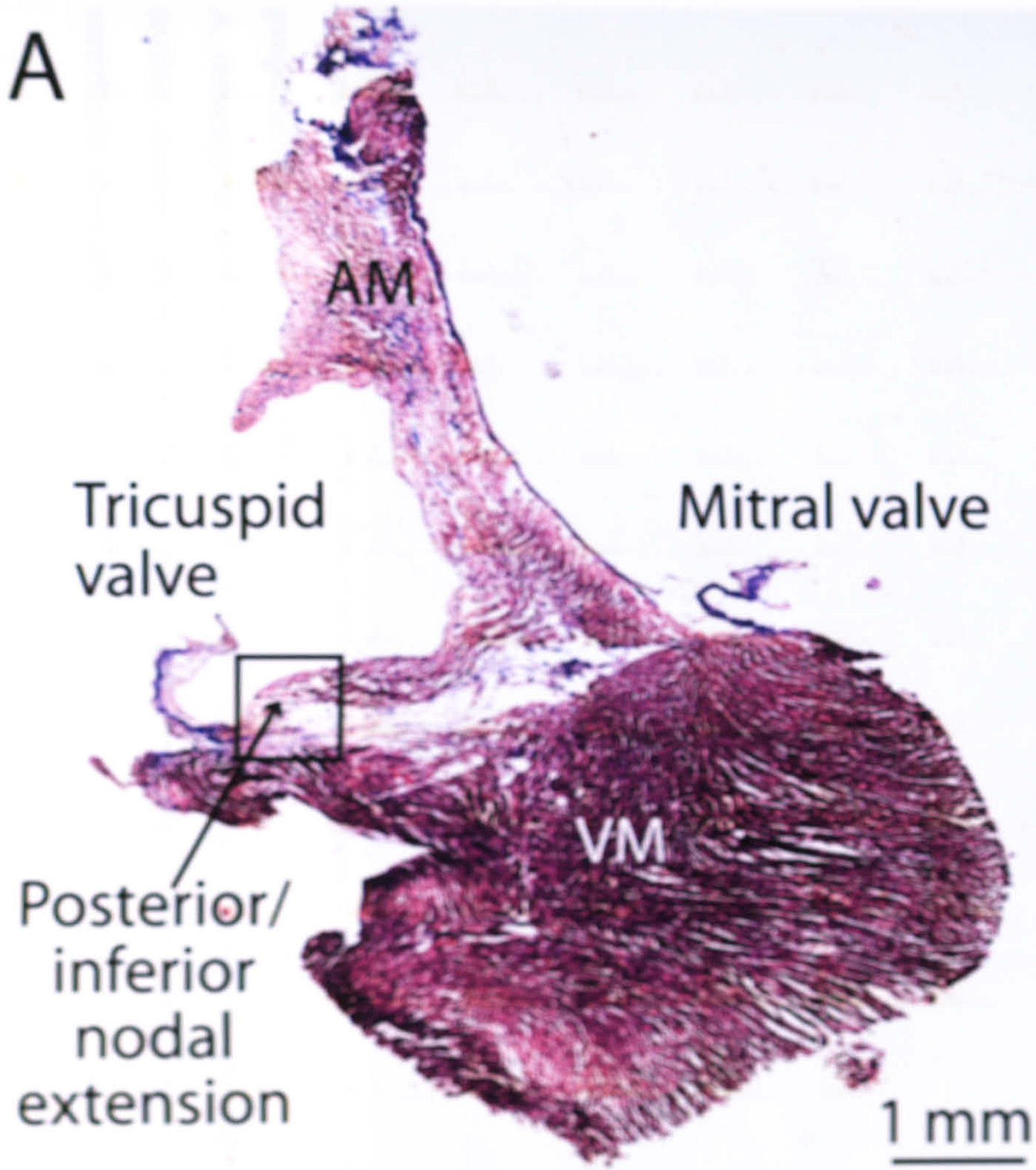
A
AM
Tricuspid valve
Mitral valve
VM
Posterior/ inferior nodal extension
1 mm

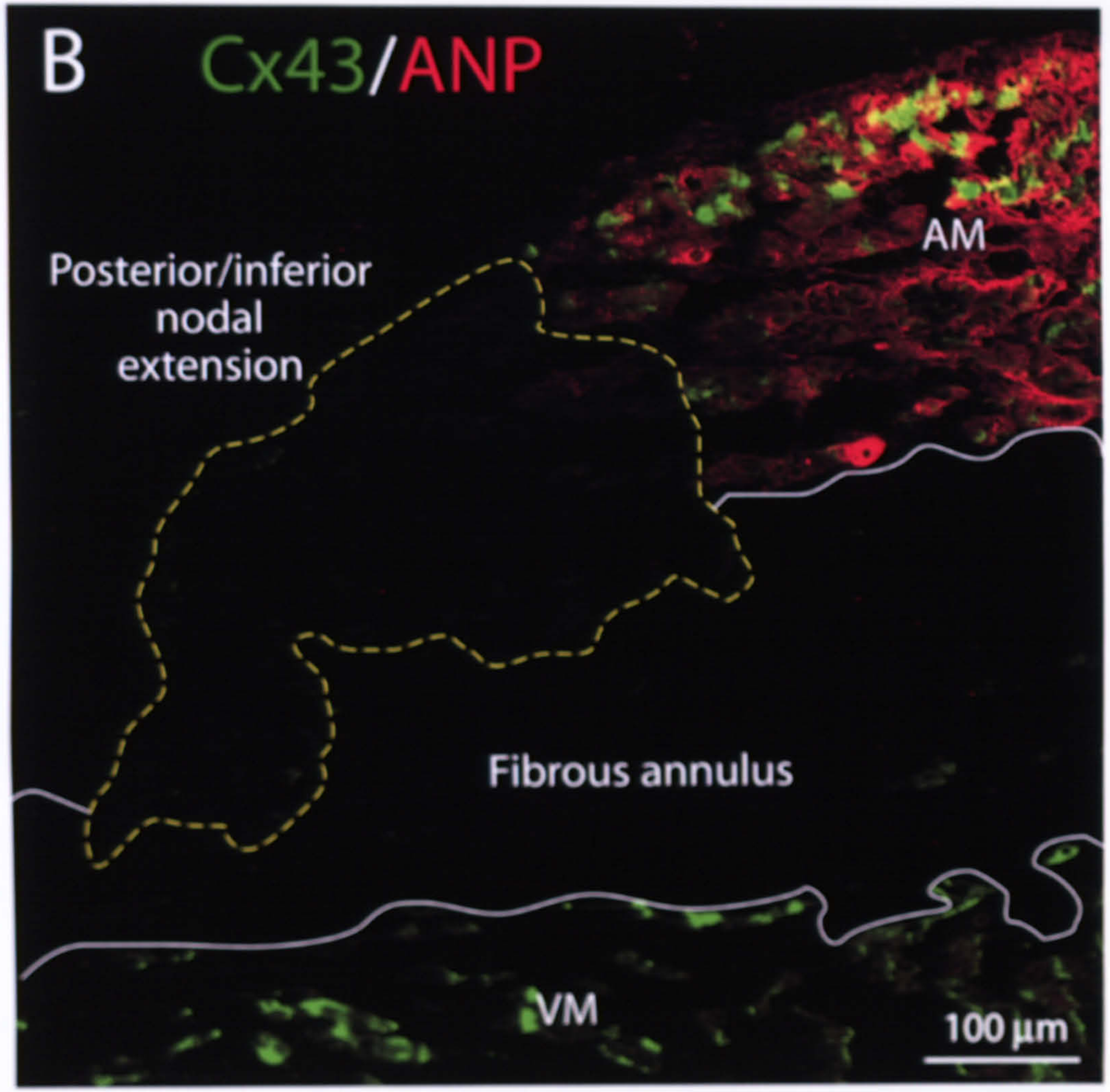
B
Cx43/ANP
AM
Posterior/inferior nodal extension
Fibrous annulus
VM
100 µm

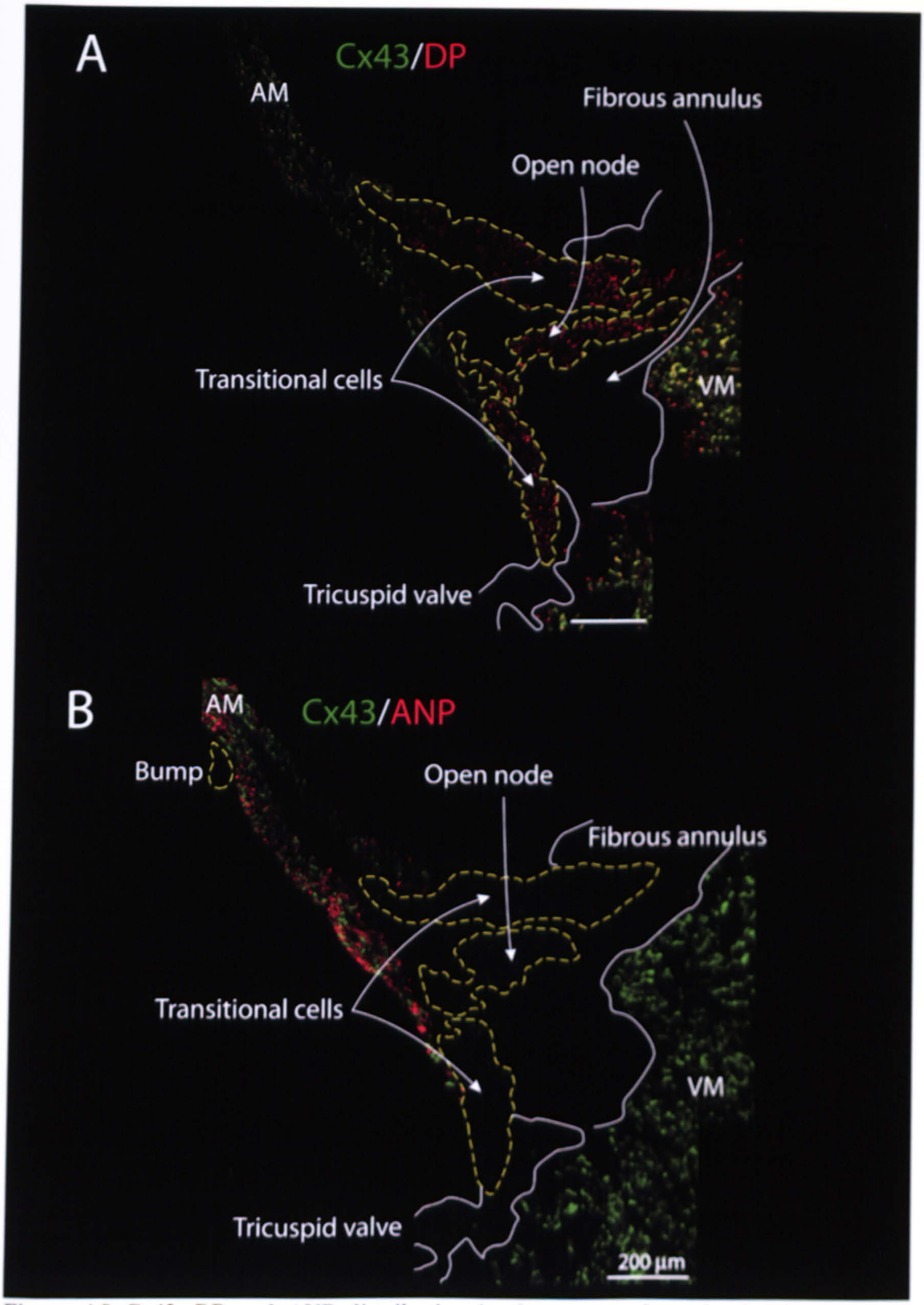

Figure 4.8 Cx43, DP and ANP distribution in the open node at level 6 in the main preparation studied (Fig. 2.1B)

A, montage of section double labelled for Cx43 (green) and DP (red). B, montage of adjacent section double labelled for Cx43 (green) and ANP (red). AM, atrial myocardium; VM, ventricular myocardium. Scale bars, 200 µm.

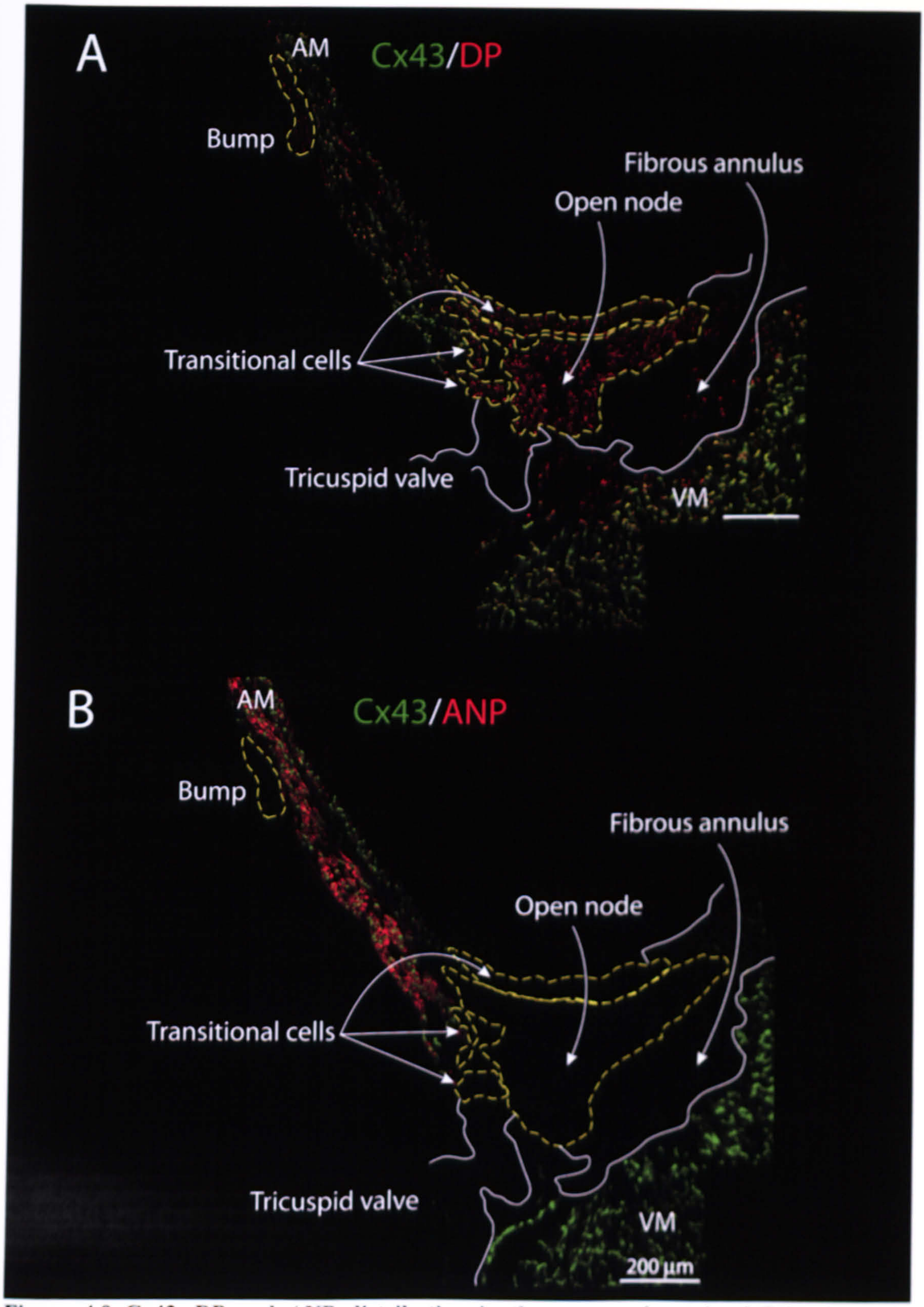

Figure 4.9 Cx43, DP and ANP distribution in the open node at level 7 in the main preparation studied (Fig. 2.1B)

A, montage of section double labelled for Cx43 (green) and DP (red). B, montage of adjacent section double labelled for Cx43 (green) and ANP (red). AM, atrial myocardium; VM, ventricular myocardium. Scale bars, 200 µm.

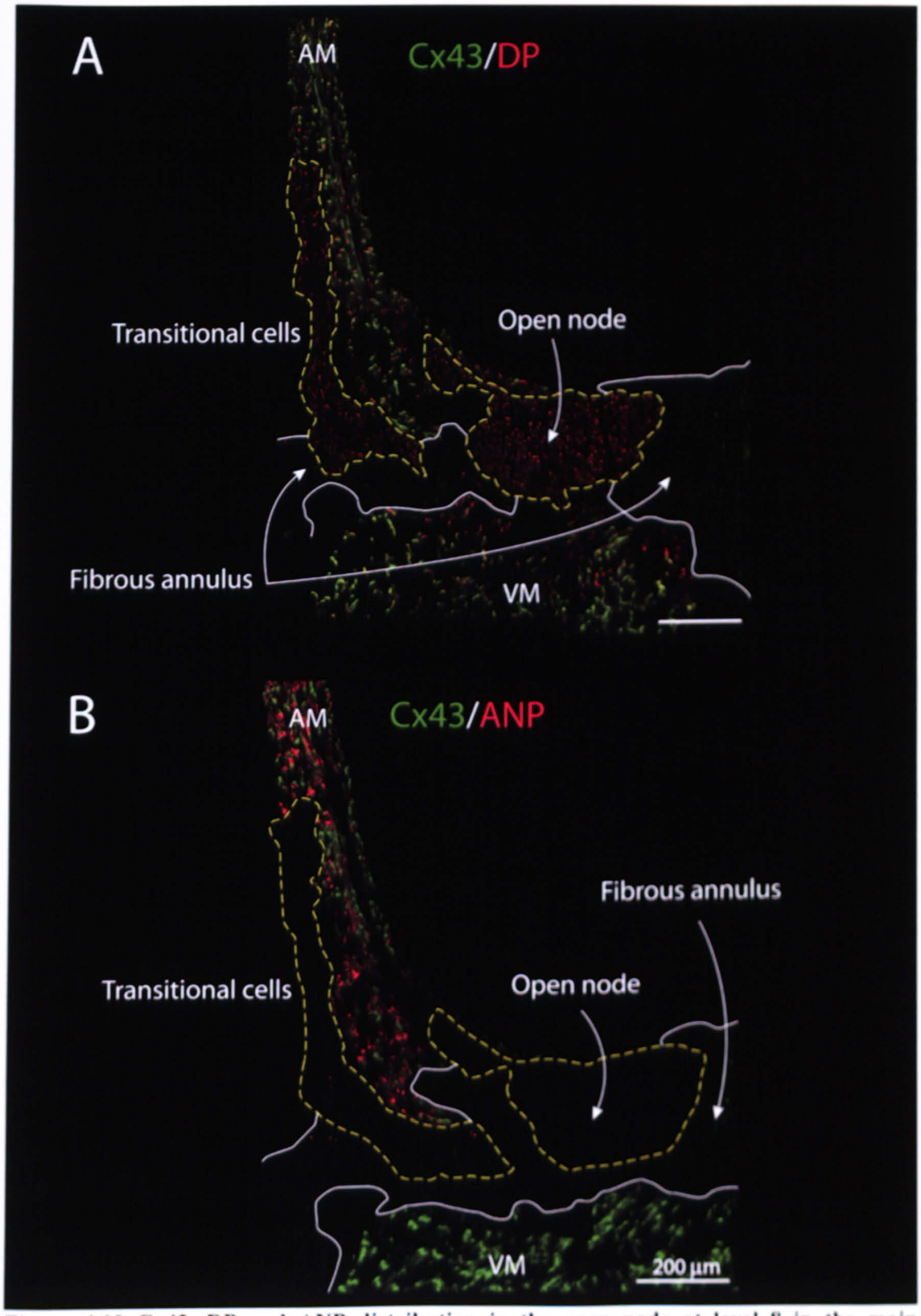

Figure 4.10 Cx43, DP and ANP distribution in the open node at level 8 in the main preparation studied (Fig. 2.1B)

A, montage of section double labelled for Cx43 (green) and DP (red). B, montage of adjacent section double labelled for Cx43 (green) and ANP (red). AM, atrial myocardium; VM, ventricular myocardium. Scale bars, 200 µm.

showed co-localisation of Cx43 and DP at intercalated disks and intracellular ANP labelling (Figs. 4.8 to 4.10). The open node showed DP labelling only at intercalated disks (Figs. 4.8 to 4.10). The fibrous annulus did not show fluorescence above background (Figs. 4.8 to 4.10). The ventricular myocardium showed co-localisation of Cx43 and DP at intercalated disks as in the atrial myocardium (Figs. 4.8 to 4.10). In summary, the open node is Cx43-negative, DP-positive and ANP-negative like the posterior/inferior nodal extension and can be distinguished from the surrounding atrial myocardium, fibrous annulus and ventricular myocardium. In addition to the nodal myocytes of the open node, nodal-like myocytes existed in two other separated regions, above the open node (Figs 4.8A and 4.9) and above the tricuspid valve (Figs. 4.8 to 4.10). These two regions will be referred to as the "bump" (Figs 4.8B and 4.9) and the zone of the transitional cells (Figs. 4.8 to 4.10). The open node, the collection of the cells in the "bump" and the transitional cells show the same immunolabelling by Cx43, DP and ANP (Figs. 4.8 to 4.10). The zone of transitional cells and the open node are not physically connected (Figs. 4.8 to 4.10). The definition and boundary of transitional cells will be given in the following chapters, which are concerned with Na^+ channel expression in the AV node junctional area. Fig. 4.11 shows double labelling of Cx43 and ANP of the open node at level 3 of the second preparation (Fig. 4.6A). The pattern of labelling of Cx43 and ANP is similar to that shown in panel B in Figs. 4.8 to 4.10.

4.3.3. Enclosed node

Figs. 4.12 and 4.13 show immunolabelling of the immunohistochemical markers in the enclosed node in sections at levels 9 and 10 of the main preparation (Fig. 2.1B). The enclosed node, ringed in yellow, is located above the ventricular myocardium and fibrous annulus (or tricuspid valve), outlined in white, and beneath the atrial myocardium (Figs. 4.12 and 4.13). The atrial myocardium showed co-localisation of Cx43 and DP at intercalated disks and intracellular ANP labelling (Figs. 4.12 and 4.13). The enclosed node showed DP labelling only at intercalated disks (Figs. 4.12 and 4.13). The fibrous annulus did not show fluorescence above background (Figs. 4.12 and 4.13). The ventricular myocardium showed co-localisation of Cx43 and DP at intercalated disks as in the atrial myocardium (Figs. 4.12 and 4.13). In summary, the enclosed node is Cx43-negative, DP-positive and ANP-negative like the posterior/inferior nodal extension and the open node and can be distinguished from the surrounding atrial myocardium, fibrous annulus and ventricular myocardium. The zone of the transitional cells again existed above the tricuspid valve (Figs. 4.12 to 4.13), but the bump had disappeared. Fig. 4.14 shows double labelling of Cx43 and ANP of the enclosed node at level 4 of the second preparation (shown in Fig. 4.6A). The pattern of labelling of Cx43 and ANP is similar to that shown in panel B in Figs. 4.12 and 4.13.

4.3.4. Common bundle

Figure 4.11 Cx43 and ANP distribution in the open node at level 3 in the second preparation (Fig. 4.6A)

Section double labelled for Cx43 (green) and ANP (red) shown. AM, atrial myocardium; VM, ventricular myocardium.

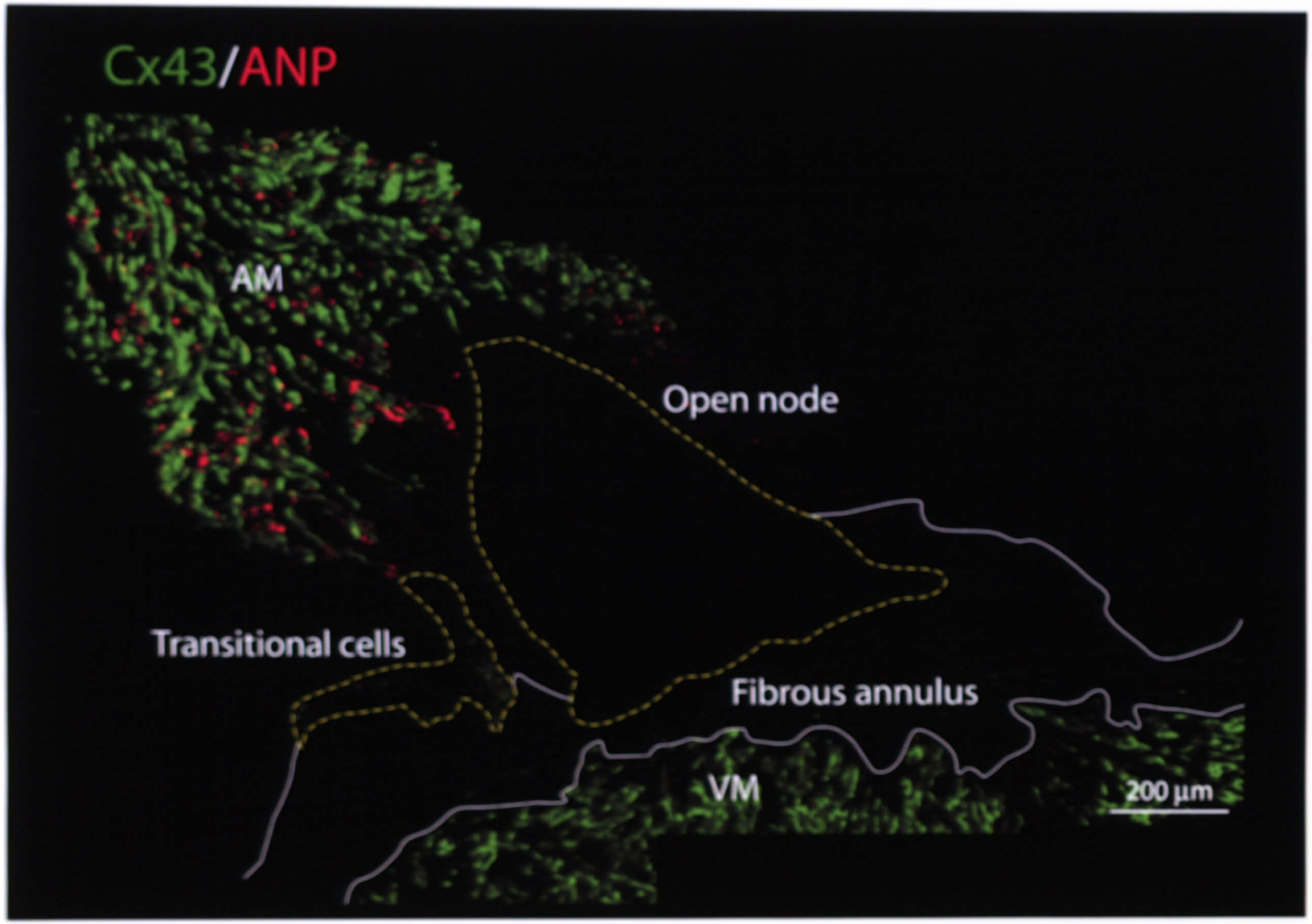
Cx43/ANP
AM
Open node
Transitional cells
Fibrous annulus
VM
200 µm

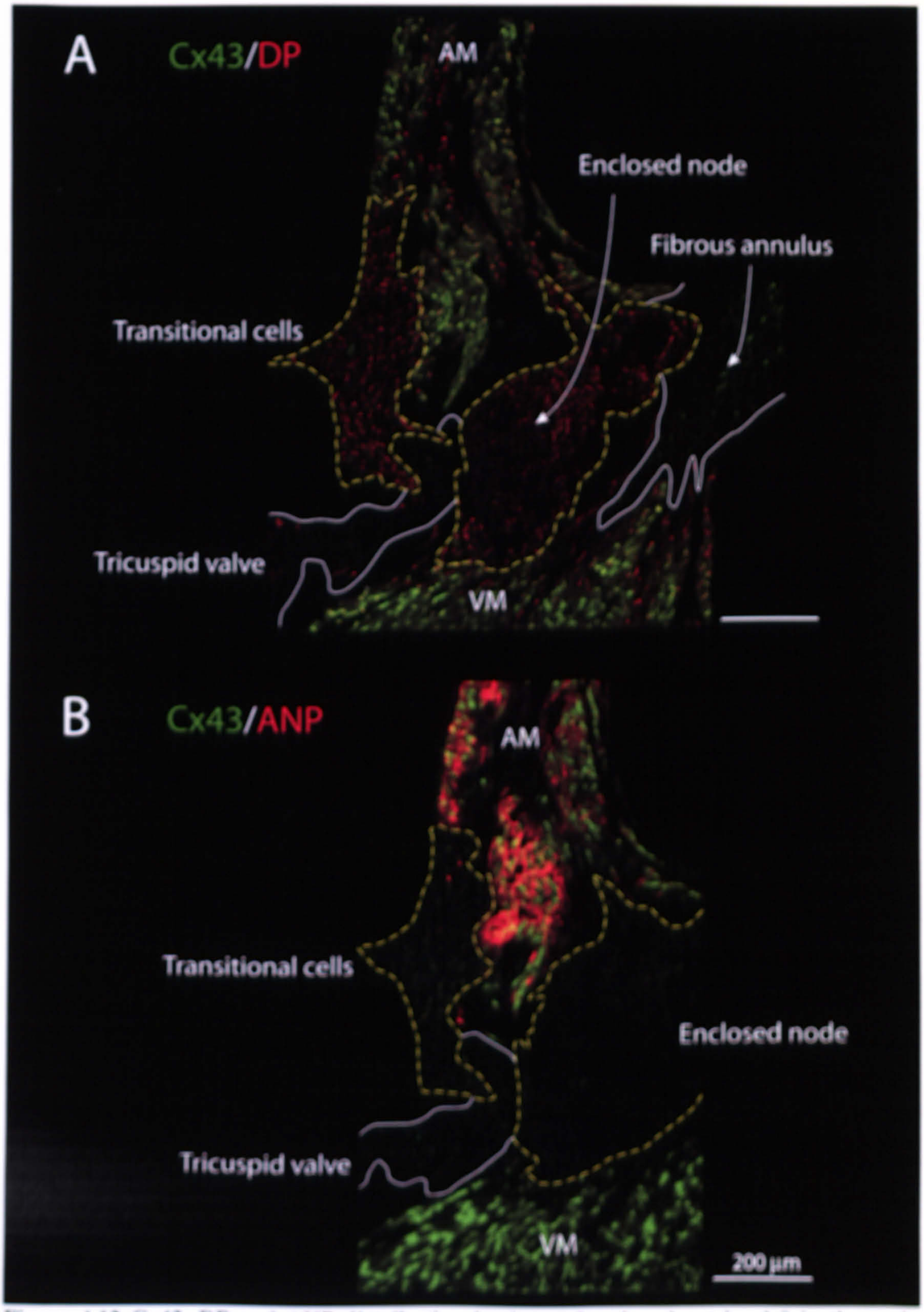

Figure 4.12 Cx43, DP and ANP distribution in the enclosed node at level 9 in the main preparation studied (Fig. 2.1B)

A, montage of section double labelled for Cx43 (green) and DP (red). B, montage of adjacent section double labelled for Cx43 (green) and ANP (red). AM, atrial myocardium; VM, ventricular myocardium. Scale bars, 200 µm.

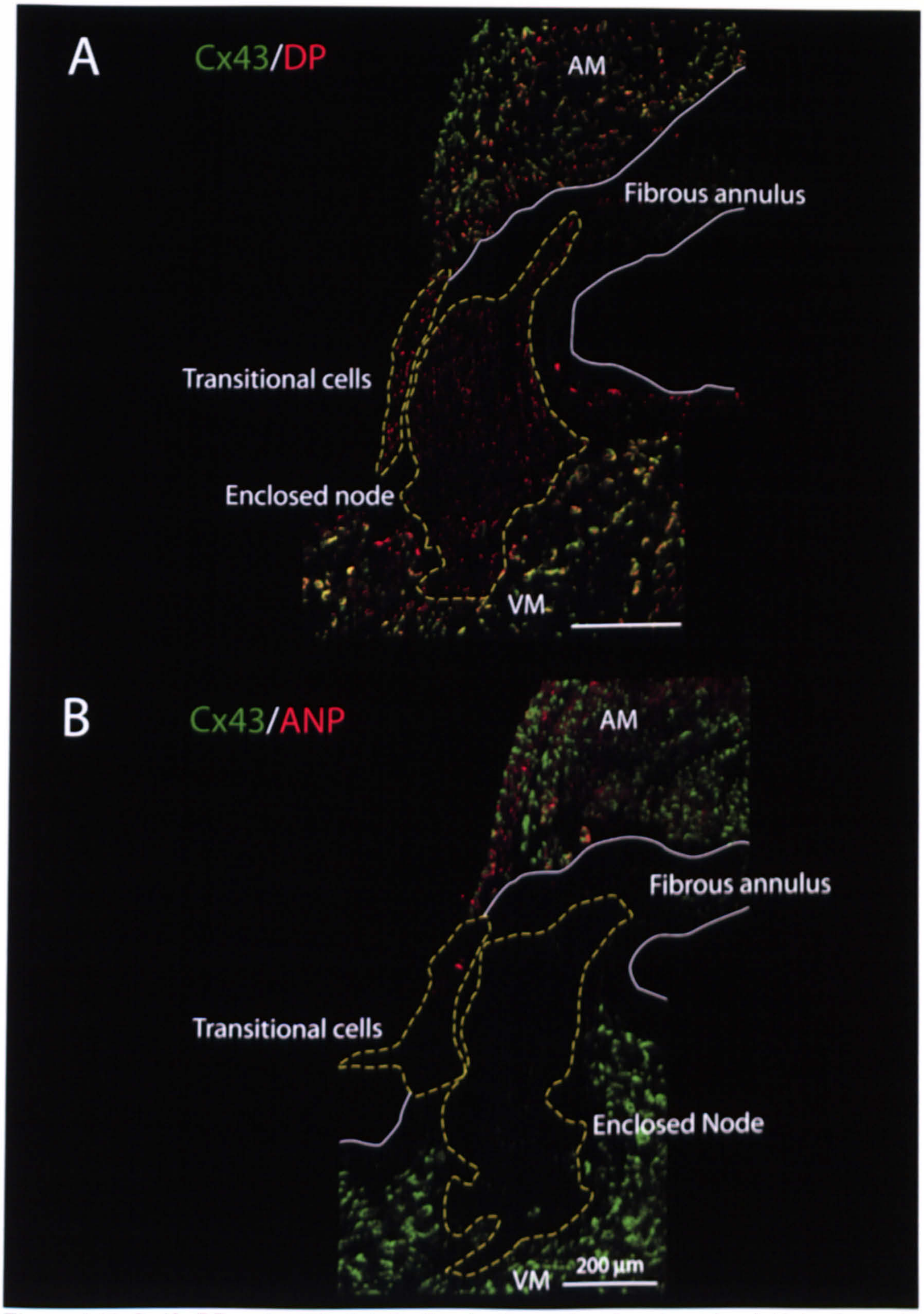

Figure 4.13 Cx43, DP and ANP distribution in the enclosed node at level 10 in the main preparation studied (Fig. 2.1B)

A, montage of section double labelled for Cx43 (green) and DP (red). B, montage of adjacent section double labelled for Cx43 (green) and ANP (red). AM, atrial myocardium; VM, ventricular myocardium. Scale bars, 200 µm.

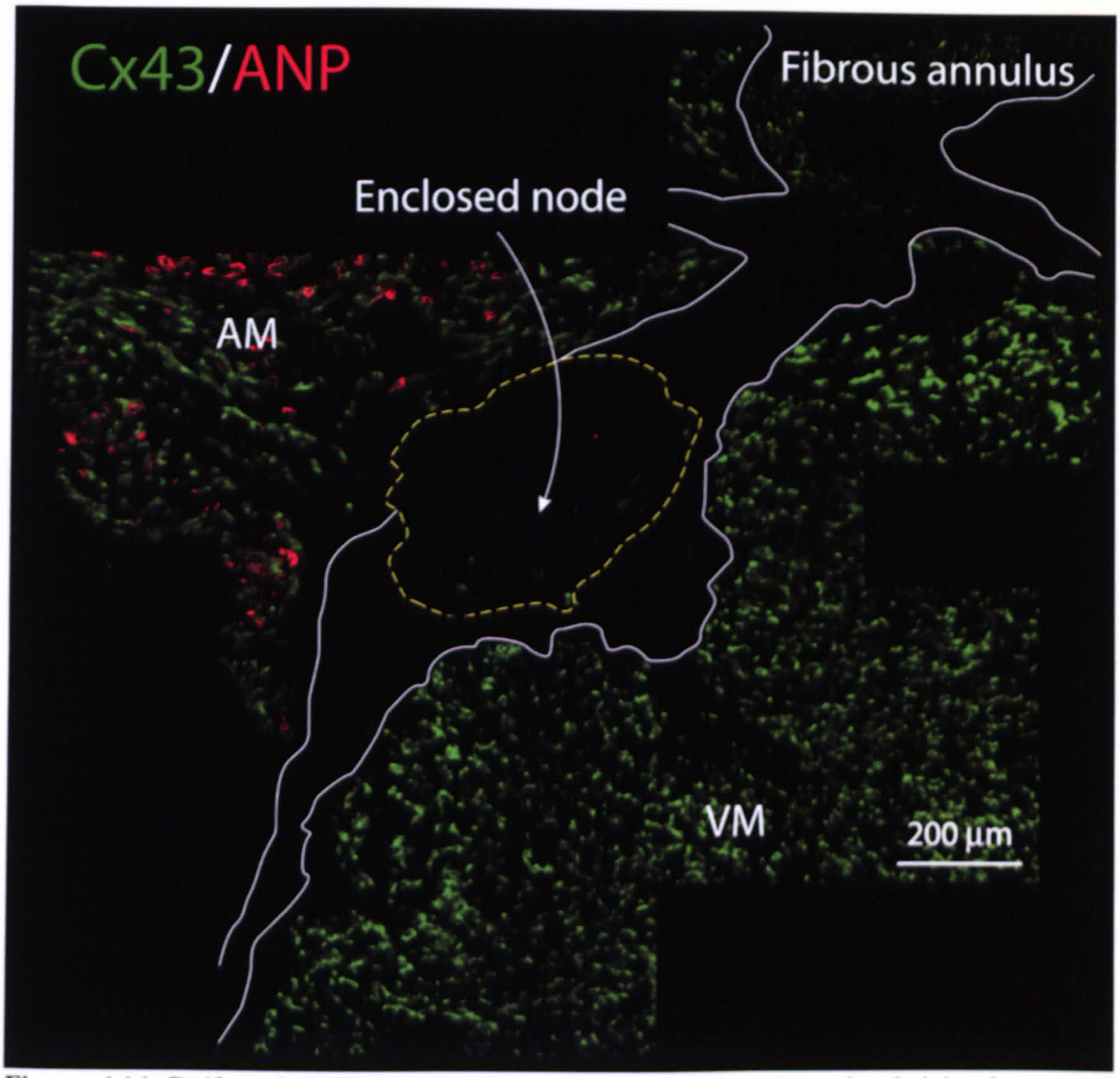

Figure 4.14 Cx43 and ANP distribution in the enclosed node at level 4 in the second preparation (Fig. 4.6A)

Section double labelled for Cx43 (green) and ANP (red) shown. AM, atrial myocardium; VM, ventricular myocardium.

Figs. 4.15 and 4.16 show immunolabelling of the immunohistochemical markers in the common bundle in sections at levels 11 and 12 of the main preparation (Fig. 2.1B). The common bundle, ringed in yellow, is located above the ventricular myocardium and fibrous annulus (or tricuspid valve), outlined in white, and beneath the atrial myocardium (Figs. 4.15 and 4.16). The atrial myocardium showed co-localisation of Cx43 and DP at intercalated disks and intracellular ANP labelling (Figs. 4.15 and 4.16). The common bundle showed DP labelling only at intercalated disks (Figs. 4.15 and 4.16). The fibrous annulus did not show fluorescence above background (Figs. 4.15 and 4.16). The ventricular myocardium showed co-localisation of Cx43 and DP at intercalated disks as in the atrial myocardium (Figs. 4.15 and 4.16). In summary, the common bundle is Cx43-negative, DP-positive and ANP-negative like the posterior/inferior nodal extension, the open node and the enclosed node and can be distinguished from the surrounding atrial myocardium, fibrous annulus and ventricular myocardium. In addition to the myocytes of the common bundle, nodal-like myocytes existed in two other separate regions, i.e. the zone of transitional cells and the termination of the AV ring bundle (Figs. 4.15 and 4.16). The transitional cells again existed above the tricuspid valve as at previous levels (Figs. 4.12 and 4.13). The termination of the AV ring bundle was located above the common bundle and was separated from it by the zone of transitional cells and atrial myocardium (Figs. 4.15 and 4.16). Fig. 4.17 shows double labelling of Cx43 and ANP of the common bundle at level 5 of the second preparation (Fig. 4.6A). The pattern of labelling of Cx43 and ANP in the common bundle, the zone of transitional cells and the termination of the AV ring bundle is the same as in the main preparation. In addition to these regions, nodal-like myocytes also existed in the left bundle branch (Fig. 4.17). It is noteworthy that some myocytes of the left bundle branch express ANP (Fig. 4.17).

4.3.5. Termination of the AV ring bundle

Figs. 4.18 and 4.19 show immunolabelling of the immunohistochemical markers in the termination of the AV ring bundle in sections at levels 13 and 14 of the main preparation (Fig. 2.1B). The termination of the AV ring bundle, ringed in yellow, is located at the AV junction (Figs. 4.18 and 4.19). Note that at levels 13 and 14 the common bundle can no longer be seen. The atrial myocardium showed co-localisation of Cx43 and DP at intercalated disks and intracellular ANP labelling (Figs. 4.18 and 4.19). The termination of the AV ring bundle showed DP labelling only at intercalated disks (Figs. 4.18 and 4.19). The fibrous annulus did not show fluorescence above background (Figs. 4.18 and 4.19). The ventricular myocardium showed co-localisation of Cx43 and DP at intercalated disks as in the atrial myocardium (Figs. 4.18 and 4.19). In summary, the termination of the AV ring bundle is Cx43-negative, DP-positive and ANP-negative like the posterior/inferior nodal extension, the open node, the enclosed node and the common bundle and can be distinguished from the surrounding atrial and ventricular myocardium.

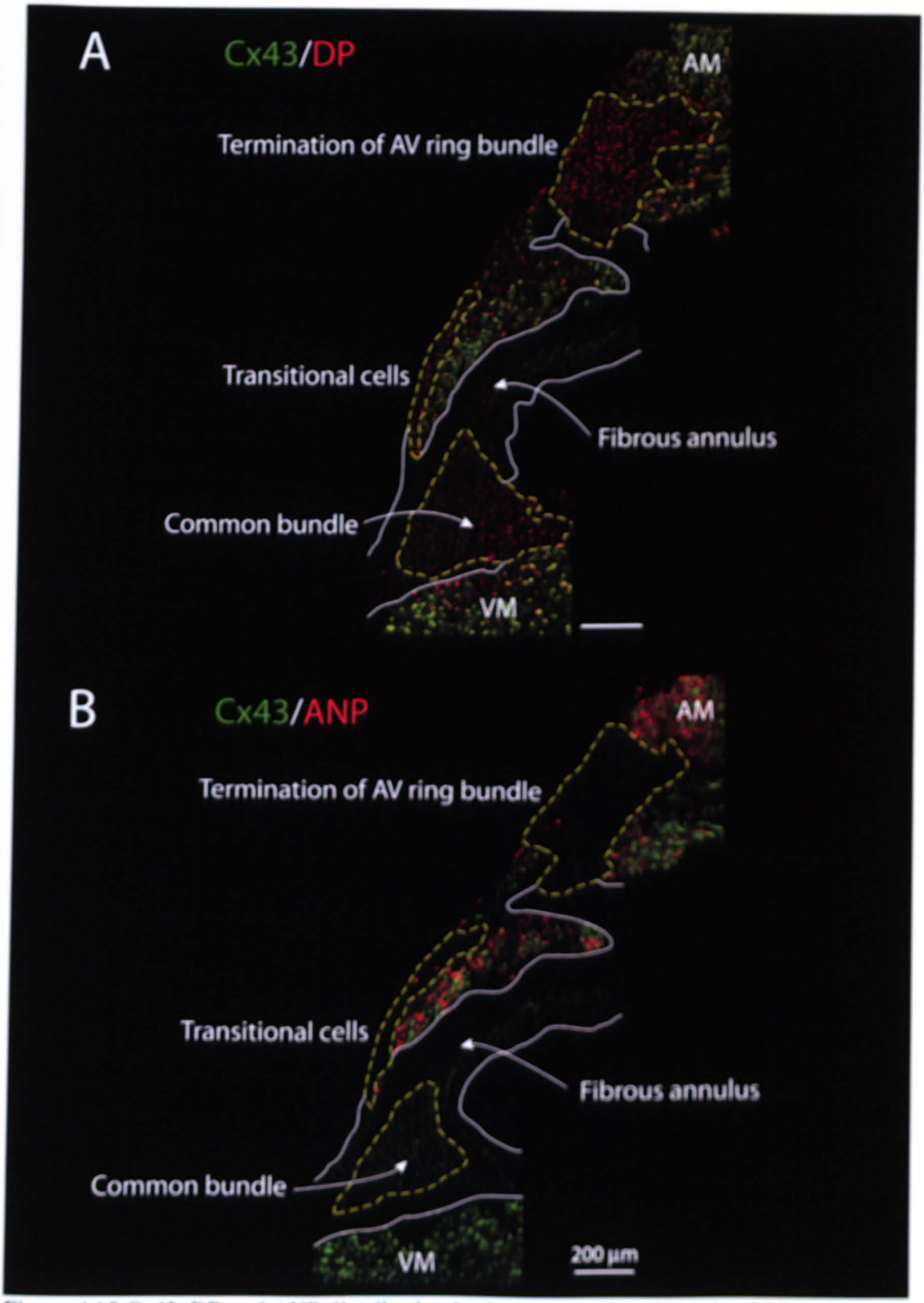

Figure 4.15 Cx43, DP and ANP distribution in the common bundle at level 11 in the main preparation studied (Fig. 2.1B)

A, montage of section double labelled for Cx43 (green) and DP (red). B, montage of adjacent section double labelled for Cx43 (green) and ANP (red). AM, atrial myocardium; VM, ventricular myocardium. Scale bars, 200 µm.

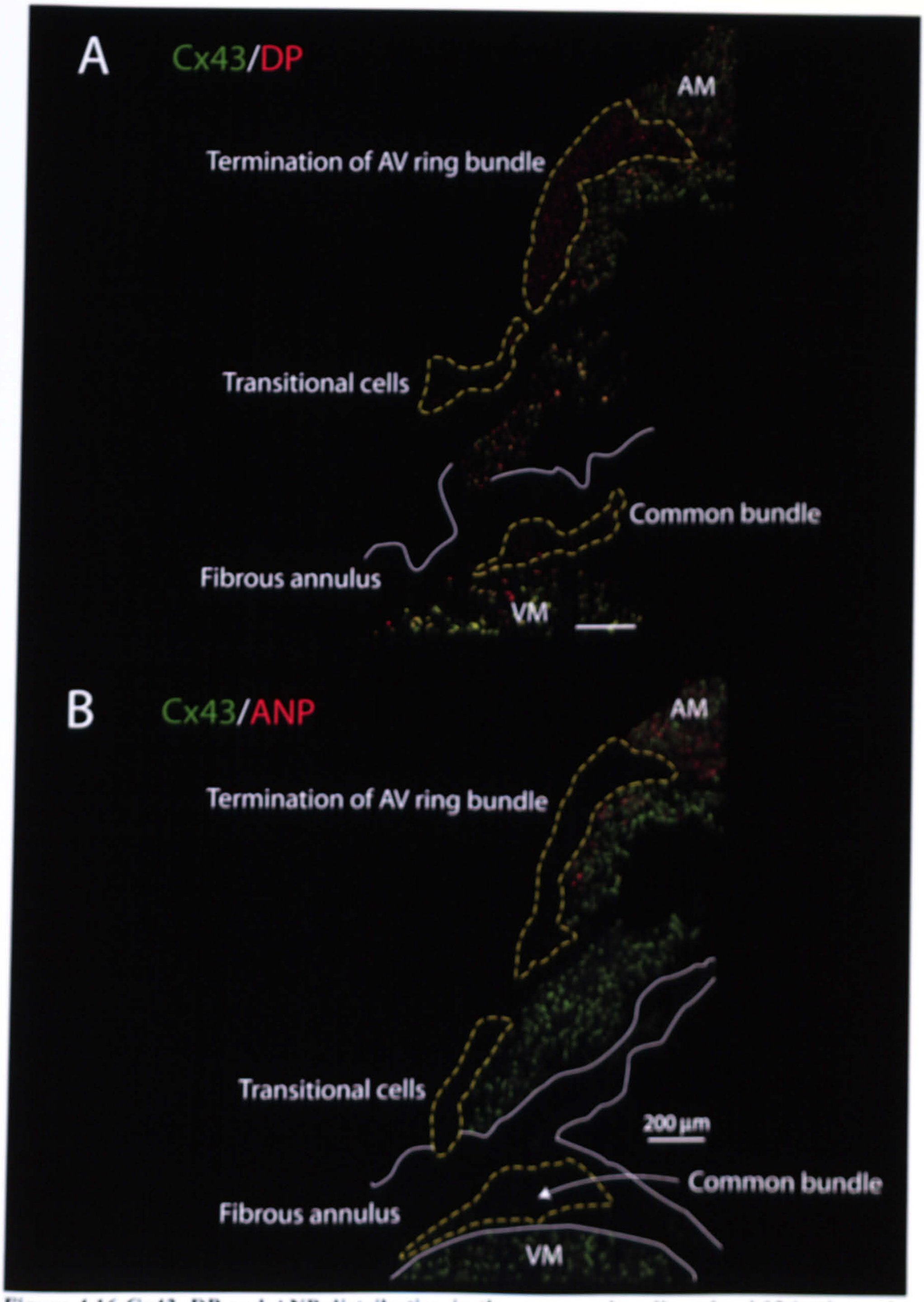

Figure 4.16 Cx43, DP and ANP distribution in the common bundle at level 12 in the main preparation studied (Fig. 2.1B)

A, montage of section double labelled for Cx43 (green) and DP (red). The tissue was slightly damaged. B, montage of adjacent section double labelled for Cx43 (green) and ANP (red). AM, atrial myocardium; VM, ventricular myocardium. Scale bars, 200 µm.

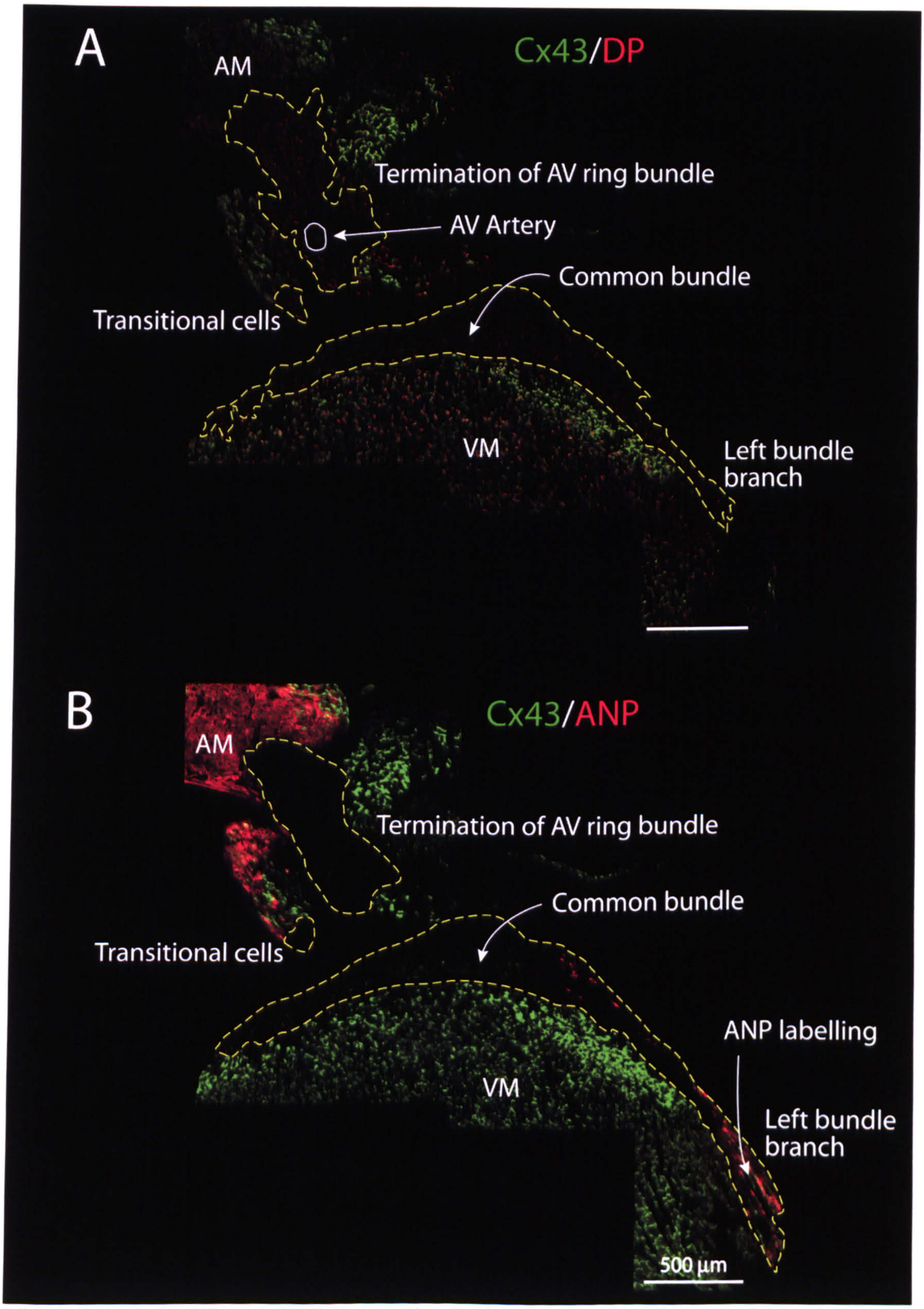

Figure 4.17 Cx43, DP and ANP distribution in the common bundle at level 5 in the second preparation (Fig. 4.6A)

A, section double labelled for Cx43 (green) and DP (red). B, section double labelled for Cx43 (green) and ANP (red). AM, atrial myocardium; VM, ventricular myocardium. Scale bars, 500 µm.

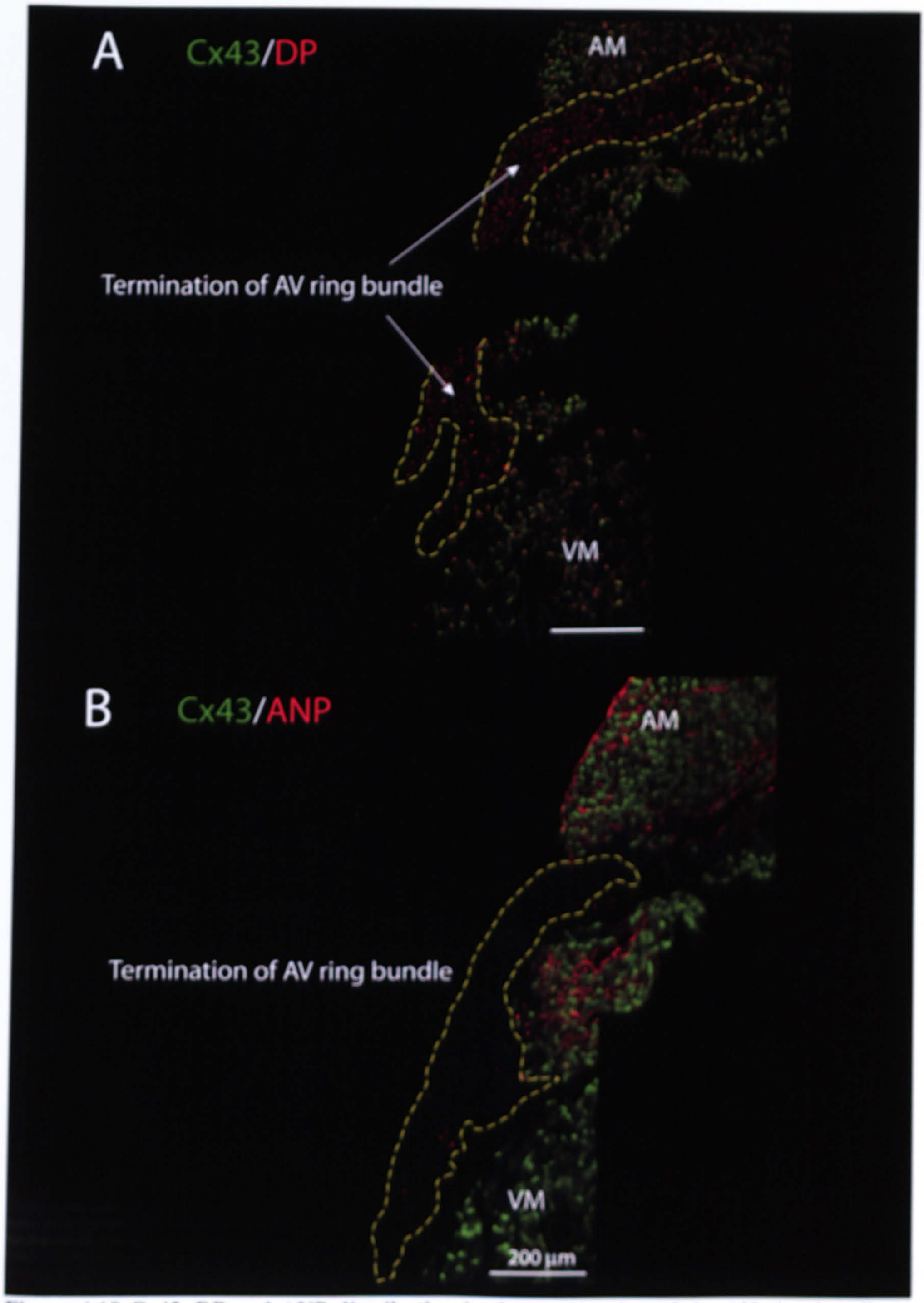

Figure 4.18 Cx43, DP and ANP distribution in the termination of the AV ring bundle at level 13 in the main preparation studied (Fig. 2.1B)

A, montage of section double labelled for Cx43 (green) and DP (red). The tissue was broken into two pieces. B, montage of adjacent section double labelled for Cx43 (green) and ANP (red). AM, atrial myocardium; VM, ventricular myocardium. Scale bars, 200 µm.

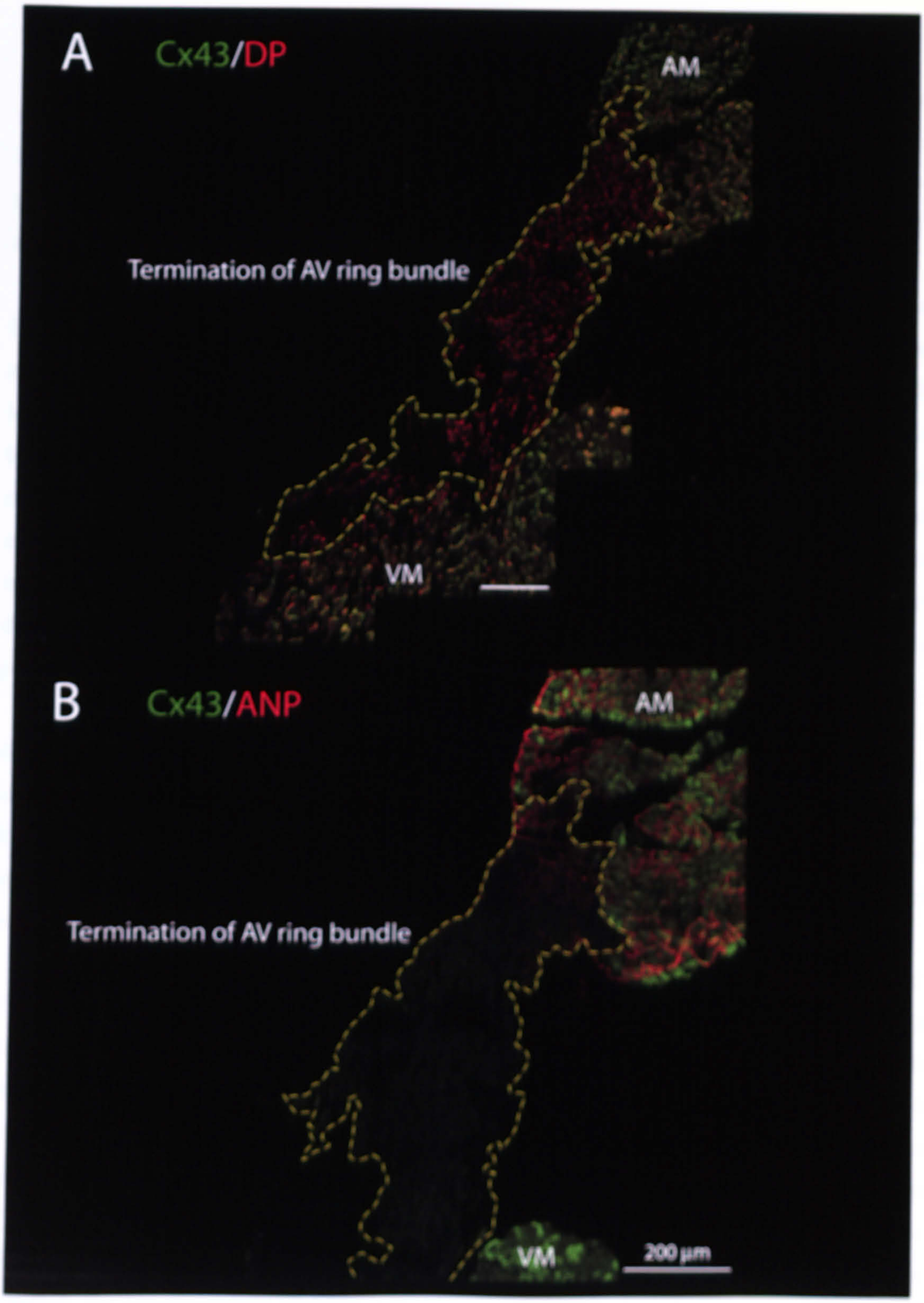

Figure 4.19 Cx43, DP and ANP distribution in the termination of the AV ring bundle at level 14 in the main preparation studied (Fig. 2.1B)

A, montage of section double labelled for Cx43 (green) and DP (red). B, montage of adjacent section double labelled for Cx43 (green) and ANP (red). AM, atrial myocardium; VM, ventricular myocardium. Scale bars, 200 µm.

4.4. Discussion

In accordance with previous reports, DP labelling was observed in all myocytes throughout the AV node. As nodal myocytes are Cx43-negative and ANP-negative, DP labelling of nodal myocytes is useful to confirm the existence of myocytes in regions where there is no labelling of Cx43 and ANP (the fibrous annulus, for example, is also Cx43-negative and ANP-negative).

In the atrial and ventricular myocardium, Cx43 and DP labelling was co-localised at the intercalated disks, whereas in the nodal cell regions of the AV junction Cx43 labelling was absent, but DP labelling was present. The absence of Cx43 labelling and presence of DP labelling in the nodal cell regions of the AV junction, therefore, enabled the nodal cell regions to be distinguished from atrial myocardium, fibrous annulus and ventricular myocardium. In the rabbit AV node, a tract of Cx43-expressing myocytes has been reported in the lower half of the enclosed node (Nikolski *et al.*, 2003; Ko *et al.*, 2004). However, in rat, Cx43 was not detected in the enclosed as well as the other nodal cell regions (Figs. 4.12 to 4.14). The rat, therefore, differs from the rabbit in that the lower nodal cells do not express Cx43 (alternatively Cx43 was present, but below the detection limit of immunohistochemistry).

In this chapter, labelling of Cx43 was carried out using mouse Cx43 antibody. A different Cx43 antibody raised in rabbit (data not shown) produced the same pattern of labelling. In this chapter, Cx43 and ANP or DP were labelled simultaneously (double labelling). It was checked that single labelling of Cx43 was not different from double labelling of Cx43 and another target protein. It is concluded that the Cx43 antibody used was reliable and suitable for use on rat tissue.

In agreement with previous reports (Skeper, 1989; Sola *et al.*, 1990; Benvenuti *et al.*, 1997), ANP was present in the atrial myocardium, but absent in nodal tissues and ventricular myocardium (Figs. 4.1 to 4.19). There was an unexpected ANP labelling in the left bundle branch (Fig. 4.17). Back *et al.* (1986) reported ANP immunoreactivity in the sub-endocardial layers of rat ventricles, but they were unable to determine whether it resided in Purkinje cells or in ventricular cells. ANP has also been suggested to exist in a small proportion of the ventricular myocytes underlying the terminal ramifications of the ventricular conducting system (Skeper, 1989). Thus, the finding of ANP in the left bundle branch is consistent with these reports. However, the functional role of ANP expression in left bundle branch observed in the present study or ANP expression in the Purkinje cells of the ventricular conducting system needs further investigation. It may be relevant to this issue that, under certain pathological conditions, general ventricular myocytes may express ANP (Ding *et al.*, 1987) and early neonates may also express ANP within the ventricular myocardium (Scott & Jennes, 1987; Toshimori *et al.*, 1987).

In conclusion, Cx43-negative, DP-positive and ANP-negative nodal cells were distributed throughout the AV junction in a complex three-dimensional manner and can be

distinguished from the surrounding working myocardium and the fibrous annulus.

Chapter 5

HCN4 expression in the AV node

5.1. Introduction

The hyperpolarization-activated inward current (termed I_f, I_h or I_q) plays a key role in the initiation and modulation of cardiac and neuronal pacemaker depolarizations (Biel *et al.*, 2002). Several cDNAs encoding I_f channels have been isolated by molecular cloning (Kaupp & Seifert, 2001). The I_f channels were termed HCN channels because their gating requires membrane hyperpolarization instead of depolarization and, in addition, is modulated by binding of cAMP (DiFrancesco, 1993; Pape, 1996; Mitsuiye *et al.*, 2000).

HCN channel types can be classified on the basis of their activation kinetics. HCN1 is the fastest channel (time constant of activation, τ, 25-300 ms) followed by HCN2 and HCN3 (τ, 180-500 ms) and HCN4. HCN4 is by far the slowest channel, displaying activation time constants ranging between a few hundred milliseconds at strongly hyperpolarized voltages (-140 mV) up to several seconds at the normal resting potential (-70 mV) (Biel *et al.*, 2002).

cAMP increases the activity of native and cloned I_f channels by accelerating activation kinetics in a voltage-dependent manner and by shifting the voltage of half-maximal activation to more positive values (Moosmang *et al.*, 2001). Based on the systematic analysis of a series of deletion mutants and HCN1/HCN2 chimeras, Wainger *et al.* (2001) and Wang *et al.* (2001) have proposed a model to explain the action of cAMP. In this model, the cyclic nucleotide binding domain (CNBD) located at the C terminus fulfills the role of an autoinhibitory channel domain. In the absence of cAMP, the C terminus inhibits HCN channel gating by interacting with the channel core and thereby shifting the activation to more hyperpolarized voltages. Binding of cAMP to the CNBD relieves this inhibition. HCN2 and HCN4 channels show a large response to cAMP, because they are efficiently inhibited in the absence of cyclic nucleotide. In contrast, HCN1 is only weakly affected by cAMP, because in this channel the inhibitory effect of the CNBD is weak. Thus, HCN2 and HCN4 are set apart from HCN1 with regard to their activation kinetics and their response to cyclic nucleotides.

Although HCN channels conduct both K^+ and Na^+, they are not non-selective. For example, HCN channels are almost impermeable to Li^+ and are even blocked by millimolar concentrations of Cs^+. Similarly, divalent cations and anions do not pass through the channels (Ludwig *et al.*, 1998; Gauss *et al.*, 1998; Santoro *et al.*, 1998). Although HCN channels carry an inward Na^+ current under physiological conditions, the primary sequence of the HCN pore region is clearly related to that of highly selective K^+ channels (Xue *et al.*, 2002; Azene *et al.*, 2003). The motif of the K^+ channel selectivity filter was found in the HCN channel pore region (Zhou *et al.*, 2001; Xue *et al.*, 2002; Azene *et al.*, 2003). However, it is clearly not sufficient to confer selectivity for K^+.

In vertebrates, the HCN channel family comprises four members (HCN1-4). Whereas HCN3 seems to be specifically expressed in neurones (Ludwig *et al.*, 1998; Moosmang *et al.*, 2001), the other three channels (HCN1, 2 and 4) have been detected in both heart and brain (Ludwig *et al.*, 1998; Santoro *et al.*, 1998; Shi *et al.*, 1999; Ludwig *et al.*, 1999; Moosmang *et al.*, 2001). In murine and rabbit SA node, HCN4 is by far the predominant HCN channel type, suggesting that this particular isoform plays a key role in the generation of primary pacemaker potentials (Ishii *et al.*, 1999; Moosmang *et al.*, 2001). In addition to HCN4, low to moderate amounts of HCN1 and HCN2 transcripts were detected in SA node (Shi *et al.*, 1999; Moosmang *et al.*, 2001). HCN channels are also present in atrial and ventricular myocytes. HCN2 is the only isoform in rabbit ventricle, and its mRNA expression is minimal (Shi *et al.*, 1999; Ludwig *et al.*, 1999). Low-level HCN expression in ventricle is consistent with the ventricle's lack of automaticity (Shi *et al.*, 1999). These data suggest that HCN4 expression is associated with the spontaneously active cells of the conduction tissue, whereas HCN2 expression is associated with non-spontaneously-active myocytes. This conclusion is supported by the finding that HCN channel expression changes during embryonic development (Yasui *et al.*, 2001). In early ventricular myocytes that beat spontaneously, HCN4 and HCN1 are predominantly expressed.

In late embryonic myocytes that have lost their ability to beat spontaneously, HCN2 becomes the principal isoform.

The existence of I_f or HCN4 in the AV node is as certain as in the SA node. However, within the AV node, there is a discrepancy between I_f recording and HCN4 expression detected by immunohistochemistry. I_f has been recorded from ovoid and rod-shaped cells isolated from the rabbit AV node (Noma *et al.*, 1980; Hancox & Levi, 1994; Habuchi *et al.*, 1995; Munk *et al.*, 1996). I_f is present in 95 % of ovoid cells versus 10 % of rod-shaped cells, and I_f density is 25 fold larger in ovoid cells (Munk *et al.*, 1996). However, Dobrzynski *et al.* (2003) based on immunohistochemistry reported that HCN4 expression was uniformly detected in the conduction tissue throughout the rabbit AV node.

5.2. Methods

The procedures of AV node tissue dissection are described in chapter 2 (section 2.1.2). The general immunohistochemistry procedures are described in chapter 2 (section 2.6). Details of procedures (tissue fixation, membrane permeabilisation, blocking of non-specific sites, type of labelling, type of primary and secondary antibodies used, incubation time and temperature during incubation with antibodies, washing and mounting of tissue) are described in chapter 4 (section 4.2).

5.3. Results

As shown in the previous chapter, based on histological staining and immunohistochemical labelling, the AV node (within the triangle of Koch) can be divided into five regions: the posterior/inferior nodal extension, the open node, the enclosed node, the common bundle and the termination of the AV ring bundle. In this chapter, the distribution of HCN4 investigated by immunohistochemical staining in three AV node preparations is shown. In the third preparation, not previously shown in this thesis, 14 levels at 500 μm intervals were studied. Information on the main preparation (Fig. 2.1B) and the second preparation (Fig. 4.6A) was given in chapter 4 (section 4.3). Typically, HCN4 labelling was detected at the membrane of myocytes.

5.3.1. Posterior/inferior nodal extension

Fig. 5.1 shows immunolabelling of HCN4 in the posterior/inferior nodal extension at level 4 in the main preparation (Fig. 2.1B), level 2 in the second preparation (Fig. 4.6A) and level 6 in the third preparation. The posterior/inferior nodal extension, outlined in yellow, is

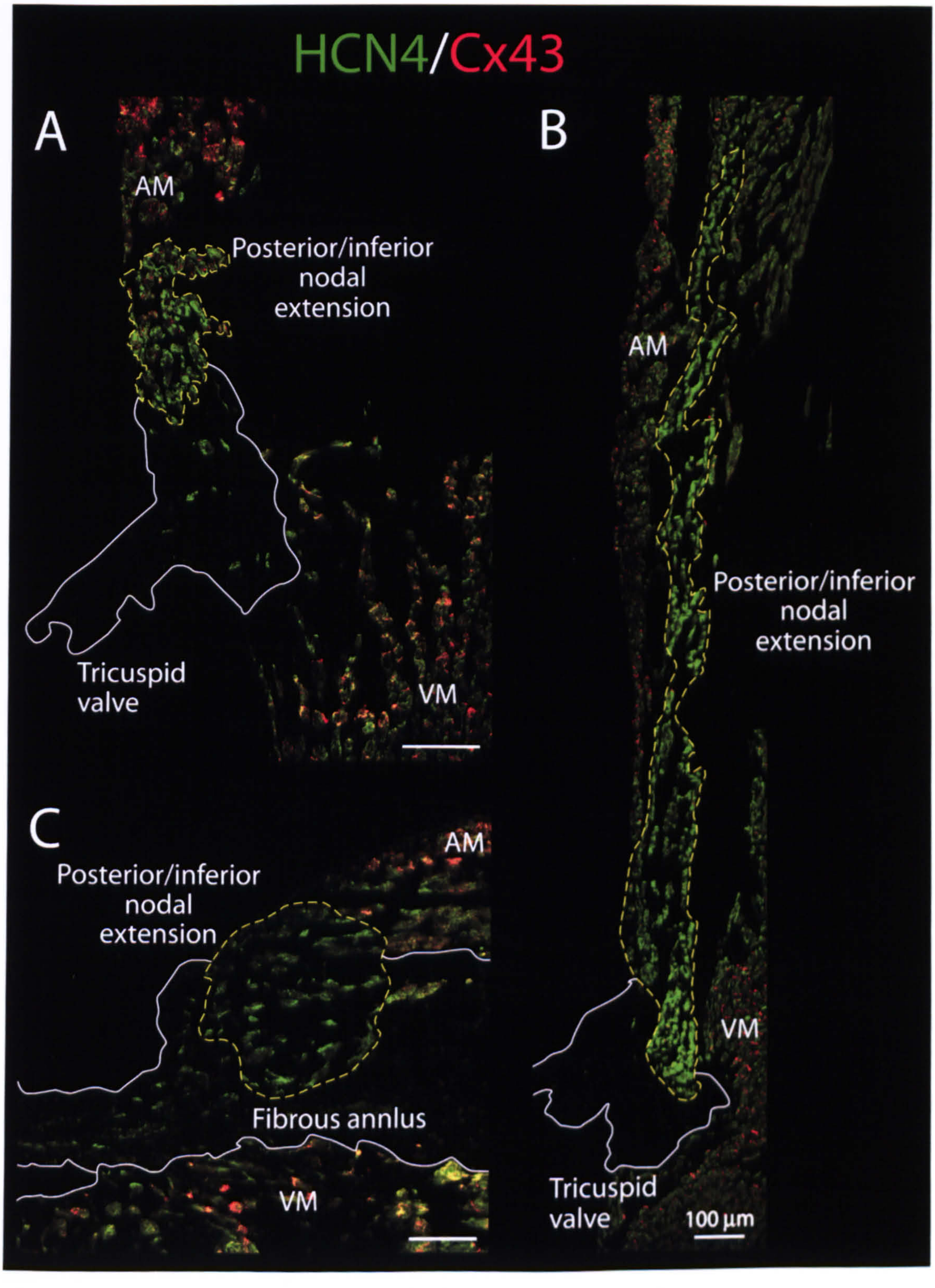

Figure 5.1 HCN4 labelling in the posterior/inferior nodal extension

A-C, montages of sections double labelled for HCN4 (green) and Cx43 (red) from three preparations. AM, atrial myocardium; VM, ventricular myocardium. In the atrial and ventricular myocardium, there is green labelling, but *it is background only. Scale bars, 100 µm.*

located above the ventricular myocardium and tricuspid valve and beneath the atrial myocardium (Fig. 5.1). Atrial and ventricular myocardium showed labelling of Cx43 at the intercalated disks, but did not show labelling of HCN4 (Fig. 5.1). The fibrous annulus, outlined in white, did not show fluorescence above background (Fig. 5.1). The posterior/inferior nodal extension did not show labelling of Cx43, but did show labelling of HCN4 at the outer cell membrane (Fig. 5.1). Putting the results of HCN4 and immunohistochemical markers (section 4.3.1) together, the posterior/inferior nodal extension is Cx43-negative, DP-positive, ANP-negative and HCN4-positive.

5.3.2. Open node

Fig. 5.2 shows immunolabelling of HCN4 in the open node at level 8 in the main preparation (Fig. 2.1B), level 3 in the second preparation (Fig. 4.6A) and level 9 in the third preparation. The open node, outlined in yellow, is located at the centre of the montage, i.e. between the atrial myocardium and the ventricular myocardium, in which Cx43 labelling is abundant (Fig. 5.2). The open node showed HCN4 labelling at the outer cell membrane (Fig. 5.2). Putting the results of HCN4 and immunohistochemical markers (section 4.3.2) together, the open node is Cx43-negative, DP-positive, ANP-negative and HCN4 positive. In addition to the open node, the zone of transitional cells, which is located above the tricuspid valve, is HCN4-positive and Cx43-negative (and also DP-positive and ANP-negative as shown in section 4.3.2).

5.3.3. Enclosed node

Fig. 5.3 shows immunolabelling of HCN4 in the enclosed node at level 9 in the main preparation (Fig. 2.1B), level 4 in the second preparation (Fig. 4.6A) and level 10 in the third preparation. The enclosed node, outlined in yellow, is located at the centre of the montage, i.e. between the atrial and ventricular myocardium, in which Cx43 labelling is abundant (Fig. 5.3). The enclosed node showed the same labelling pattern as the open node, i.e. HCN4-positive and Cx43-negative (Fig. 5.3). Putting the results of HCN4 and immunohistochemical markers (section 4.3.3) together, the enclosed node is Cx43-negative, DP-positive, ANP-negative and HCN4 positive. As described in the previous section, the zone of transitional cells is also HCN4-positive and Cx43-negative (and also DP-positive and ANP-negative as shown in section 4.3.3).

5.3.4. Common bundle

Fig. 5.4 shows immunolabelling of HCN4 in the common bundle at level 11 in the main preparation (Fig. 2.1B) and level 11 in the third preparation. The common bundle, outlined in yellow, is located at the centre of the montage, i.e. between the atrial and ventricular myocardium, in which Cx43 labelling is abundant (Fig. 5.4). The common bundle

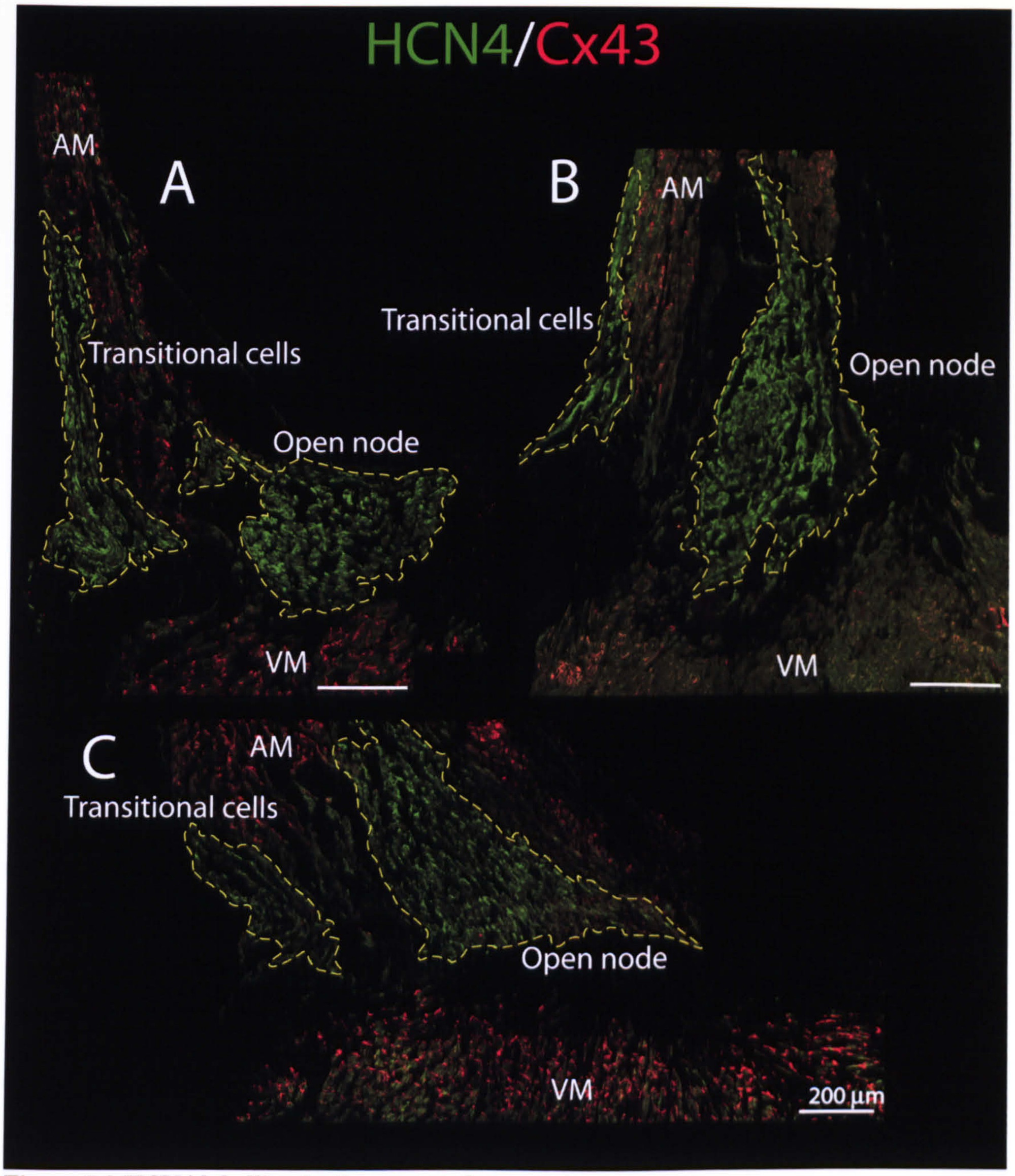

Figure 5.2 HCN4 labelling in the open node

A-C, montages of sections double labelled for HCN4 (green) and Cx43 (red) from three preparations. AM, atrial myocardium; VM, ventricular myocardium. Scale bars, 200 µm.

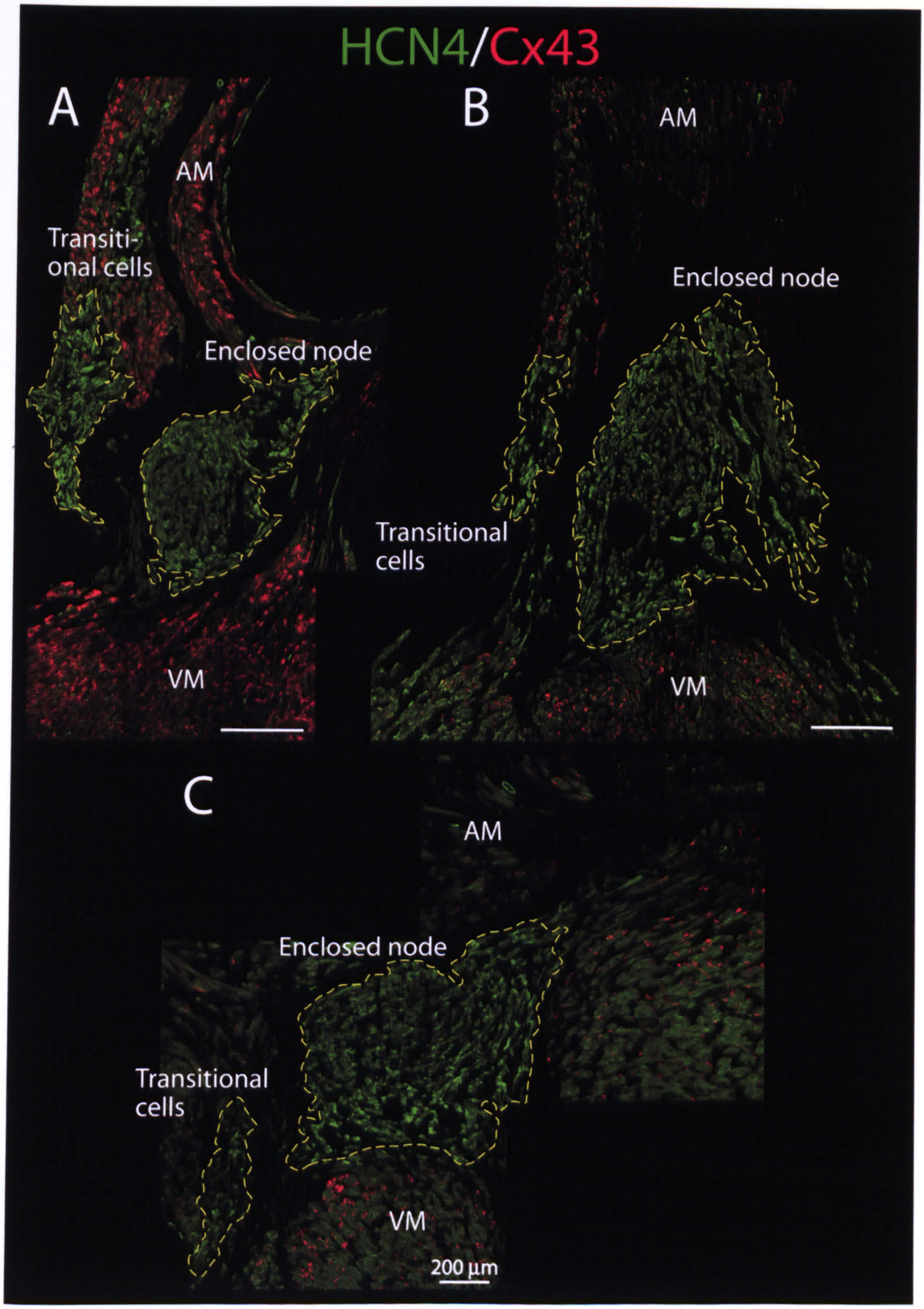

Figure 5.3 HCN4 labelling in the enclosed node

A-C, montages of sections double labelled for HCN4 (green) and Cx43 (red) from three preparations. AM, atrial myocardium; VM, ventricular myocardium. Scale bars, 200 µm.

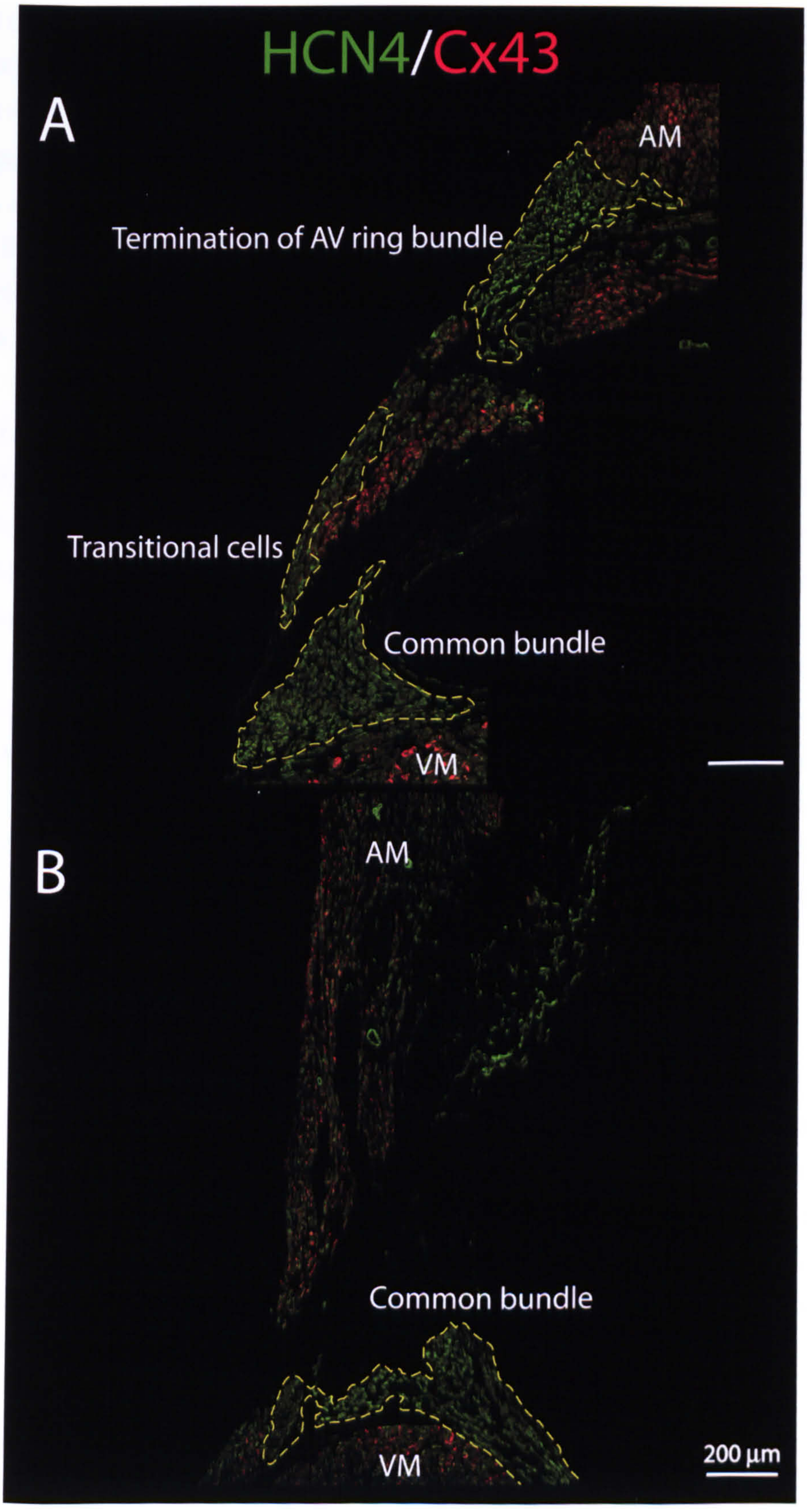

Figure 5.4 HCN4 labelling in the common bundle

A, B, montages of sections double labelled for HCN4 (green) and Cx43 (red) from two preparations. AM, atrial myocardium; VM, ventricular myocardium. Scale bars, 200 µm.

showed the same labelling pattern as the open node and the enclosed node, i.e. HCN4-positive and Cx43-negative (Fig. 5.4). Putting the results of HCN4 and immunohistochemical markers (section 4.3.4) together, the common bundle is Cx43-negative, DP-positive, ANP-negative and HCN4 positive. At this level, the zone of transitional cells again existed as in the two previous sections and the termination of AV ring bundle is also located vertically above the common bundle. Both the zone of transitional cells and the cells of the termination of the AV ring bundle are HCN4-positive and Cx43-negative (and also DP-positive and ANP-negative as shown in section 4.3.4).

5.3.5. Left bundle branch

Fig. 5.5 shows immunolabelling of HCN4 in the common bundle and the left bundle branch from two preparations. Fig. 5.5A corresponds to level 5 in the second preparation (Fig. 4.6A). Although the section shown in Fig. 5.5B (from another preparation not one of the preparations mentioned above) was cut in a different plane to the section in Fig. 5.5A, the image has been rotated so as to be placed in the same orientation and the architecture of the tissue is similar to that in Fig. 5.5A. As already described in the previous section, the common bundle was Cx43-negative and HCN4-positive (and also DP-positive and ANP-negative as shown in section 4.3.5). In addition to the common bundle, HCN4-positive and Cx43-negative myocytes were located in the left bundle branch (Fig. 5.5). Unlike other HCN4-positve and Cx43-negative regions, the left bundle branch was not ANP-negative (as described in chapter 4, sections 4.3.5 and 4.4).

5.3.6. Termination of the AV ring bundle

Fig. 5.6 shows immunolabelling of HCN4 in the termination of the AV ring bundle at level 14 in the main preparation (Fig. 2.1B) and level 13 in the third preparation. The termination of the AV ring bundle, outlined in yellow, is located above the ventricular myocardium and beneath the atrial myocardium, in which Cx43 labelling is abundant (Fig. 5.6). In agreement with data shown in chapter 4 (section 4.3.6) and section 5.3.4, the termination of the AV ring bundle was Cx43-negative, DP-positive, ANP-negative and HCN4-positive (the same labelling pattern as other nodal myocytes).

5.4. Discussion

In this study, the distribution of HCN4 in the rat AV node was investigated. In agreement with a previous investigation (Dobrzynski *et al.*, 2003), HCN4-positive, Cx43-negative cells were detected throughout the AV node and these cells correspond to nodal cells described as DP-positive and ANP-negative in chapter 4. There appears to be a perfect overlap of immunohistochemical markers and HCN4. The uniform distribution of HCN4 in nodal myocytes cannot explain the different electrophysiological properties of the different cell types

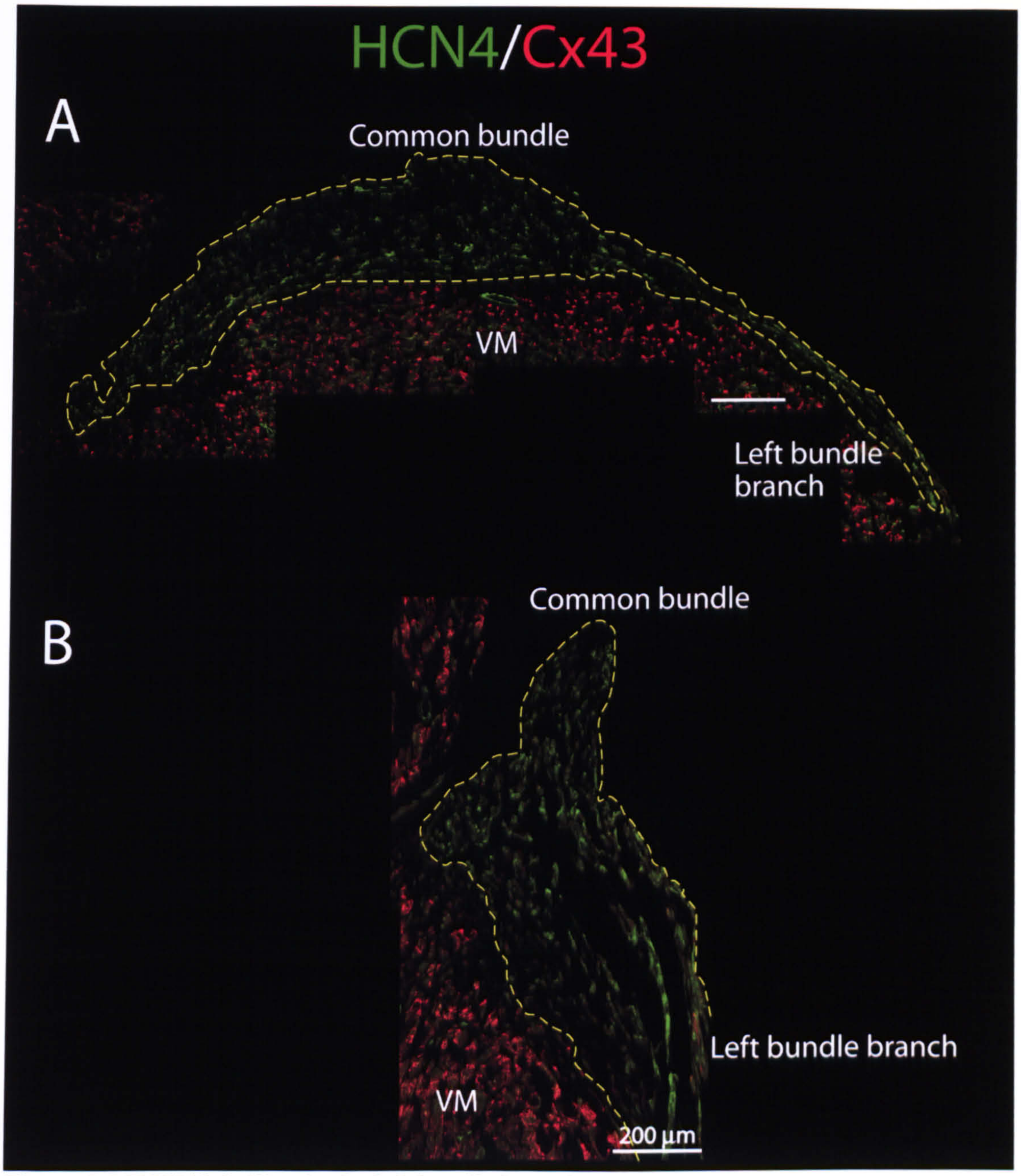

Figure 5.5 HCN4 labelling in the left bundle branch

A, B, montages of sections double labelled for HCN4 (green) and Cx43 (red) from two preparations. AM, atrial myocardium; VM, ventricular myocardium. Scale bars, 200 µm.

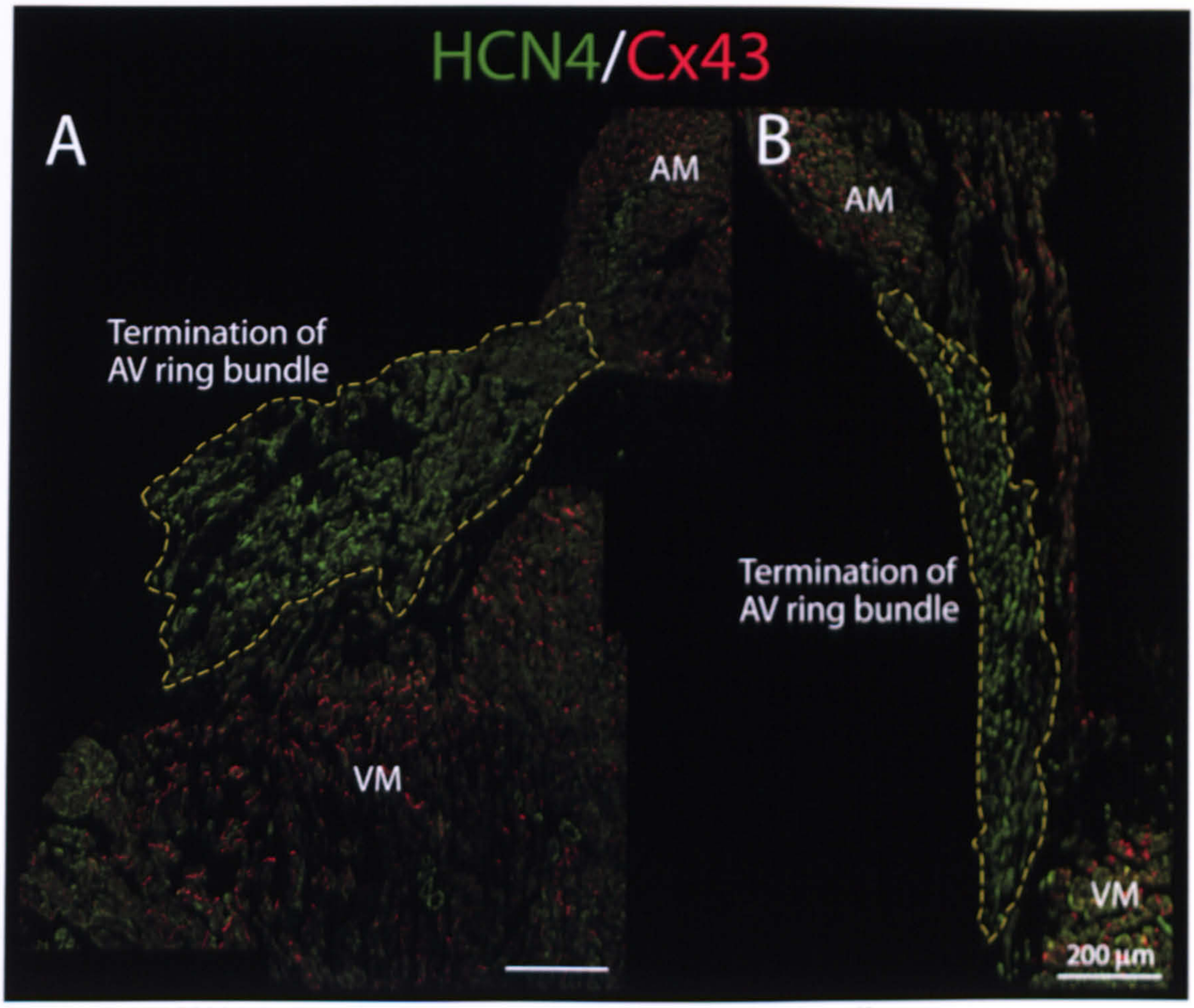

Figure 5.6 HCN4 labelling in the termination of the AV ring bundle

A, B, montages of sections double labelled for HCN4 (green) and Cx43 (red) from two preparations. AM, atrial myocardium; VM, ventricular myocardium. Scale bars, 200 µm.

in the AV node. The distribution of Na^+ channel isoforms in the AV node (chapter 6 and 7) may provide clues to this mystery. The distribution of the largest conductance gap junction protein (chapter 8) may also be useful.

Chapter 6

Expression of Na^+ channel isoforms in isolated atrial and ventricular myocytes and tissue sections

6.1. Introduction

Voltage-gated Na^+ channels are critical elements for action potential initiation and propagation in excitable cells, because they are responsible for the initial depolarization of the membrane (Goldin *et al.*, 2000). For the delay and regulation of electrical impulse conduction between the atria and the ventricles, the absence of the cardiac Na^+ channel in some fraction of myocytes in the AV node is also important (Munk *et al.*, 1996; Petrecca *et al.*, 1997).

As already explained in chapter 1 (section 1.5.2), recent studies have shown that some of the neuronal Na^+ channel isoforms are expressed in the heart and are functionally important (Maier *et al.*, 2002; Maier *et al.*, 2003; Lei *et al.*, 2004). $Na_v1.1$, $Na_v1.3$ and $Na_v1.6$ are expressed in isoloated mouse ventricular myocytes (Maier *et al.*, 2002). $Na_v1.1$ and $Na_v1.3$ are expressed in mouse SA node and $Na_v1.1$ is expressed in rat SA node (Maier *et al.*, 2003).

However, the distribution of neuronal Na^+ channel isoforms in the AV node is unknown. Before discussing the distribution of Na^+ channel isoforms in the AV node in following chapter, Na^+ channel expression outside of the AV node is discussed in this chapter. Using subtype-specific antibodies and immunocyto- or immunohisto-chemistry, Na^+ channel isoforms are identified and localised in rat cardiac myocytes and myocardium.

6.2. Methods

6.2.1. Immunocytochemistry for Na^+ channel isoforms in isolated atrial and ventricular myocytes

The atrial and ventricular myocytes were isolated as described in chapter 2 (section 2.2). The general immunocytochemistry procedures were similar to those described in chapter 2 (section 2.6). The myocytes were placed on pieces of coverslips coated with flamed carbon for 30 min and were then washed in PBS for 10 min, fixed in 10 % neutral buffered formalin at room temperature for 15 min and washed three times in PBS over 30 min to remove excess fixative. The myocytes were treated with 0.1 % (or 0.3 % for $Na_v1.5$) Triton X-100 in PBS for 10 min at room temperature. The myocytes were incubated with 10 % normal donkey serum and 1 % BSA, in PBS for 60 min at room temperature. Primary antibodies were diluted in 1 % BSA in PBS (or 1 % BSA/ 10 % normal donkey serum in PBS for $Na_v1.5$). The myocytes were incubated with a suitable concentration of each primary antibody in a humid box at -4°C overnight. Information on three different $Na_v1.5$ antibodies and other primary antibodies are summarised in Table 6.1 and Table 2.1, respectively. The secondary antibodies were diluted with same manner as the primary antibodies. The secondary antibodies were applied for 1 h at room temperature in the dark. Information on secondary antibodies can be obtained from chapter 2 (section 2.6.9 and Table 2.3). After application of the primary and secondary antibodies, the myocytes were thoroughly washed in PBS three times for 30 min. Finally, the myocytes were mounted under coverslips with the anti-fade reagent, Vectashield (Vector Laboratories). The myocytes were viewed by confocal laser scanning microscopy (section 2.7).

6.2.2. Immunohistochemistry for cardiac Na^+ channel isoforms in tissue sections

The general immunohistochemistry procedures are described in chapter 2 (section 2.6). Details of procedures (tissue fixation, membrane permeabilisation, blocking of non-specific sites, type of labelling, type of primary and secondary antibodies used, incubation time and temperature during incubation with antibodies, washing and mounting of tissue) are described here. The AV node tissue was prepared and cryosectioned as described in chapter 2 (section 2.1 and 2.3). Prior to immunofluorescence labelling, sections were fixed in 10 % neutral buffered formalin at room temperature and washed three times in PBS over 30 min to remove excess fixative. Tissue sections were treated with 0.3 % Triton X-100 in PBS for 10 min at room

Table 6.1 Summary of $Na_v1.5$ antibodies used

$Na_v1.5$ antibody	Host	Recognition peptide (epitope), location of epitope	Dilution
Alomone (Cohen, 1996; Kucera *et al.*, 2002)	Rabbit	Residues 493-511 of rat $Na_v1.5$, intracellular loop between domains I and II	1:30
Catterall (Rogart *et al.*, 1989)	Rabbit	Residues 1122-1137 of rat $Na_v1.5$, intracellular loop between domains II and III	1:30
Dumaine (Haufe *et al.*, 2005)	Rabbit	Residues 1985-2000 of dog $Na_v1.5$, intracellular, C-terminus	1:30, 1:50

temperature. Tissue sections were incubated with 10 % normal donkey serum and 1 % BSA in PBS for 60 min at room temperature. Primary antibodies were diluted in 1 % BSA/ 10 % normal donkey serum in PBS. The tissue sections were incubated with a suitable concentration of each primary antibody in a humid box at -4°C overnight. The secondary antibodies were diluted in 1 % BSA/ 10 % normal donkey serum in PBS. The secondary antibodies were applied for 1 h at room temperature in the dark. For multiple labelling experiments, combinations of secondary antibodies were used. Information regarding the incubation time and antibody concentration for the secondary antibodies can be obtained from chapter 2 (section 2.6.9 and Table 2.3). After application of the primary and secondary antibodies, the samples were thoroughly washed in PBS three times for 30 min. Finally, the sections were mounted under coverslips with the anti-fade reagent, Vectashield (Vector Laboratories). The immunolabelled tissue sections were viewed by confocal laser scanning microscopy and montages were constructed as described in chapter 2 (section 2.7).

6.3. Results

Immunohistochemistry was used to investigate the expression of neuronal and cardiac Na^+ channel isoforms in isolated atrial and ventricular myocytes and myocardium; the skeletal isoform, $Na_v1.4$, was not investigated. The expression of Na^+ channel isoforms in and around the AV node will be described in following chapters.

6.3.1. Expression of neuronal Na^+ channel isoforms

To investigate whether neuronal Na^+ channel isoforms are present in atrial and ventricular myocytes and myocardium, I used specific antibodies recognizing the specific neuronal α subunit isoforms, $Na_v1.1$, $Na_v1.2$, $Na_v1.3$ and $Na_v1.6$.

6.3.1.1. Expression of neuronal Na^+ channels in isolated atrial myocytes

Fig. 6.1 shows immunolabelling of neuronal Na^+ channel isoforms in isolated atrial myocytes. $Na_v1.1$ labelling was located at the outer cell membrane (Fig. 6.1A). The staining in the nucleus is assumed to be non-specific. $Na_v1.2$ and $Na_v1.3$ were not detected (Fig. 6.1B and C) - the fluorescence in Fig. 6.1B and C is assumed to be background only. Fig. 6.1D shows that there was labelling of $Na_v1.6$ around the nucleus. This labeling was not present when the antibody was preincubated with the antigenic peptide (data not shown) and this suggests that the labelling was specific. As already shown in chapter 2, there was no fluorescence above background in a control experiment in which no primary antibody was used (Fig. 2.3).

6.3.1.2. Expression of neuronal Na^+ channels in isolated ventricular myocytes

Fig. 6.2 shows immunolabelling of neuronal Na^+ channel isoforms in isolated ventricular myocytes. $Na_v1.1$ labelling was located in the t-tubules (Fig. 6.2A, arrow 1) and the

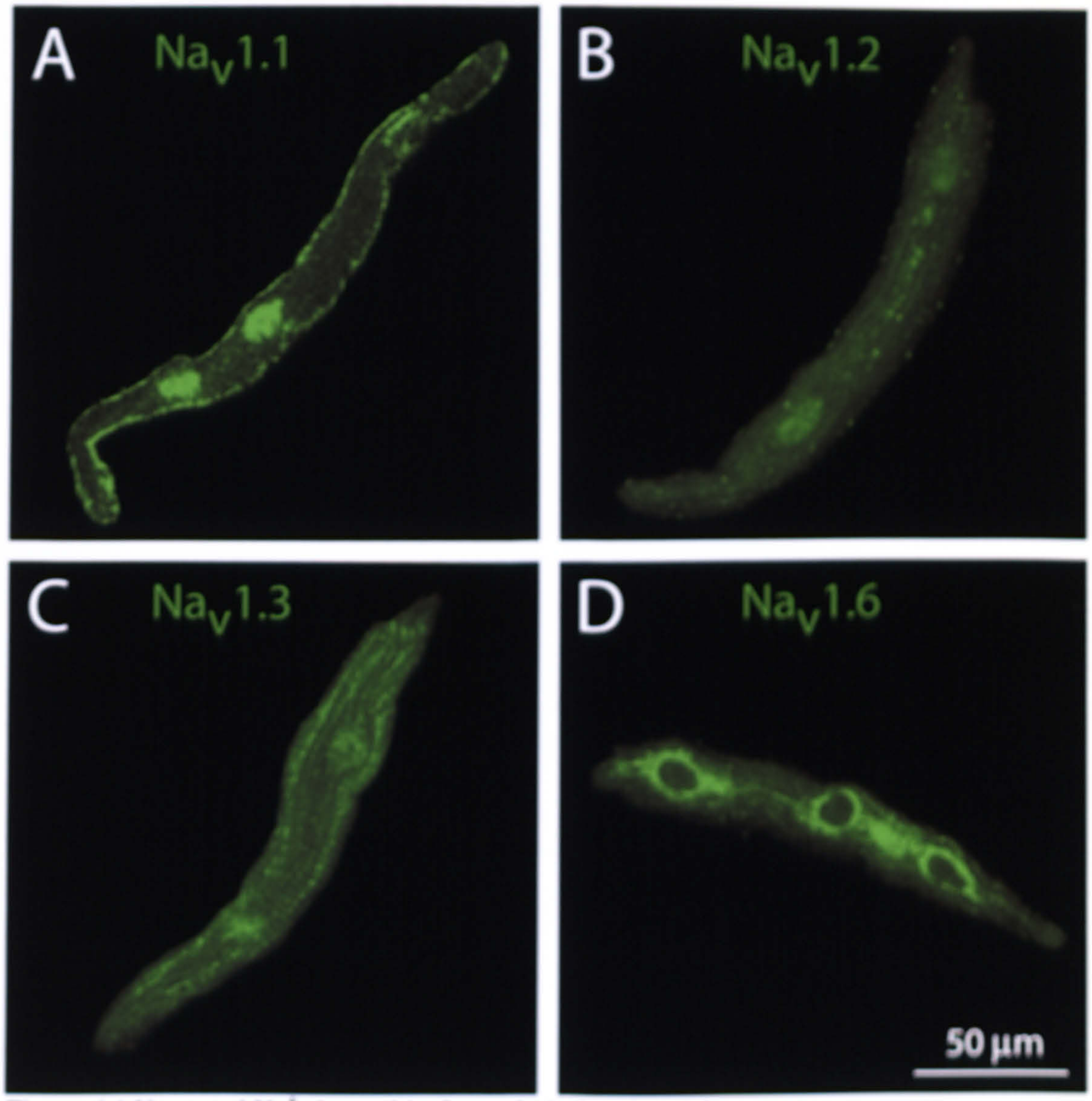

Figure 6.1 Neuronal Na^+ channel isoforms in isolated atrial myocytes

A-D, high magnification images of labelling of neuronal Na^+ channel isoforms ($Na_V1.1$, $Na_V1.2$, $Na_V1.3$ and $Na_V1.6$) in isolated atrial myocytes. Scale bar, 50 µm.

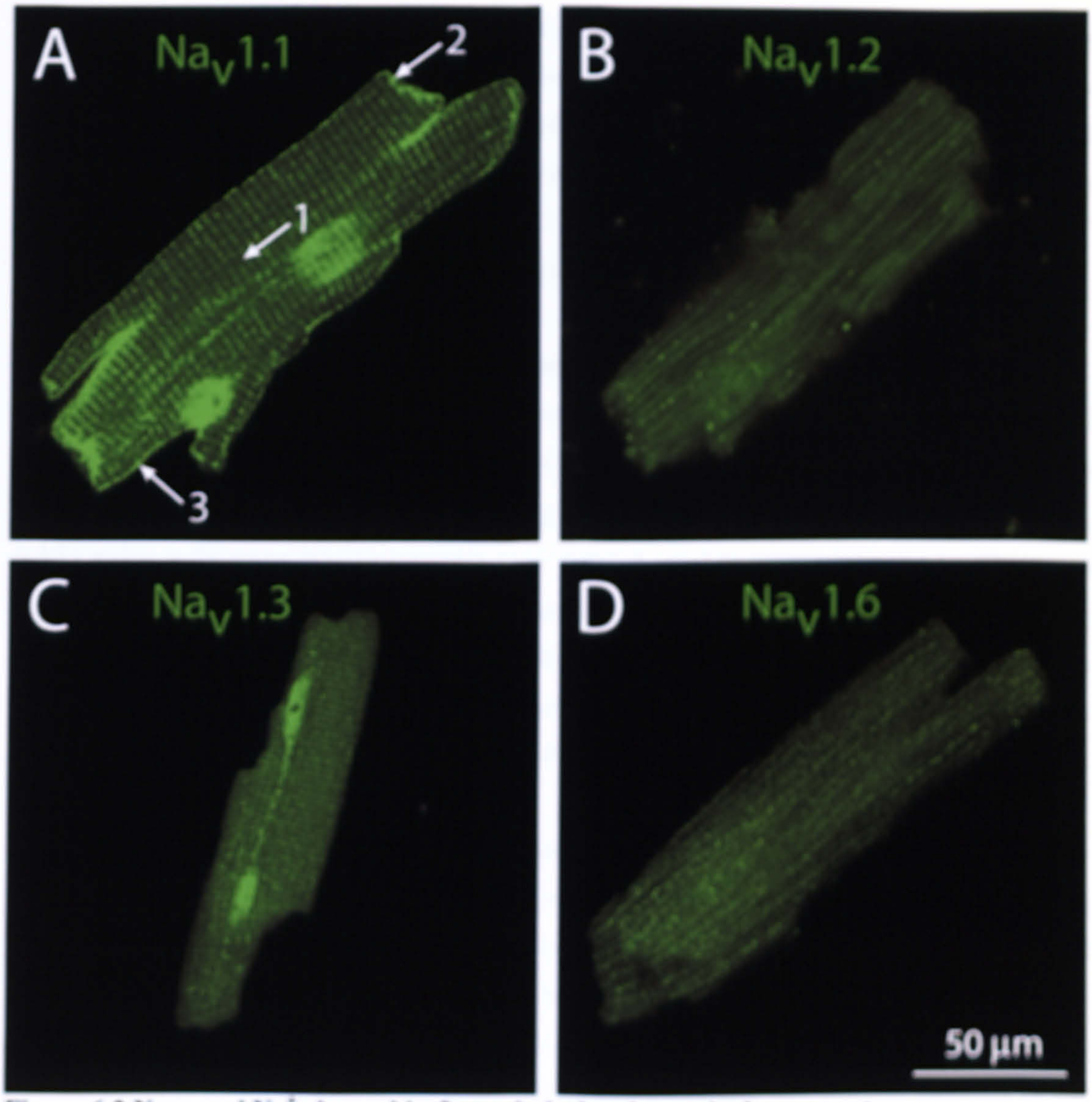

Figure 6.2 Neuronal Na$^+$ channel isoforms in isolated ventricular myocytes

A-D, high magnification images of labelling of neuronal Na$^+$ channel isoforms (Na$_v$1.1, Na$_v$1.2, Na$_v$1.3 and Na$_v$1.6) in isolated ventricular myocytes. In A, the white arrows designate labelling at t-tubules (1), at the intercalated disks (2) and at the outer cell membrane (3) by the Na$_v$1.1 antibody. Scale bar, 50 µm.

intercalated disks (Fig. 6.2A, arrow 2) as well as at the outer cell membrane (Fig. 6.2A, arrow 3). The staining in the nucleus is assumed to be non-specific (Fig. 6.2A). $Na_v1.2$ labelling was not detected (Fig. 6.2B). $Na_v1.3$ and $Na_v1.6$ labelling was detected at t-tubules (Fig. 6.2C and D). There was no fluorescence above background in a control experiment in which no primary antibody was used (data not shown). Table 6.2 shows a summary of labelling of neuronal Na^+ channel isoforms in isolated atrial and ventricular myocytes.

6.3.1.3. Expression of neuronal Na^+ channels in atrial myocardium

Fig. 6.3 shows double labelling of neuronal Na^+ channel isoforms and Cx43 in atrial myocardium. As already shown in chapter 4, Cx43 labelling exists at the intercalated disks in atrial myocardium (Fig. 6.3). $Na_v1.1$ labelling was located at the outer cell membrane (Fig. 6.3A) and it is the same labelling pattern as in isolated atrial myocytes (Fig. 6.1A). There was also non-specific labelling of $Na_v1.1$ in the nucleus (Fig. 6.3A) as in isolated myocytes (Fig. 6.1A). $Na_v1.2$, $Na_v1.3$ and Nav1.6 were not detected in the atrial myocardium (Fig. 6.3B-D). As already shown in chapter 2, there was no fluorescence above background in control experiments in which no primary antibody was used (Fig. 2.4).

6.3.1.4. Expression of neuronal Na^+ channels in ventricular myocardium

Fig. 6.4 shows double labelling of neuronal Na^+ channel isoforms and Cx43 in ventricular myocardium. As already shown in chapter 4, Cx43 labelling exists at the intercalated disks in ventricular myocardium (Fig. 6.4). $Na_v1.1$ labelling was located at the outer cell membrane and was also co-localised with Cx43 at the intercalated disks (Fig. 6.4A). There was also intracellular labelling at t-tubules (not clear in Fig. 6.4D) and non-specific labelling of the nucleus (clear in Fig. 6.4A). The labelling of $Na_v1.1$ in ventricular myocardium is the same labelling pattern as in isolated ventricular myocytes (Fig. 6.2A). $Na_v1.2$ and $Na_v1.3$ labelling was either absent or weak in ventricular myocardium (Fig. 6.4B-C). $Na_v1.6$ labelling was localised at t-tubules (Fig. 6.4D; for example see arrow) and was the same labelling pattern as in isolated ventricular myocytes. There was no fluorescence above background in control experiments (data not shown). Table 6.3 shows a summary of labelling of neuronal Na^+ channel isoforms in atrial and ventricular myocardium.

6.3.2. Expression of the cardiac Na^+ channel isoform

In order to investigate the cellular or tissue localisation of the cardiac Na^+ channel isoform ($Na_v1.5$), three independent antibodies were applied to isolated atrial and ventricular myocytes and myocardium.

6.3.2.1. Expression of the cardiac Na^+ channel in isolated ventricular myocytes

Table 6.2 Summary of labelling of neuronal Na^+ channel isoforms in isolated myocytes

		Atrial myocytes		Ventricular myocytes	
		No. of hearts	No. of cells	No. of hearts	No. of cells
$Na_v1.1$	Without peptide	6	33	5	26
		Membrane labelling		Membrane, t-tubule and intercalated disk labelling	
	With peptide	2	13	2	11
		No labelling		No labelling	
$Na_v1.2$	Without peptide	2	8	2	10
		No labelling		No labelling	
	With peptide	-	-	-	-
$Na_v1.3$	Without peptide	5	40	5	26
		No labelling		t-tubule labelling	
	With peptide	1	6	2	7
		No labelling		No labelling	
$Na_v1.6$	Without peptide	4	24	5	22
		No labelling except around nuclues		t-tubule labelling	
	With peptide	2	9	3	13
		No labelling		No labelling	
No primary antibody		1	8	1	3
		No labelling		No labelling	

All control experiments (preincubation of antibody with antigen or no primary antibody) showed background levels of immunolabelling.

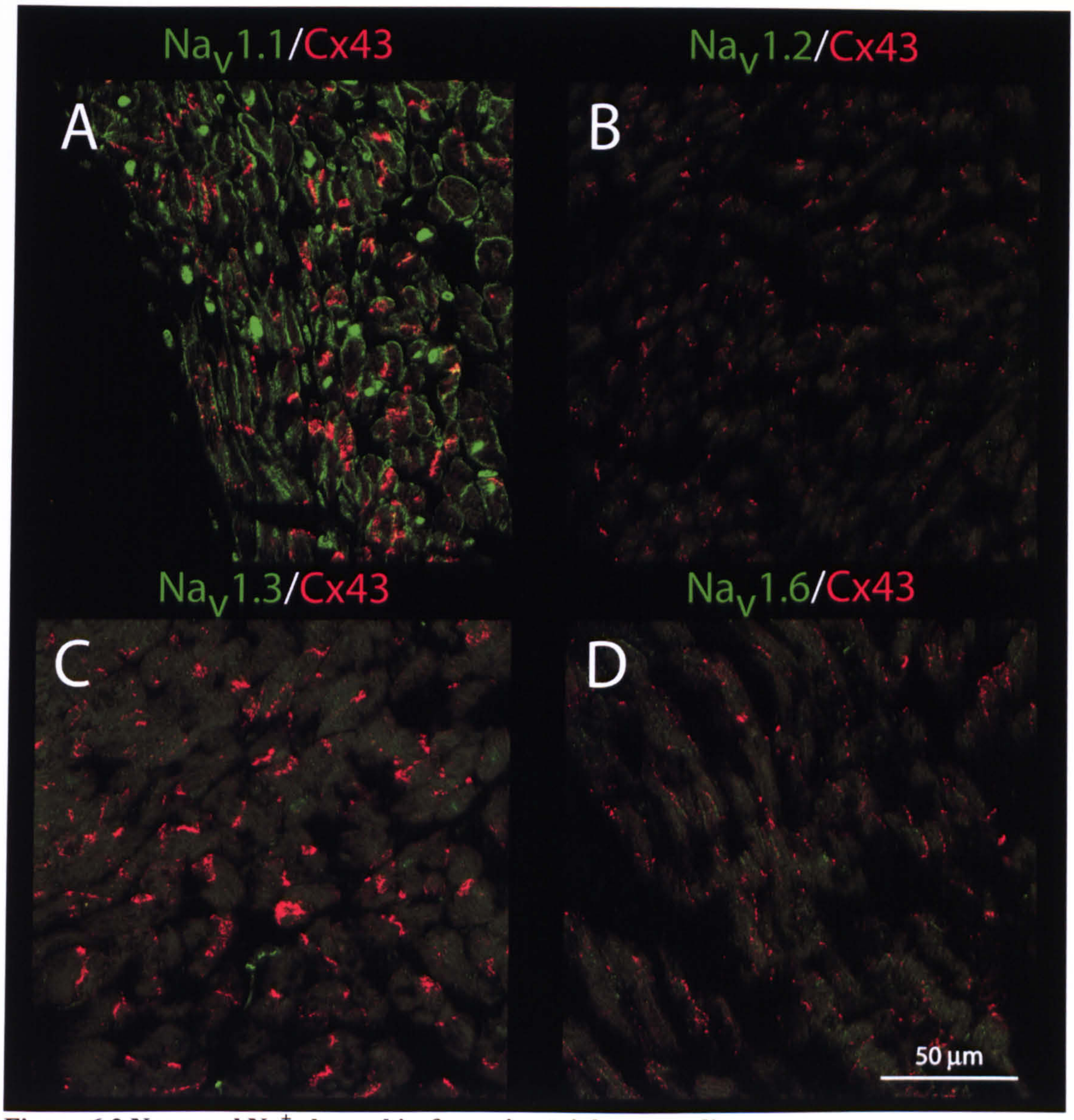

Figure 6.3 Neuronal Na^+ channel isoforms in atrial myocardium

A-D, high magnification images of double labelling of neuronal Na^+ channel isoforms (green; $Na_v1.1$, $Na_v1.2$, $Na_v1.3$ and $Na_v1.6$) and Cx43 (red) in atrial myocardium. Scale bar, 50 µm.

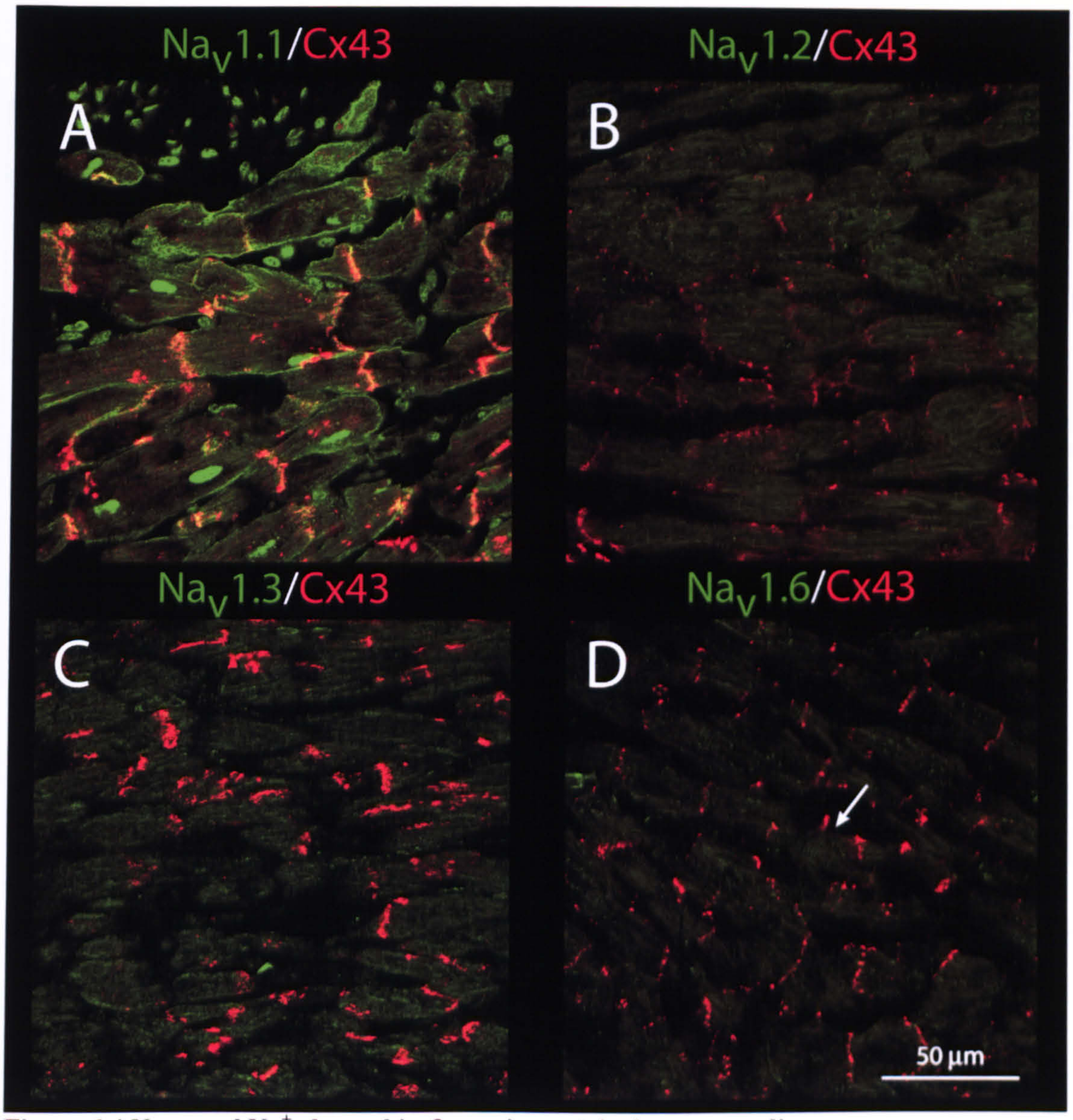

Figure 6.4 Neuronal Na^+ channel isoforms in ventricular myocardium

A-D, high magnification images of double labelling of neuronal Na^+ channel isoforms (green; $Na_v1.1$, $Na_v1.2$, $Na_v1.3$ and $Na_v1.6$) and Cx43 (red) in ventricular myocardium. In D, the white arrow indiciates very weak striation of $Na_v1.6$. Scale bar, 50 µm.

Table 6.3 Summary of labelling of neuronal Na^+ channel isoforms in myocardium

	No. of hearts	Atrial myocardium	Ventricular myocardium
$Na_v1.1$	5	Membrane labelling	Membrane, intracellular labelling (t-tubule) and intercalated disk labelling
$Na_v1.2$	3	No labelling	No labelling
$Na_v1.3$	4	No labelling	No labelling
$Na_v1.6$	3	No labelling	Intracellular (t-tubule) labelling
No primary antibody	6	No labelling	No labelling

The control experiments (no primary antibody) showed background levels of immunolabelling.

Fig. 6.5 shows immunolabelling by two different $Na_v1.5$ antibodies in isolated ventricular myocytes. Although the epitopes against which these antibodies were raised are different (Table 6.1), both antibodies produced labelling at t-tubules in isolated ventricular myocytes. There is also labelling by the Catterall $Na_v1.5$ antibody at the intercalated disks (the bright green labelling, highlighted by arrow, in Fig. 6.5A). As the concentration of antibodies decreased from 1:30 to 1:100 and 1:300, the immunofluorescence signal became weaker. Thus, the immunofluorescence signal produced by these antibodies is unlikely to be non-specific.

6.3.2.2. Comparison of labelling by different cardiac Na^+ channel antibodies in isolated atrial and ventricular myocytes

Fig. 6.6 shows immunolabelling by three different $Na_v1.5$ antibodies in isolated atrial and ventricular myocytes. Labelling by the Alomone $Na_v1.5$ antibody was located at the outer cell membrane in isolated atrial myocytes and at t-tubules in isolated ventricular myocytes (Fig. 6.6A). Labelling by the Catterall $Na_v1.5$ antibody was located at the outer cell membrane in isolated atrial myocytes (left panel in Fig. 6.6B). In an isolated ventricular myocyte, labelling by the Catterall $Na_v1.5$ antibody was located at t-tubules (right panel in Fig. 6.6B) and there was some intercalated disk labelling (highlighted by arrow in right panel of Fig. 6.6B). Labelling by the Dumaine $Na_v1.5$ antibody was located at the outer cell membrane in isolated atrial myocytes and at t-tubules in isolated ventricular myocytes (Fig. 6.6C). In summary, there was surface labelling in isolated atrial myocytes and t-tubular labelling in ventricular myocytes. Note that intercalated disk labelling was only observed with the Catterall $Na_v1.5$ antibody. However, also note that in atrial cells there was some (or a hint of) intracellular striated labelling with all three antibodies.

6.3.2.3. Comparison of labelling by different cardiac Na^+ channel antibodies in AV node tissue sections

A comparison of labelling by three $Na_v1.5$ antibodies of AV node tissue sections is shown in Fig. 6.7. It has been reported that high levels of Na^+ channel immunofluorescence are observed in the atrial and ventricular myocardium, whereas the myocytes of the mid nodal cell region of the AV node are $Na_v1.5$-negative (Petrecca *et al.*, 1997). Although I will address the complex distribution of Na^+ channel isoforms in the AV node in the following chapters, this characteristic labelling pattern is useful at this stage. In the low-magnification montage of labelling by the Alomone $Na_v1.5$ antibody in Fig. 6.7A, there is abundant labelling in the atrial and ventricular myocardium, but no labelling in the enclosed node (Fig. 6.7A). This is equivalent to the labelling pattern observed by Petrecca *et al.* (1997). The high-magnification images shown as insets in Fig. 6.7A show intracellular striated labelling in both the atrial and ventricular myocytes. In the case of the ventricular myocytes, the intracellular striated labelling could correspond to t-tubules, but this is unlikely to be the case of atrial myocytes, because the

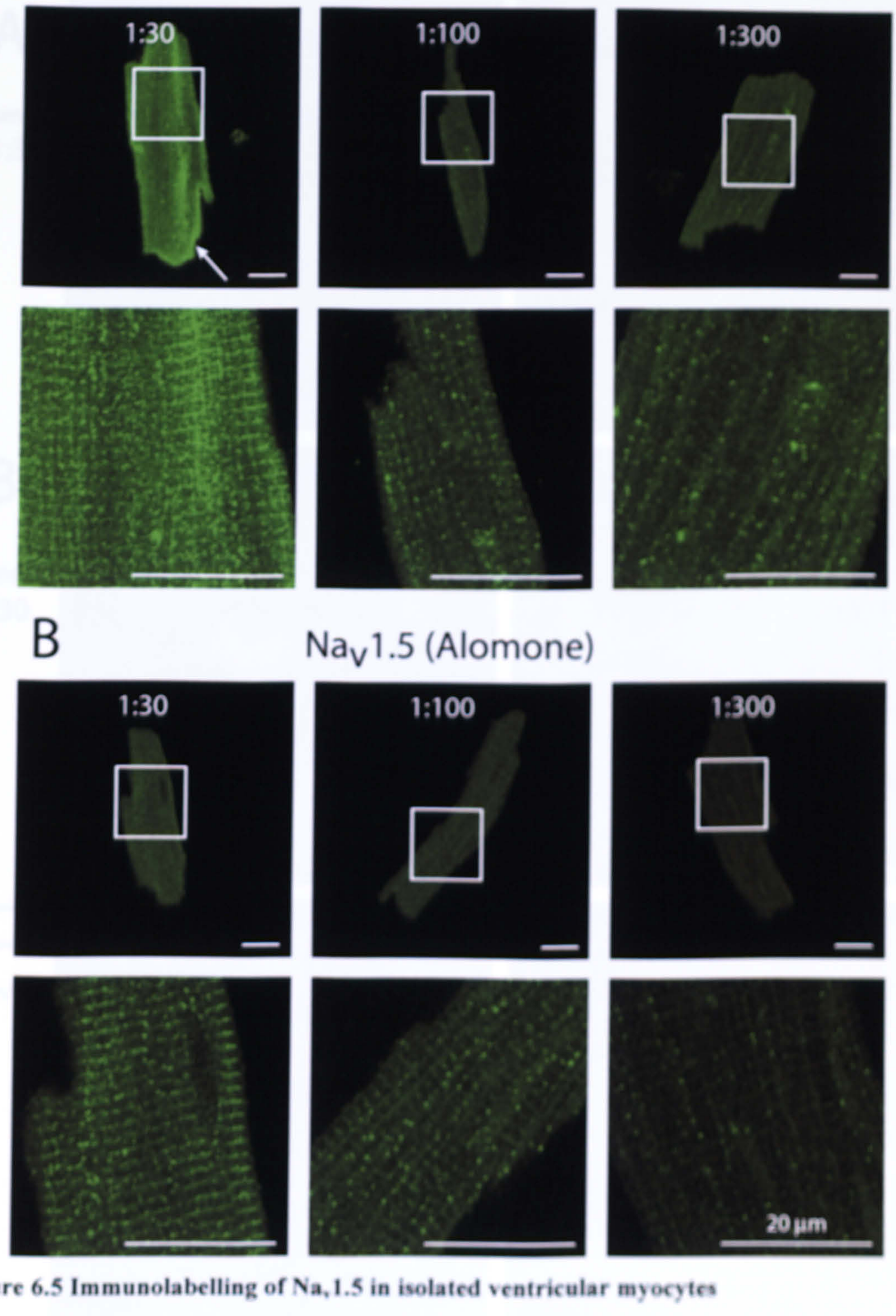

Figure 6.5 Immunolabelling of Na$_V$1.5 in isolated ventricular myocytes

A, high magnification images of labelling by the Catterall Na$_V$1.5 antibody (used at 1:30, 1:100 or 1:300; for more detail information see text) in isolated ventricular myocytes. Zoomed images in the bottom panels correspond to the framed areas in the top panels. The white arrow highlights intercalated disk labelling by the Catterall Na$_V$1.5 antibody. B, high magnification images of labelling by the Alomone Na$_V$1.5 antibody (used at 1:30, 1:100 or 1:300) in isolated ventricular myocytes. Zoomed images in the bottom panels correspond to the framed areas in the top panels. Scale bars, 20 µm.

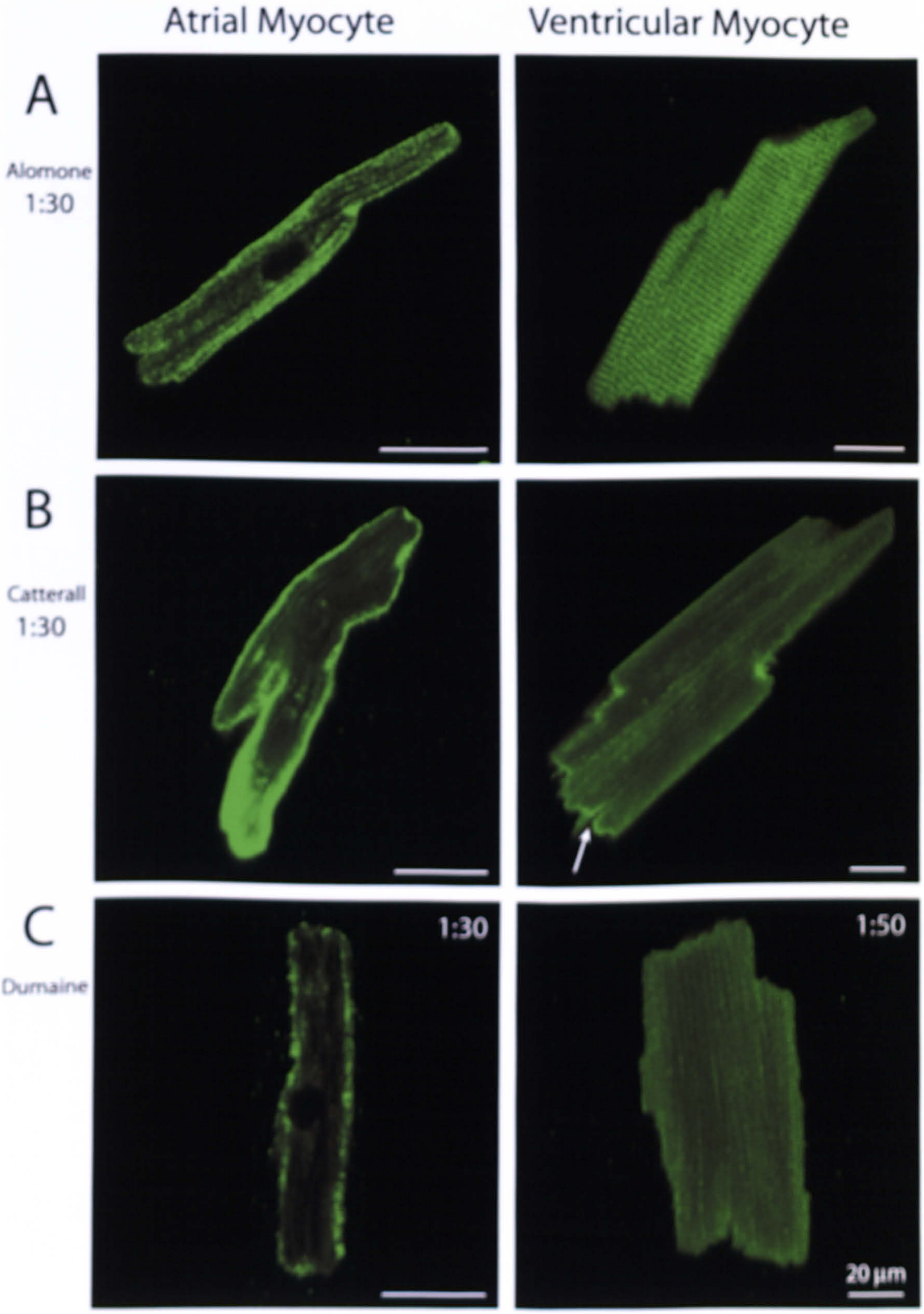

Figure 6.6 Comparison of immunolabelling by different Na$_v$1.5 antibodies in isolated atrial and ventricular myocytes

A-C, high magnification images of labelling by the Alomone Na$_v$1.5 antibody (used at 1:30), the Catterall Na$_v$1.5 antibody (used at 1:30) and the Dumaine Na$_v$1.5 antibody (used at 1:30 or 1:50; for more detail information see text) in isolated atrial and ventricular myocytes. In B, the white arrow highlights intercalated disk labelling by the Catterall Na$_v$1.5 antibody. Scale bars, 20 µm.

Figure 6.7 Comparison of immunolabelling by different $Na_v1.5$ antibodies of AV node tissue sections

A-C, labelling by Alomone, Catterall and Dumaine, respectively, $Na_v1.5$ antibodies. Low-magnification montages are shown on the left and high magnification images are shown on the right. All antibodies were used at a concentration of 1:30. AM, atrial myocardium; EN, enclosed node; ON, open node; VM, ventricular myocardium. Scale bars for montages (left): 400 μm (A), 200 μm (B) and 100 μm (C). Scale bars for high magnification images (right), 20 μm.

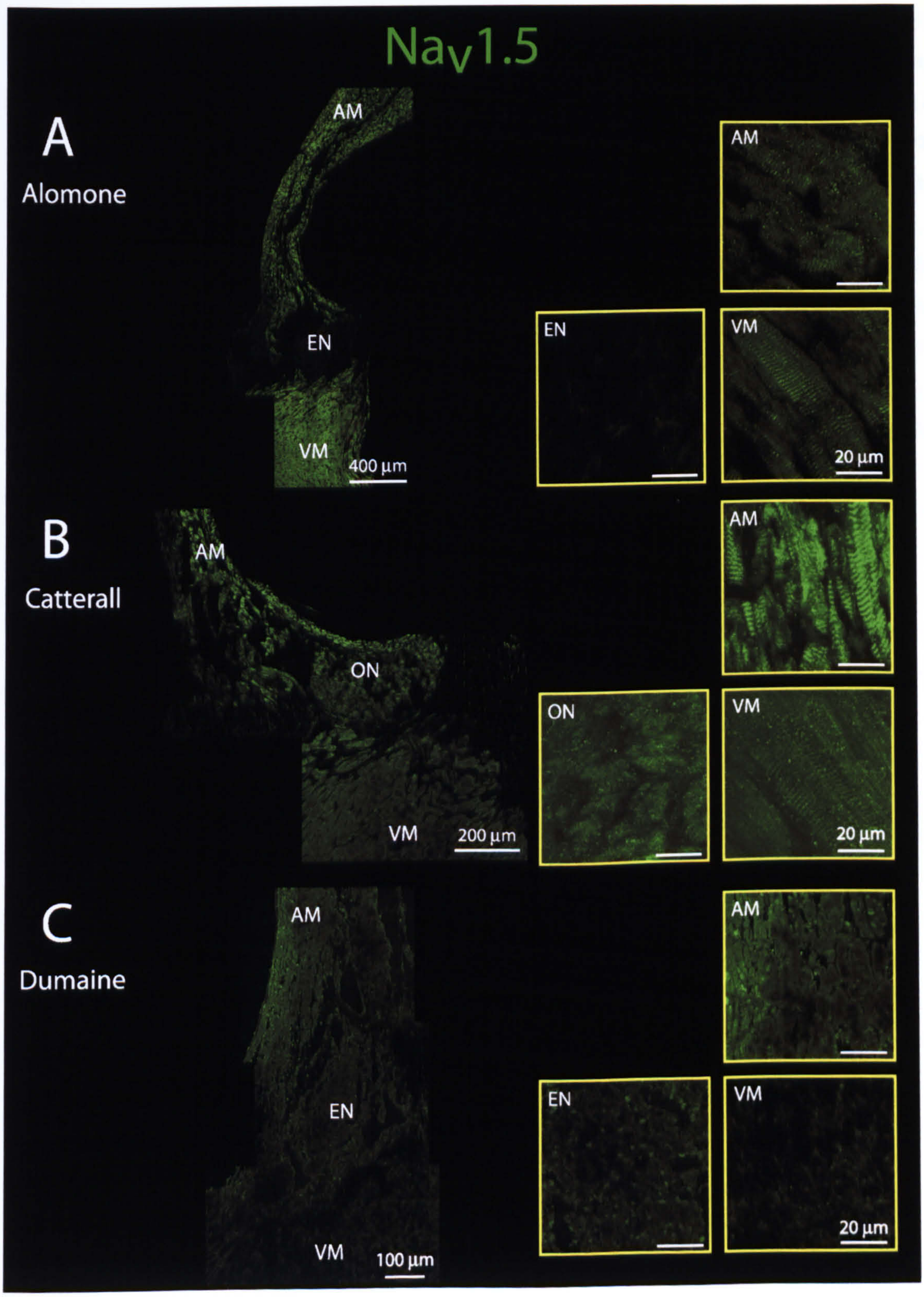
Nav1.5
A
Alomone
AM
EN
VM
400 µm
AM
EN
VM
20 µm
B
Catterall
AM
ON
VM
200 µm
AM
ON
VM
20 µm
C
Dumaine
AM
EN
VM
100 µm
AM
EN
VM
20 µm

majority of atrial myocytes are reported to have no or only rudimentary t-tubules (Cohen, 1996). In the case of the atrial myocytes (and perhaps the ventricular myocytes) the striated labelling could correspond to channel protein before trafficked to and from the outer cell membrane (if the trafficking apparatus is organised in a striated manner) (Fig. 6.7A) (Zhou *et al.*, 1998; Rahkila *et al.*, 2001). Fig. 6.7B and C show low magnification montages and high-magnification images of labelling by the two other $Na_v1.5$ antibodies. The Catterall $Na_v1.5$ antibody produced a similar pattern of labelling (at both the tissue and myocyte levels) as the Alomone $Na_v1.5$ antibody (Fig. 6.7A, B). The Dumaine $Na_v1.5$ antibody produced labelling of the atrial myocardium (the labelling was at the outer cell membrane) (Fig. 6.7C). The Dumaine $Na_v1.5$ antibody produced no labelling in the enclosed node (apart from non-specific labelling of nuclei; Fig. 6.7C). Finally, the Dumaine $Na_v1.5$ antibody produced patchy labelling at the outer cell membrane of the ventricular myocardium; the patchness of labelling may be the result of limited or no access of the antibody to the large mass of ventricular myocardium. In summary, there was abundant intracellular striated labelling in the atrial and ventricular myocardium and no labelling in the enclosed node by the Alomone and Catteral $Na_v1.5$ antibodies, whereas the Dumaine Nav1.5 antibody produced outer cell membrane labelling in the atrial myocardium, no labelling in the enclosed node and patchy outer membrane labelling in the ventricular myocardium.

6.3.2.4. Control experiments for the Alomone $Na_v1.5$ antibody

Based on the data presented in this chapter, the Alomone $Na_v1.5$ antibody was chosen for subsequent studies. In order to confirm whether labelling of this antibody was genuine or not, control experiments were carried out. Control experiments either without the primary antibody or with preincubation of the antibody with the antigenic peptide did not produce immunofluorescence above background in sections through the enclosed node (Fig. 6.8). Fig. 6.9 shows another control experiments for the Alomone $Na_v1.5$ antibody. As the concentration of the antibody was decreased, the intensity of the immunofluorescence became weaker as expected. Putting these results together, it is concluded that the Alomone $Na_v1.5$ antibody is a reliable antibody.

6.4. Discussion

6.4.1. Expression of neuronal Na^+ channel isoforms

$Na_v1.1$ labelling was present in atrial and ventricular myocytes and myocardium (Figs. 6.1 and 6.3). The labelling was in the outer cell membrane in atrial myocytes and myocardium (Figs. 6.1 and 6.3). The labelling was localised in intercalated disks, the outer cell membrane and in the cytoplasm (presumably t-tubular labelling) in ventricular myocytes and myocardium (Figs. 6.2 and 6.4). In atrial and ventricular myocytes and myocardium, there was also a presumably non-specific labelling of the nuclei (Figs. 6.1-6.4). $Na_v1.2$ labelling was absent in

Figure 6.8 Control experiments for the Alomone $Na_v1.5$ antibody

A, low magnification montage of section containing the enclosed node double labelled for $Na_v1.5$ (green) and Cx43 (red). The Alomone $Na_v1.5$ antibody was used. B, low magnification montage of an adjacent section double labelled for $Na_v1.5$ (green) and Cx43 (red). The procedure for labelling $Na_v1.5$ with the Alomone $Na_v1.5$ antibody was followed, but the primary antibody was not added. C, low magnification montage of an adjacent section double labelled for $Na_v1.5$ (green) and Cx43 (red). In this experiment, prior to the incubation of the section with the Alomone antibody for Nav1.5, the antibody was preincubated with the antigenic peptide. AM, atrial myocardium; EN, enclosed node; VM, ventricular myocardium. Scale bars, 200 μm.

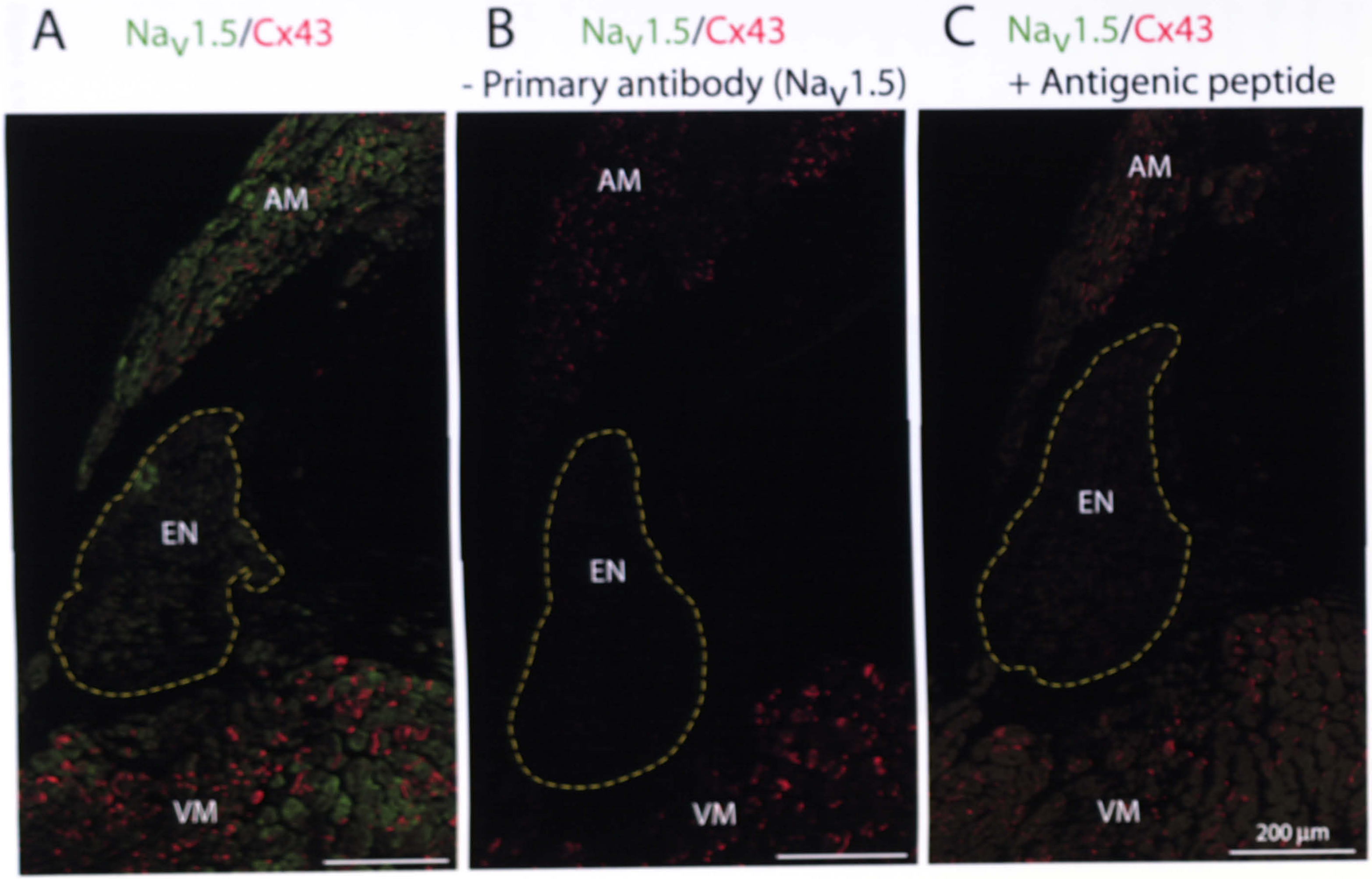
A
$Na_V1.5$/Cx43
B
$Na_V1.5$/Cx43
- Primary antibody ($Na_V1.5$)
C
$Na_V1.5$/Cx43
+ Antigenic peptide
AM
EN
VM
200 µm

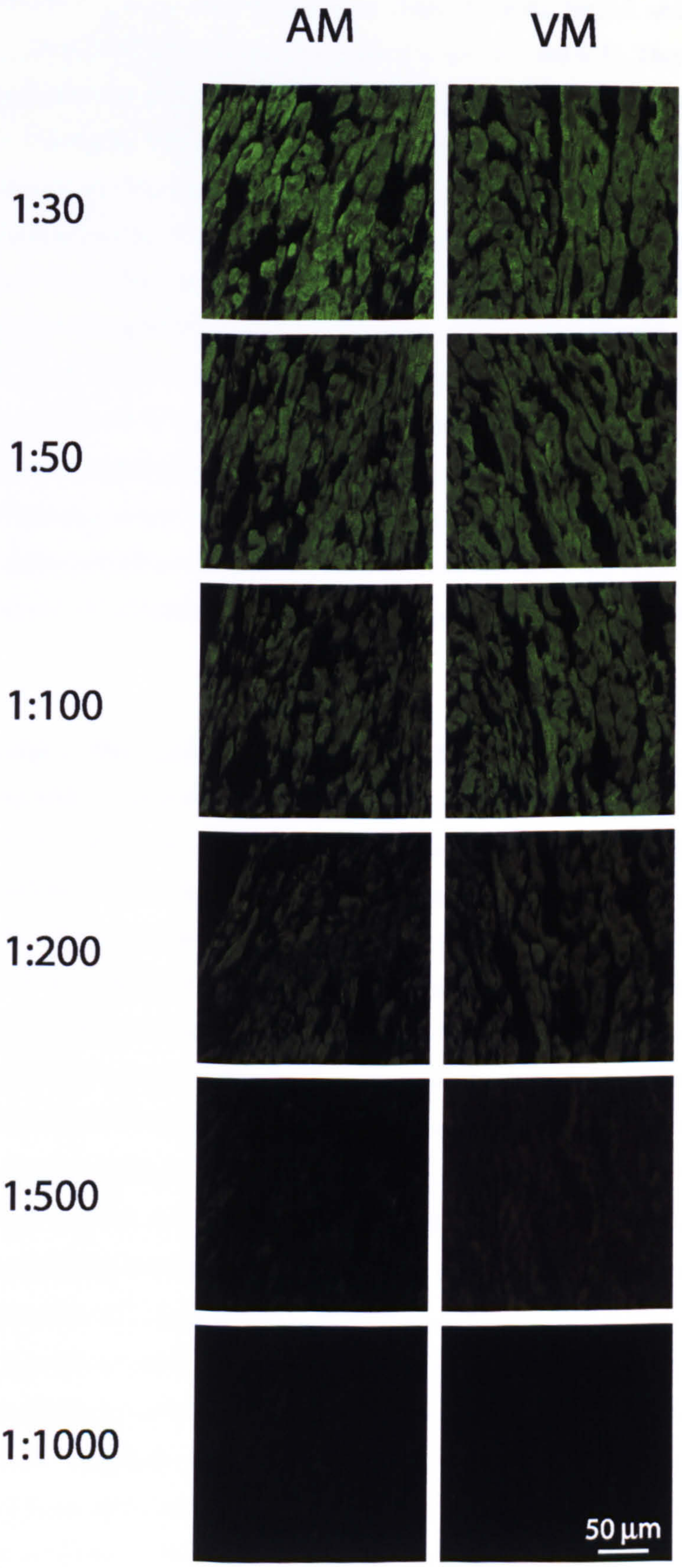

Figure 6.9 Control experiment with a series of concentrations of the Alomone $Na_v1.5$ antibody on atrial and ventricular myocardium

Applied antibody concentrations are shown on left. AM, atrial myocardium; VM, ventricular myocardium. Scale bar, 50 µm.

atrial and ventricular myocytes and myocardium (Figs. 6.1-6.4). $Na_v1.3$ and $Na_v1.6$ labelling was not detected in atrial myocytes and myocardium (Figs. 6.1 and 6.3). There was $Na_v1.3$ and $Na_v1.6$ labelling at t-tubules in isolated ventricular myocytes (Fig. 6.2), but $Na_v1.3$ labelling was not observed in ventricular tissue sections under my experimental conditions (Fig. 6.4). The reason for the absence of t-tubular labelling of $Na_v1.3$ in tissue sections is uncertain. A possible explanation is that the access of the antibody to the epitope in tissue section is limited, unlike in isolated myocytes. Generally, the experience of our laboratories is that antibodies have better access to the epitope in isolated myocytes than in tissue sections (Dobrzynski *et al.*, 2000).

Malhotra *et al.* (2001) using a specific antibody for $Na_v1.1$, called SP11, reported that $Na_v1.1$ labelling is detected at t-tubules in the mouse heart. Maier *et al.* (2002) using specific commercial antibodies reported that the neuronal Na^+ channel isoforms, $Na_v1.1$, $Na_v1.3$ and $Na_v1.6$, are localised in t-tubules in mouse ventricular myocytes. However, we observed $Na_v1.1$ labelling at the surface membrane and intercalated disks as well as in the t-tubules in isolated rat ventricular myocytes. A possible explanation of this discrepancy may be the difference in species.

6.4.2. Expression of the cardiac Na^+ channel isoform

The intracellular localisation of $Na_v1.5$ labelling is uncertain. Cohen (1996) reported that $Na_v1.5$ labelling was in the surface membrane and in the cytoplasm in both atrial and ventricular myocardium of rat. The labelling in the cytoplasm was striated and, therefore, could correspond to the t-tubular system, although atrial myocytes have no or only rudimentary t-tubules. Although the striated labelling could correspond to $Na_v1.5$ being trafficked to and from the surface membrane, labelling at the intercalated disk was stronger than in the surface membrane and t-tubular system with the $Na_v1.5$ antibody, which recognises peptide rH1, corresponding to residues 492-511 of the α subunit of rat $Na_v1.5$ (Cohen, 1996). This antibody is nearly identical to the Alomone $Na_v1.5$ antibody (which recognises residues 493-511 of the α subunit of rat $Na_v1.5$, Table 6.1) used in this study. Kucera *et al.* (2002) observed $Na_v1.5$ labelling at the intercalated disk in cultures of neonatal rat ventricular myocytes with antibody which recognises peptide rH1, corresponding to residues 492-510 of the α subunit of rat $Na_v1.5$. This antibody is also nearly identical to the Alomone $Na_v1.5$ antibody (Table 6.1). Maier *et al.* (2002) only observed $Na_v1.5$ labelling at intercalated disks in mouse ventricular myocytes with $Na_v1.5$ antibody that recognises peptide SH1, corresponding to residues 1122-1137 of the α subunit of rat $Na_v1.5$ (i.e. the Catterall $Na_v1.5$ antibody, Table 6.1) and argued that rH1 antibody used in the study of Cohen (1996) would also have recognised $Na_v1.3$, based on a BLAST amino acid sequence search.

In the present study, three independent $Na_v1.5$ antibodies were used (Table 6.1). These antibodies produced similar labelling in isolated atrial and ventricular myocytes (Fig. 6.6). There was striated intracellular labelling in rat ventricular myocytes and myocardium by all

three antibodies (Figs. 6.6 and 6.7) except in the case of the Dumaine $Na_v1.5$ antibody and rat ventricular myocardium (Fig. 6.7). This is in agreement with Cohen (1996), but in contrast to Kucera *et al.* (2002) and Maier *et al.* (2002). This difference could be due to a difference in antibody, because the SH1 antibody was used both in this study and by Maier *et al.* (2002). The difference could be a species difference, because rat was used both in this study and the study by Cohen (1996), whereas mouse was used by Maier *et al.* (2002). Finally, the difference could be result of two pools of $Na_v1.5$ (one at the intercalated disk and one at or next to the t-tubules) and different procedures being required to access the pools. In the present study, labelling in rat atrial myocytes at the surface membrane by all three antibodies was observed (Fig. 6.6). In contrast, in the present study, intracellular striated labelling was observed in rat atrial myocardium when the Alomone and Catterall (but not the Dumaine) antibodies were used (Fig. 6.7). The intracellular striated labelling is consistent with the result of Cohen (1996) on rat atrial myocardium. The difference between labelling of atrial myocytes and myocardium in the present study could once again be the result of different pools of $Na_v1.5$ in a cell that require different conditions to access. It is noteworthy that there was a hint of intracellular striated labelling in atrial myocytes (Fig. 6.6). The intracellular striated labelling in atrial myocardium is possibly the result of $Na_v1.5$ being trafficked to and from the membrane.

Before deciding whether the Alomone $Na_v1.5$ antibody would be used for the remainder of the study or not, control experiments were carried out: preadsorption of the primary antibody with the antigenic peptide and the omission of the primary antibody (Fig. 6.8). All control experiments produced background levels of immunofluorescence. In proportion to the Alomone $Na_v1.5$ antibody concentration, the intensity of the immunofluorescence varied (Fig. 6.9). These results are consistent with the Nav1.5 labelling by the Alomone antibody being genuine.

In order to confirm the specificity of the Alomone $Na_v1.5$ antibody, $Na_v1.5$ with GFP was transfected into HEK-293 cells by Dr. S. Xu. $Na_v1.5$ labelling by the Alomone antibody was only observed in transfected HEK-293 cells (data not shown). In addition, Western blot analysis was carried by Dr. S. Jones. Using the Alomone $Na_v1.5$ antibody, the expression of $Na_v1.5$ in rat ventricular myocardium was detected and there was a single band at the correct molecular weight (data not shown).

$Na_v1.5$ has been reported to be absent from the mouse SA node using the Catterall $Na_v1.5$ antibody (Maier *et al.*, 2003; Lei *et al.*, 2004). Consistent with this, in the present study, $Na_v1.5$ labelling was not detected in the centre of SA node using the Alomone antibody (Figs. 10.3 and 10.4). The Alomone Nav1.5 antibody is ,therefore, assumed to be selective and effective.

Chapter 7

Na^+ channel expression in the AV node

7.1. Introduction

The cardiac voltage-gated Na^+ channel isoform ($Na_v1.5$) is known to play a major role not only in the initiation of the action potential, but also in action potential conduction in the heart (Schram *et al.*, 2002). It has been reported that neither membrane hyperpolarization nor the addition of TTX modifies the upstroke phase of the action potential in the AV node, leading to the proposal that the action potential of AV node cells is generated by a slow current system (i.e. $I_{Ca,L}$) and that these cells do not express functional Na^+ channels (Meijler & Janse, 1988). However, other investigators have shown that hyperpolarization can increase the upstroke velocity of the action potential and render some AV node preparations sensitive to TTX (Kokubun *et al.*, 1982). Therefore, it is unclear whether the slow action potential upstroke in the AV node is due to a voltage-dependent inactivation of Na^+ channels or the absence of Na^+ channels in these cells. There may also be a gradation of Na^+ protein expression as one proceeds from the peripheral nodal region to the central nodal region: the upstroke velocity of the action

potential is low in the compact part of the AV node, >20 V/s (Billette, 1987; Patterson & Scherlag, 2002), as compared to that in the atrial muscle (150 - 300 V/s; Schram *et al.*, 2002; Patterson & Scherlag, 2002). In the fast and slow pathways into the AV node the upstroke velocity is intermediate (41 or 60 V/s; Patterson & Scherlag, 2002) between that in the compact node and atrial muscle.

Petrecca *et al.* (1997) previously reported a lack of or a low density of Na^+ channels in mid-nodal region using a Na^+ channel antibody generated against a conserved region of the Na_v1 subfamily and this can explain the slow upstroke, low amplitude and low conduction velocity of the action potential in the compact AV node. However, besides $Na_v1.5$, some neuronal Na^+ channel isoforms have been recently reported to be expressed in mouse ventricular myocytes and adult rat and mouse SA node. The neuronal Na^+ channels have a physiological function at both sites: a role in excitation-contraction coupling in the ventricular myocardium and as a pacemaker current in the SA node (Maier *et al.*, 2002; Maier *et al.*, 2003). The expression and distribution of Na^+ channel isoforms in the AV node has not been determined. The previous investigation of Na^+ channel distribution in the rabbit AV node by Petrecca *et al.* (1997) did not use an antibody against a specific Na^+ channel isoform.

7.2. Methods

The general immunohistochemistry procedures are described in chapter 2 (section 2.6). Details of procedures for neuronal and cardiac Na^+ channel isoforms are given in chapter 6 (section 6.2.2 and 6.2.3, respectively).

7.2.1. Semi-quantitative assessment of immunofluorescence

The relative level of $Na_v1.5$ expression was determined in a semi-quantitative manner with Scion image (release: Alpha 4.0.3.2). The image displayed levels of pixel intensity ranging from 0 to 255 on a linear scale. In order to compare intensities of different regions throughout the AV node tissue sections, all measured intensities in one section were divided by the highest intensity value (from the ventricular myocardium) and converted into a percentage.

7.3. Results

Immunohistochemistry was used to investigate the distribution of neuronal and cardiac Na^+ channel isoforms in the AV node. The skeletal isoform, $Na_v1.4$, was not investigated.

7.3.1. Expression of neuronal Na^+ channel isoforms

To investigate whether neuronal Na^+ channel isoforms are present in the AV node, I used specific antibodies raised against $Na_v1.1$, $Na_v1.2$, $Na_v1.3$ and $Na_v1.6$. Among three complete serial sectioned preparations, $Na_v1.1$ and $Na_v1.3$ were studied in two preparations. In

addition, similar data for $Na_v1.1$ and $Na_v1.3$ were obtained from three other preparations (level of the enclosed node only). $Na_v1.2$ and $Na_v1.6$ were not detected in atrial and ventricular myocardium (chapter 6). Furthermore, these isoforms were not detected in the nodal myocytes of the AV node in sections from three hearts (data not shown). Thus these isoforms will not be considered further.

7.3.1.1. Expression of $Na_v1.1$ in the AV node

Fig. 7.1 shows high magnification images of $Na_v1.1$ labelling in different regions at levels 4 (B), 8 (A and C), 9 (D and E), 10 (I) and 11 (F and H) of the main preparation studied (Fig. 2.1B) (except left bundle branch; at level 5 of the second preparation, Fig. 4.6A). Similar data were obtained from the second preparation (Fig. 4.6A). In accordance with data from isolated myocytes shown in chapter 6 (section 6.3.1), $Na_v1.1$ labelling was located at the cell membrane in the atrial myocardium (Fig. 7.1I). In the ventricular myocardium, $Na_v1.1$ labelling was located at the cell membrane and also co-localised with Cx43 at the intercalated disks (Fig. 7.1A). There was also a non-specific labelling of nuclei. $Na_v1.1$ labelling was also present in the posterior/inferior nodal extension and the zone of transitional cells (Fig. 7.1B and D). The absence of Cx43 in these regions suggests that myocytes in these regions differ from myocytes in the atrial and ventricular myocardium. There was no $Na_v1.1$ labelling (apart from the non-specific labelling of nuclei) in the open node, enclosed node, common bundle and termination of the AV ring bundle (Fig. 7.1C, E, F and H, respectively). The absence of $Na_v1.1$ as well as Cx43 in these regions suggests that the myocytes in these regions differ from myocytes in the posterior/inferior nodal extension and the zone of transitional cells. Although $Na_v1.1$ labelling was absent in the conduction tissue from the open node to common bundle, $Na_v1.1$ was expressed in the left bundle branch (Fig. 7.1G).

7.3.1.2. Expression of $Na_v1.3$ in the AV node

Whereas Cx43 was absent, there was labelling of $Na_v1.3$ in the enclosed node from two different preparations (Fig. 7.2, left panels). In accordance with data already shown in chapter 6 (section 6.3.1), there was no labelling of $Na_v1.3$ in the atrial and ventricular myocardium (Fig. 7.2). Neurofilament160 (NF160) is a neuronal cytoskeleton protein. The right panels in Fig. 7.2 show adjacent sections double labelled for $Na_v1.3$ and NF160 and $Na_v1.3$ and NF160 were co-localised in the enclosed node. The co-localisation of $Na_v1.3$ and NF160 labelling demonstrates that $Na_v1.3$ was only expressed in nerve fibres and nerve cell bodies innervating the enclosed node (i.e. not in the nodal myocytes; Fig. 7.2).

Fig. 7.3 shows double labelling of $Na_v1.3$ and Cx43 in different regions at levels 4, 8, 9, 11 and 13 of the main preparation (Fig. 2.1B). Similar data were obtained from the third preparation (not shown). To facilitate comparison, high-magnification images of the yellow framed areas in Fig. 7.3 were taken (Fig. 7.4). As already shown, there was no labelling of

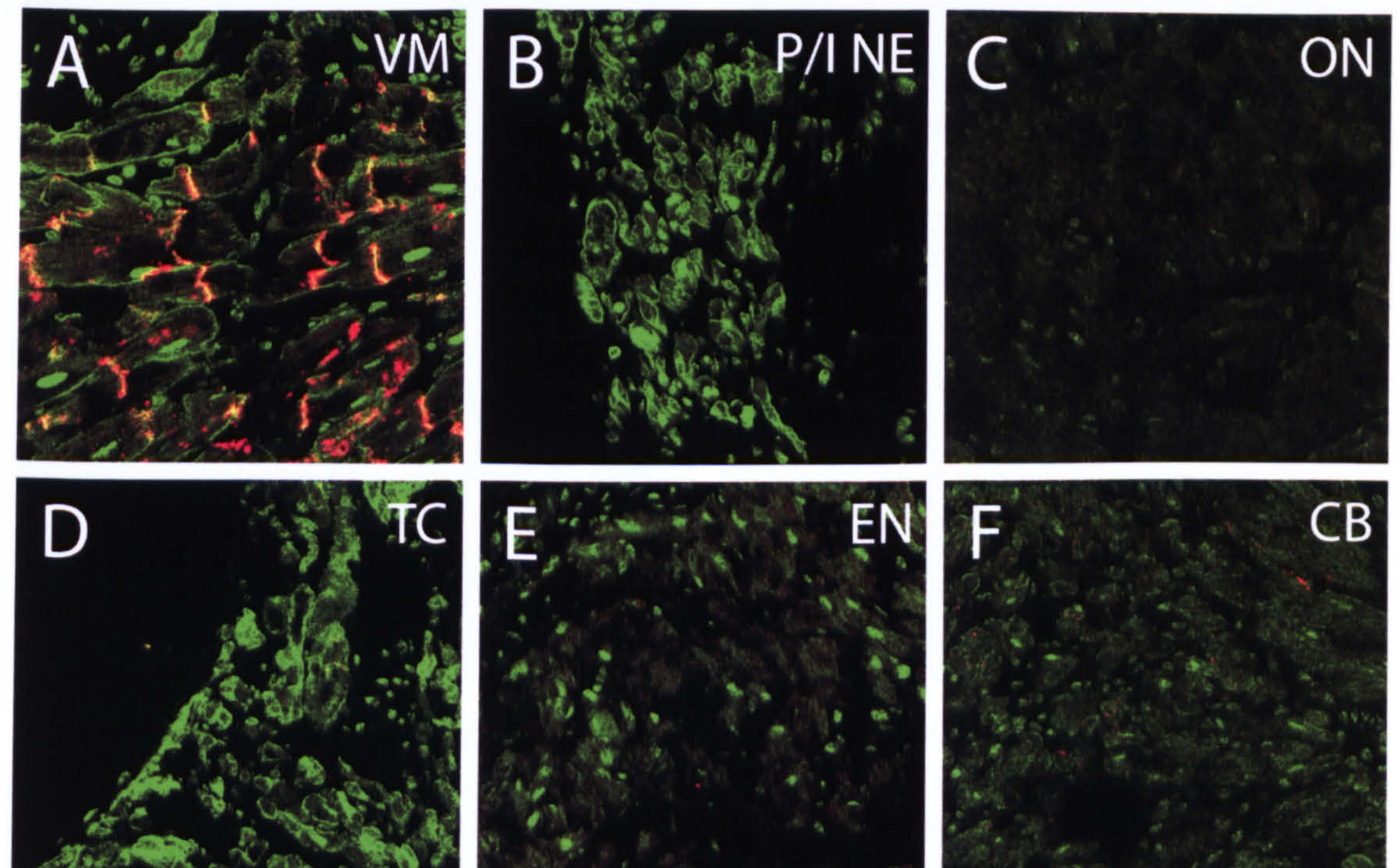

Figure 7.1 $Na_v1.1$ labelling in the different regions of the AV node in the main preparation (Fig. 2.1B)

High-magnification images of double labelling for $Na_v1.1$ (green) and Cx43 (red) in different regions of the AV node. AM, atrial myocardium; CB, common bundle; EN, enclosed node; LBB, left bundle branch; ON, open node; P/I NE, posterior/inferior nodal extension; TAVRB, termination of the AV ring bundle; TC, transitional cells; VM, ventricular myocardium. Scale bar, 50 µm.

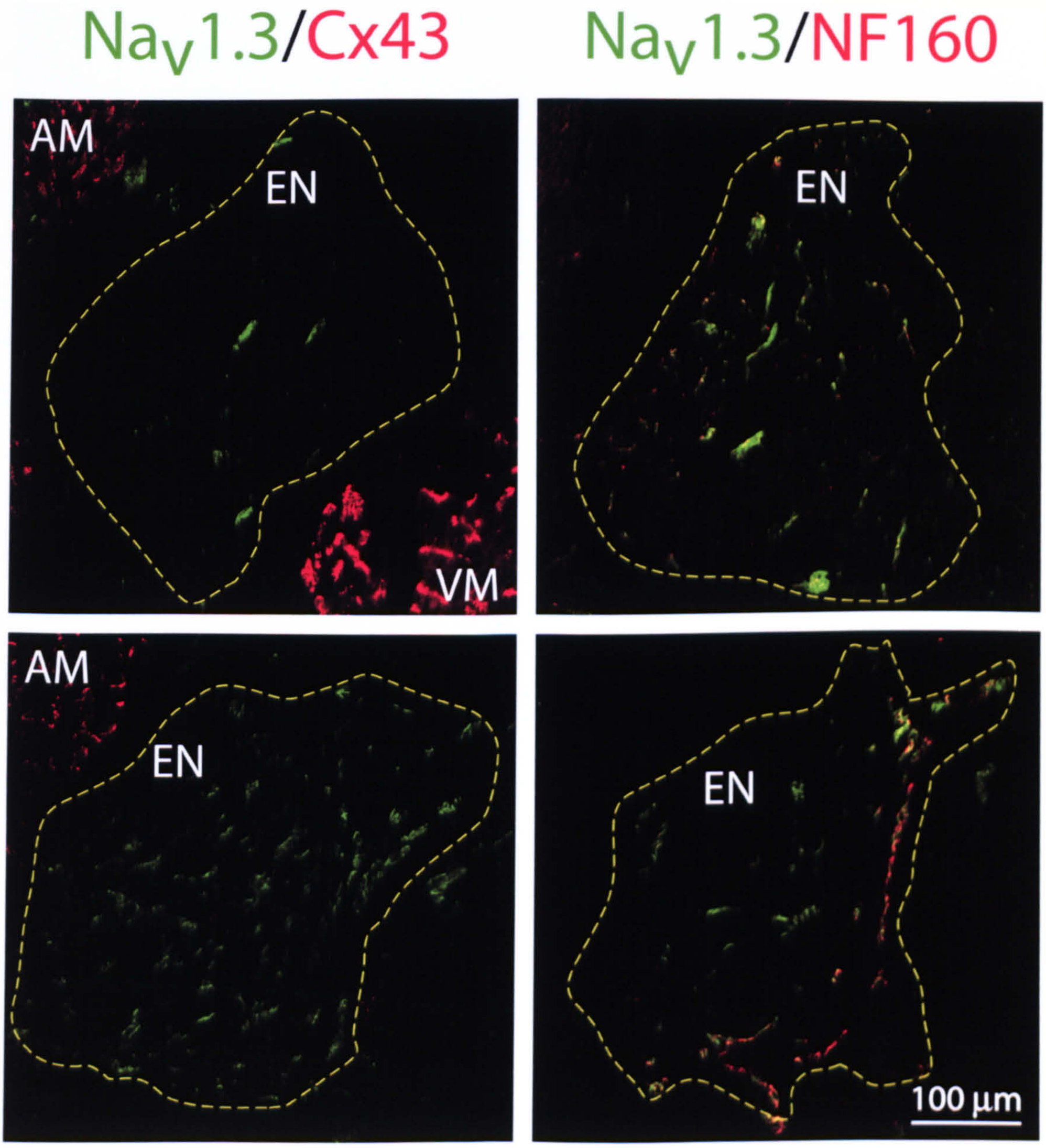

Figure 7.2 Co-localisation of $Na_v1.3$ and neurofilament in the enclosed node

High-magnification images of double labelling in the enclosed node for $Na_v1.3$ (green) with Cx43 (red, left) and NF160 (red, right). Where the $Na_v1.3$ and NF160 labels are co-localised, there is a yellow colour. Yellow ringed areas represent the enclosed node. AM, atrial myocardium; EN, enclosed node; VM, ventricular myocardium. Scale bar, 100 µm.

Figure 7.3 $Na_v1.3$ labelling in the different regions of the AV node

A-E, montages of sections double labelled for $Na_v1.3$ (green) and Cx43 (red) in different regions of the AV node. The posterior/inferior nodal extension is shown in A, the open node is shown in B, the enclosed node is shown in C, the common bundle is shown in D and the termination of the AV ring bundle is shown in E. High magnification images of the yellow framed areas are shown in Fig. 7.4. Framed areas are numbered according to the sequence of images in Fig. 7.4. AM, atrial myocardium; CB, common bundle; EN, enclosed node; LBB, left bundle branch; ON, open node; P/I NE, posterior/inferior nodal extension; TAVRB, termination of the AV ring bundle; TC, transitional cells; VM, ventricular myocardium. Scale bars, 100 μm (A and B) and 200 μm (C to E).

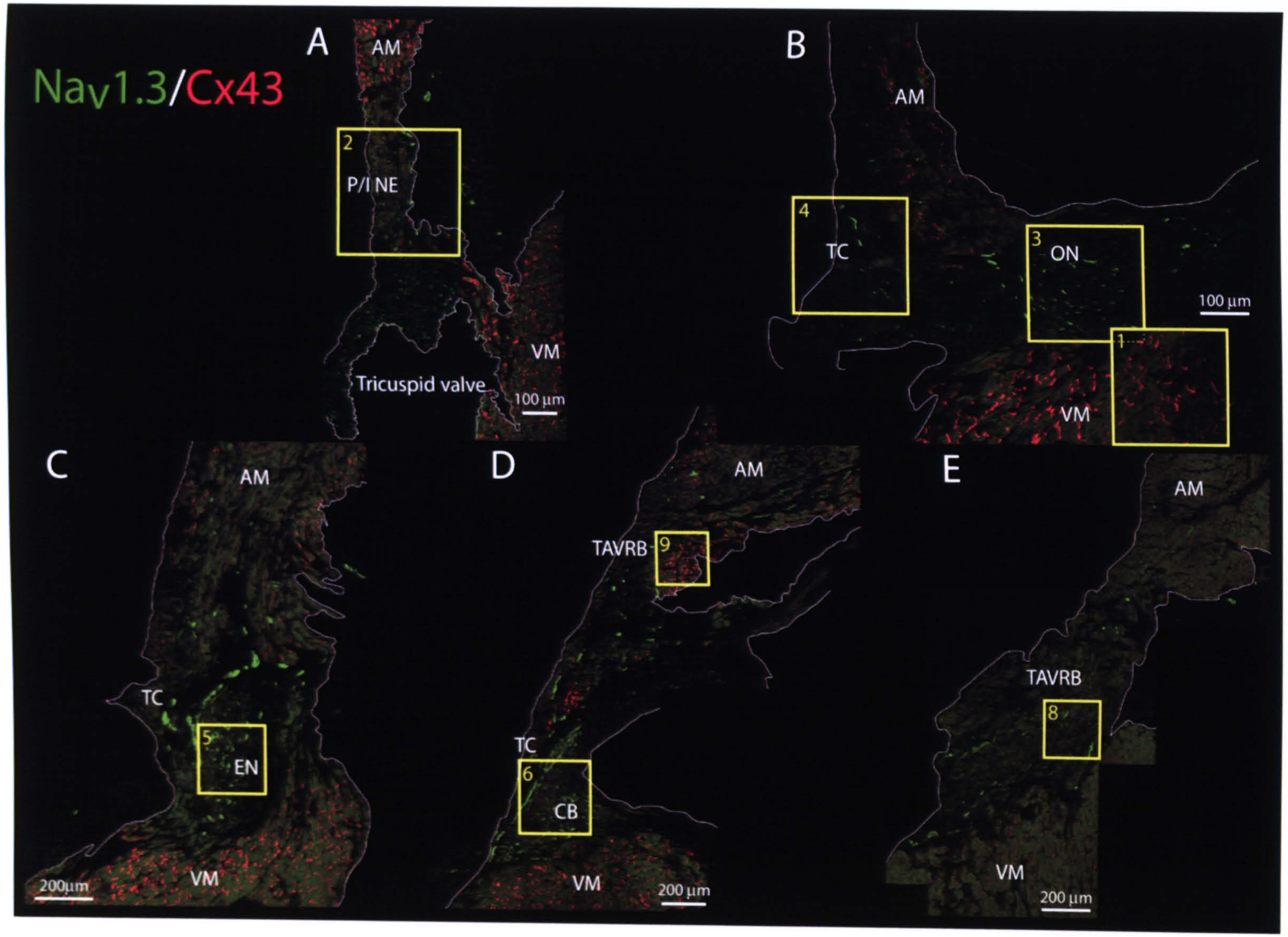
Nav1.3/Cx43
A
AM
2
P/I NE
VM
Tricuspid valve
100 µm
B
AM
4
TC
3
ON
100 µm
1
VM
C
AM
TC
5
EN
VM
200µm
D
AM
TAVRB
9
TC
6
CB
VM
200 µm
E
AM
TAVRB
8
VM
200 µm

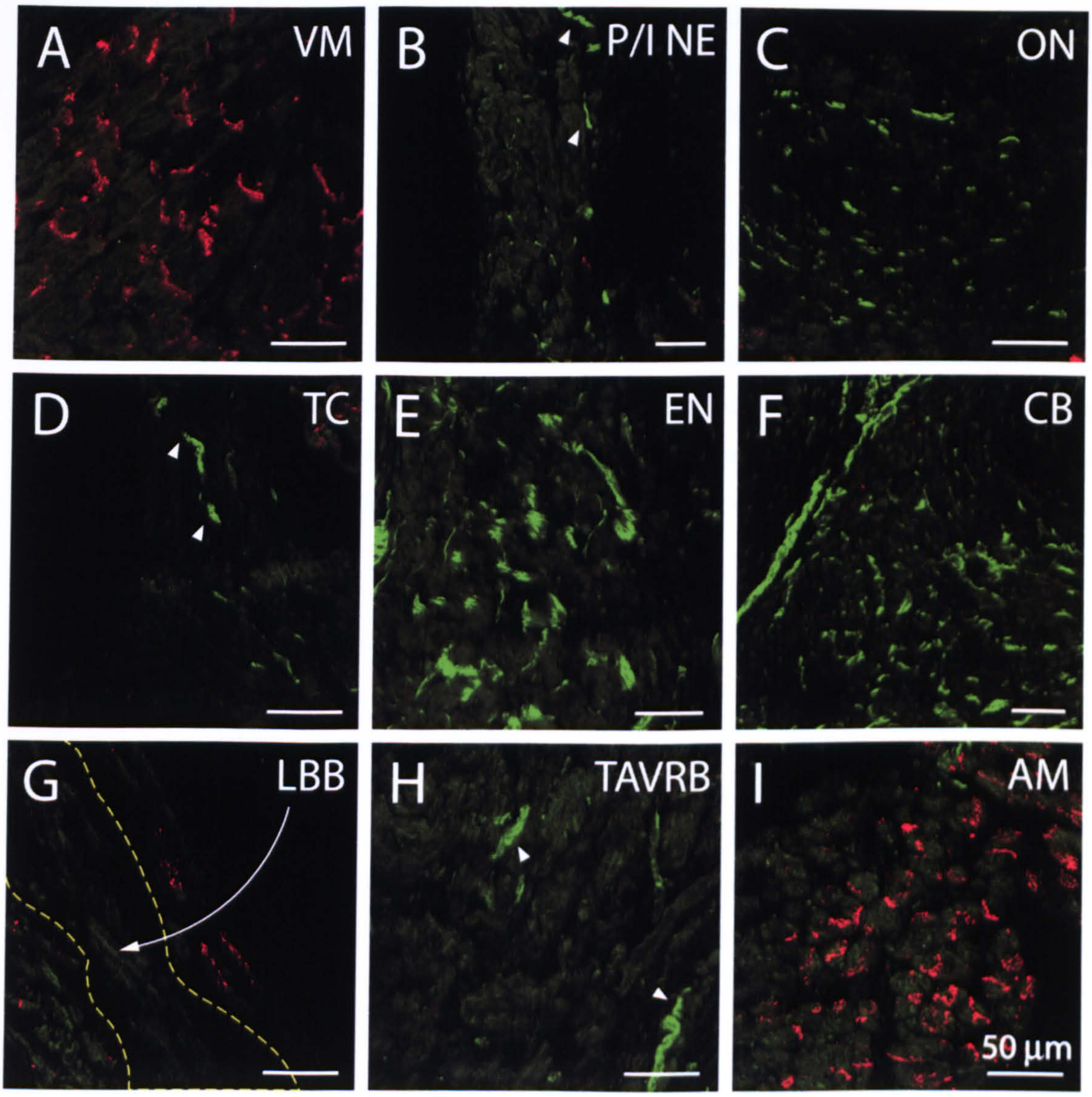

Figure 7.4 $Na_v1.3$ labelling in the different regions of the AV node

High-magnification images of double labelling for $Na_v1.3$ (green) and Cx43 (red) in different regions of the AV node. White arrowheads designate nerve cell bodies labelled for $Na_v1.3$ in B, D and H. AM, atrial myocardium; CB, common bundle; EN, enclosed node; LBB, left bundle branch; ON, open node; P/I NE, posterior/inferior nodal extension; TAVRB, termination of the AV ring bundle; TC, transitional cells; VM, ventricular myocardium. Scale bars, 50 µm.

$Na_v1.3$ in atrial and ventricular myocardium (the dull green labelling in Fig. 7.4A and I is background only). $Na_v1.3$ labelling was present but much less abundant in the posterior/inferior nodal extension and the zone of transitional cells (Fig. 7.4B and D). $Na_v1.3$ labelling was abundant in the open node, enclosed node and common bundle (Fig. 7.4 C, E and F). There was little or no labelling in the termination of the AV ring bundle and left bundle branch (Fig. 7.4G and H).

7.3.2. Expression of the cardiac Na^+ channel isoform, $Na_v1.5$

In order to investigate expression of the cardiac Na^+ channel isoform in the AV node, the Alomone $Na_v1.5$ antibody was used on sections from three serially sectioned preparations. Data from the main main preparation (Fig. 2.1B) and the third preparation are shown here. Similar data were obtained from the second preparation. Also similar data for $Na_v1.5$ were obtained from one other preparation (level of the enclosed node only).

7.3.2.1. Posterior/inferior nodal extension

Fig. 7.5 shows immunolabelling of $Na_v1.5$ in the posterior/inferior nodal extension from two different preparations. Fig. 7.5A shows a section at level 4 in the main preparation (Fig. 2.1B) and Fig. 7.5B shows a section at level 3 in the third preparation. The posterior/inferior nodal extension, ringed in yellow in Fig. 7.5B, is located above the ventricular myocardium and tricuspid valve and beneath the atrial myocardium. There was dense labelling of $Na_v1.5$ in the atrial and ventricular myocardium (Fig. 7.5). As already shown in chapter 4 (section 4.3.1), Cx43 was absent in the posterior/inferior nodal extension (Fig. 7.5B). There was labelling of $Na_v1.5$ in the posterior/inferior nodal extension (but weaker than that in the atrial and ventricular myocardium) (Fig. 7.5). As expected, there was no labelling of $Na_v1.5$ in connective tissue (Fig. 7.5A). A high-magnification image of the framed area in Fig. 7.5A (labelled 2) is shown in Fig. 7.11B.

7.3.2.2. Open node

Fig. 7.6 shows immunolabelling of $Na_v1.5$ in the open node from two different preparations. Fig. 7.6A shows a section at level 7 in the main preparation (Fig. 2.1B) and Fig. 7.6B shows a section at level 7 in the third preparation. The open node is located at the centre of the montage, i.e. between the atrial and ventricular myocardium, in which $Na_v1.5$ labelling is abundant. As already shown in chapter 4 (section 4.3.1), the open node and the zone of transitional cells (ringed in yellow in Fig. 7.6) are Cx43-negative (Fig. 7.6B). There was little or no labelling of $Na_v1.5$ in the open node (Fig. 7.6). The "bump", ringed in yellow, was localised far above the open node in Fig. 7.6A. As shown in Fig. 7.6, the "bump" is Nav1.5-negative. As shown previously (Fig. 4.9), the "bump" is also Cx43-negative, DP-positive and ANP-negative. Thus, labelling in the "bump" is same as in the open node, the enclosed node, the common

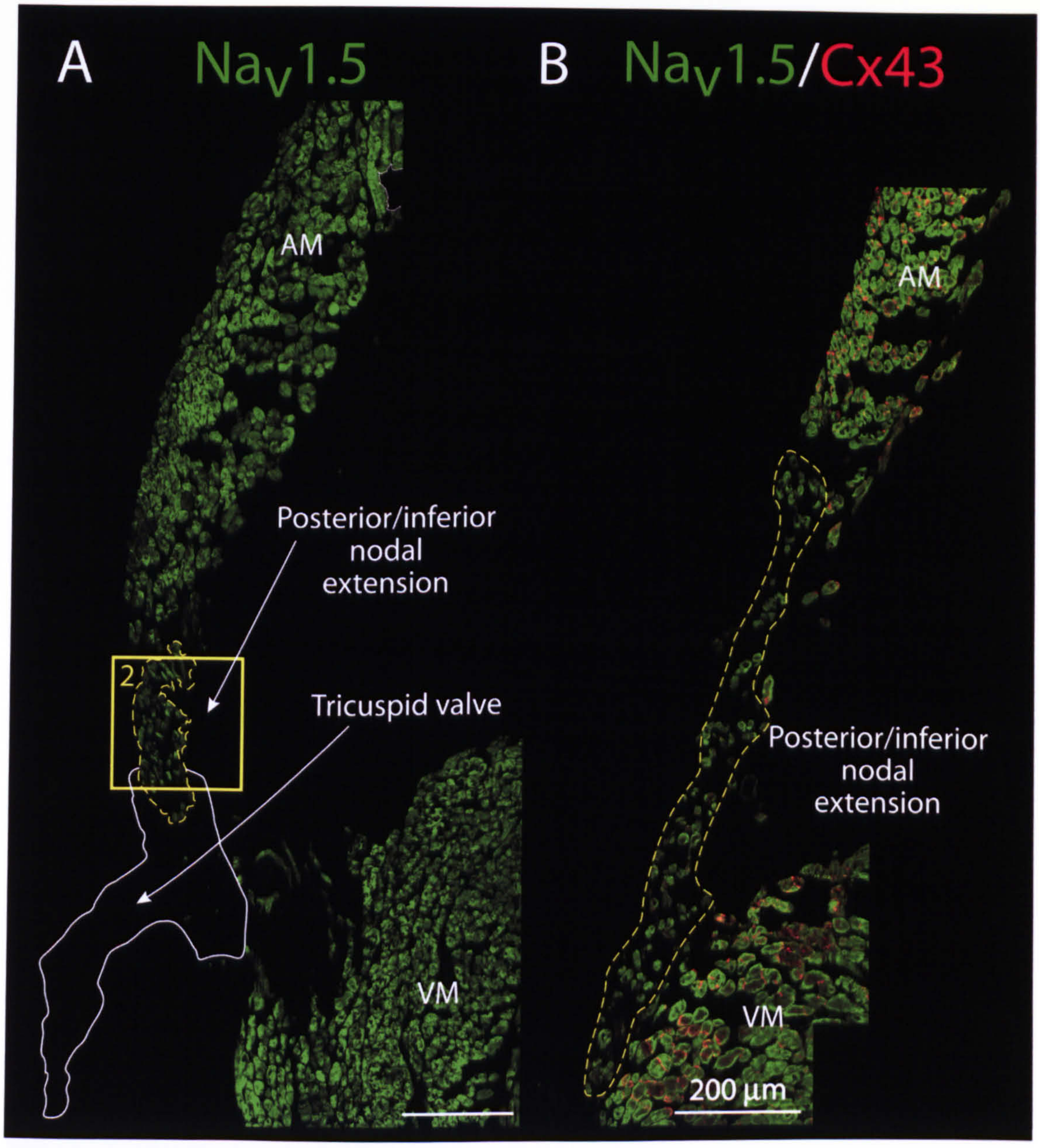

Figure 7.5 Na$_v$1.5 labelling in the posterior/inferior nodal extension

A, montage of Na$_v$1.5 (green) labelled section at level 4 in the main preparation (Fig. 2.1B). B, montage of Na$_v$1.5 (green) and Cx43 (red) double labelled section at level 3 in the third preparation. A high magnification image of the yellow framed area (labelled 2) in A is shown in Fig. 7.11B. AM, atrial myocardium; VM, ventricular myocardium. Scale bars, 200 µm.

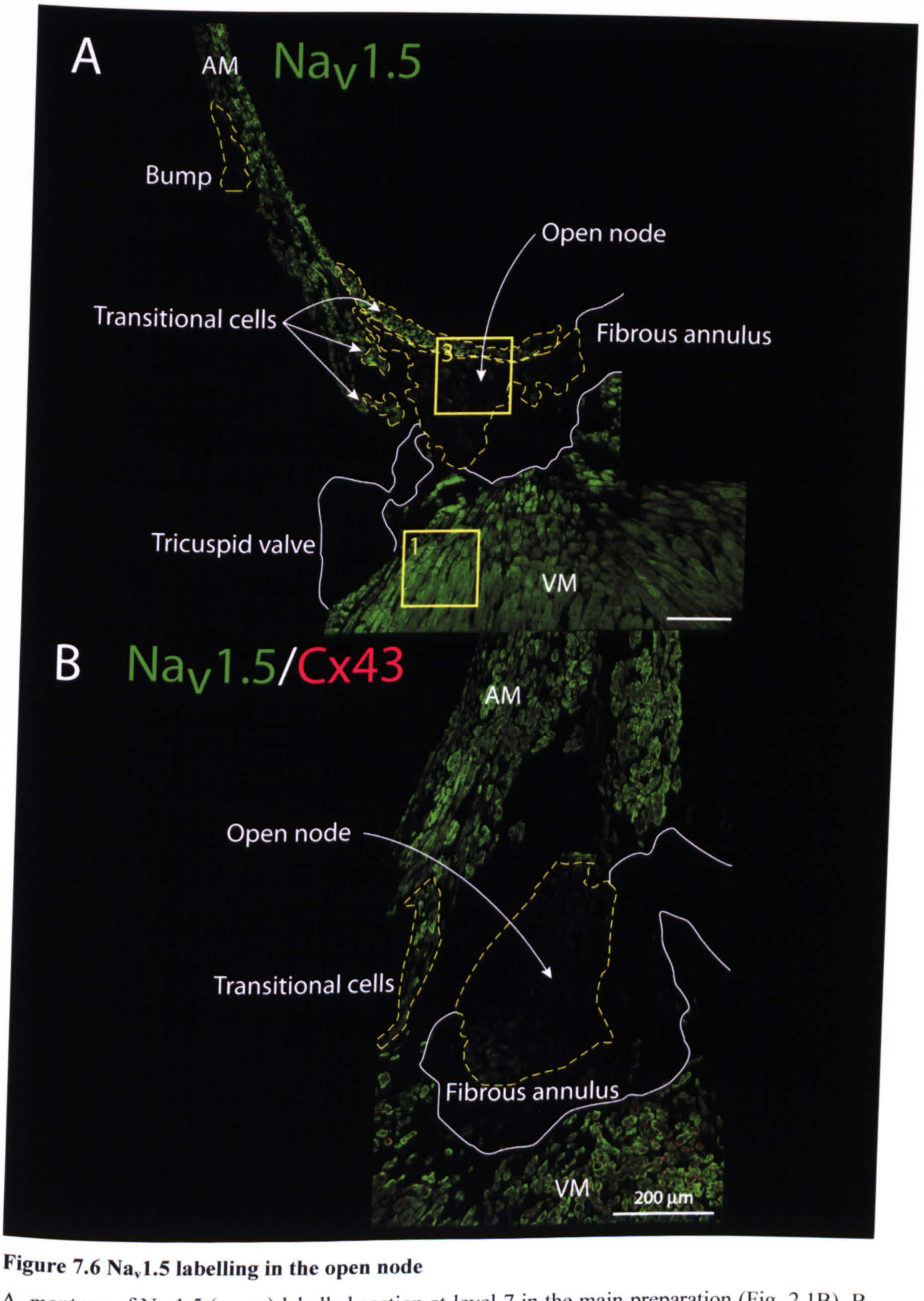

Figure 7.6 $Na_v1.5$ labelling in the open node

A, montage of $Na_v1.5$ (green) labelled section at level 7 in the main preparation (Fig. 2.1B). B, montage of $Na_v1.5$ (green) and Cx43 (red) double labelled section at level 7 in the third preparation. High magnification images of the yellow framed areas (labelled 1 and 3) in A are shown in Fig. 7.11A and C, respectively. AM, atrial myocardium; VM, ventricular myocardium. Scale bars, 200 μm.

bundle, and the termination of the AV ring bundle (see next sections). However, the continuation of the "bump" to other parts of the preparation (for example, the level of the enclosed node or the common bundle) is not certain. In addition to the termination of the AV ring bundle, the surprising appearance of the "bump" may be an example of the exceptional structural complexity of the AV node. In the zone of transitional cells, there was labelling of $Na_v1.5$ – it was generally weaker than that in the atrial and ventricular muscle (as in the case of the posterior/inferior nodal extension, Fig. 7.5) (Fig. 7.6). The zone of transitional cells and the posterior/inferior nodal extension are part of the AV ring bundle around the tricuspid annulus. High-magnification images of the framed areas in Fig. 7.6A (labelled 1 and 3) are shown in Fig. 7.11A and C, respectively.

7.3.2.3. Enclosed node

Fig. 7.7 shows immunolabelling of $Na_v1.5$ in the enclosed node from two different preparations. Fig. 7.7A shows a section at level 9 in the main preparation (Fig. 2.1B) and Fig. 7.7B shows a section at level 9 in the third preparation. The enclosed node, ringed in yellow in Fig. 7.7B, is located in the centre of the tissue between the atrial and ventricular myocardium, in which $Na_v1.5$ and Cx43 labelling is abundant (Fig. 7.7). The enclosed node shows the same labelling pattern as the open node, i.e. $Na_v1.5$-negative and Cx43-negative (Fig. 7.7). The zone of transitional cells exists again above the tricuspid valve and shows the same labelling pattern as the zone of transitional cells in the open node region (Fig. 7.7). High-magnification images of the framed areas in Fig. 7.7A (labelled 4 and 5) are shown in Fig. 7.11D and E, respectively.

7.3.2.4. Common bundle

Fig. 7.8 shows immunolabelling of $Na_v1.5$ in the common bundle region from two different preparations. Fig. 7.8A shows a section at level 11 in the main preparation (Fig. 2.1B) and Fig. 7.8B shows a section at level 10 in the third preparation. The common bundle, ringed in yellow in Fig. 7.8B, is located between the atrial and ventricular myocardium, in which $Na_v1.5$ and Cx43 labelling is abundant, close to the tricuspid valve (Fig. 7.8). At this level, $Na_v1.5$ labelling was present, but less abundant (as compared to the labelling in the atrial and ventricular myocardium), in the zone of transitional cells and absent from the common bundle and the termination of the AV ring bundle (Fig. 7.8). At this level, Cx43 labelling was absent in the zone of transitional cells, the common bundle and the termination of the AV ring bundle as expected (Fig. 7.8B). A high-magnification image of the framed area in Fig. 7.8A (labelled 6) is shown in Fig. 7.11F.

7.3.2.5. Left bundle branch

Fig. 7.9 shows immunolabelling of $Na_v1.5$ in the common bundle and the left bundle branch from two different preparations. Fig. 7.9A shows a section at level 5 in the second

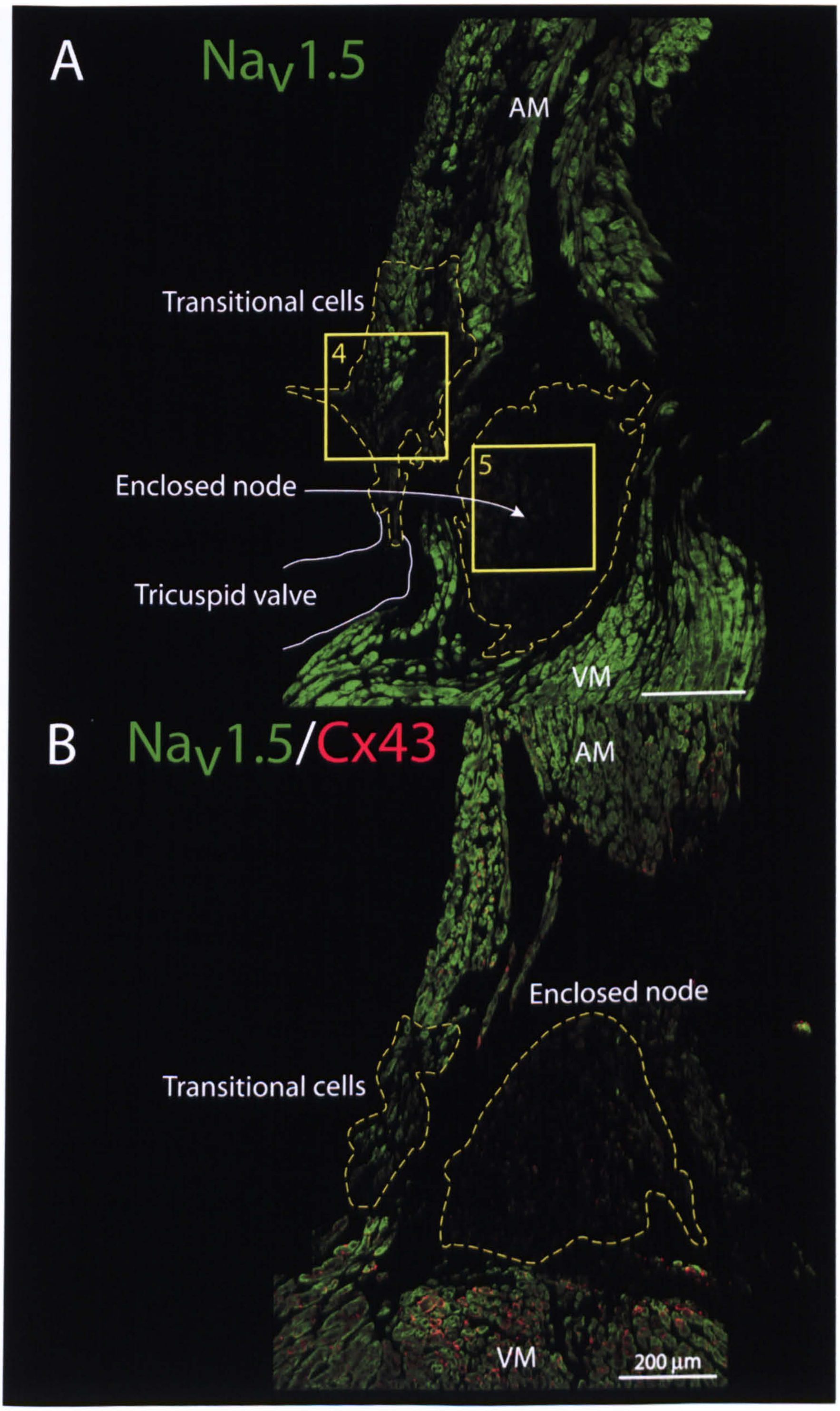

Figure 7.7 $Na_v1.5$ labelling in the enclosed node

A, montage of $Na_v1.5$ (green) labelled section at level 9 in the main preparation (Fig. 2.1B). B, montage of $Na_v1.5$ (green) and Cx43 (red) double labelled section at level 9 in the third preparation. High magnification images of the yellow framed areas (labelled 4 and 5) in A are shown in Fig. 7.11D and E, respectively. AM, atrial myocardium; VM, ventricular myocardium. Scale bars, 200 µm.

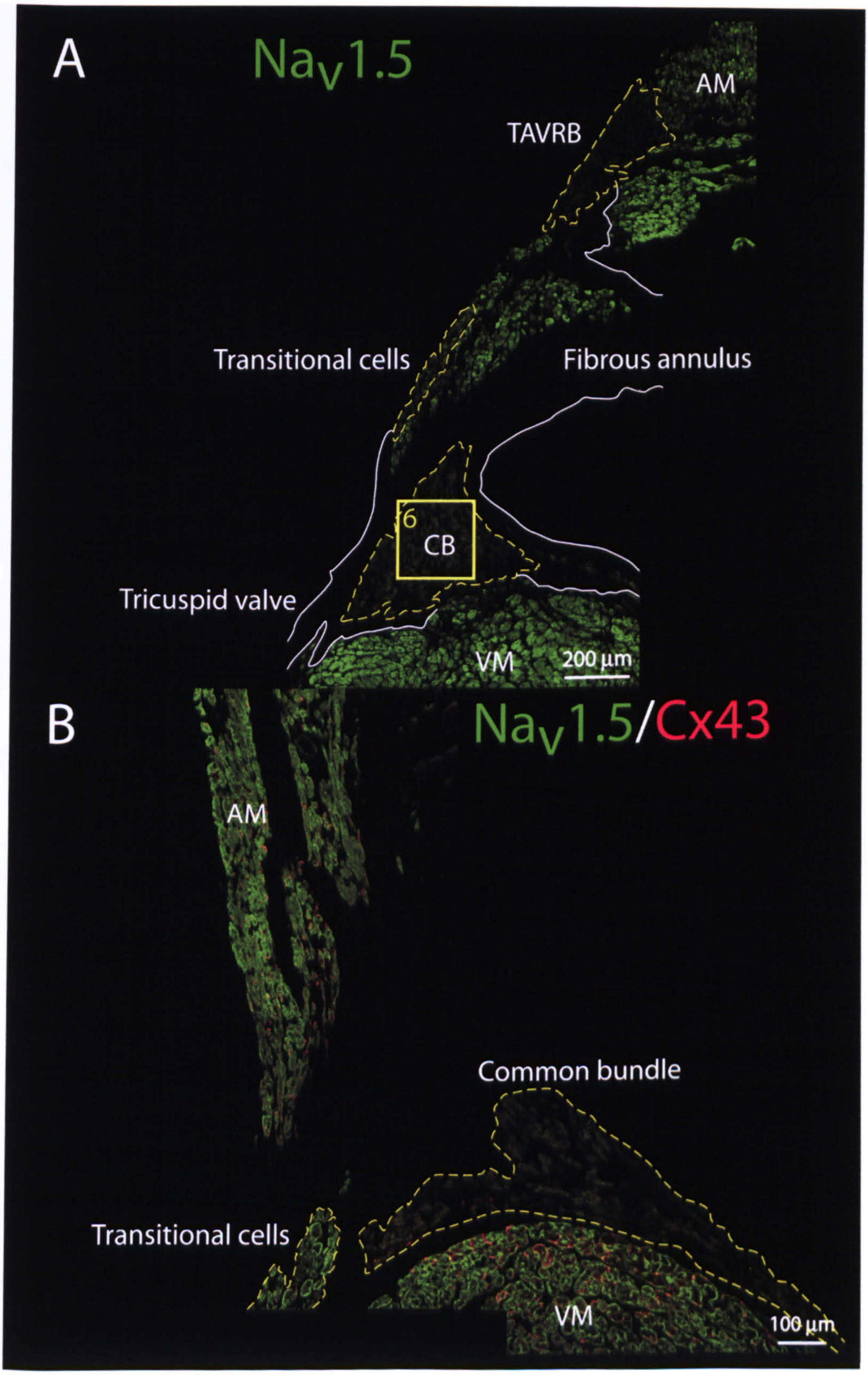

Figure 7.8 $Na_v1.5$ labelling in the common bundle

A, montage of $Na_v1.5$ (green) labelled section at level 11 in the main preparation (Fig. 2.1B). B, montage of $Na_v1.5$ (green) and Cx43 (red) double labelled section at level 10 in the third preparation. A high magnification image of the yellow framed area (labelled 6) in A is shown in Fig. 7.11F. AM, atrial myocardium; VM, ventricular myocardium. Scale bars, 200 µm (A) and 100 µm (B).

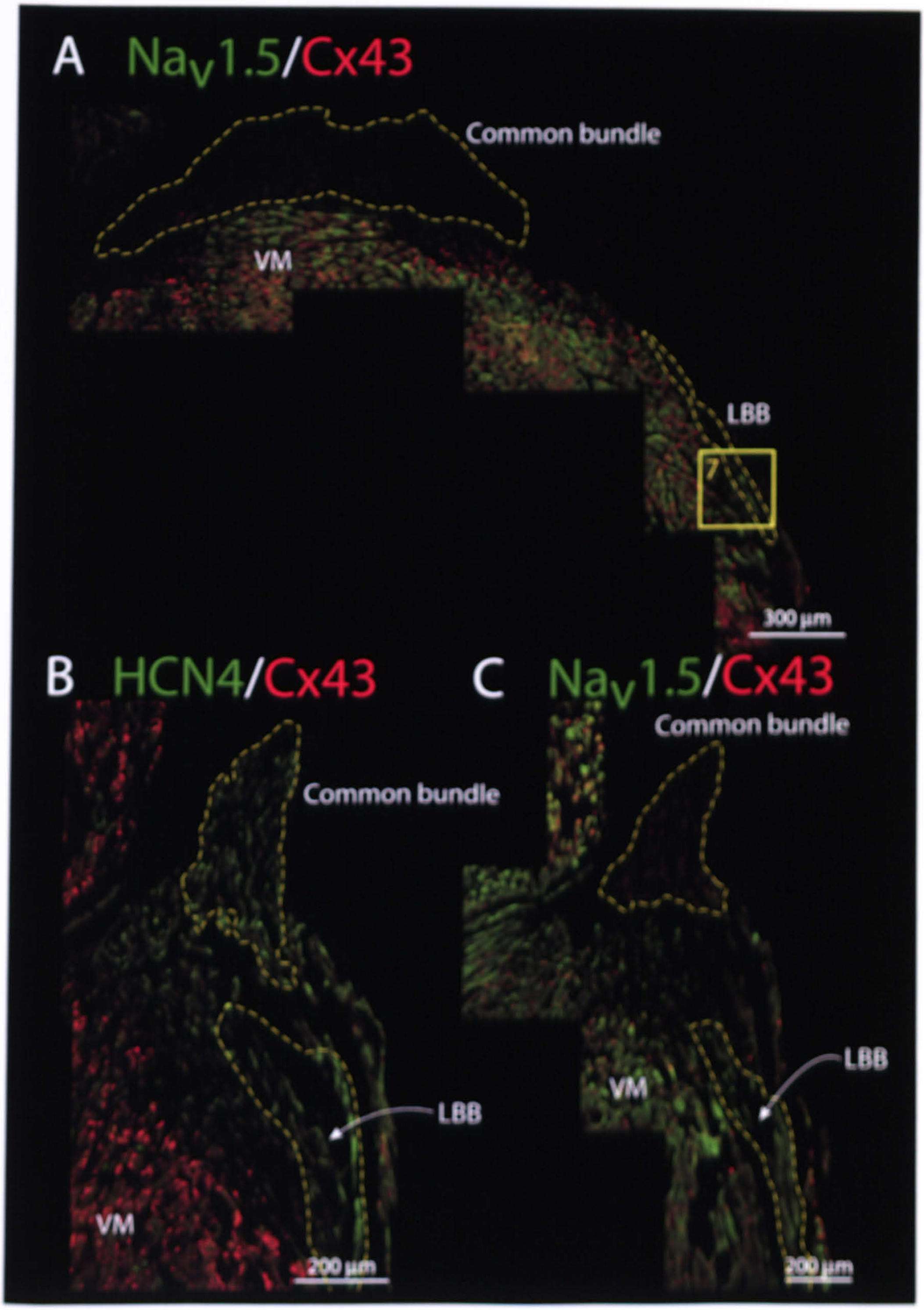

Figure 7.9 Na$_v$1.5 labelling in the left bundle branch

A, montage of Na$_v$1.5 (green) labelled section at level 5 in the second preparation (Fig. 4.6A). B and C, montages of adjacent sections, cut parallel to the tricuspid valve, double labelled for HCN4 (green) and Na$_v$1.5 (green) and Cx43 (red). A high magnification image of the yellow framed area (labelled 7) in A is shown in Fig. 7.11G. LBB, left bundle branch; VM, ventricular myocardium. Scale bars, 300 µm (A) and 200 µm (B and C).

preparation (Fig. 4.6A). Although the adjacent sections shown in Fig. 7.9B and C from another preparation (not one of three serially-sectioned preparations) were cut parallel to the tricuspid valve, the architecture is similar to that in Fig. 7.9A. The common bundle is located between the atrial and the ventricular myocardium, in which $Na_v1.5$ and Cx43 labelling is abundant (Fig. 7.9). For the sake of comparison, the common bundle with the left bundle branch double labelled for HCN4 and Cx43, already shown in Fig. 5.5B, is shown again in Fig. 7.9B. Whereas HCN4 labelling was present in both the common bundle and the left bundle branch (Cx43 was not expressed in both regions, Fig. 7.9B), $Na_v1.5$ was not expressed in the common bundle, but was expressed in the left bundle branch, 1.5 mm from the common bundle (Fig. 7.9A and C). A high-magnification image of the framed area in Fig. 7.9A (labelled 7) is shown in Fig. 7.11G.

7.3.2.6. Termination of the AV ring bundle

Fig. 7.10 shows immunolabelling of $Na_v1.5$ in the termination of the AV ring bundle from two different preparations. Fig. 7.10A shows a section at level 13 in the main preparation (Fig. 2.1B) and Fig. 7.10B shows a section at level 11 in the third preparation. The termination of the AV ring bundle, ringed in yellow in Fig. 7.10, is located between the atrial and ventricular myocardium, in which $Na_v1.5$ and Cx43 labelling is abundant, and shows the same immunolabelling pattern as the open node, the enclosed node and the common bundle, i.e. it is $Na_v1.5$-negative and Cx43-negative (Fig. 7.10). High-magnification images of the framed areas in Fig. 7.10A (labelled 8 and 9) are shown in Fig. 7.11H and I, respectively.

7.3.2.7. Summary of expression of $Na_v1.5$ in the AV node

Figs. 7.11 and 7.12 summarise the results in this chapter. As already shown in chapter 6 (section 6.3.2), there was abundant labelling of $Na_v1.5$ in atrial and ventricular myocardium (Fig. 7.11A and I). As normalized by the intensity in the ventricular myocardium, the intensity in the atrial myocardium was 84 ± 10 % (Fig. 7.12). $Na_v1.5$ labelling was present, but less abundant in the posterior/inferior nodal extension and the zone of transitional cells (Fig. 7.11B and D) and normalized expression levels were 45 ± 2 and 44 ± 12 %, respectively (Fig. 7.12). There was no or a reduced level of expression in the open node, the enclosed node, the common bundle and the termination of the AV ring bundle (Fig. 7.11C, E, F and H) and the degree of expression was semi-quantified as 27 ± 9 % in the open node, 22 ± 4 % in the bump, 30 ± 8 % in the enclosed node, 35 ± 13 % in the common bundle and 24 ± 8 % in the termination of the AV ring bundle (Fig. 7.12). These regions showed a lower level of expression than the posterior/inferior nodal extension and the zone of transitional cells. Significant differences to the posterior/inferior nodal extension and the zone of transitional cells are shown with asterisks (* and **: $P < 0.05$ vs P/I NE and TC, respectively; Fig. 7.12). It is interesting that the expression in the common bundle was slightly higher than in the enclosed node or the open node. This may represent onset of $Na_v1.5$ expression in the distal part of the conduction axis. The level of

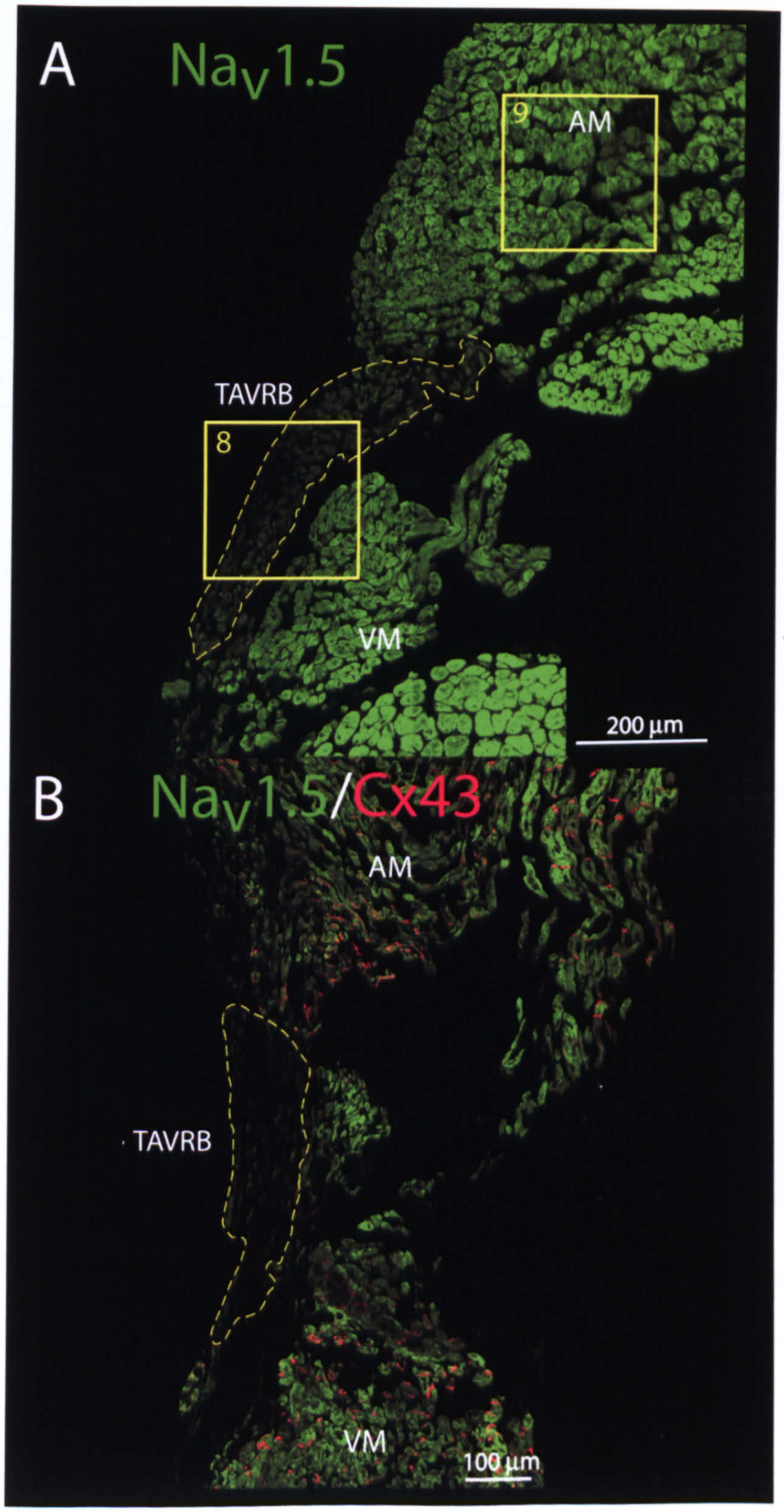

Figure 7.10 $Na_v1.5$ labelling in the termination of the AV ring bundle

A, montage of $Na_v1.5$ (green) labelled section at level 13 in the main preparation (Fig. 2.1B). B, montage of $Na_v1.5$ (green) and Cx43 (red) double labelled section at level 11 in the third preparation. High magnification images of the yellow framed areas (labelled 8 and 9) in A are shown in Fig. 7.11H and I, respectively. AM, atrial myocardium; TAVRB, termination of the AV ring bundle; VM, ventricular myocardium. Scale bars, 200 µm (A) and 100 µm (B).

$Na_V1.5$

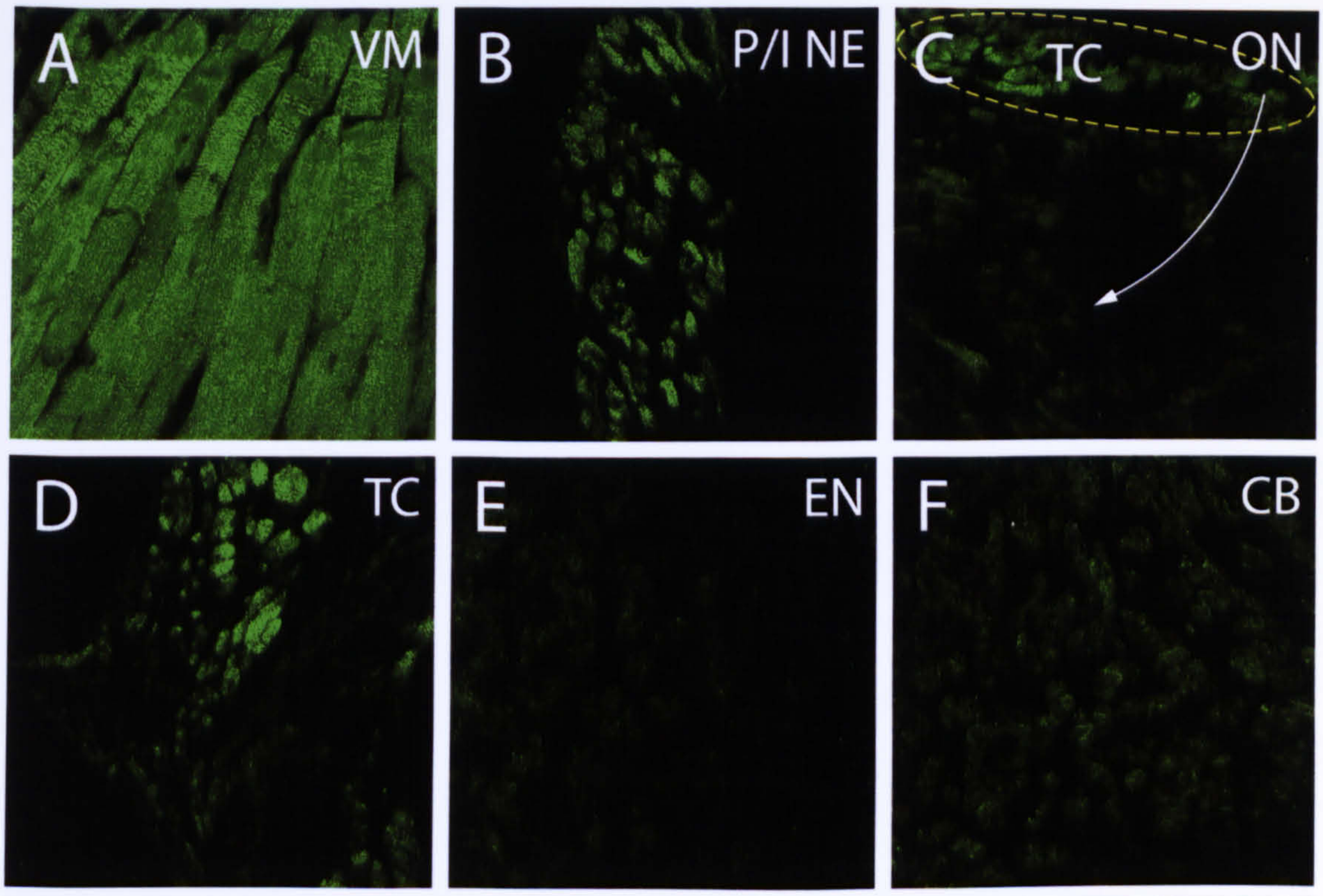

Figure 7.11 $Na_v1.5$ labelling in the different regions of the AV node

High-magnification images of the different regions of the AV node labelled for $Na_v1.5$ (green) (G shows a section double labelled for $Na_v1.5$, green, and Cx43, red). The yellow ringed areas shown in C and G highlight transitional cells and the left bundle branch, respectively. AM, atrial myocardium; CB, common bundle; EN, enclosed node; LBB, left bundle branch; ON, open node; P/I NE, posterior/inferior nodal extension; TAVRB, termination of the AV ring bundle; TC, transitional cells; VM, ventricular myocardium. Scale bar, 50 µm.

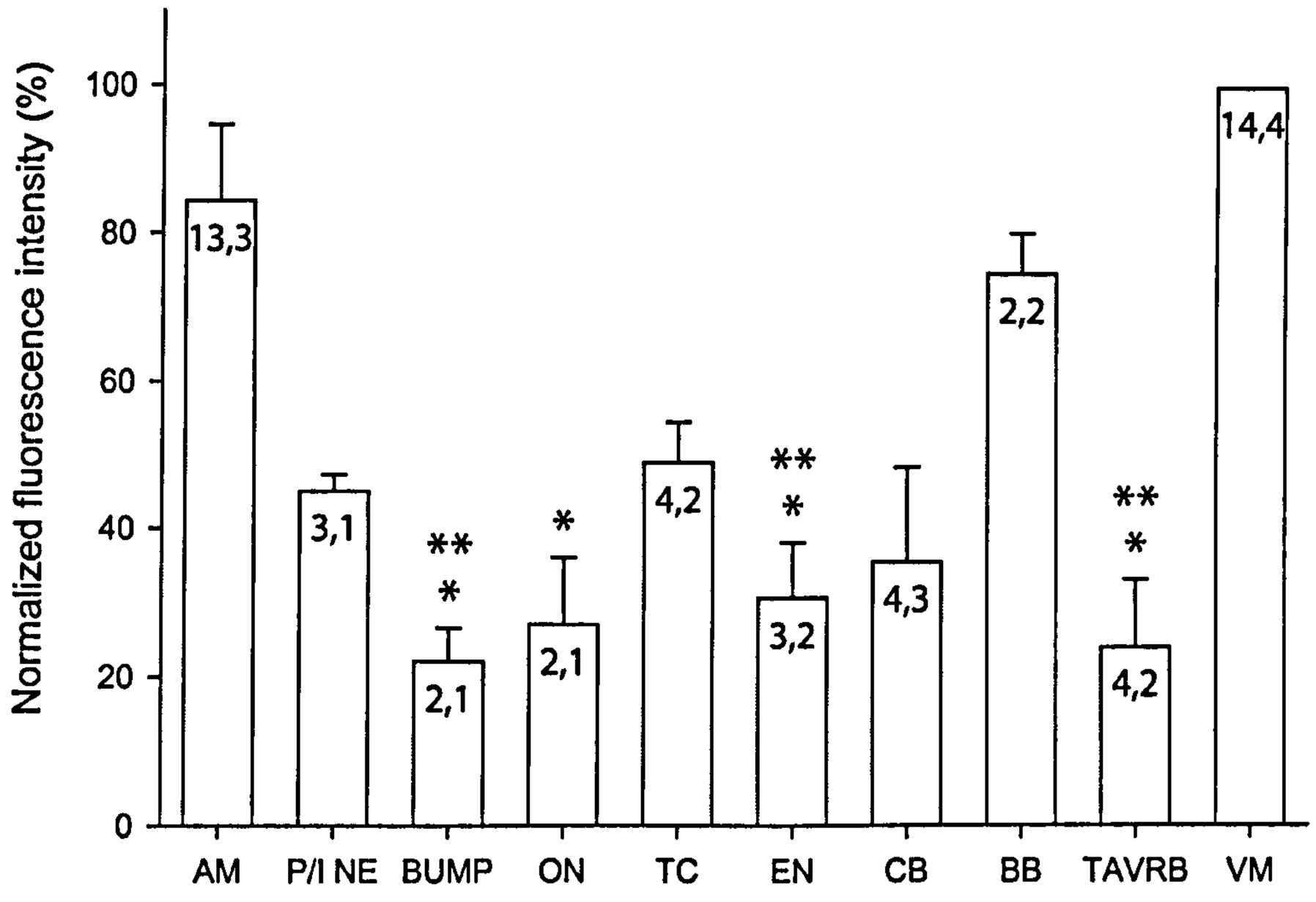

* P < 0.05 vs P/I NE; ** P < 0.05 vs TC

Figure 7.12 Semi-quantitative assessment of $Na_v1.5$ expression in the different regions of the AV node

The bar graph illustrates $Na_v1.5$ expression in the different regions of the AV node. Intensity of the different regions in a particular $Na_v1.5$-labelled section was normalized by the intensity in ventricular myocardium. Data are represented as mean ± SEM. * P < 0.05 vs P/I NE; ** P < 0.05 vs TC (student's *t*-test). Number of levels and number of preparations are shown in the middle of each bar. AM, atrial myocardium; CB, common bundle; EN, enclosed node; LBB, left bundle branch; ON, open node; P/I NE, posterior/inferior nodal extension; TAVRB, termination of the AV ring bundle; TC, transitional cells; VM, ventricular myocardium.

$Na_v1.5$ expression in the left bundle branch was 74 ± 5 % (Fig. 7.12). This is higher than in the common bundle and approximately the same as in the ventricular myocardium.

Comparison of Figs. 7.1 and 7.11 shows that, qualitatively, the expression pattern of $Na_v1.1$ is the same as that of $Na_v1.5$. However, due to non-specific nuclear labelling, semi-quantitative assessment of $Na_v1.1$ expression in the different regions of the AV node is not possible.

7.4. Discussion

7.4.1. Relation to previous studies

Petrecca *et al.* (1997) previously reported evidence of a lower level of expression of Na_v channels in the mid-nodal cells of rabbit. However, an antibody raised against a portion of the conserved inter-domain 3-4 region of the Na_v1 subfamily of Na^+ channels was used and, therefore, Petrecca *et al.* (1997) could not discriminate between different Na^+ channel isoforms. The possibility of the existence of neuronal Na^+ channel isoforms in the AV node was not expected (Petrecca *et al.*, 1997). Although Petrecca *et al.* (1997) reported the expression of Na^+ channels in lower nodal cells, I observed the absence of all Na^+ channel isoforms throughout the enclosed node (both mid-nodal and lower nodal cells). Furthermore, the labelling in the atrial myocardium in the study of Petrecca *et al.* (1997) was sparse and this raises doubts concerning the veracity of the labelling.

7.4.2. The roles of Na^+ channels in AV node electrophysiology

As explained in chapter 1 (section 1.2.1), the cells of the AV junction are frequently described as atrionodal (AN), nodal (N) and nodal-His (NH) (Mazgalev *et al.*, 2001). The maximum upstroke velocity of the action potential in these cells is substantially lower than in the atrium or His bundle. Moreover, within the triangle of Koch, the upstroke velocity of the N-type cell is slower than that of the AN or NH-type cell (McGuire *et al.*, 1996; Patterson & Scherlag, 2002). This is in keeping with my findings, because some Na^+ channels are expressed in the zone of transitional cells (44 ± 12 %, Fig. 7.12; possibly AN cells) and the posterior/inferior nodal extension (45 ± 2 %, Fig. 7.12; containing, possibly, AN cells), whereas no Na^+ channels are expressed in the open node and enclosed node (27 ± 9 % and 30 ± 8 %, respectively, Fig. 7.12; containing, possibly, N cells). The reduced level of Na^+ channel expression in the enclosed node explains the slow-rising upstroke of the action potential here. The mid-level of expression of $Na_v1.1$ (not quantified) and $Na_v1.5$ in the zone of transitional cells and the posterior/inferior nodal extension explains the faster upstroke velocity here. The conduction velocity of the AV node is low and this is responsible for the delay between the activation of the atria and ventricles in the cardiac cycle. The reduced level of $Na_v1.5$ and $Na_v1.1$ from the open node to the proximal left and right bundle branches will, at least, contribute to the low conduction velocity.

7.4.3. Other roles for neuronal Na^+ channels in conduction tissue?

As already reported in the SA node (Dobrzynski *et al.*, 2003), $Na_v1.3$ labelling was only observed in nerve fibres and nerve cell bodies innervating the nodal myocytes. Although there is a rich innervation by the autonomic nervous system of both the SA and AV nodes, the innervation of the two nodes seems to be different. From a study of the canine heart, the SA node is especially responsive to parasympathetic regulation, whereas the AV conduction is preferentially sensitive to sympathetic adrenergic regulation (Randall, 1988). The exact distribution and destination of these nerves are still uncertain.

One of the interesting findings in this study is the distribution of $Na_v1.3$ in the AV node. $Na_v1.3$ is expressed in nerve fibres and cell bodies rather than myocytes. $Na_v1.3$ labelling is absent in the atrial and ventricular myocardium, present (but not abundant) in the specialised pathways into the AV node (posterior/inferior nodal extension and the zone of transitional cells) and abundant in the open and enclosed nodes. Therefore, innervation appears to be controlling AV conduction at the point at which conduction will be the most severely constrained by the absence of $Na_v1.5$ and $Na_v1.1$.

Besides the presence of $Na_v1.1$ in the posterior/inferior nodal extension and the zone of transitional cells, $Na_v1.1$ is expressed in the left bundle branch. It is well known that Na^+ channels exist from the distal part of the common bundle until the terminal Purkinje fibres and contributes to the high upstroke velocity and long duration of the action potential in the His-Purkinje system (Carmeliet, 1987). The role of $Na_v1.1$ in the left bundle branch needs investigation.

Chapter 8

Cx40 expression in the AV node

8.1. Introduction

8.1.1. The contribution of gap junctions to atrial-AV nodal conduction

Activation of cardiac contraction requires an orderly spread of electrical excitation from one myocyte to the next throughout the heart. Gap junctions are essentially clusters of transmembrane channels that connect the cytoplasmic compartments of neighbouring myocytes, forming sites of low resistance electrical coupling and conduits for the direct exchange of small molecules and ions.

Particularly in the enclosed node, a reduced level of or an absence of high-conductance gap junction channel isoforms (Cx43 and Cx40; Severs *et al.*, 2001) and the presence of a low conductance isoform (Cx45; Severs *et al.*, 2001) can explain the slow conduction through the AV node (Shaw & Rudy, 1997). As already described in the previous chapter (section 7.4.2), the absence of $Na_v1.5$ and $Na_v1.1$ from the open node to the proximal left and right bundle branches will, at least, also contribute to the low conduction velocity of the AV node. However,

it has been suggested that the contribution of Na^+ channels to slow conduction is lower than that of connexins, because a reduction of Na^+ conductance can produce only a three-fold reduction in conduction velocity, whereas a decrease in coupling by connexins can cause a 100-fold reduction (Shaw & Rudy, 1997).

In this chapter, the distribution of Cx40 in the rat AV node is investigated from the point of view of AV conduction. It is widely accepted that Cx40 expression is scant or absent in the working ventricular myocardium of most mammals and Cx40 is mainly expressed in the atria and the His-Purkinje system, in which rapid conduction occurs (Gourdie *et al.*, 1993; Kanter *et al.*, 1993; Bastide *et al.*, 1993; Davis *et al.*, 1994; Gros *et al.*, 1994; Van Kempen *et al.*, 1995; Gros & Jongsma, 1996; Vozzi *et al.*, 1999).

8.1.2. Mid-nodal and lower nodal cells

In the enclosed node, mid-nodal cells and lower nodal cells can be discriminated from each other. The "typical" AV nodal cells constitute the so-called mid-nodal or compact node region. These are the cells forming a dense discoid-shaped network for which Tawara coined the term "node" (Tawara, 2000), now always used for description of the entire region. In addition to being closely packed together (i.e. compact), the mid-nodal cells are typically small, have random orientation (DeFelice & Challice, 1969) and contain few nexuses (Kawamura & James, 1971). Lower nodal cells start posteriorly/inferiorly as a thin bundle of small cells that make scarce contacts with transitional cells. Closer to the enclosed node, one can recognise larger individual bundles separated by fibrous tissue, and as the lower cells progress even more anteriorly/superiorly they form, without any sharp boundary, the bundle of His. The above description has been originally proposed for the rabbit heart (Anderson *et al.*, 1974), although similar subdivisions have been observed in other species as well (Truex & Smythe, 1965; Truex & Smythe, 1967; Anderson *et al.*, 1975).

8.2. Methods

The general immunohistochemistry procedures are described in chapter 2 (section 2.6). Details of procedures (tissue fixation, membrane permeablisation, blocking of non-specific sites, type of labelling, type of primary and secondary antibodies used, incubation time and temperature during incubation with antibodies, washing and mounting of tissue) are also described in chapter 4 (section 4.2). As Cx40 antibody can detect Cx43 protein in tissue sections (data not shown), a very low concentration of Cx40 antibody was used (1:2000 or 1:5000) to avoid misleading results.

8.3. Results

Fig. 8.1 shows high magnification images of Cx40 labelling in the AV conduction axis in the second preparation (Fig. 4.6A). Cx40 was expressed in the enclosed node (only in the lower half; Fig. 8.1A), common bundle (Fig. 8.1B), and left bundle branch (Fig. 8.1C). The high abundance of Cx40 in these areas contributes to the fast conduction in the His-Purkinje system.

Fig. 8.2 shows high maginification images of Cx40 labelling in other sub-regions in the AV node in the same preparation. In accordance with previous reports (Van Kempen *et al.*, 1995; Vozzi *et al.*, 1999), Cx40 was absent in ventricular myocardium, but present in the atrial myocardium (Fig. 8.2A and F). Compared to the labelling in the conduction axis (Fig. 8.1), Cx40 labelling in the atrial myocardium was quite weaker. In the part of AV conduction axis, there was Cx40-negative areas from the posterior/inferior nodal extension to the enclosed node (upper part) (Figs. 8.2B-D and 8.1A). The termination of the AV ring bundle was also Cx40-negative (Fig. 8.2E).

8.4. Discussion

From the open node to the proximal left and right bundle branches, the medium conductance gap junction protein, Cx43, is not expressed or poorly expressed (chapter 4, sections 4.3.2-4.3.5), although from the enclosed node to the left and right bundle branches (and, presumably, onto the terminal Purkinje fibres) the high conductance gap junction isoform, Cx40, is expressed (Fig. 8.1). In the open node and part of the enclosed node, Cx40 is not expressed (Figs. 8.2C and 8.1A, upper half of the enclosed node) and Cx43 is either not or poorly expressed (chapter 4, sections 4.3.2 and 4.3.3) and instead the low-conductance gap junction protein, Cx45, is expressed (Dobrzynski *et al.*, 2003) and this pattern of expression, at least, is expected to contribute to the low conduction velocity of the AV node.

In the compact AV node of the rabbit, Mazgalev *et al.* (2001) has described distinct electrophysiologies in the mid and lower nodal cells. Does this correspond to the mid Cx40-negative nodal cells and lower Cx40-positive nodal cells in this study (Fig. 8.1A)? In the rabbit the lower nodal cells express Cx43 rather than Cx40 (Dobrzynski & Greener, unpublished data).

CX40

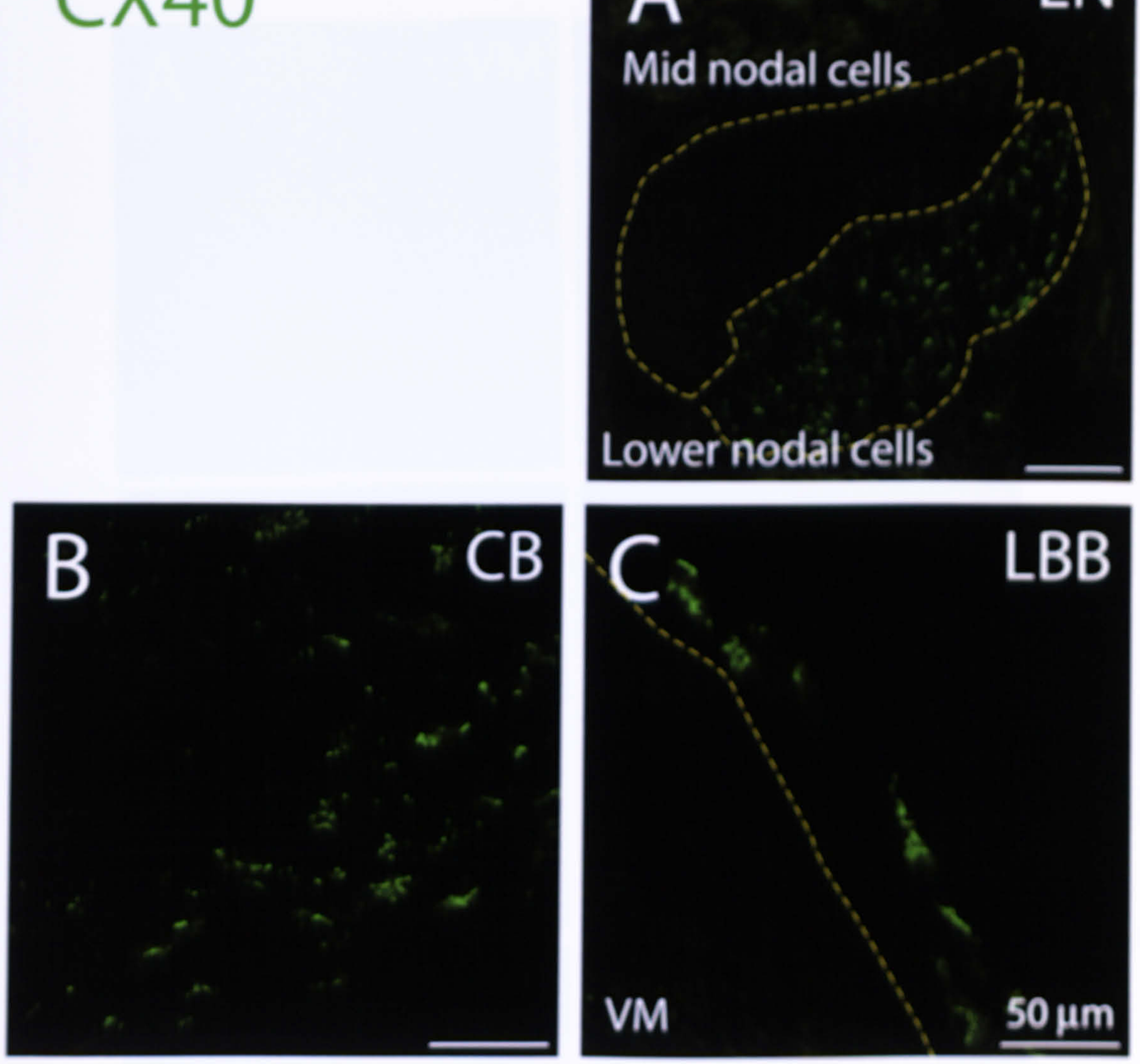

Figure 8.1 The presence of Cx40 labelling in the AV conduction axis in the second preparation (Fig. 4.6A)

High magnification images of Cx40 in the AV conduction axis are shown. CB, common bundle; EN, enclosed node; LBB, left bundle branch; VM, ventricular myocardium. Scale bars, 50 µm.

Figure 8.2 The absence of Cx40 labelling in other sub-regions of the AV node (outside of the AV conduction axis) in the second preparation (Fig. 4.6A)

High magnification images of Cx40 (green) in different sub-regions of the AV node are shown. AM, atrial myocardium; ON, open node; P/I NE, posterior/inferior nodal extension; TAVRB, termination of the AV ring bundle; TC, transitional cells; VM, ventricular myocardium. Scale bar, 50 µm.

Chapter 9

Expansion to the AV ring bundle (around the tricuspid annulus)

9.1. Introduction

Advances in the radiofrequency therapy of AVNRT with preservation of AV conduction have revived interest in the detailed morphology of the AV node and its atrial inputs (Schluter *et al.*, 1991; Jazayeri *et al.*, 1992; Keim *et al.*, 1992; Becker, 1994). For instance, in patients with AVNRT, a "slow pathway" is considered part of the reentrant circuit and catheter ablation near the coronary sinus orifice is the most favoured and highly successful approach (Mitrani *et al.*, 1993; Jazayeri & Akhtar, 1993; Sousa *et al.*, 1994).

Many experimental (mostly electrophysiological) and clinical observations support the idea that reentry involves not only the compact AV node but also atrial tissue (Lin *et al.*, 1994; Wu *et al.*, 2001) and the posterior/inferior nodal extension (Haissaguerre *et al.*, 1992; Medkour

et al., 1998; Inoue & Becker, 1998). The posterior/inferior nodal extension could be the slow pathway.

Nodal-like cells from the posterior/inferior nodal extension continue around the tricuspid annulus and form the AV ring bundle (McGuire *et al.*, 1994; Thery *et al.*, 1994; Uchida *et al.*, 1998; Xie *et al.*, 2004). The existence of this ring of conduction tissue was shown by earlier anatomical studies in the 1970's (Anderson & Taylor, 1972; Anderson, 1972). Some morphological studies have recently found that some bundles and collections of cells with different morphological characteristics and arrangements exist in the AV junctional area, and connect with the compact AV node in humans and in some animals (Inoue & Becker, 1998; Anderson & Ho, 1998). Inoue & Becker (1998) reported that rightward posterior and leftward posterior extensions showed similar cellular and architectural characteristics as those of the compact AV node. The cells in the extensions were small and closely packed, with an interweaving architecture and, occasionally, a distinct node-like cellular arrangement. This specialised conduction tissue outside the triangle of Koch is assumed to be a remnant of the AV canal tissue demonstrated in embryonic hearts (Arguello *et al.*, 1986). Clearly, this tissue remains present into adult life, because Mcguire *et al.* (1994) reported electrophysiological evidence for a ring of nodal-like cells around the tricuspid annulus in mature dog heart.

Although Mcguire *et al.* (1996) reported a lack of Cx43 in AV junctional cells around both the tricuspid and mitral valves, the expression pattern of proteins responsible for conduction in these cells has not been investigated. The aim of the experiments described in this chapter was to investigate the expression pattern of ion channels (especially Na^+ channels) and gap junction channel isoforms in the AV ring bundle around the tricuspid valve. The part of the AV ring bundle of the tricuspid valve opposite the AV node was investigated.

9.2. Methods

The general immunohistochemistry procedures are described in chapter 2 (section 2.6). Details of procedures for each probe are described in previous chapters (DP, ANP and Cx43, section 4.2; HCN4, section 5.2; Na^+ channels, section 6.2; Cx40, section 8.2).

9.3. Results

To investigate the expression of various ion channels including some Na^+ channel isoforms ($Na_v1.1$ and $Na_v1.5$) and gap junction channels in the AV ring bundle, sections were cut along the sagittal plane. The position of the cutting plane is shown as a dotted line in Fig. 11.1C.

9.3.1. Anatomy and histology of the AV ring bundle

Fig. 9.1 shows Masson's trichrome staining of a 'four chamber section'. Because all four chambers in the heart can be seen, sections cut along the sagittal plane are called 'four chamber sections'. Fig. 9.1B shows a high magnification image of the framed area in A: the common bundle (and the zone of transitional cells) is on one side (in box D) and the AV ring bundle is on the opposite side (in box C). As already described in chapter 3 (sections 3.3.3 and 3.3.4), the common bundle was situated in the middle of the AV junctional region (box D in Fig. 9.1B) and it was separated from the atrial and ventricular myocardium (stained red) by connective tissue (stained blue). Compared to the surrounding atrial and ventricular myocardium, the myocytes in the AV ring bundle and the common bundle (boxes C and D, respectively, in Fig. 9.1B) were stained a lighter red, were smaller, and were loosely packed.

9.3.2. Immunolabelling of immunohistochemical markers and HCN4

Fig. 9.2 shows immunolabelling of immunohistochemical markers (Cx43, DP and ANP) and HCN4 in the common bundle and the AV ring bundle on the opposite side of the tricuspid valve to the AV node in adjacent sections. The common bundle, yellow ringed, is located above the ventricular myocardium and beneath the atrial myocardium (Fig. 9.2B, D and F). Atrial myocardium showed co-localisation of Cx43 and DP at intercalated disks (Fig. 9.2B) and intracellular ANP labelling (Fig. 9.2D). The common bundle showed DP labelling at intercalated disks and HCN4 labelling at the outer cell membrane (Fig. 9.2B and F). Ventricular myocardium showed co-localisation of Cx43 and DP at intercalated disks as in atrial myocardium (Fig. 9.2B). As already described in chapters 4 and 5 (sections 4.3.4 and 5.3.4), the common bundle is Cx43-negative, DP-positive, ANP-negative and HCN4-positive. In addition to the myocytes of the common bundle, nodal-like myocytes existed in the other yellow ringed areas (the zone of transitional cells and the AV ring bundle (lateral side)) (Fig. 9.2). The expression pattern in the AV ring bundle on the lateral side was the same as that in the zone of transitional cells and the common bundle: DP-positive, Cx43-negative, ANP-negative and HCN4-positive (Fig. 9.2).

9.3.3. Immunolabelling of Na^+ channel isoforms

Fig. 9.3 shows immunolabelling of $Na_v1.1$ and $Na_v1.5$ in the common bundle, the zone of transitional cells next to the common bundle and the AV ring bundle (lateral side) in adjacent sections. As already described in chapter 7 (section 7.3.2.4), all these structures, ringed in yellow, are located between the atrial and ventricular myocardium, in which $Na_v1.1$, $Na_v1.5$ and Cx43 labelling are abundant (Fig. 9.3B and D). $Na_v1.1$ and $Na_v1.5$ labelling was present,

Figure 9.1 Anatomy and histology of a four chamber section

A, low-magnification montage of Masson's trichrome stained section which was cut along with sagittal plane (the cutting plane is shown as a dotted line in Fig. 11.1C). The section was provided and stained by Dr. M. Yamamoto. B, zoomed image of framed area in A. Framed areas C and D are regions of interest. AS, atrial septum; CT, crista terminalis; LA, left atrium; LV, left ventricle; MV, mitral valve; RA, right atrium; RV, right ventricle; SVC, superior vena cava; TV, tricuspid valve; VS, ventricular septum. Scale bars, 1 mm (A) and 400 μm (B).

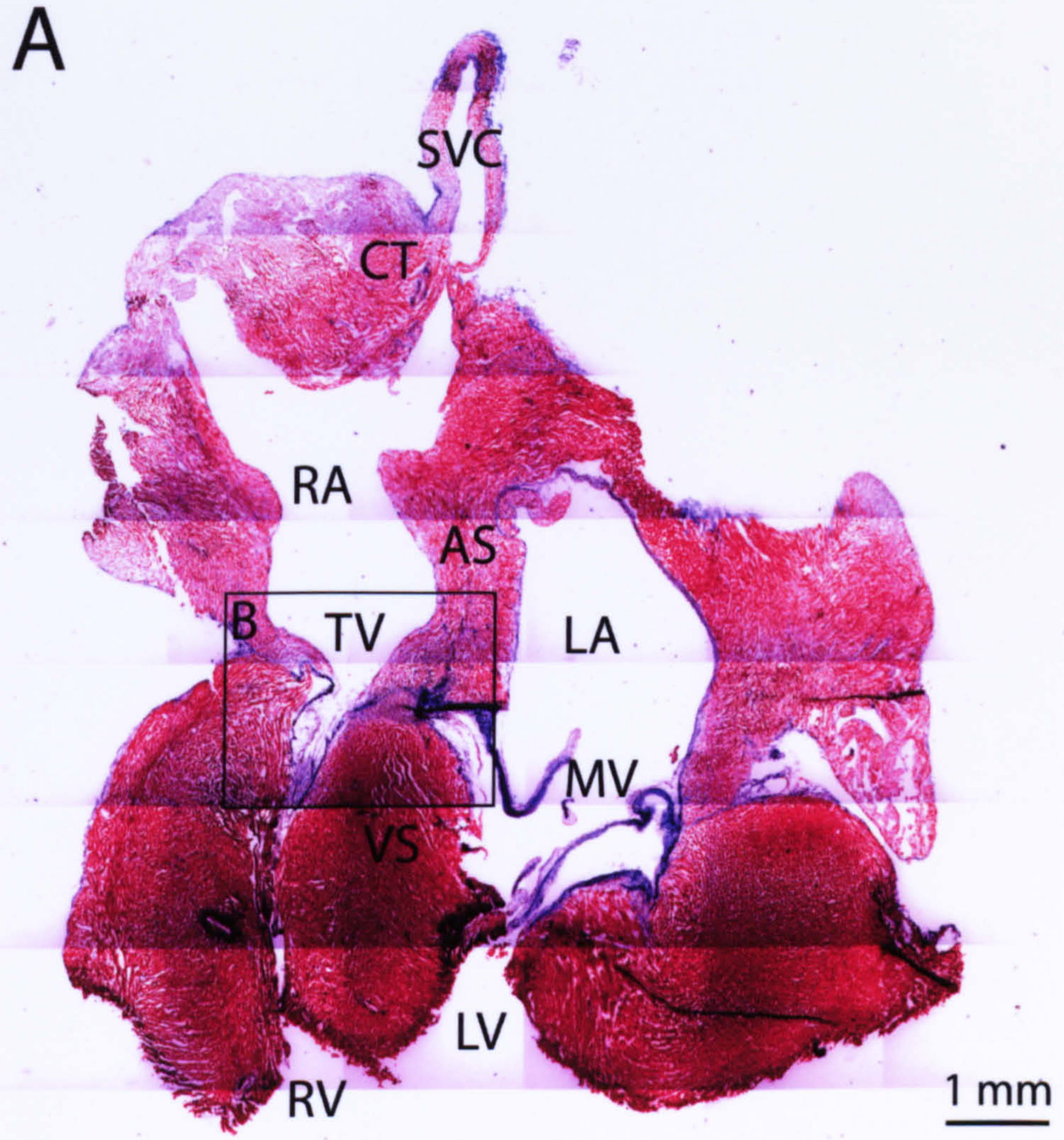
A
SVC
CT
RA
AS
B
TV
LA
MV
VS
LV
RV
1 mm

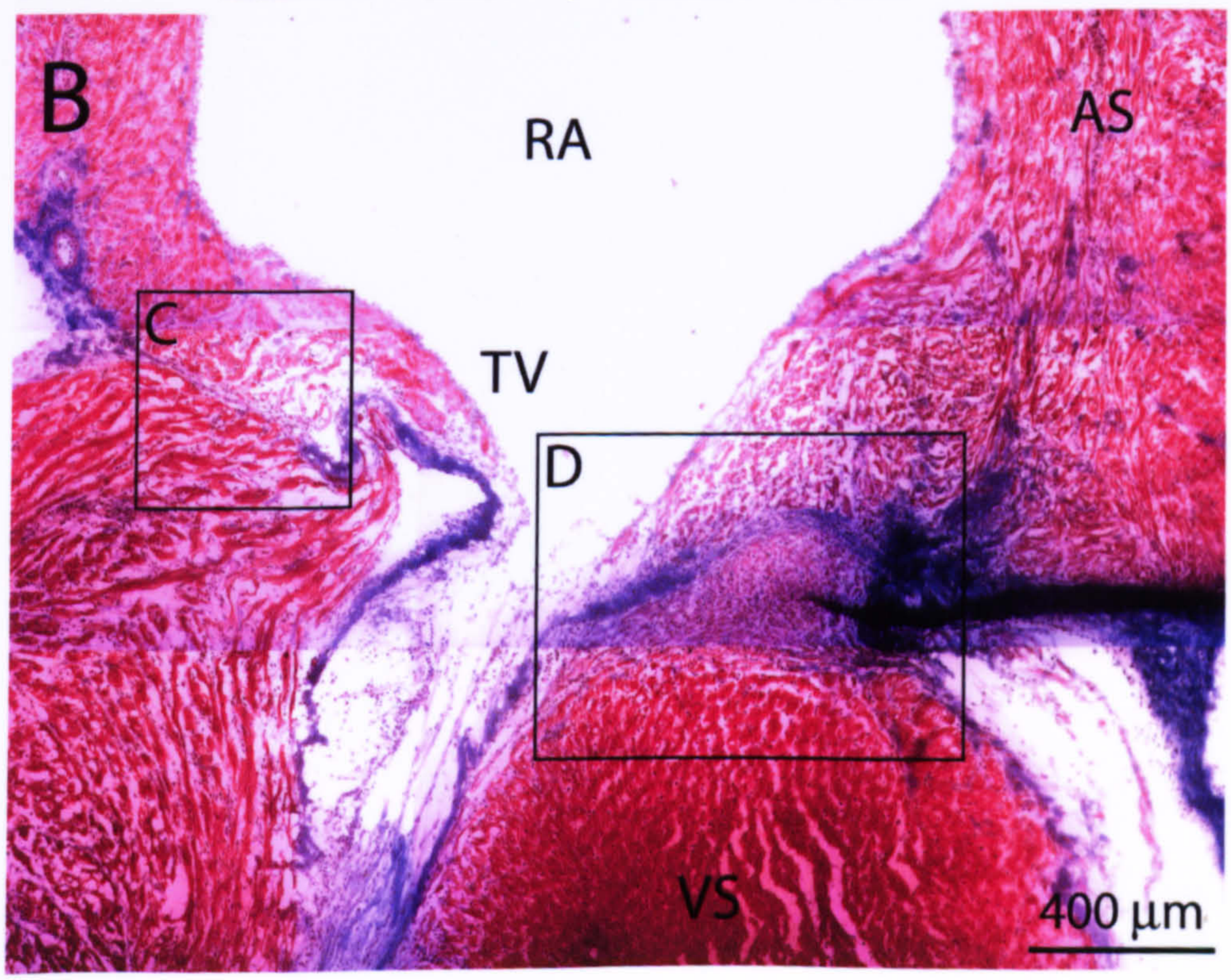
B
RA
AS
C
TV
D
VS
400 µm

Figure 9.2 Labelling of immunohistochemical markers in a four chamber section

Left (A and B), middle (C and D) and right (E and F) panels show montages of sections double labelled for Cx43 (green) and DP (red), Cx43 (green) and ANP (red), and HCN4 (green) and Cx43 (red), respectively. Sections were provided by Dr. M. Yamamoto. Top (A, C, and E) and bottom (B, D, and F) panels correspond to the framed areas in Fig. 9.1 (C and D, respectively). AM, atrial myocardium; CB, common bundle; TC, transitional cells; VM, ventricular myocardium. Scale bars, 200 μm.

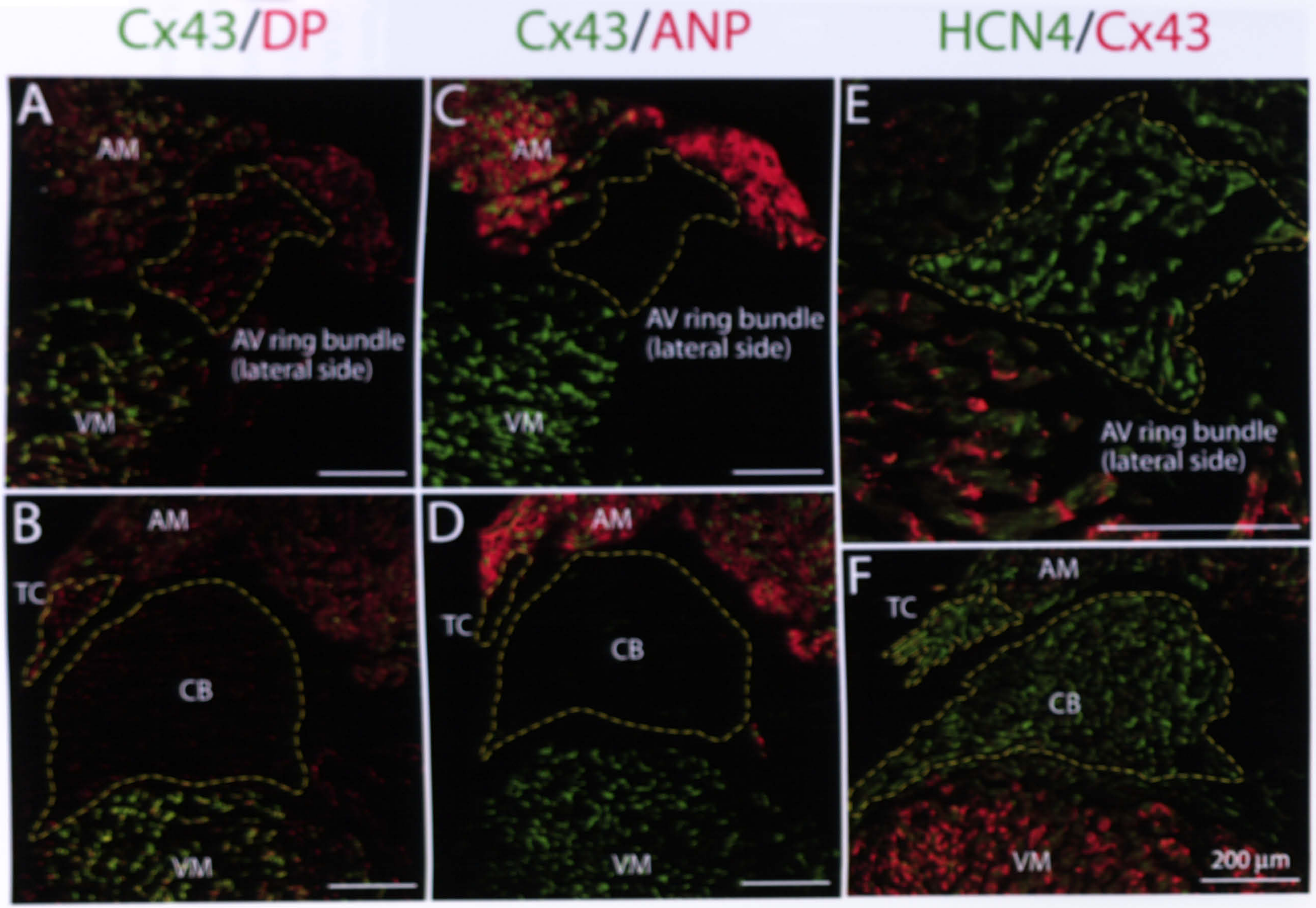
Cx43/DP
Cx43/ANP
HCN4/Cx43
A
AM
AV ring bundle
(lateral side)
VM
C
AM
AV ring bundle
(lateral side)
VM
E
AV ring bundle
(lateral side)
B
AM
TC
CB
VM
D
AM
TC
CB
VM
F
AM
TC
CB
VM
200 µm

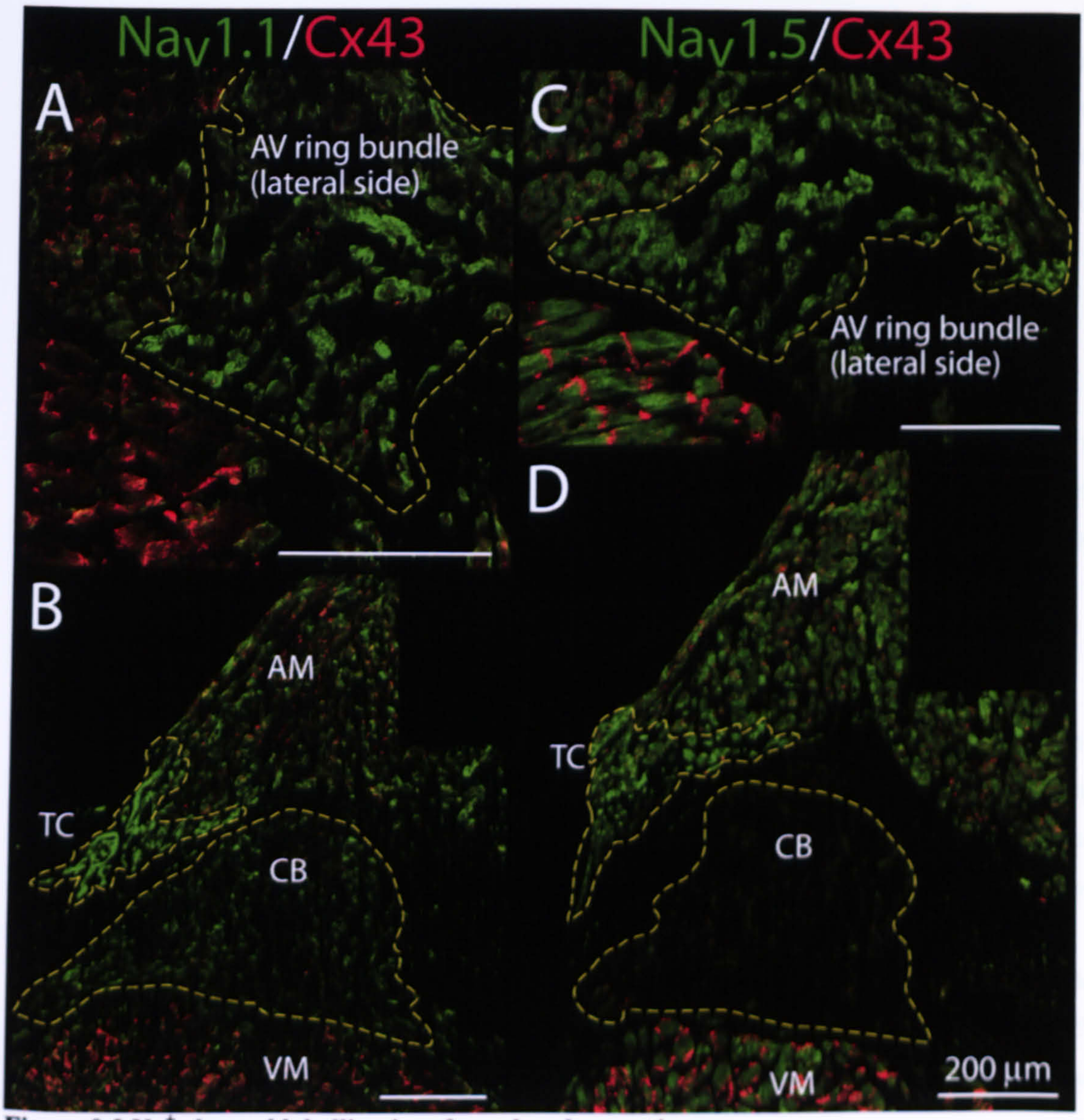

Figure 9.3 Na^+ channel labelling in a four chamber section

Left (A and B) and right (C and D) panels show montages of sections double labelled for $Na_v1.1$ (green) and Cx43 (red) and $Na_v1.5$ (green) and Cx43 (red), respectively. The section were provided by Dr. M. Yamamoto. Top (A and C) and bottom (B and D) panels correspond to the framed areas in Fig. 9.1 (C and D, respectively). AM, atrial myocardium; CB, common bundle; TC, transitional cells; VM, ventricular myocardium. Scale bars, 200 µm

but less abundant (as compared to the surrounding working myocardium), in the zone of transitional cells and the AV ring bundle (lateral side), but was not present in the common bundle (Fig. 9.3). Cx43 labelling was absent in the zone of transitional cells, the AV ring bundle (lateral side) and the common bundle (Fig. 9.3). The expression pattern in the AV ring bundle (lateral side) was the same as that in the zone of transitional cells, but different from that in the common bundle; the AV rung bundle (lateral side) was $Na_v1.1$-positive (Fig. 9.3A), $Na_v1.3$-positive (not abundant; data not shown) and $Na_v1.5$-positive (Fig. 9.3C).

9.3.4. Immunolabelling of the large conductance connexin isoform, Cx40

Fig. 9.4 shows immuolabelling of Cx40. As already described in chapter 8 (section 8.3), Cx40 was abundantly expressed in the common bundle, but it was not present in the zone of transitional cells (Fig. 9.4). Fig. 9.4 shows that Cx40 was also not present in the AV ring bundle (lateral side).

9.4. Discussion

Cx43 has been reported to be absent in the AV junctional cells (the AV ring bundle) around both the tricuspid and mitral valves (McGuire *et al.*, 1996). In this study, Cx43 labelling was also not detected in the AV ring bundle (lateral side). The expression of the other immunohistochemical markers (DP, ANP and HCN4) in the AV ring bundle (lateral side) was the same as in the common bundle (Fig. 9.2).

In this chapter, the distribution of different Na^+ channel isoforms in the AV ring bundle is shown for the first time. The labelling pattern of Na^+ channel isoforms ($Na_v1.1$ and $Na_v1.5$, Fig. 9.3) and Cx40 (Fig. 9.4) in the AV ring bundle (lateral side) is the same as that in the zone of transitional cells next to the common bundle, but is different from that in the common bundle. Such a difference in labelling pattern makes it possible to classify different cell types around the tricuspid annulus (an area larger than the triangle of Koch). This issue is discussed in detail in chapter 11.

The presence of a ring of nodal-like cells around the tricuspid annulus is supported by electrophysiological evidence. Mcguire *et al.* (1994) reported that the ring of nodal-like cells was not part of the compact AV node. Xie *et al.* (2004) reported that the action potential characteristics of the AV ring bundle were similar to those of the AV node, Although the repolarization characteristics in the AV ring bundle were different from those in the AV node. The distribution of the ion channels responsible for repolarization may provide a clue to the electrophysiology of this specialised region, but this is outside of the scope of the present study.

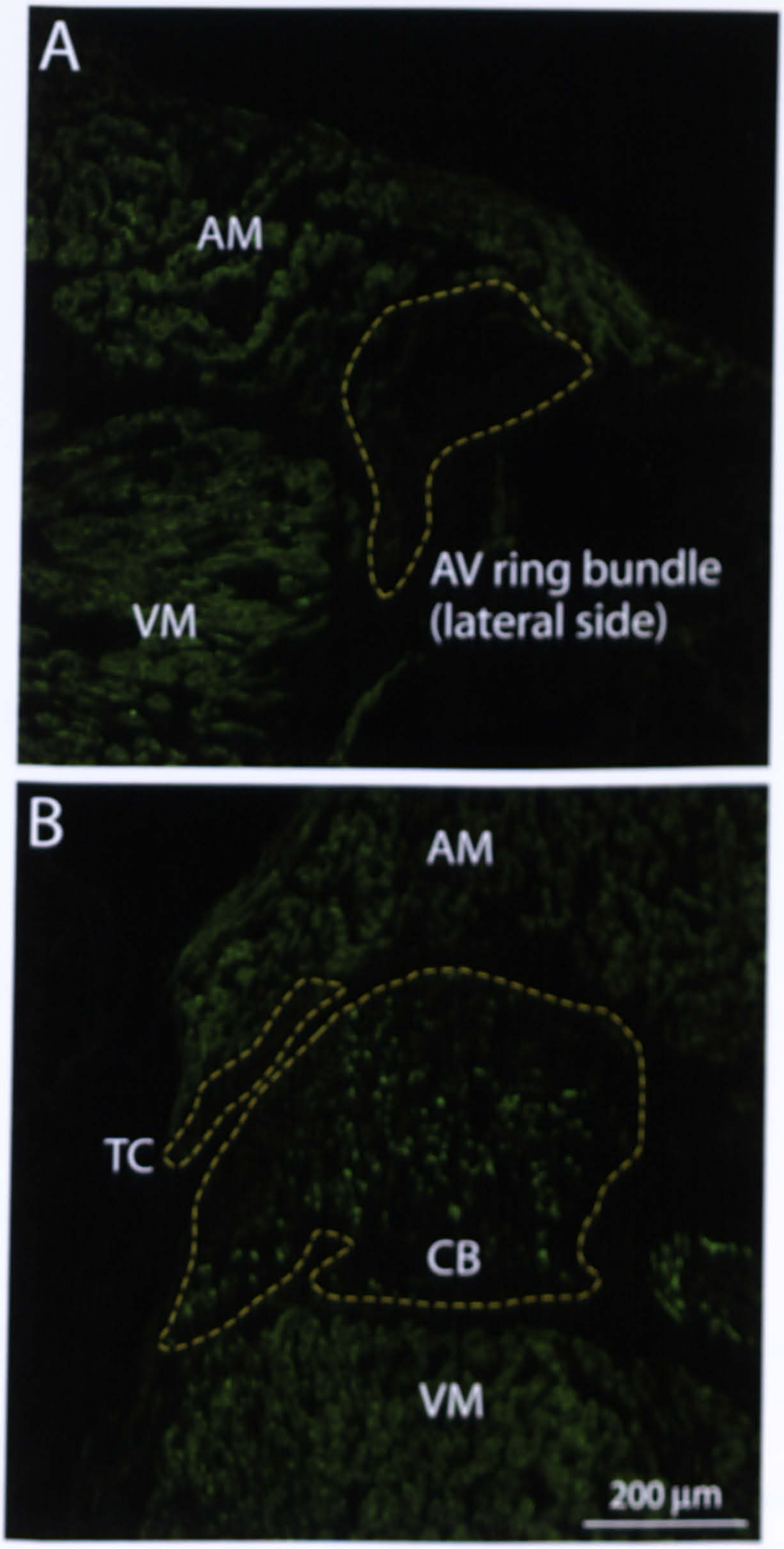

Figure 9.4 Cx40 labelling in a four chamber section

Montages of a section labelled for Cx40 (green). A and B correspond to framed areas in Fig. 9.1 (C and D, respectively). Section was provided by Dr. M. Yamamoto. The general green fluorescence is background fluorescence; the only genuine Cx40 labelling is in the form of spots in the common bundle. AM, atrial myocardium; CB, common bundle; TC, transitional cells; VM, ventricular myocardium. Scale bar, 200 µm.

Chapter 10

The different architecture of the SA node

10.1. Introduction

10.1.1. SA node: a heterogenous tissue

The SA node is a complex and inhomogeneous tissue in terms of cell morphology and electrophysiological activity. There are two models of the cellular organization of the SA node: the gradient and mosaic models (Verheijck *et al.*, 1998; Boyett *et al.*, 2000).

In favour of the gradient model, action potentials recorded from the centre of the rabbit SA node have a more positive take-off potential, slower upstroke, longer duration and less negative maximum diastolic potential than action potentials recorded from the periphery; the intrinsic pacemaker activity of the centre is also slower than that of periphery (Boyett *et al.*, 1999; Kodama & Boyett, 1985; Bleeker *et al.*, 1980). Between the centre and periphery, there is a smooth gradient in action potential properties. Similar heterogeneities of the action potential characteristics have been observed in isolated SA nodal myocytes (Honjo *et al.*, 1996). Furthermore, cell size also increases from the centre to the periphery of the SA node (Bleeker *et*

al., 1980; Boyett *et al.*, 2000) and there are significant correlations between the densities of i_{Na}, 4-AP sensitive current, rapidly activating delayed rectifier K^+ current ($i_{K,r}$), slowly activating delayed rectifier K^+ current ($i_{K,s}$), hyperpolarization-activated inward current (i_f), L-type Ca^{2+} current ($i_{Ca,L}$) and cell capacitance (a measure of cell size) in rabbit SA node cells (Honjo *et al.*, 1996; Honjo *et al.*, 1999; Lei *et al.*, 2000; Lei *et al.*, 2001; Musa *et al.*, 2002). Besides electrophysiological evidence, the expression patterns of several proteins relevant to the excitability of the SA node including gap junction channels and various Ca^{2+} handling proteins (L-type Ca^{2+} channel, Na^+-Ca^{2+} exchanger, sarcoplasmic reticulum Ca^{2+} release channel, and sarcoplasmic reticulum Ca^{2+} pump) vary from the centre to the periphery of the SA node (Honjo *et al.*, 2003; Musa *et al.*, 2002).

However, there are other reports which support the mosaic model. In the rabbit SA node, Verheijck *et al.* (1998) reported that there exists a substantial number of atrial cells (as well as SA node cells) even in the centre of the SA node, and the ratio of atrial cells:SA node cells gradually increases from the centre of the SA node to the periphery and morphological differences in the SA node cells are not associated with differences in action potential configuration and pacemaker activity. Based on these results, the mosaic model was suggested, in which there is a random mix of the two cell types and the ratio of atrial cells:SA node cells increases from the centre to the periphery of the SA node. Dobrzynski *et al.* (2005) recently showed that contrary to the gradient model and consistent in part with the mosaic model, there is a mix of atrial and SA node myocytes in the periphery.

Thus, according to the gradient model there is a gradual transition in morphology and electrophysiological properties of SA nodal myocytes from the centre to the periphery of the SA node. In contrast, according to the mosaic model, there is a variable mix of atrial and SA nodal myocytes from the centre to the periphery; each cell type has nearly constant morphological and electrophysiological properties. It is possible that elements of both models are correct.

10.1.2. Centre and periphery of the SA node

The action potential is usually first initiated in the centre of the SA node (distant from the surrounding atrial myocardium). Normally, the function of the periphery of the SA node (at the border of the SA node with the atrial muscle) is to conduct the action potential from the centre to the surrounding atrial muscle, although it can take over the role as the leading pacemaker site (Boyett *et al.*, 2000).

Many studies have reported that Cx43, the predominant connexin in the heart, is absent in the centre of the SA node (Verheule *et al.*, 2001; Davis *et al.*, 1994; Dobrzynski *et al.*, 2001; Coppen *et al.*, 1999). Dobrzynski *et al.* (2005) recently distinguished between the centre and periphery of the SA node using SA node specific markers: middle (160/165-kDa) neurofilament (NF-M) and ANP. The periphery of the SA node was NF-M-positive, ANP-negative and Cx43-

positive, whereas the centre of the SA node was NF-M-positive, ANP-negative, and Cx43-negative.

10.1.3. The expansion of the SA node

Early histological studies reported that the SA node is only found at the junction between the superior vena cava and the right atrium (Truex *et al.*, 1967; James, 1961). However, it has been reported that electrophysiologically the SA node occupies a larger area than does the histological distribution of the SA node (Betts *et al.*, 2002; Kalman *et al.*, 1995; Boineau *et al.*, 1988; Boineau *et al.*, 1980). Consistent with this, other histological studies have shown that the SA node is a more extensive structure than originally thought and runs from the superior vena cava alongside the crista terminalis towards the inferior vena cava (Sanchez-Quintana *et al.*, 2002). SA nodal myocytes, as identified by the presence of HCN4 and Cx45, are also found in the interatrial groove in the vicinity of the right superior pulmonary vein (Dr. M. Yamamoto, unpublished observations).

10.1.4. Gap junction channel expression in the SA node

Gap junction channels are the basis of intercellular coupling (Beyer *et al.*, 1990). Nodal myocytes are small, with a reduced amount of contractile elements and small, sparse, dispersed gap junctions. The latter correlates with poor electrical coupling, which, in the SA node, is important for the ability of the SA node to drive the large mass of surrounding atrial tissue while remaining protected from its hyperpolarizing influence (Severs *et al.*, 2001).

It is widely accepted that Cx43 is absent in the centre of the SA node (Verheule *et al.*, 2001; Dobrzynski *et al.*, 2001; Davis *et al.*, 1994; Coppen *et al.*, 1999). Other connexins (possibly Cx40 and certainly Cx45), expressed in heart, are major components of the very small gap junctions of the SA node (Coppen *et al.*, 1999; Kwong *et al.*, 1998).

10.1.5. Na^+ channel expression in the SA node

Recent studies have shown that $Na_v1.5$ is not only the Na^+ channel isoform in the adult heart and neuronal isoforms are also present (Maier *et al.*, 2002; Maier *et al.*, 2003). Some work in this chapter was published in a paper concerning the presence of neuronal Na^+ channels and absence of $Na_v1.5$ in the SA node (Maier *et al.*, 2003).

It was recently reported that the distribution of $Na_v1.5$ is complex in the mouse SA node: $Na_v1.5$ was not expressed in small SA nodal cells (likely to be from the centre of the SA node) and in the region of the SA node located in the intercaval region (the centre). However, $Na_v1.5$ was expressed in large SA nodal cells (likely to be from the periphery of the SA node) and in the region of the SA node located on the endocardial face of the crista terminalis (the periphery) (Lei *et al.*, 2004).

10.2. Methods

The general immunohistochemistry procedures are described in chapter 2 (section 2.6). Details of procedures for each probe are described in previous chapters (DP, ANP and Cx43, section 4.2; HCN4, section 5.2; Na^+ channels, section 6.2). SA node tissue sections, cut along perpendicular to the crista terminalis, as well as four chamber sections, cut along the sagittal plane, were used.

10.3. Results

10.3.1. Immunolabelling of immunohistochemical markers: the discrimination between the the centre and periphery of the SA node

To discriminate between the centre and periphery of the SA node, Cx43, ANP and HCN4 were used as immunohistochemical markers. Cx43 is expressed in the atrial myocardium and in the periphery of the SA node, but is absent in the centre of the SA node. ANP is expressed in the atrial myocardium, but is absent in the SA node. HCN4 is the principal isoform responsible for the pacemaker current, I_f, and is known to be present throughout the SA node, but not in the atrial myocardium (Boyett *et al.*, 2003). DP is a component of desmonsomes (which mediate cell-to-cell linkage of the intermediate filament cytoskeleton) and is expressed in all myocytes (atrial myocardium and SA node).

Typical immunolabelling of immunohistochemical markers in SA node tissue sections is shown in Fig. 10.1. Fig. 10.1 shows immunolabelling of Cx43, ANP and HCN4 as well as Masson's trichrome staining of a four chamber section. Fig. 10.1A shows the gross anatomy of section (already shown in Fig. 9.1A) and Fig. 10.1B shows a high magnification image of the framed area in A. The SA node tissue appears lighter in colour (Fig. 10.1B). ANP labelling was largely a mirror image of HCN4 labelling: SA node tissue showing HCN4 labelling showed no ANP labelling, whereas atrial myocardium showing no HCN4 labelling showed ANP labelling (Fig. 10.1). As expected, there was no Cx43 labelling in the centre of SA node, but there was labelling in the atrial myocardium (Fig. 10.1). However, Fig. 10.1C shows that there was Cx43 labelling in the periphery of SA node. The centre of the SA node was Cx43-negative, ANP-negative and HCN4-positive, whereas the periphery of the SA node was Cx43-positive, ANP-negative and HCN4-positive (Fig. 10.1). In addition to the SA node in the intercaval region (Fig. 10.1C and E), there was another region in which nodal myocytes occupied: the interatrial groove (Fig. 10.1D and F).

Fig. 10.2 shows another example of labelling of immunohistochemical markers in a SA node tissue section. SA node sections were cut perpendicular to the crista terminalis through the SA node and were immunolabelled by Dr. H. Dobrzynski. The labelling pattern was same as that in Fig. 10.1. It is noteworthy that the myocytes in the centre of the SA node are small, Cx43-negative, ANP-negative and HCN4-positive; none of these are the attributes of atrial

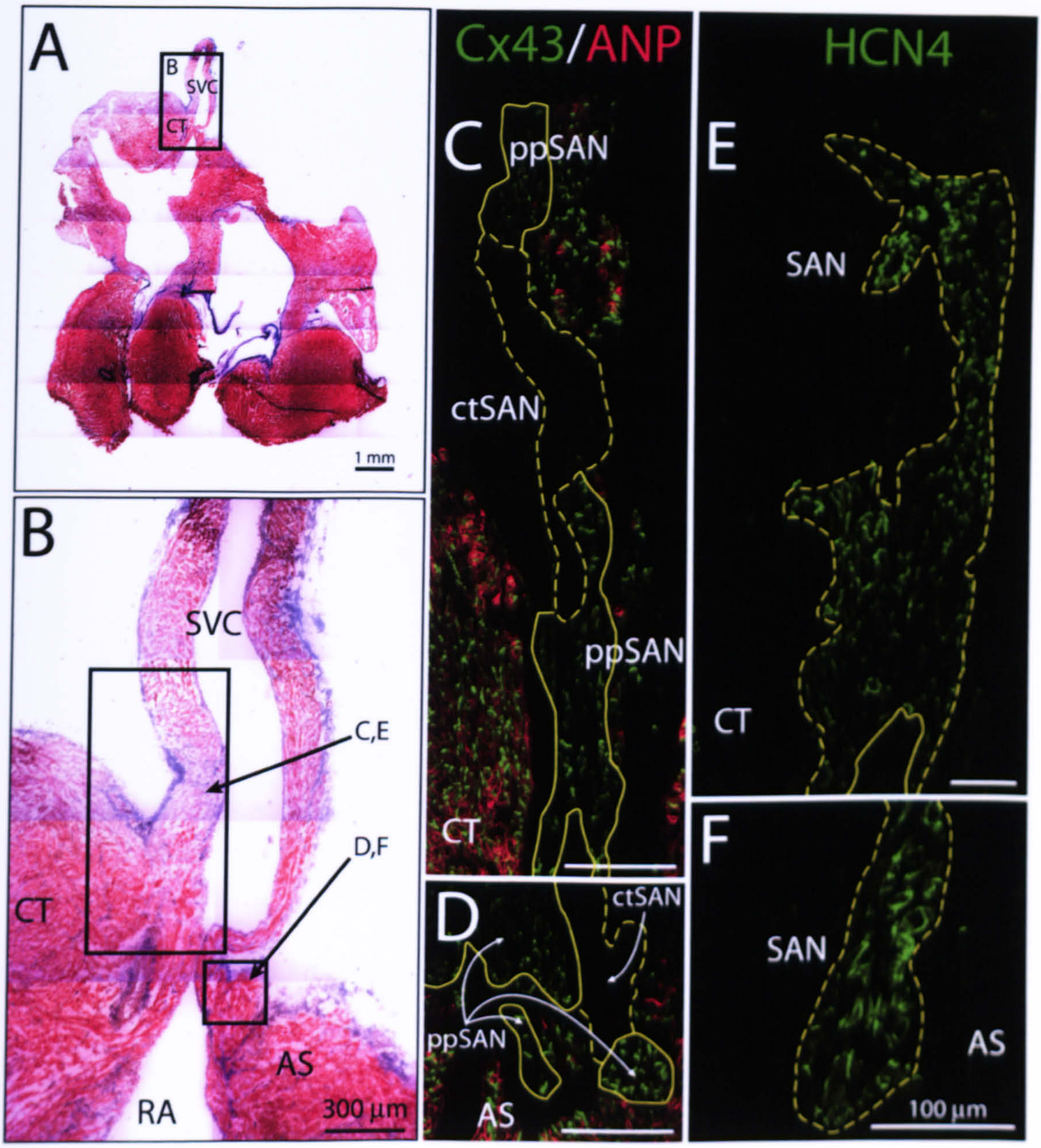

Figure 10.1 Anatomy of and immunolabelling of immunohistochemical markers in a four chamber section

A, Masson's trichrome stained section. B, zoomed image of the framed area in A. Sections were provided and histologically stained by Dr. M. Yamamoto. C, D, montages of section double labelled for Cx43 (green) and ANP (red). E, F, montages of section labelled for HCN4 (green). C to F correspond to the framed areas in B. AS, atrial septum; CT, crista terminalis; ctSAN, centre of the SA node; ppSAN, periphery of the SA node; RA, right atrium; SAN, SA node; SVC, superior vena cava. Scale bars, 1 mm (A), 300 µm (B), and 100 µm (C - F).

Figure 10.2 Labelling of immunohistochemical markers in a rat SA node tissue section

A, montage of section double labelled for ANP (green) and Cx43 (red). B, montage of section labelled for HCN4 (green). Sections were provided and immunolabelled by Dr. H. Dobrzynski. CT, crista terminalis; SAN, SA node; SEP, interatrial septum; ctSAN, centre of the SA node; ppSAN, periphery of the SA node. Scale bars, 100 μm.

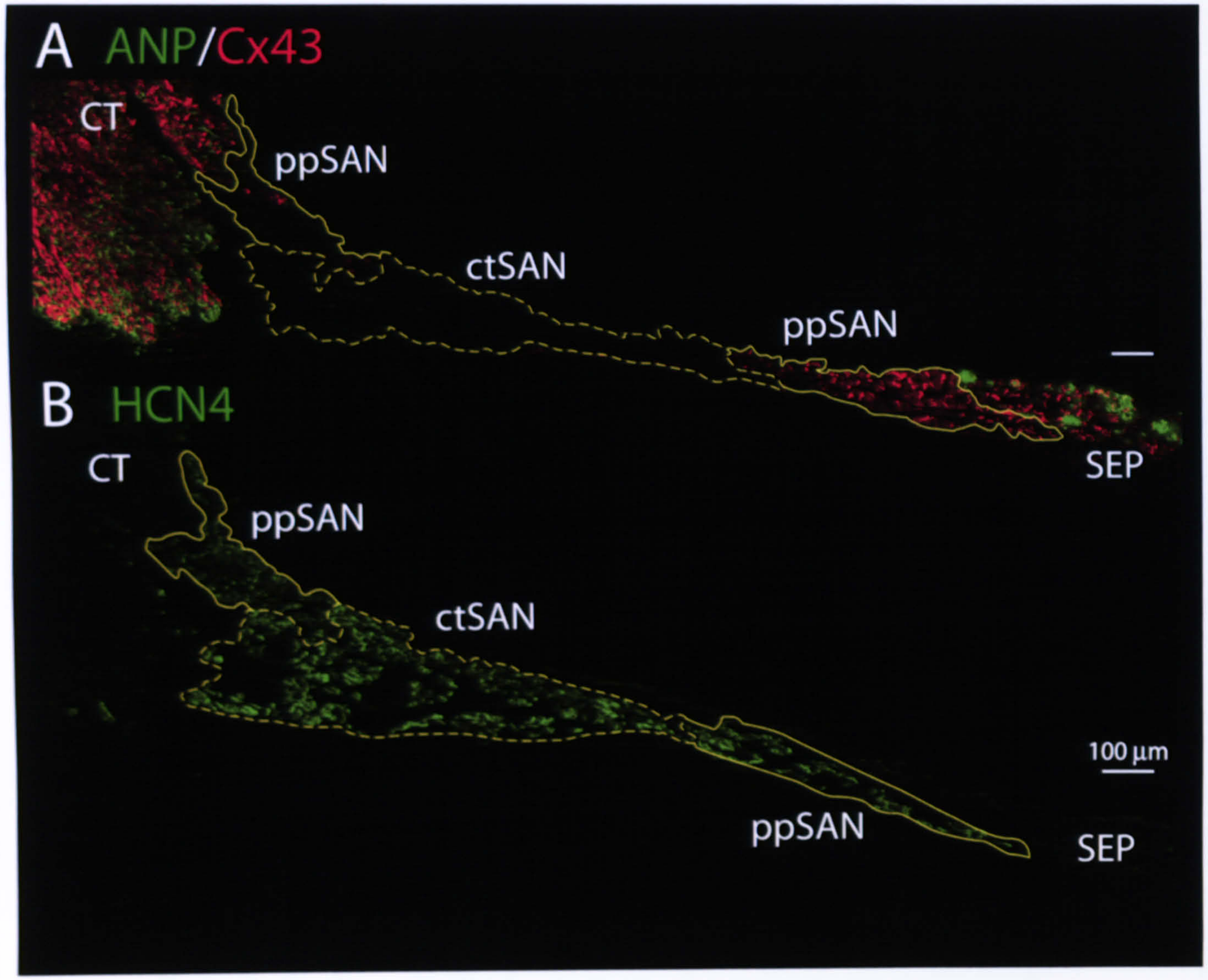
A ANP/Cx43
CT
ppSAN
ctSAN
ppSAN
SEP
B HCN4
CT
ppSAN
ctSAN
ppSAN
SEP
100 µm

myocytes, and this is inconsistent with the mosaic model (there should be some atrial myocytes in the centre of the SA node according to the mosaic model).

10.3.2. Immunolabelling of Na^+ channel isoforms

Immunolabelling of Na^+ channel isoforms in adjacent four chamber sections is shown in Fig. 10.3. Myocytes showing no Cx43 labelling show $Na_v1.1$ labelling in Fig. 10.3A and B; $Na_v1.1$ was expressed in the centre of the SA node (Cx43-negative region) as well as in the surrounding myocardium (Cx43-positive). Myocytes showing no Cx43 labelling show *no* $Na_v1.5$ labelling in Fig. 10.3C and D, but $Na_v1.5$ and Cx43 were expressed elsewhere. Although the exact border of the periphery of the SA node is not certain, the presence of $Na_v1.5$ in the periphery of the SA node is a possibility (the periphery of the SA node region is around the Cx43-negative region).

Fig. 10.4 shows $Na_v1.1$ and $Na_v1.5$ labelling in SA node sections adjacent to those shown in Fig. 10.2. The $Na_v1.1$ labelling pattern is the same as shown in Fig. 10.3; $Na_v1.1$ was present throughout the tissue. The centre and periphery of the SA node region can perhaps be distinguished by considering the difference between HCN4 labelling (Fig. 10.2B) and $Na_v1.5$ labelling (Fig. 10.4B). The centre of the SA node is HCN4-positive and $Na_v1.5$-negative, whereas the periphery is HCN4-positive and $Na_v1.5$-positive (Figs 10.2 and 10.4) As already reported in the mouse SA node (Maier *et al.*, 2003; Lei *et al.*, 2004), the present study shows that $Na_v1.5$ is present in the periphery of the SA node of the rat (Fig. 10.4B).

Fig. 10.5 shows high magnification images of sections double labelled for $Na_v1.1$ and DP or Cx43. As already shown in chapter 4 (section 4.3), DP was expressed at the intercalated disks in all myocytes (Fig. 10.5). As already shown in Figs. 10.3 and 10.4, $Na_v1.1$ was present throughout the tissue (Fig. 10.5). In the right-middle panel in Fig. 10.5, there is no labelling of Cx43 in the SA node except in the SA node artery, whereas there is labelling of $Na_v1.1$ in the SA node myocytes.

Fig. 10.6 shows $Na_v1.3$ labelling in the SA node. Cx43 labelling (red in Fig. 10.6A) is largely absent, confirming that the tissue is SA node. There was no labelling of $Na_v1.3$ in SA node myocytes, but as already shown in chapter 7 (section 7.3.1.2), $Na_v1.3$ labelling was present in nerve fibres and nerve cell bodies innervating the nodal myocytes. Fig. 10.6B shows co-localisation (yellow colour) of $Na_v1.3$ and NF160 in the SA node.

Some parts of this study (Figs. 10.4A, 10.5 and 10.6) have already been published (Maier *et al.*, 2003).

10.4. Discussion

The SA and AV nodes are specialised tissues in the heart: the SA node is specialised for pacemaking (it is the pacemaker of the heart), whereas the AV node is specialised for slow conduction of the action potential (to introduce a delay between atrial and ventricular activation

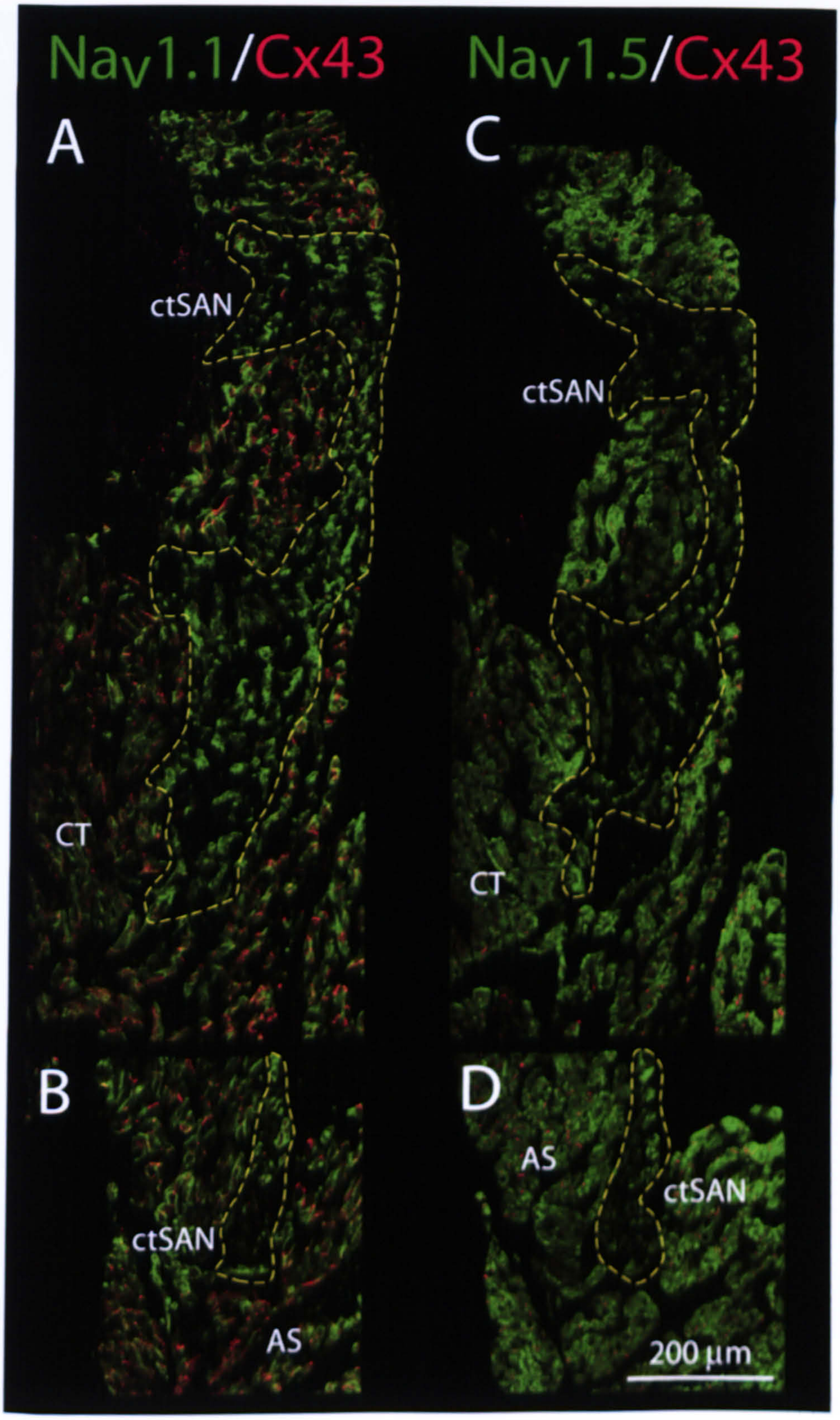

Figure 10.3 $Na_v1.1$ and $Na_v1.5$ labelling in four chamber sections

Left (A and B) and right (C and D) panels show montages of sections double labelled for $Na_v1.1$ (green) and Cx43 (red) and $Na_v1.5$ (green) and Cx43 (red), respectively. Top (A and C) and bottom (B and D) panels correspond to the framed areas in Fig. 10.2B (C and E and D and F, respectively). AS, atrial septum; CT, crista terminalis; ctSAN, centre of the SA node. Scale bars, 200 µm.

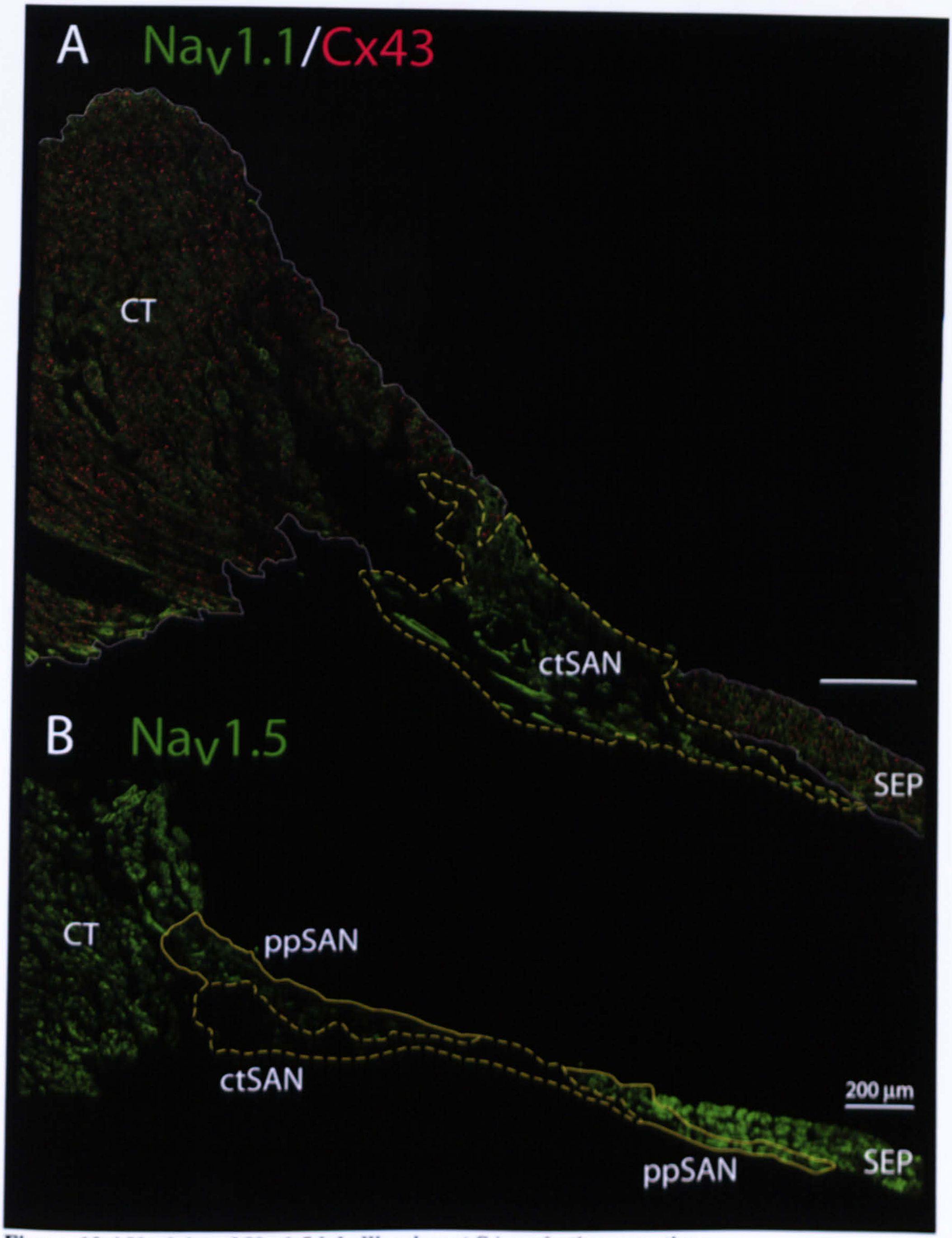

Figure 10.4 $Na_v1.1$ and $Na_v1.5$ labelling in rat SA node tissue sections

A, montage of section double labelled for $Na_v1.1$ (green) and Cx43 (red). B, montage of section labelled for $Na_v1.5$. Section was provided and immunolabelled by Dr. H. Dobrzynski. CT, crista terminalis; ctSAN, centre of the SA node; ppSAN, periphery of the SA node; SEP, interatrial septum. Scale bars, 200 µm.

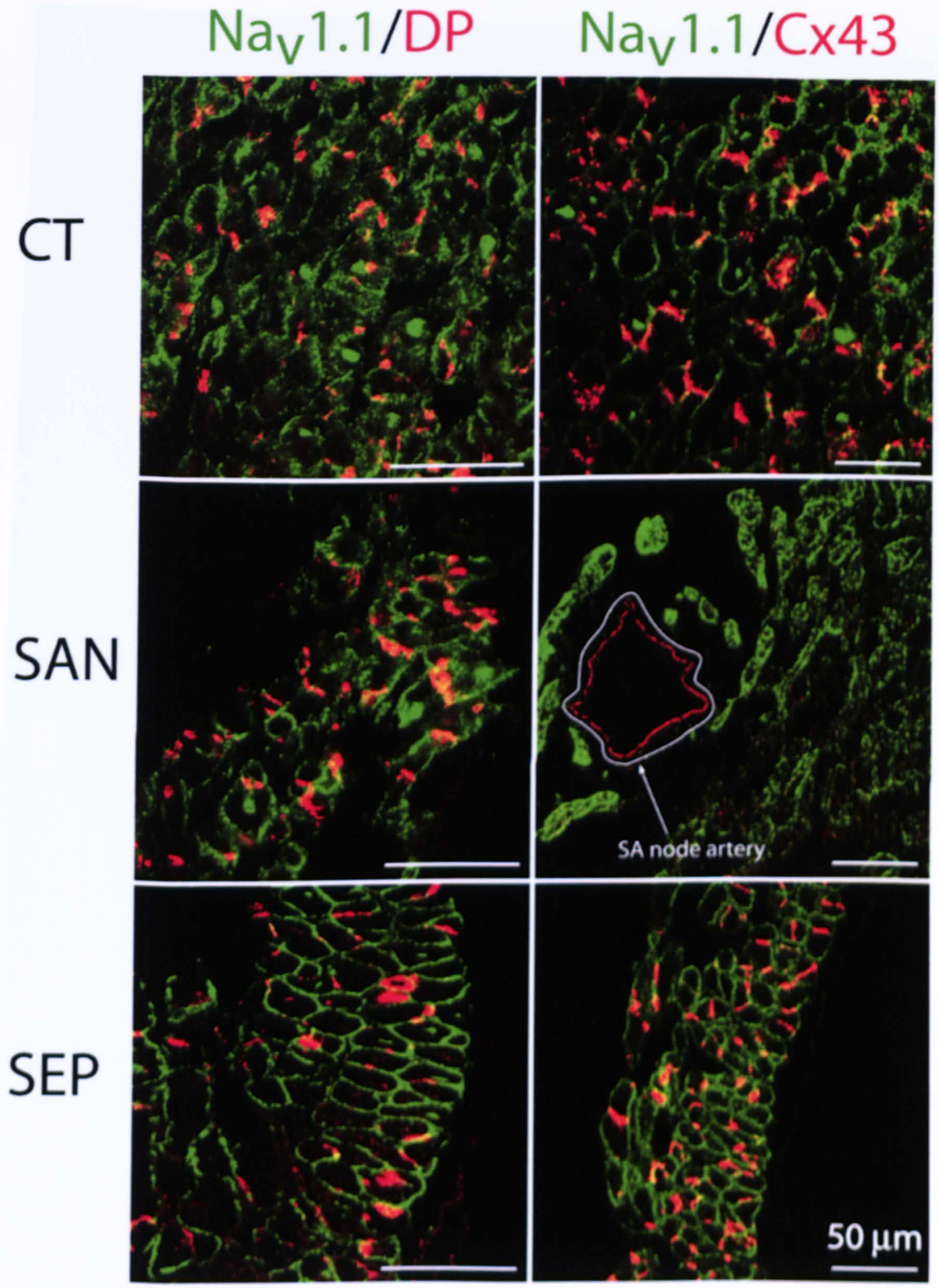

Figure 10.5 Double labelling of Na$_v$1.1 with DP and Cx43 in SA node tissue sections

Left and right panels show high magnification images of sections double labelled for Na$_v$1.1 (green) and DP (red) and Na$_v$1.1 (green) and Cx43 (red), respectively. Top, middle and bottom panels correspond to the crista terminalis (CT), SA node (SAN), and interatrial septum (SEP), respectively. Scale bars, 50 µm.

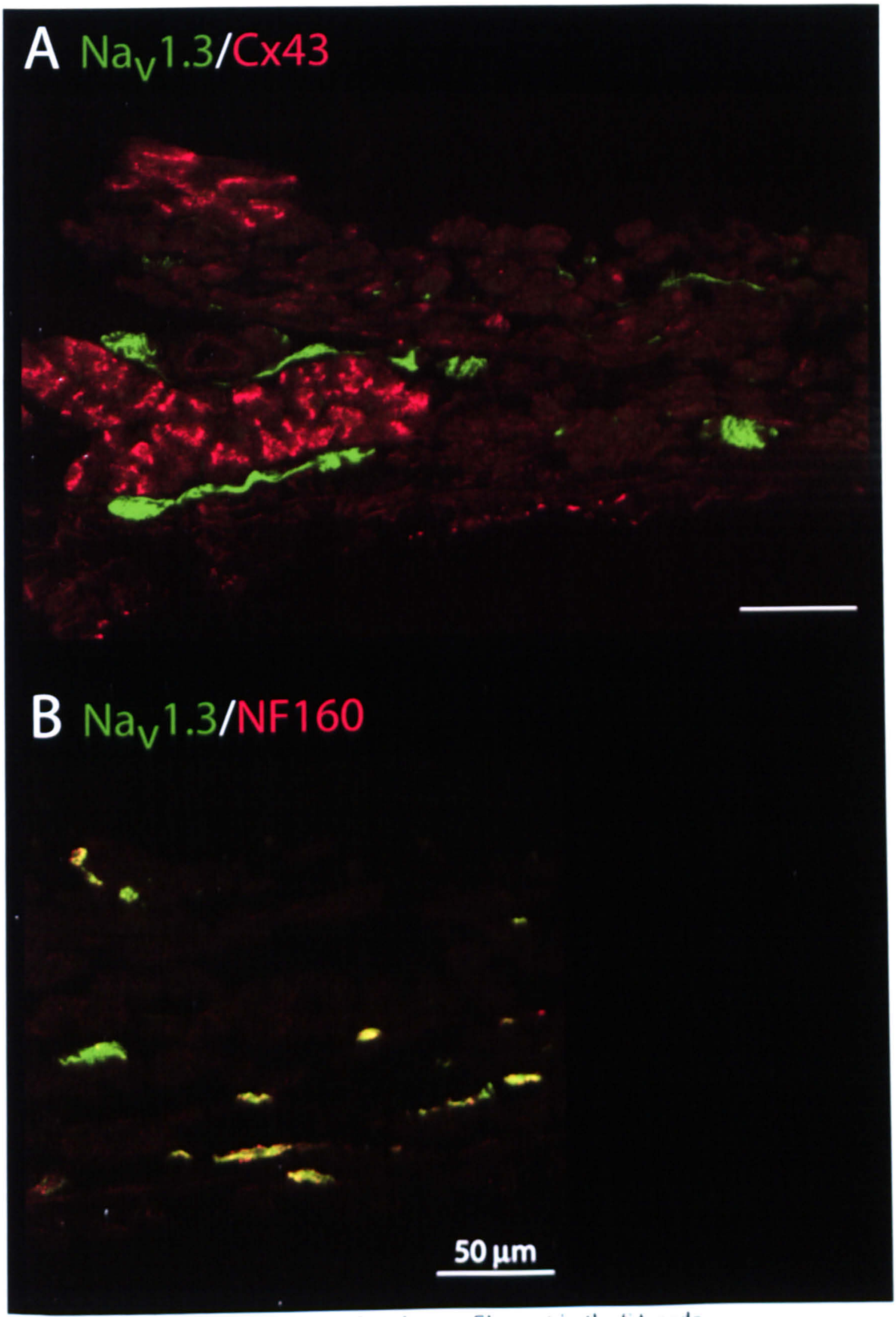

Figure 10.6 Co-localisation of Na$_V$1.3 and neurofilament in the SA node

A, B, high magnification images of adjacent sections double labelled for Na$_V$1.3 (green) and Cx43 (red, top) and NF160 (red, bottom), respectively. The yellow colour in B shows co-localisation of Na$_V$1.3 (green) and NF160 (red). Scale bars, 50 µm.

during the cardiac cycle). In order to fulfill their specialised functions, the SA and AV nodes have (i) a different pattern of expression of ion channels and, as a result, different action potential configurations (as compared to the working myocardium), (ii) poor electrical coupling between cells and (iii) specialised structures.

At the single cell level, their electrophysiological activity is reasonably well understood (Schram *et al.*, 2002; Irisawa *et al.*, 1993). From the point of view of impulse generation and conduction, poor electrical coupling protects the SA node from the hyperpolarizing influence of the surrounding atrial myocardium and, in case of the AV node, because of the resulting slow conduction, the poor electrical coupling ensures coordinated contractions of the atria and ventricles (Boyett *et al.*, 2000; Severs *et al.*, 2001).

More than any other tissue in the heart, the SA and AV nodes are complex tissues and their function depends on the complexity. The SA and AV nodes are made up of networks of histologically palely stained, small and slender cells closely packed in a dense matrix of fibrous tissue (Severs *et al.*, 2001; Mazgalev *et al.*, 2001). However, there are gradual transitions from the centre of the nodes to the surrounding atrial myocardium (Bleeker *et al.*, 1982; Masson-Pévet *et al.*, 1984; Mazgalev *et al.*, 2001; Meijler & Janse, 1988; Tawara, 2000). The transitional areas, i.e. intermediate myocardium (myocytes with a mixture of nodal and atrial properties), may be important physiologically. For example, the leading pacemaker site can move from the centre of the SA node to the periphery (or even further, to nodal cells in the interatrial groove) and the posterior/inferior nodal extension can drive AV junctional pacemaking (Kalman *et al.*, 1995; Boyett *et al.*, 2000; Dobrzynski *et al.*, 2003; Yamamoto *et al.*, unpublished observations). Functionally important and complex phenomena in the SA and AV nodes include the non-radial spread of the action potential from the leading pacemaker site in the SA node, the block of conduction from the leading pacemaker site in the SA node towards the atrial septum, (which protects the SA node from reentry and invasion from action potentials from outside the SA node) and the dual inputs into the AV node responsible for AV transmission, respectively (Nikolski & Efimov, 2001; Jazayeri *et al.*, 1992; Keim *et al.*, 1992; Patterson & Scherlag, 1999; Lo *et al.*, 1995; Amellal & Billette, 1996) (Bleeker *et al.*, 1982; Boyett *et al.*, 1999).

In this study, using immunohistochemistry with antibodies against ion channels and proteins important to the SA node structurally and functionally, different cell types were identified in the rat SA node: the myocytes in the centre of the SA node are Cx43-negative, ANP-negative, HCN4-positive, $Na_v1.1$-positive and $Na_v1.5$-negative; the myocytes in the periphery of the SA node are Cx43-positive, ANP-negative, HCN4-positive, $Na_v1.1$-positive and $Na_v1.5$-positive; the atrial myocytes are Cx43-positive, ANP-positive, HCN4-negative, $Na_v1.1$-positive and $Na_v1.5$-positive. These results are consistent with previous reports (Dobrzynski *et al.*, 2005; Lei *et al.*, 2004; Maier *et al.*, 2003).

The sub-regions in the SA and the AV nodes can be compared in terms of expression pattern. Cx43 was absent in the nodal myocytes in the AV node, whereas Cx43 was present in the periphery of the SA node (Figs 10.1 and 10.2). The existence of the Cx43 in the periphery of the SA node represents a gradual increase in electrical coupling, which is thought to be important in enabling the SA node to resist the hyperpolarizing influence of the atrial myocardium and yet still be able to drive the atrial myocardium. The absence of the Cx43 in the AV node may contribute to the slowing of conduction, which makes sure the sequential contraction of the atria and ventricles (Severs *et al.*, 2001).

The distribution of $Na_v1.1$ and $Na_v1.5$ differs in the SA and AV nodes. In agreement with previous reports (Maier *et al.*, 2003; Lei *et al.*, 2004), $Na_v1.5$ labelling was not detected in the centre of the SA node (Figs 10.3 and 4). Lei *et al.* (2004) showed $Na_v1.5$ labelling in the periphery of the mouse SA node using the Catterall $Na_v1.5$ antibody. In the present study, evidence of $Na_v1.5$ in the periphery of the rat SA node was obtained (Fig. 10.4). In the present study, in contrast of $Na_v1.5$, $Na_v1.1$ was observed throughout the SA node (Figs. 10.3 and 4). However, in the AV node, the distributions of $Na_v1.1$ and $Na_v1.5$ were the same. Both isoforms were expressed in the transitional cells and the posterior/inferior nodal extension and both were not expressed in the enclosed node. As already discussed in chapter 7 (section 7.4.2), the expression of $Na_v1.1$ and $Na_v1.5$ in the transitional cells and posterior/inferior nodal extension may contribute the faster upstroke velocity of the action potential in these sub-regions and the absence of both isoforms in the enclosed node may contribute to the low upstroke velocity of the action potential in this sub-region.

Chapter 11

Summary

11.1. Summary: three different cell types in and around the AV node

Table 11.1 summarises the expression pattern in the different tissues in and around the AV node. Based on the expression pattern, three types of nodal cells were identified: type 1 nodal cells were present in the posterior/inferior nodal extension, the zone of transitional cells and the AV ring bundle on the opposite side of the tricuspid valve to the AV node; type 2 nodal cells were expressed in the open node, enclosed node and the termination of the AV ring bundle; type 3 nodal cells only differed from type 2 nodal cells in their expression of Cx40 and were located in the enclosed node (lower part), common bundle and bundle branches.

For all 14 levels investigated from the preparation shown in Fig. 2.1B, the distribution of the different tissues and the three types of nodal myocytes are summarised in Fig. 11.1A. The distribution of the three types of nodal myocytes was mapped onto the original preparation (Fig. 11.1B). Figure 11.1B shows that the type 1 nodal myocytes in the posterior/inferior nodal extension continued as the transitional cells adjacent to the open node; type 2 nodal myocytes in

Table 11.1 Summary of expression of marker proteins and Na^+ channel isoforms in and around the AV node

	Colour code (Fig. 11.1)	DP	Cx40	Cx43	ANP	HCN4	$Na_v1.1$	$Na_v1.2$	$Na_v1.3$*	$Na_v1.5$	$Na_v1.6$
Atrium	Pink	+	+	+	+	-	+	-	-	+	-
Ventricle	Red	+	-	+	-	-	+	-	-	+	-
Type 1 nodal myocytes Posterior/inferior nodal extension and zone of transitional cells	Light blue	+	-	-	-	+	+	-	+	+	-
Type 2 nodal myocytes Open node, enclosed node (mid-nodal cells) and termination of the AV ring bundle	Green	+	-	-	-	+	-	-	+	-	-
Type 3 nodal myocytes Enclosed node (lower nodal cells) and common bundle	Purple	+	+	-	-	+	-	-	+	-	-
Left bundle branch	Not shown	+	+	-	-	+	+	-	-	+	-
Connective tissue	Dark blue	-	-	-	-	-	-	-	-	-	-
Fatty tissue	Yellow	-	-	-	-	-	-	-	-	-	-

* labelling present in nerve fibres and nerve cell bodies

Figure 11.1 Summary of nodal tissue distribution in the rat AV junctional area

A, diagrams summarising the distribution of different cell types in the 14 levels shown in B. Scale bars, 200 μm. B, summary of nodal tissue distribution in the main preparation studied. Numbers at the bottom of the panel show the position of the different levels studied. Labels in yellow and white show conventional orientation and correct orientation, respectively. Scale bar, 1 mm. C, schematic diagram summarising nodal tissue distribution in the entire tricuspid annulus. The dotted line indicates the cutting plane of sagittal sections shown in chapters 9 and 10. Light blue, type 1 nodal myocytes; green, type 2 nodal myocytes; purple, type 3 nodal myocytes. A, anterior; AM, atrial myocardium; Ao, aorta; AoV, aortic valve; CB, common bundle; CS, coronary sinus; EN, enclosed node; I, inferior; LNC, lower nodal cells; MNC, mid-nodal cells; MV, mitral valve; ON, open node; P, posterior; P/I NE, posterior/inferior nodal extension; S, superior; TAVRB, termination of the AV ring bundle; TT, tendon of Todaro; TV, tricuspid valve; VM, ventricular myocardium.

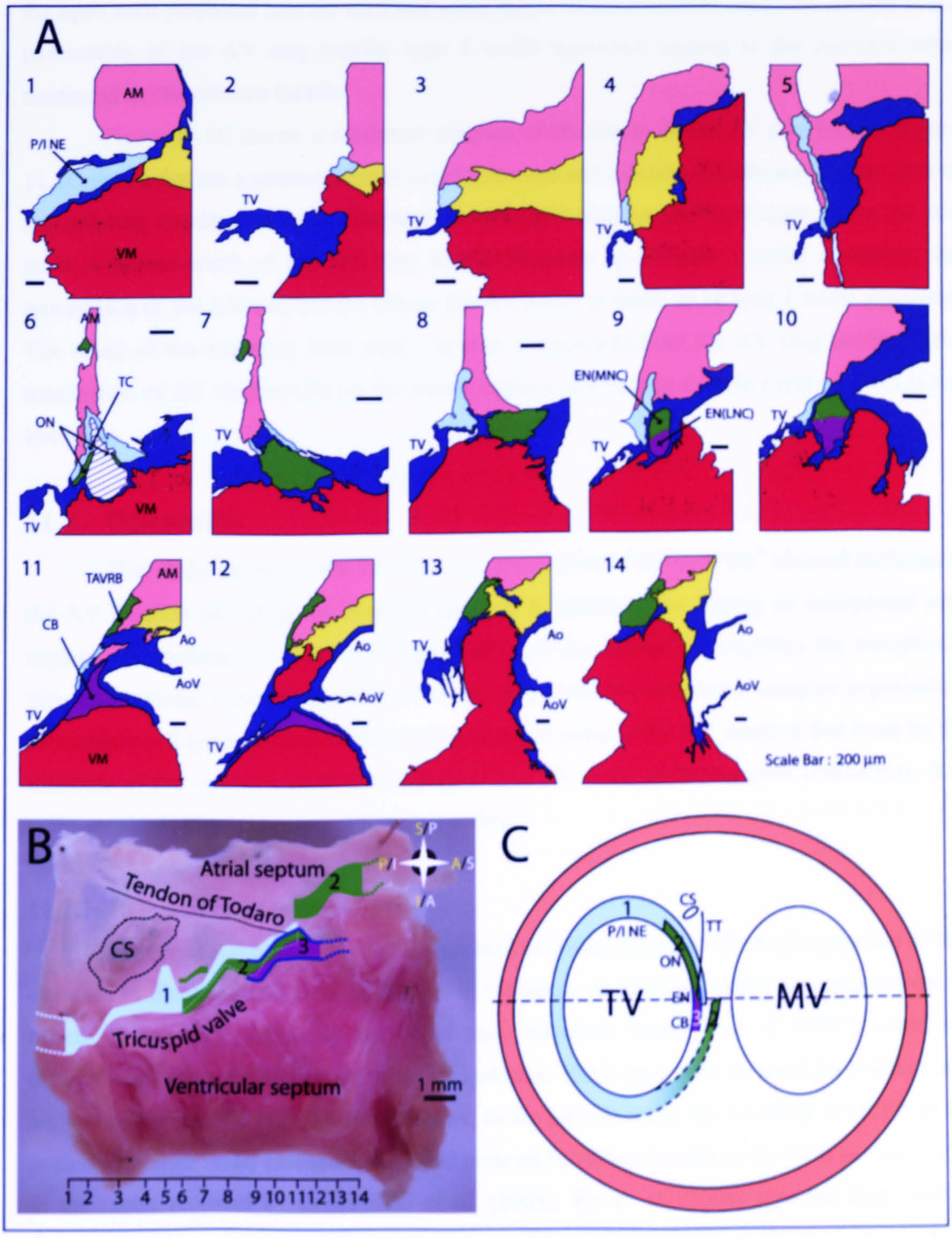
A
1
AM
P/I NE
VM
2
TV
3
TV
4
TV
5
TV
6
AM
TC
ON
VM
TV
7
TV
8
TV
9
EN(MNC)
EN(LNC)
TV
10
TV
11
TAVRB
AM
CB
Ao
AoV
TV
VM
12
Ao
AoV
TV
13
TV
Ao
AoV
14
Ao
AoV
Scale Bar : 200 µm
B
S/P
P/I
A/S
I/A
Atrial septum
Tendon of Todaro
CS
1
2
3
Tricuspid valve
Ventricular septum
1 mm
1 2 3 4 5 6 7 8 9 10 11 12 13 14
C
CS
TT
1
P/I NE
ON
TV
EN
CB
MV

the open node projected into the enclosed node; type 2 nodal myocytes were also present in the termination of the AV ring bundle; type 3 nodal myocytes starting in the enclosed node continued in the common bundle.

Figure 11.1C shows a schematic diagram of the whole of the AV ring bundle. Figure 11.1C shows that the posterior/inferior nodal extension and transitional cells are just one part of the AV ring bundle that projects around the tricuspid annulus and terminates above the AV node. Whereas much of the AV ring bundle is made up of type 1 nodal myocytes, the termination of the AV ring bundle (above the AV node) is made up of type 2 nodal myocytes. The detail of the transition from type 1 to type 2 myocytes from the AV ring bundle to the termination of AV ring bundle (in the region between the dashed lines in Figure 11.1C) is not known.

11.2. Discussion

This study shows for the first time the distribution of different Na^+ channel isoforms at the AV junction including the tricuspid annulus. In addition, the finding of unexpected sub-regions (the termination of the AV ring bundle and the "bump") exemplifies the exceptional three-dimensional complexity of the AV node. The study has revealed a complex organisation of multiple cell types (including three types of nodal cells) at the AV junction that must be the substrate of the complex electrophysiology of the AV node, including slow conduction, dual pathway electrophysiology and AV nodal reentry.

11.2.1. Relation to previous studies

Petrecca *et al.* (1997) previously reported evidence of a lower level of expression of Na^+ channels in the mid-nodal cells of the rabbit. However, an antibody raised against a conserved region of the Na$_v$1 subfamily was used and, therefore, Petrecca *et al.* (1997) could not discriminate between different Na^+ channel isoforms. There have been no previous studies using antibodies for specific Na^+ channel isoforms. In the present study, the labelling of HCN4 in the posterior/inferior nodal extension, enclosed node and common bundle in the rat is similar to that in the rabbit reported by Dobrzynski *et al.* (2003). Ko *et al.* (2004) reported that Cx43 is expressed in the posterior nodal extension of the rabbit, whereas in this study and in the study of the rabbit AV node by Dobrzynski *et al.* (2003), the posterior nodal extension was Cx43-negative. However, this discrepancy is likely to be only the result of confused nomenclature – the "posterior nodal extension" in the study of Ko *et al.* (2004) probably corresponds to the tract of type 3, Cx40-expressing (in the rat – Fig. 8.1) or Cx43-expressing (in the rabbit; unpublished observations) lower nodal cells. Above the "posterior nodal extension" in the study of Ko *et al.* (2004), there is a tract of Cx43-negative cells (termed "transitional cells" by Ko *et al.*, 2004) and this corresponds to the posterior/inferior nodal extension in the present study (Fig. 11.1) and the study of Dobrzynski *et al.* (2003)

11.2.2. Understanding the electrophysiology of the AV junction

The AV node has dual inputs (slow and fast pathways) from the atrial myocardium and this is the substrate for AV node reentry (Moe *et al.*, 1956; Mendez & Moe, 1966). The slow pathway proceeds parallel to the tricuspid valve annulus from beneath the coronary sinus to the open node near the apex of the triangle of Koch, whereas the fast pathway enters the open node superiorly from the direction of the atrial septum. The results from the present study help to understand this dual pathway electrophysiology as well as other aspects of the electrophysiology of the AV junction.

The upstroke velocity and amplitude of the action potential in the atrial (and ventricular) myocardium are high (dog atrial myocardium: 158 V/s and 108 mV, Patterson & Scherlag, 2002) and this is because the voltage-dependent Na^+ current, I_{Na}, is responsible for it. In accordance with this, in the present study, labelling of both $Na_v1.5$ and $Na_v1.1$ was observed in the atrial myocardium (chapters 6 and 7; Table 11.1). The fast conduction velocity (70 cm/s in rabbit, Meijler & Janse, 1988) in atrial myocardium can be explained by the high upstroke velocity (as a result of the expression of $Na_v1.5$ and $Na_v1.1$), the abundant expression of the medium conductance gap junction protein, Cx43 (chapter 4; Table 11.1) and the expression of the high-conductance gap junction protein, Cx40 (chapter 8, Table 11.1), in the atrial myocardium, because the conduction velocity is dependent on both the upstroke velocity of the action potential and the coupling conductance between cells.

Simultaneous optical mapping of action potentials and immunohistochemical delineation of the posterior/inferior nodal extension in the rabbit has shown that the posterior/inferior nodal extension is the slow pathway (unpublished observations). The upstroke velocity and amplitude of the action potential in the slow pathway (dog: 41 V/s and 70 mV, Patterson & Scherlag, 2002) are intermediate between those in the atrial myocardium and the enclosed node. Consistent with this, in the present study, labelling of both $Na_v1.5$ and $Na_v1.1$ was observed in the posterior/inferior nodal extension ($Na_v1.5$: 45 ± 2 %; Fig. 7.12) but the labelling was less abundant than in the atrial myocardium ($Na_v1.5$: 84 ± 10 %; Fig. 7.12). In the rabbit, Nikolski *et al.* (2003) measured the conduction velocity of the slow pathway to be 7.9 ± 3.4 cm/s (in the nearby atrial myocardium, it was 35.1 ± 17.2 cm/s). The slow conduction in the posterior/inferior nodal extension could be the result of the lack of expression of the medium conductance gap junction protein, Cx43 (chapter 4, Table 11.1), and the high-conductance gap junction protein, Cx40 (chapter 8, Table 11.1), in the posterior/inferior nodal extension as well as the lower expression of Na^+ channels (chapter 7). In the posterior/inferior nodal extension, it is known that the low conductance connexin, Cx45, is expressed (Dobrzynski *et al.*, 2003).

Figure 11.1A, B shows three pathways into the open/enclosed node: (i) the posterior/inferior nodal extension (Fig. 11.1B shows that the posterior/inferior nodal extension and the open node are continuous), (ii) the zone of transitional cells (6 and 7 in Fig. 11.1A show connections between the zone of transitional cells and the open node) and (iii) atrial

myocardium (8 in Fig. 11.1A shows an apparent contact). The location of the zone of transitional cells means that it could be the fast pathway from the direction of the atrial septum to the open node. The upstroke velocity and amplitude of the action potential in the fast pathway (dog: 60 V/s and 71 mV, Patterson & Scherlag, 2002) is again intermediate between that in the atrial myocardium and the enclosed node. Consistent with this, in the present study, labelling of both $Na_v1.5$ and $Na_v1.1$ was observed in the zone of transitional cells ($Na_v1.5$: 44 ± 12 %; Fig. 7.12), but the labelling was less abundant than in the atrial muscle ($Na_v1.5$: 84 ± 10 %; Fig. 7.12). The conduction velocity of the fast pathway could be faster than that of the slow pathway. If the zone of transitional cells does constitute the fast pathway, the possible difference in conduction velocity between the slow and fast pathways (i.e. between the posterior/inferior nodal extension and zone of transitional cells) is unlikely to be the result of I_{Na} (because the Na^+ channel expression in the two regions was similar; Fig. 7.12; Table 11.1) or electrical coupling (because the expression of connexins was similar; Table 11.1). However, the terms fast and slow were originally introduced to describe differences in the observed time intervals not velocities during AV node reentrant tachycardia. In fact, it has never been demonstrated that the wavefronts deserve their adjectives (Mazgalev & Tchou, 2000a; Mazgalev & Tchou, 2000b). The faster conduction of the fast pathway is perhaps the result of the shortness (~1 mm) of the tract of Cx43-negative myocytes with reduced $Na_v1.5$ and $Na_v1.1$ expression in the zone of transitional cells that the action potential has to propagate across in order to reach the open node (the length of the slow pathway, i.e. posterior/inferior nodal extension, is much greater) (Fig. 11.1B). Across such a short distance, the electrotonic influence of the atrial muscle will be important. Alternatively, or in addition, the faster conduction of the fast pathway is perhaps the consequence of the "back door" connection between the atrial muscle and the open node (8 in Fig. 11.1A).

In contrast to the atrial muscle, the upstroke velocity and amplitude of the action potential in the enclosed node are low (dog: 18 V/s and 54 mV, Patterson & Scherlag, 2002) and this is because the L-type Ca^{2+} current, I_{Ca}, rather than I_{Na} is responsible for it. In cells likely to be from the enclosed node, there is no I_{Na} (Petrecca *et al.*, 1997). Consistent with this, in the present study, no or reduced labelling of either $Na_v1.5$ or $Na_v1.1$ was observed in the enclosed node (Figs. 7.1E, 7.11E and 7.12). The absence or reduced level of $Na_v1.5$ or $Na_v1.1$ expression continued from the open node, through the enclosed node and common bundle to the proximal left (and presumably right) bundle branch. Consistent with this, the upstroke velocity and amplitude of the action potential is still low in the N11 cells in this region (dog: 29 V/s and 61 mV, Patterson & Scherlag, 2002). The slow conduction through the AV node (0.7 cm/s in chick embryo, Arguello *et al.*, 1986) is responsible for the delay between the activation of the atria and ventricles in the cardiac cycle. The absence or reduced level of $Na_v1.5$ and $Na_v1.1$ expression from the open node to the proximal left and right bundle branches will, at least, contribute to the slow conduction. The expression pattern of connexins may also contribute:

from the open node to the proximal left and right bundle branches, the medium conductance gap junction protein, Cx43, is not expressed (or poorly expressed), although, from the enclosed node to the left and right bundle branches (and, presumably, onto the terminal Purkinje fibres), the high-conductance gap junction protein, Cx40, is expressed (chapter 8). In the open node and part of the enclosed node, Cx40 is not expressed and Cx43 is either not or poorly expressed and instead the low-conductance gap junction protein, Cx45, is expressed (Dobrzynski *et al.*, 2003) and this pattern of expression, at least, is expected to contribute to the slow conduction of the AV node.

In the dog, the upstroke velocity and amplitude of the action potential (dog: 140 V/s and 111 mV, Patterson & Scherlag, 2002) and conduction velocity (100-150 cm/s in dog, Hofmann & Cranefield, 1960) in the common bundle are high. The high upstroke velocity and amplitude of the action potential in the common bundle in the dog are not consistent with the lack or reduced level of expression of $Na_v1.5$ and $Na_v1.1$ in the common bundle in the rat (Figs. 7.1 and 7.11). It is possible that there is a difference between species and the upstroke velocity and action potential amplitude are low in the common bundle of the rat. The rapid conduction velocity in the common bundle in the dog may either not be true of the rat or it is the result of the abundant expression of Cx40 in the common bundle (Fig. 8.1). A reduction of Na^+ conductance can produce only a three-fold reduction in conduction velocity, whereas a decrease in coupling via connexin can cause a 100-fold reduction (Shaw & Rudy, 1997). In the common bundle, previous reports (Mazgalev *et al.*, 2001; Nikolski *et al.*, 2003) have described distinct electrophysiologies in the mid and lower nodal cells – does this correspond to the mid Cx40-negative and lower Cx40-positive nodal cells in the rat as shown in Fig. 8.1?

$Na_v1.3$ labelling (arguably an indication of innervation) was minimal in the atrial and ventricular muscle, present (but not abundant) in the specialised pathways into the AV node (posterior/inferior nodal extension and zone of the transitional cells) and abundant in the open and enclosed nodes. Therefore, innervation appears to be controlling AV conduction at the point at which conduction will be the most severely constrained by the absence of $Na_v1.5$, $Na_v1.1$, Cx40 (in part at least) and Cx43 (to a large degree at least).

11.2.3. Why do mutations in or knockout of $Na_v1.5$ (SCN5A) result in AV conduction defects?

The role of $Na_v1.5$ in AV conduction has recently been highlighted by the discovery of inherited AV conduction disturbances (AV conduction block or slowing of AV conduction) linked to mutations in SCN5A (Schott *et al.*, 1999; Tan *et al.*, 2001; Lupoglazoff *et al.*, 2001; Kyndt *et al.*, 2001) and the discovery that $SCN5A^{+/-}$ mice have impaired AV conduction (as well as other cardiac conduction defects) (Papadatos *et al.*, 2002). Our findings provide the substrate for these conduction disturbances. There is no $Na_v1.5$ expressed in a long tract from the open node to the proximal part of the left and presumably right bundle branches (Table 11.1

and Fig. 11.1). However, $Na_v1.5$ is expressed in the pathways into the open node (posterior/inferior nodal extension and transitional cells) (Fig. 11.1), but less abundantly than in the working myocardium, and these are the most likely regions that conduction defects will occur on impairing $Na_v1.5$ (because the safety factor for conduction is already likely to be low in these regions as a result of the lower expression of $Na_v1.5$). This raises the possibility that the AV conduction abnormalities could be corrected by local up-regulation of $Na_v1.5$ (perhaps by local transfection with further copies of SCN5A). Alternatively (or as well) the AV conduction abnormalities could be the result of impaired conduction in the bundle branches, because the bundle branches do express $Na_v1.5$ (Fig. 7.9) and indeed there is evidence of this (Papadatos *et al.*, 2002).

11.2.4. Mapping the AV conduction system

Recently, a three-dimensional anatomical model of the human AV node has been generated based on histological information only (Mutharasan *et al.*, 2004). Although an appreciation of the complex anatomy of the AV junction is undoubtedly important for the understanding of AV conduction, it is also important to understand the distribution of the proteins involved in the action potential and its conduction. Dobrzynski *et al.* (2003) mapped the distribution of HCN4 in the rabbit AV node, but HCN4 is involved in pacemaking. Ko *et al.* (2004) mapped the distribution of connexins in the rabbit AV node and this is important in understanding action potential conduction. In the present study, I not only largely confirmed the findings of Dobrzynski *et al.* (2003) and Ko *et al.* (2004) as regards HCN4 and connexins, I extended them to the whole of the AV junction. Although connexins play an important role in the conduction, Na^+ channels also play a major role and this is the first study to map in detail the distribution of Na^+ channels throughout the AV junction. The expression of the Na^+ channels was non-uniform at the AV junction and allowed the identification of various types of nodal myocytes.

11.3. Limitations of this study

The expression of protein is often qualitatively and quantitatively heterogeneous, both spatially within an organ or tissue and temporally in relation to development or disease. Cytochemistry is indispensable to the analysis of these heterogeneities in the pattern of expression.

In this study, immunohistochemistry was the experimental technique most frequently used. Several intrinsic technical difficulties, including reliability and specificity of antibody probes and quality and interpretation of the image data, have been encountered during the investigation. In particular, the identification of genuine $Na_v1.5$ labelling was the most troublesome. In the present study, three independent $Na_v1.5$ antibodies were used (Table 6.1). These antibodies produced intracellular labelling in most cases. This labelling pattern was not

consistent with other investigators' observations. This difference could be due to a difference in antibody, a difference in species or the result of two pools of $Na_v1.5$ (with different antibody accessibility). The validity of Alomone $Na_v1.5$ antibody was confirmed with several control experiments including control immunolabelling, transfection experiments carried out by Dr. S. Xu and Western blot experiments carried out by Dr. S. Jones.

There were some other difficulties and disadvantages in the methods and experimental conditions used. The number of levels studied was not enough to construct a precise 3D model of the AV node. As tissue deformation is inevitable in freezing and cryosectioning, jumps in the tissue architecture always happened from one level to the next.

In the present study, morphological aspects of the AV node were investigated. It is possible that sections cut at a different angle would have made it possible to construct a more precise and information-rich 3D model. Although the importance of Na^+ channels has been reported in transgenic animal studies, elucidating the functional role of the Na^+ channels in the different cell types at the AV junction needs to be carried out.

References

Akamatsu N, Inenaga K & Yamashita H (1993). Inhibitory effects of natriuretic peptides on vasopressin neurons mediated through cGMP and cGMP-dependent protein kinase in vitro. *Journal of Neuroendocrinology* **5**, 517-522.

Altman PL & Dittmer DS (1971). *Biological Handbooks: Respiration and Circulation* Federation of American Societies for Experimental Biology, Bethesda, MD.

Amellal F & Billette J (1996). Selective functional properties of dual atrioventricular nodal inputs. Role in nodal conduction, refractoriness, summation, and rate-dependent function in rabbit heart. *Circulation* **94**, 824-832.

Anderson RH (1972b). Histologic and histochemical evidence concerning the presence of morphologically distinct cellular zones within the rabbit atrioventricular node. *Anatomical Record* **173**, 7-23.

Anderson RH (1972a). The disposition and innervation of atrioventricular ring specialized tissue in rats and rabbits. *Journal of Anatomy* **113**, 197-211.

Anderson RH, Becker AE, Brechenmacher C, Davies MJ & Rossi L (1975). The human atrioventricular junctional area. A morphological study of the A-V node and bundle. *European Journal of Cardiology* **3**, 11-25.

Anderson RH & Ho SY (2000). The atrial connections of the specialized axis responsible for AV conduction. In *Atrial-AV nodal electrophysiolog: a view from the millennium*, eds. Mazgalev TN & Tchou PJ, pp. 3-24. Futura Publishing Company., Armonk, NY.

Anderson RH & Ho SY (1998). The architecture of the sinus node, the atrioventricular conduction axis, and the internodal atrial myocardium. *Journal of Cardiovascular Electrophysiology* **9**, 1233-1248.

Anderson RH, Janse MJ, van Capelle FJ, Billette J, Becker AE & Durrer D (1974). A combined morphological and electrophysiological study of the atrioventricular node of the rabbit heart. *Circulation Research* **35**, 909-922.

Anderson RH & Taylor IM (1972). Development of atrioventricular specialized tissue in human heart. *British Heart Journal* **34**, 1205-1214.

Angst BD, Khan LU, Severs NJ, Whitely K, Rothery S, Thompson RP, Magee AI & Gourdie RG (1997). Dissociated spatial patterning of gap junctions and cell adhesion junctions during postnatal differentiation of ventricular myocardium. *Circulation Research* **80**, 88-94.

Antunes-Rodrigues J, de Castro M, Elias LL, Valenca MM & McCann SM (2004). Neuroendocrine control of body fluid metabolism. *Physiological Reviews* **84**, 169-208.

Antz M, Scherlag BJ, Otomo K, Pitha J, Tondo C, Patterson E, Jackman WM & Lazzara R (1998). Evidence for multiple atrio-AV nodal inputs in the normal dog heart. *Journal of Cardiovascular Electrophysiology* **9**, 395-408.

Arguello C, Alanis J, Pantoja O & Valenzuela B (1986). Electrophysiological and ultrastructural study of the atrioventricular canal during the development of the chick embryo. *Journal of Molecular Cellular Cardiology* **18**, 499-510.

Aschoff L (1910). Referat uber die Herzstorungen in ihren Bezeihungen zu den spezifischen Muskelsystem des Herzens. *Verhandlungen DerDeutschen Gesellschaft Für Pathologie* **14**, 3-35.

Azene EM, Xue T & Li RA (2003). Molecular basis of the effect of potassium on heterologously expressed pacemaker (HCN) channels. *Journal of Physiology* **547**, 349-356.

Back H, Stumpf WE, Ando E, Nokihara K & Forssmann WG (1986). Immunocytochemical evidence for CDD/ANP-like peptides in strands of myoendocrine cells associated with the ventricular conduction system of the rat heart. *Anatomia, Histologia, Embryologia (Berlin)* **175**, 223-226.

Bancroft JD & Gamble M (2002). *Theory and Practice of Histological Techniques.*, 5th ed. Harcourt Publishers Ltd.

Baruscotti M, Westenbroek R, Catterall WA, DiFrancesco D & Robinson RB (1997). The newborn rabbit sino-atrial node expresses a neuronal type I-like Na^+ channel. *Journal of Physiology* **498**, 641-648.

Bastide B, Neyses L, Ganten D, Paul M, Willecke K & Traub O (1993). Gap junction protein connexin40 is preferentially expressed in vascular endothelium and conductive bundles of rat myocardium and is increased under hypertensive conditions. *Circulation Research* **73**, 1138-1149.

Bean BP (1985). Two kinds of calcium channels in canine atrial cells. Differences in kinetics, selectivity, and pharmacology. *Journal of General Physiology* **86**, 1-30.

Beblo DA, Wang HZ, Beyer EC, Westphale EM & Veenstra RD (1995). Unique conductance, gating, and selective permeability properties of gap junction channels formed by connexin40. *Circulation Research* **77**, 813-822.

Becker AE (1994). Atrioventricular nodal anatomy revisited. *Lerning Center Highlights* **9**, 17-22.

Belardinelli L, Shryock JC, Song Y, Wang D & Srinivas M (1995). Ionic basis of the electrophysiological actions of adenosine on cardiomyocytes. *FASEB Journal* **9**, 359-365.

Benvenuti LA, Aiello VD, Higuchi ML & Palomino SA (1997). Immunohistochemical expression of atrial natriuretic peptide (ANP) in the conducting system and internodal atrial myocardium of human hearts. *Acta Histochemica (Jena)* **99**, 187-193.

Betts TR, Ho SY, Sanchez-Quintana D, Roberts PR, Anderson RH & Morgan JM (2002). Three-dimensional mapping of right atrial activation during sinus rhythm and its relationship to endocardial architecture. *Journal of Cardiovascular Electrophysiology* **13**, 1152-1159.

Beyer EC (1993). Gap junctions. *International Review of Cytology (New York, NY)* **137C, 1-37.**

Beyer EC, Paul DL & Goodenough DA (1987). Connexin43: a protein from rat heart homologous to a gap junction protein from liver. *Journal of Cell Biology* **105**, 2621-2629.

Beyer EC, Paul DL & Goodenough DA (1990). Connexin family of gap junction proteins. *Journal of Membrane Biology* **116**, 187-194.

Bharati S (2000). Anatomic-morphologic relation between AV nodal structure and function in the normal and diseased heart. In *Atrial-AV nodal electrophysiology: a view from the millennium*, eds. Mazgalev TN & Tchou PJ, pp. 25-48. Futura Publishing Company, Armonk, NY.

Biel M, Schneider A & Wahl C (2002). Cardiac HCN channels: structure, function, and modulation. *Trends in Cardiovascular Medicine* **12**, 206-212.

Billette J (1987). Atrioventricular nodal activation during periodic premature stimulation of the atrium. *American Journal of Physiology* **252**, H163-H177.

Billette J (2002). What is the atrioventricular node? Some clues in sorting out its structure-function relationship. *Journal of Cardiovascular Electrophysiology* **13**, 515-518.

Billette J & Amellal F (2000). Functional properties of the AV node. In *Atrial-AV nodal electrophysiology: a view from the millennium*, eds. Mazgalev TN & Tchou PJ, pp. 155-173. Futura Publishing Company, Armonk, NY.

Bleeker WK, Mackaay AJ, Masson-Pevet M, Bouman LN & Becker AE (1980). Functional and morphological organization of the rabbit sinus node. *Circulation Research* **46**, 11-22.

Bleeker WK, Mackaay AJ, Masson-Pevet M, Op't HT, Jongsma HJ & Bouman LN (1982). Asymmetry of the sino-atrial conduction in the rabbit heart. *Journal of Molecular Cellular Cardiology* **14**, 633-643.

Bogdanov KY, Vinogradova TM & Lakatta EG (2001). Sinoatrial nodal cell ryanodine receptor and Na^{+}-Ca^{2+} exchanger: molecular partners in pacemaker regulation. *Circulation Research* **88**, 1254-1258.

Boineau JP, Canavan TE, Schuessler RB, Cain ME, Corr PB & Cox JL (1988). Demonstration of a widely distributed atrial pacemaker complex in the human heart. *Circulation* **77**, 1221-1237.

Boineau JP, Schuessler RB, Hackel DB, Miller CB, Brockus CW & Wylds AC (1980). Widespread distribution and rate differentiation of the atrial pacemaker complex. *American Journal of Physiology* **239**, H406-H415.

Boyett MR, Dobrzynski H, Lancaster MK, Jones SA, Honjo H & Kodama I (2003). Sophisticated architecture is required for the sinoatrial node to perform its normal pacemaker function. *Journal of Cardiovascular Electrophysiology* **14**, 104-106.

Boyett MR, Honjo H & Kodama I (2000). The sinoatrial node, a heterogeneous pacemaker structure. *Cardiovascular Research* **47**, 658-687.

Boyett MR, Honjo H, Yamamoto M, Nikmaram MR, Niwa R & Kodama I (1999). Downward gradient in action potential duration along conduction path in and around the sinoatrial node. *American Journal of Physiology* **276**, H686-H698.

Bruzzone R, White TW & Goodenough DA (1996a). The cellular internet: on-line with connexins. *Bioessays* **18**, 709-718.

Bruzzone R, White TW & Paul DL (1996b). Connections with connexins: the molecular basis of direct intercellular signaling. *European Journal of Biochemistry* **238**, 1-27.

Burt JM & Spray DC (1988). Single-channel events and gating behavior of the cardiac gap junction channel. *Proceedings of the National Academy of Sciences of the United States of America* **85**, 3431-3434.

Cantin M & Huet M (1975). Chemical nature of atrial specific granules. *Recent Advances in Studies on Cardiac Structure and Metabolism* **6**, 313-322.

Carmeliet E (1987). Slow inactivation of the sodium current in rabbit cardiac Purkinje fibres. *Pflügers Arch* **408**, 18-26.

Catterall WA (2000). From ionic currents to molecular mechanisms: the structure and function of voltage-gated sodium channels. *Neuron* **26**, 13-25.

Cheng X & Koch PJ (2004). In vivo function of desmosomes. *Journal of Dermatology* **31**, 171-187.

Clapham DE & Neer EJ (1997). G protein beta gamma subunits. *Annual Review of Pharmacology and Toxicology* **37**, 167-203.

Clemo HF & Belardinelli L (1986). Effect of adenosine on atrioventricular conduction. I: Site and characterization of adenosine action in the guinea pig atrioventricular node. *Circulation Research* **59**, 427-436.

Clapham DE & Neer EJ (1997). G protein βγ subunits. *Annual Review of Pharmacology and Toxicology* **37**, 167-203.

Cohen SA (1996). Immunocytochemical localization of rH1 sodium channel in adult rat heart atria and ventricle. Presence in terminal intercalated disks. *Circulation* **94**, 3083-3086.

Convery MK & Hancox JC (2000). Na^+-Ca^{2+} exchange current from rabbit isolated atrioventricular nodal and ventricular myocytes compared using action potential and ramp waveforms. *Acta Physiologica Scandinavica* **168**, 393-401.

Copenhaver WM (1981). A restudy of cardiac conduction pathways by techniques for visualization of cholinesterase reaction. *Anatomical Record* **201**, 51-54.

Coppen SR, Dupont E, Rothery S & Severs NJ (1998). Connexin45 expression is preferentially associated with the ventricular conduction system in mouse and rat heart. *Circulation Research* **82**, 232-243.

Coppen SR, Kodama I, Boyett MR, Dobrzynski H, Takagishi Y, Honjo H, Yeh HI & Severs NJ (1999a). Connexin45, a major connexin of the rabbit sinoatrial node, is co-expressed with connexin43 in a restricted zone at the nodal-crista terminalis border. *Journal of Histochemistry and Cytochemistry* **47**, 907-918.

Coppen SR, Severs NJ & Gourdie RG (1999b). Connexin45 (alpha 6) expression delineates an extended conduction system in the embryonic and mature rodent heart. *Developmental Genetics* **24**, 82-90.

Cosio FG, Anderson RH, Kuck KH, Becker A, Borggrefe M, Campbell RW, Gaita F, Guiraudon GM, Haissaguerre M, Rufilanchas JJ, Thiene G, Wellens HJ, Langberg J, Benditt DG, Bharati S, Klein G, Marchlinski F & Saksena S (1999). Living anatomy of the atrioventricular junctions. A guide to electrophysiologic mapping. A Consensus Statement from the Cardiac Nomenclature Study Group, Working Group of Arrhythmias, European Society of Cardiology, and the Task Force on Cardiac Nomenclature from NASPE. *Circulation* **100**, e31-e37.

Davis LM, Kanter HL, Beyer EC & Saffitz JE (1994). Distinct gap junction protein phenotypes in cardiac tissues with disparate conduction properties. *Journal of the American College of Cardiology* **24**, 1124-1132.

de Bold AJ, Borenstein HB, Veress AT & Sonnenberg H (1981). A rapid and potent natriuretic response to intravenous injection of atrial myocardial extract in rats. *Life Sciences* **28**, 89-94.

de Carvalho A & de Almeida D (1960). Spread of activity through the atrioventricular node. *Circulation Research* **8**, 801-809.

DeFelice LJ & Challice CE (1969). Anatomical and ultrastructural study of the electrophysiological atrioventricular node of the rabbit. *Circulation Research* **24**, 457-474.

DiBona GF (2000). Nervous kidney. Interaction between renal sympathetic nerves and the renin-angiotensin system in the control of renal function. *Hypertension* **36**, 1083-1088.

DiFrancesco D (1993). Pacemaker mechanisms in cardiac tissue. *Annual Review of Physiology* **55**, 455-472.

Ding J, Thibault G, Gutkowska J, Garcia R, Karabatsos T, Jasmin G, Genest J & Cantin M (1987). Cardiac and plasma atrial natriuretic factor in experimental congestive heart failure. *Endocrinology* **121**, 248-257.

Dobrzynski H, Li J, Tellez J, Greener ID, Nikolski VP, Wright SE, Parson SH, Jones SA, Lancaster MK, Yamamoto M, Honjo H, Takagishi Y, Kodama I, Efimov IR, Billeter R & Boyett MR (2005). Computer three-dimensional reconstruction of the sinoatrial node. *Circulation* **111**, 846-854.

Dobrzynski H, Marples DD, Musa H, Yamanushi TT, Henderson Z, Takagishi Y, Honjo H, Kodama I & Boyett MR (2001). Distribution of the muscarinic K^+ channel proteins

Kir3.1 and Kir3.4 in the ventricle, atrium, and sinoatrial node of heart. *Journal of Histochemistry and Cytochemistry* **49**, 1221-1234.

Dobrzynski H, Nikolski VP, Sambelashvili AT, Greener ID, Yamamoto M, Boyett MR & Efimov IR (2003). Site of origin and molecular substrate of atrioventricular junctional rhythm in the rabbit heart. *Circulation Research* **93**, 1102-1110.

Dobrzynski H, Rothery SM, Marples DD, Coppen SR, Takagishi Y, Honjo H, Tamkun MM, Henderson Z, Kodama I, Severs NJ & Boyett MR (2000). Presence of the Kv1.5 K^+ channel in the sinoatrial node. *Journal of Histochemistry and Cytochemistry* **48**, 769-780.

Epstein LM, Scheinman MM, Langberg JJ, Chilson D, Goldberg HR & Griffin JC (1989). Percutaneous catheter modification of the atrioventricular node. A potential cure for atrioventricular nodal reentrant tachycardia. *Circulation* **80**, 757-768.

Favaretto AL, Ballejo GO, buquerque-Araujo WI, Gutkowska J, ntunes-Rodrigues J & McCann SM (1997). Oxytocin releases atrial natriuretic peptide from rat atria in vitro that exerts negative inotropic and chronotropic action. *Peptides* **18**, 1377-1381.

Flagg-Newton J, Simpson I & Loewenstein WR (1979). Permeability of the cell-to-cell membrane channels in mammalian cell juncton. *Science* **205**, 404-407.

Flynn TG, de Bold ML & de Bold AJ (1983). The amino acid sequence of an atrial peptide with potent diuretic and natriuretic properties. *Biochemical and Biophysical Research Communications* **117**, 859-865.

Forssmann WG, Richter R & Meyer M (1998). The endocrine heart and natriuretic peptides: histochemistry, cell biology, and functional aspects of the renal urodilatin system. *Histochemistry and Cell Biology* **110**, 335-357.

Fozzard HA & Hanck DA (1996). Structure and function of voltage-dependent sodium channels: comparison of brain II and cardiac isoforms. *Physiological Reviews* **76**, 887-926.

Gauss R, Seifert R & Kaupp UB (1998). Molecular identification of a hyperpolarization-activated channel in sea urchin sperm. *Nature* **393**, 583-587.

Goldin AL (2001). Resurgence of sodium channel research. *Annual Review of Physiology* **63**, 871-894.

Goldin AL, Barchi RL, Caldwell JH, Hofmann F, Howe JR, Hunter JC, Kallen RG, Mandel G, Meisler MH, Netter YB, Noda M, Tamkun MM, Waxman SG, Wood JN & Catterall WA (2000). Nomenclature of voltage-gated sodium channels. *Neuron* **28**, 365-368.

Gourdie RG, Severs NJ, Green CR, Rothery S, Germroth P & Thompson RP (1993). The spatial distribution and relative abundance of gap-junctional connexin40 and connexin43 correlate to functional properties of components of the cardiac atrioventricular conduction system. *Journal of Cell Science* **105**, 985-991.

Gros D, Jarry-Guichard T, Ten V, I, de MA, Van Kempen MJ, Davoust J, Briand JP, Moorman AF & Jongsma HJ (1994). Restricted distribution of connexin40, a gap junctional protein, in mammalian heart. *Circulation Research* **74**, 839-851.

Gros DB & Jongsma HJ (1996). Connexins in mammalian heart function. *Bioessays* **18**, 719-730.

Guo W, Li H, London B & Nerbonne JM (2000). Functional consequences of elimination of $i_{to,f}$ and $i_{to,s}$: early afterdepolarizations, atrioventricular block, and ventricular arrhythmias in mice lacking Kv1.4 and expressing a dominant-negative Kv4 alpha subunit. *Circulation Research* **87**, 73-79.

Gutstein DE, Liu FY, Meyers MB, Choo A & Fishman GI (2003). The organization of adherens junctions and desmosomes at the cardiac intercalated disc is independent of gap junctions. *Journal of Cell Science* **116**, 875-885.

Habuchi Y, Han X & Giles WR (1995). Comparison of the hyperpolarization-activated and delayed rectifier currents in rabbit atrioventricular node and sinoatrial node. *Heart Vessels* **9 (suppl)**, 203-206.

Haefliger JA, Bruzzone R, Jenkins NA, Gilbert DJ, Copeland NG & Paul DL (1992). Four novel members of the connexin family of gap junction proteins. Molecular cloning, expression, and chromosome mapping. *Journal of Biological Chemistry* **267**, 2057-2064.

Hagiwara N, Irisawa H & Kameyama M (1988). Contribution of two types of calcium currents to the pacemaker potentials of rabbit sino-atrial node cells. *Journal of Physiology* **395**, 233-253.

Haissaguerre M, Gaita F, Fischer B, Commenges D, Montserrat P, d'Ivernois C, Lemetayer P & Warin JF (1992). Elimination of atrioventricular nodal reentrant tachycardia using discrete slow potentials to guide application of radiofrequency energy. *Circulation* **85**, 2162-2175.

Haissaguerre M, Warin JF, Lemetayer P, Saoudi N, Guillem JP & Blanchot P (1989). Closed-chest ablation of retrograde conduction in patients with atrioventricular nodal reentrant tachycardia. *New England Journal of Medicine* **320**, 426-433.

Hancox J & Levi A (1994a). The hyperpolarisation-activated current, I_f, is not required for pacemaking in single cells from the rabbit atrioventricular node. *Pflügers Arch* **427**, 121-128.

Hancox JC & Levi AJ (1994b). L-type calcium current in rod- and spindle-shaped myocytes isolated from rabbit atrioventricular node. *American Journal of Physiology* **267**, H1670-H1680.

Hancox JC & Mitcheson JS (1997). Ion channel and exchange currents in single myocytes isolated from the rabbit atrioventricular node. *Canadian Journal of Cardiology* **13**, 1175-1182.

Harlow E & Lane D (1998). *Using antibodies: a laboratory manual.* Cold Spring Harbor Laboratory Press, New York.

Haufe V, Camacho JA, Dumaine R, Gunther B, Bollensdorff C, von Banchet GS, Benndorf K & Zimmer T (2005). Expression pattern of neuronal and skeletal muscle voltage-gated Na+ channels in the developing mouse heart. *Journal of Physiology* **564**, 683-696.

Hennemann H, Suchyna T, Lichtenberg-Frate H, Jungbluth S, Dahl E, Schwarz J, Nicholson BJ & Willecke K (1992). Molecular cloning and functional expression of mouse connexin40, a second gap junction gene preferentially expressed in lung. *Journal of Cell Biology* **117**, 1299-1310.

Hilgemann DW (1989). Giant excised cardiac sarcolemmal membrane patches: sodium and sodium-calcium exchange currents. *Pflügers Arch* **415**, 247-249.

Hoffman BF (1961). Physiology of atrioventricular transmission. *Circulation* **24**, 506-517.

Hoffman BF (1971). Cardiac automaticity and AV junctional rhythms. In *Research in Physiology*, eds. Kao FF, Koizumi K & Vassalle M, pp. 27-36. Aulo Gaggi, Bologna, Italy.

Hofmann BF & Cranefield PF (1960). *Electrophysiology of the Heart.* McGraw-Hill, New York.

Honjo H, Boyett MR, Kodama I & Toyama J (1996). Correlation between electrical activity and the size of rabbit sino-atrial node cells. *Journal of Physiology* **496**, 795-808.

Honjo H, Inada S, Lancaster MK, Yamamoto M, Niwa R, Jones SA, Shibata N, Mitsui K, Horiuchi T, Kamiya K, Kodama I & Boyett MR (2003). Sarcoplasmic reticulum Ca^{2+} release is not a dominating factor in sinoatrial node pacemaker activity. *Circulation Research* **92**, e41-e44.

Honjo H, Lei M, Boyett MR & Kodama I (1999). Heterogeneity of 4-aminopyridine-sensitive current in rabbit sinoatrial node cells. *American Journal of Physiology* **276**, H1295-H1304.

Hoyt RH, Cohen ML & Saffitz JE (1989). Distribution and three-dimensional structure of intercellular junctions in canine myocardium. *Circulation Research* **64**, 563-574.

Hryshko LV (2004). Membrane pumps and exchangers. In *Cardiac electrophysiology: from cell to bedside*, eds. Zipes DP & Jalife J, pp. 42-50. Saunders Co., Philadelphia.

Imanaga I, Kameyama M & Irisawa H (1987). Cell-to-cell diffusion of fluorescent dyes in paired ventricular cells. *American Journal of Physiology* **252**, H223-H232.

Inoue S & Becker AE (1998). Posterior extensions of the human compact atrioventricular node: a neglected anatomic feature of potential clinical significance. *Circulation* **97**, 188-193.

Inoue S, Becker AE, Riccardi R & Gaita F (1999). Interruption of the inferior extension of the compact atrioventricular node underlies successful radio frequency ablation of atrioventricular nodal reentrant tachycardia. *Journal of Interventional Cardiac Electrophysiology* **3**, 273-277.

Irisawa H, Brown HF & Giles W (1993). Cardiac pacemaking in the sinoatrial node. *Physiological Reviews* **73**, 197-227.

Ishii TM, Takano M, Xie LH, Noma A & Ohmori H (1999). Molecular characterization of the hyperpolarization-activated cation channel in rabbit heart sinoatrial node. *Journal of Biological Chemistry* **274**, 12835-12839.

Jackman WM, Beckman KJ, McClelland JH, Wang X, Friday KJ, Roman CA, Moulton KP, Twidale N, Hazlitt HA & Prior MI (1992). Treatment of supraventricular tachycardia due to atrioventricular nodal reentry, by radiofrequency catheter ablation of slow-pathway conduction. *New England Journal of Medicine* **327**, 313-318.

James TN (1961). Anatomy of the human sinus node. *Anatomical Record* **141**, 109-139.

James TN, Isobe JH & Urthaler F (1979). Correlative electrophysiological and anatomical studies concerning the site of origin of escape rhythm during complete atrioventricular block in the dog. *Circulation Research* **45**, 108-119.

Jankowski M, Hajjar F, Kawas SA, Mukaddam-Daher S, Hoffman G, McCann SM & Gutkowska J (1998). Rat heart: a site of oxytocin production and action. *Proceedings of the National Academy of Sciences of the United States of America* **95**, 14558-14563.

Jankowski M, Rachelska G, Donghao W, McCann SM & Gutkowska J (2001). Estrogen receptors activate atrial natriuretic peptide in the rat heart. *Proceedings of the National Academy of Sciences of the United States of America* **98**, 11765-11770.

Jankowski M, Wang D, Hajjar F, Mukaddam-Daher S, McCann SM & Gutkowska J (2000). Oxytocin and its receptors are synthesized in the rat vasculature. *Proceedings of the National Academy of Sciences of the United States of America* **97**, 6207-6211.

Janse MJ & Tranum-Jensen J (1981). Cardiac arrhythmias-some basic aspects. In *Pediatric Cardiology*, eds. Becker AE, Losekoot G, Marcelletti C & Anderson RH, pp. 91-101. Churchill Livingstone, London.

Janse MJ, Tranum-Jensen J, Kleber AG & van Capelle FJ (1978). Techniques and problems in correlating cellular electrophysiology and morphology in cardiac nodal tissues. In *The Sinus Node: Structure, function, and Clinical relevance*, ed. Bonke FIM, pp. 183-194. The Hague: Martin Nijohoff, London.

Jazayeri MR & Akhtar M (1993). Electrophysiological behavior of atrioventricular node after selective fast or slow pathway ablation in patients with atrioventricular nodal reentrant tachycardia. *Pacing and Clinical Electrophysiology* **16**, 623-628.

Jazayeri MR, Hempe SL, Sra JS, Dhala AA, Blanck Z, Deshpande SS, Avitall B, Krum DP, Gilbert CJ & Akhtar M (1992). Selective transcatheter ablation of the fast and slow pathways using radiofrequency energy in patients with atrioventricular nodal reentrant tachycardia. *Circulation* **85**, 1318-1328.

Kalman JM, Lee RJ, Fisher WG, Chin MC, Ursell P, Stillson CA, Lesh MD & Scheinman MM (1995). Radiofrequency catheter modification of sinus pacemaker function guided by intracardiac echocardiography. *Circulation* **92**, 3070-3081.

Kanter HL, Laing JG, Beau SL, Beyer EC & Saffitz JE (1993). Distinct patterns of connexin expression in canine Purkinje fibers and ventricular muscle. *Circulation Research* **72**, 1124-1131.

Kaupp UB & Seifert R (2001). Molecular diversity of pacemaker ion channels. *Annual Review of Physiology* **63**, 235-257.

Kawamura K & James TN (1971). Comparative ultrastructure of cellular junctions in working myocardium and the conduction system under normal and pathologic conditions. *Journal of Molecular and Cellular Cardiology* **3**, 31-60.

Keating MT & Sanguinetti MC (2001). Molecular and cellular mechanisms of cardiac arrhythmias. *Cell* **104**, 569-580.

Keim S, Werner P, Jazayeri M, Akhtar M & Tchou P (1992). Localization of the fast and slow pathways in atrioventricular nodal reentrant tachycardia by intraoperative ice mapping. *Circulation* **86**, 919-925.

Ko YS, Yeh HI, Ko YL, Hsu YC, Chen CF, Wu S, Lee YS & Severs NJ (2004). Three-dimensional reconstruction of the rabbit atrioventricular conduction axis by combining histological, desmin, and connexin mapping data. *Circulation* **109**, 1172-1179.

Koch W (1909). Weitere Mitteilungen uber den Sinusknoten des Herzens. *Verhandlungen DerDeutschen Gesellschaft Für Pathologie* **13**, 85-92.

Kodama I & Boyett MR (1985). Regional differences in the electrical activity of the rabbit sinus node. *Pflügers Arch* **404**, 214-226.

Kokubun S, Nishimura M, Noma A & Irisawa H (1982). Membrane currents in the rabbit atrioventricular node cell. *Pflügers Arch* **393**, 15-22.

Krapivinsky G, Gordon EA, Wickman K, Velimirovic B, Krapivinsky L & Clapham DE (1995a). The G-protein-gated atrial K^+ channel I_{KACh} is a heteromultimer of two inwardly rectifying K^+-channel proteins. *Nature* **374**, 135-141.

Krapivinsky G, Krapivinsky L, Wickman K & Clapham DE (1995b). G $\beta\gamma$ binds directly to the G protein-gated K^+ channel, I_{KACh}. *Journal of Biological Chemistry* **270**, 29059-29062.

Kubo Y, Baldwin TJ, Jan YN & Jan LY (1993). Primary structure and functional expression of a mouse inward rectifier potassium channel. *Nature* **362**, 127-133.

Kucera JP, Rohr S & Rudy Y (2002). Localization of sodium channels in intercalated disks modulates cardiac conduction. *Circulation Research* **91**, 1176-1182.

Kumar NM & Gilula NB (1996). The gap junction communication channel. *Cell* **84**, 381-388.

Kwong KF, Schuessler RB, Green KG, Laing JG, Beyer EC, Boineau JP & Saffitz JE (1998). Differential expression of gap junction proteins in the canine sinus node. *Circulation Research* **82**, 604-612.

Kyndt F, Probst V, Potet F, Demolombe S, Chevallier JC, Baro I, Moisan JP, Boisseau P, Schott JJ, Escande D & Le Marec H (2001). Novel SCN5A mutation leading either to isolated cardiac conduction defect or Brugada syndrome in a large French family. *Circulation* **104**, 3081-3086.

Lee MA, Morady F, Kadish A, Schamp DJ, Chin MC, Scheinman MM, Griffin JC, Lesh MD, Pederson D & Goldberger J (1991). Catheter modification of the atrioventricular junction with radiofrequency energy for control of atrioventricular nodal reentry tachycardia. *Circulation* **83**, 827-835.

Lei M, Honjo H, Kodama I & Boyett MR (2000). Characterisation of the transient outward K^+ current in rabbit sinoatrial node cells. *Cardiovascular Research* **46**, 433-441.

Lei M, Honjo H, Kodama I & Boyett MR (2001). Heterogeneous expression of the delayed-rectifier K^+ currents $i_{K,r}$ and $i_{K,s}$ in rabbit sinoatrial node cells. *Journal of Physiology* **535**, 703-714.

Lei M, Jones SA, Liu J, Lancaster MK, Fung SS, Dobrzynski H, Camelliti P, Maier SK, Noble D & Boyett MR (2004). Requirement of neuronal- and cardiac-type sodium channels for murine sinoatrial node pacemaking. *Journal of Physiology* **559**, 835-848.

Lewis T (1925). *The Mechanism and Graphic Registration of the Heart Beat.* Shaw and Sons, London.

Lin FY, Lin JL & Lo HM (1994). Anatomic substrate of the slow atrio-ventricular nodal pathway in an experimental atrio-ventricular nodal reentrant tachycardia. *International Journal of Cardiology* **47**, 157-163.

Lipsius SL, Huser J & Blatter LA (2001). Intracellular Ca2+ release sparks atrial pacemaker activity. *News Physiol Sci* **16**, 101-106.

Lo HM, Lin FY, Cheng JJ & Tseng YZ (1995). Anatomic substrate of the experimentally-created atrioventricular node re-entrant tachycardia in the dog. *International Journal of Cardiology* **51**, 273-282.

Ludwig A, Zong X, Jeglitsch M, Hofmann F & Biel M (1998). A family of hyperpolarization-activated mammalian cation channels. *Nature* **393**, 587-591.

Ludwig A, Zong X, Stieber J, Hullin R, Hofmann F & Biel M (1999). Two pacemaker channels from human heart with profoundly different activation kinetics. *EMBO Journal* **18**, 2323-2329.

Luke RA & Saffitz JE (1991). Remodeling of ventricular conduction pathways in healed canine infarct border zones. *Journal of Clinical Investigation* **87**, 1594-1602.

Lupoglazoff JM, Cheav T, Baroudi G, Berthet M, Denjoy I, Cauchemez B, Extramiana F, Chahine M & Guicheney P (2001). Homozygous SCN5A mutation in long-QT syndrome with functional two-to-one atrioventricular block. *Circulation Research* **89**, E16-E21.

Maack T (1992). Receptors of atrial natriuretic factor. *Annual Review of Physiology* **54**, 11-27.

Maack T, Suzuki M, Almeida FA, Nussenzveig D, Scarborough RM, McEnroe GA & Lewicki JA (1987). Physiological role of silent receptors of atrial natriuretic factor. *Science* **238**, 675-678.

Maier SK, Westenbroek RE, Schenkman KA, Feigl EO, Scheuer T & Catterall WA (2002). An unexpected role for brain-type sodium channels in coupling of cell surface depolarization to contraction in the heart. *Proceedings of the National Academy of Sciences of the United States of America* **99**, 4073-4078.

Maier SK, Westenbroek RE, Yamanushi TT, Dobrzynski H, Boyett MR, Catterall WA & Scheuer T (2003). An unexpected requirement for brain-type sodium channels for control of heart rate in the mouse sinoatrial node. *Proceedings of the National Academy of Sciences of the United States of America* **100**, 3507-3512.

Malhotra JD, Chen C, Rivolta I, Abriel H, Malhotra R, Mattei LN, Brosius FC, Kass RS & Isom LL (2001). Characterization of sodium channel alpha- and beta-subunits in rat and mouse cardiac myocytes. *Circulation* **103**, 1303-1310.

Manthey D, Bukauskas F, Lee CG, Kozak CA & Willecke K (1999). Molecular cloning and functional expression of the mouse gap junction gene connexin-57 in human HeLa cells. *Journal of Biological Chemistry* **274**, 14716-14723.

Martynyuk AE, Kane KA, Cobbe SM & Rankin AC (1995). Adenosine increases potassium conductance in isolated rabbit atrioventricular nodal myocytes. *Cardiovascular Research* **30**, 668-675.

Masson-Pévet MA, Bleeker WK, Besselsen E, Treytel BW, Jongsma HJ & Bouman LN (1984). Pacemaker cell types in the rabbit sinus node: a correlative ultrastructural and electrophysiological study. *Journal of Molecular and Cellular Cardiology* **16**, 53-63.

Mazgalev TN, Ho SY & Anderson RH (2001). Anatomic-electrophysiological correlations concerning the pathways for atrioventricular conduction. *Circulation* **103**, 2660-2667.

Mazgalev TN & Tchou PJ (2000a). The AV nodal dual pathway electrophysiology: still a controversial concept. In *Atrial-AV nodal electrophysiology: a view from the millennium*, eds. Mazgalev TN & Tchou PJ, pp. 217-236. Futura Publishing Company, Armonk, NY.

Mazgalev TN & Tchou PJ (2000b). Surface potentials from the region of the atrioventricular node and their relation to dual pathway electrophysiology. *Circulation* **101**, 2110-2117.

McGuire MA, de Bakker JM, Vermeulen JT, Moorman AF, Loh P, Thibault B, Vermeulen JL, Becker AE & Janse MJ (1996). Atrioventricular junctional tissue. Discrepancy between histological and electrophysiological characteristics. *Circulation* **94**, 571-577.

McGuire MA, de Bakker JM, Vermeulen JT, Opthof T, Becker AE & Janse MJ (1994). Origin and significance of double potentials near the atrioventricular node. Correlation of extracellular potentials, intracellular potentials, and histology. *Circulation* **89**, 2351-2360.

McGuire MA & Janse MJ (1995). New insights on anatomical location of components of the reentrant circuit and ablation therapy for atrioventricular junctional reentrant tachycardia. *Current Opinion in Cardiology* **10**, 3-8.

McGuire MA, Janse MJ & Ross DL (1993). "AV nodal" reentry: Part II: AV nodal, AV junctional, or atrionodal reentry? *Journal of Cardiovascular Electrophysiology* **4**, 573-586.

McGuire MA, Lau KC, Johnson DC, Richards DA, Uther JB & Ross DL (1991). Patients with two types of atrioventricular junctional (AV nodal) reentrant tachycardia. Evidence that a common pathway of nodal tissue is not present above the reentrant circuit. *Circulation* **83**, 1232-1246.

Medkour D, Becker AE, Khalife K & Billette J (1998). Anatomic and functional characteristics of a slow posterior AV nodal pathway: role in dual-pathway physiology and reentry. *Circulation* **98**, 164-174.

Meijler FL (1985). Atrioventricular conduction versus heart size from mouse to whale. *Journal of the American College of Cardiology* **5**, 363-365.

Meijler FL & Janse MJ (1988). Morphology and electrophysiology of the mammalian atrioventricular node. *Physiological Reviews* **68**, 608-647.

Mendez C & Moe GK (1966). Demonstration of a dual A-V nodal conduction system in the isolated rabbit heart. *Circulation Research* **19**, 378-393.

Mitcheson JS & Hancox JC (1999). Characteristics of a transient outward current (sensitive to 4-aminopyridine) in Ca^{2+}-tolerant myocytes isolated from the rabbit atrioventricular node. *Pflügers Arch* **438**, 68-78.

Mitrani RD, Klein LS, Hackett FK, Zipes DP & Miles WM (1993). Radiofrequency ablation for atrioventricular node reentrant tachycardia: comparison between fast (anterior) and slow (posterior) pathway ablation. *Journal of the American College of Cardiology* **21**, 432-441.

Mitsuiye T, Shinagawa Y & Noma A (2000). Sustained inward current during pacemaker depolarization in mammalian sinoatrial node cells. *Circulation Research* **87**, 88-91.

Moe GK, Preston JB & Burlington H (1956). Physiologic evidence for a dual A-V transmission system. *Circulation Research* **4**, 357-375.

Monckeberg JG (1910). Beitrage zur normalen und pathologischen Anatomie des Herzens. *Verhandlungen DerDeutschen Gesellschaft Für Pathologie* **14**, 64-71.

Moosmang S, Stieber J, Zong X, Biel M, Hofmann F & Ludwig A (2001). Cellular expression and functional characterization of four hyperpolarization-activated pacemaker channels in cardiac and neuronal tissues. *European Journal of Biochemistry* **268**, 1646-1652.

Moreno AP, Saez JC, Fishman GI & Spray DC (1994). Human connexin43 gap junction channels. Regulation of unitary conductances by phosphorylation. *Circulation Research* **74**, 1050-1057.

Munk AA, Adjemian RA, Zhao J, Ogbaghebriel A & Shrier A (1996). Electrophysiological properties of morphologically distinct cells isolated from the rabbit atrioventricular node. *Journal of Physiology* **493**, 801-818.

Musa H, Lei M, Honjo H, Jones SA, Dobrzynski H, Lancaster MK, Takagishi Y, Henderson Z, Kodama I & Boyett MR (2002). Heterogeneous expression of Ca^{2+} handling proteins in rabbit sinoatrial node. *Journal of Histochemistry and Cytochemistry* **50**, 311-324.

Mutharasan RK, Nagaraj A, Hamilton AJ, McPherson DD & Bharati S (2004). Computer three-dimensional reconstruction of the atrioventricular conduction system. *Pacing and Clinical Electrophysiology* **27**, 740-748.

Nakayama T & Irisawa H (1985). Transient outward current carried by potassium and sodium in quiescent atrioventricular node cells of rabbits. *Circulation Research* **57**, 65-73.

Nakayama T, Kurachi Y, Noma A & Irisawa H (1984). Action potential and membrane currents of single pacemaker cells of the rabbit heart. *Pflügers Arch* **402**, 248-257.

Nichols CG & Lopatin AN (1997). Inward rectifier potassium channels. *Annual Review of Physiology* **59**, 171-191.

Nikolski V & Efimov I (2001). Fluorescent imaging of a dual-pathway atrioventricular-nodal conduction system. *Circulation Research* **88**, E23-E30.

Nikolski VP, Jones SA, Lancaster MK, Boyett MR & Efimov IR (2003). Cx43 and dual-pathway electrophysiology of the atrioventricular node and atrioventricular nodal reentry. *Circulation Research* **92**, 469-475.

Nishimura M, Tanaka H, Homma N, Matsuzawa T & Watanabe Y (1989). Ionic mechanisms of the depression of automaticity and conduction in the rabbit atrioventricular node caused by hypoxia or metabolic inhibition and protective action of glucose and valine. *American Journal of Cardiology* **64**, 24J-28J.

Noma A, Irisawa H, Kokobun S, Kotake H, Nishimura M & Watanabe Y (1980). Slow current systems in the A-V node of the rabbit heart. *Nature* **285**, 228-229.

Page E (1992). Cardiac gap junctions. In *The Heart and Cardiovascular System*, eds. Fozzard HA, Haber E, Jennings RB, Katz AM & Morgan HE, pp. 1003-1048. Raven Press Ltd, New York, NY.

Papadatos GA, Wallerstein PM, Head CE, Ratcliff R, Brady PA, Benndorf K, Saumarez RC, Trezise AE, Huang CL, Vandenberg JI, Colledge WH & Grace AA (2002). Slowed conduction and ventricular tachycardia after targeted disruption of the cardiac sodium channel

gene Scn5a. *Proceedings of the National Academy of Sciences of the United States of America* **99**, 6210-6215.

Pape HC (1996). Queer current and pacemaker: the hyperpolarization-activated cation current in neurons. *Annual Review of Physiology* **58**, 299-327.

Patterson E & Scherlag BJ (1999). Longitudinal dissociation within the posterior AV nodal input of the rabbit: a substrate for AV nodal reentry. *Circulation* **99**, 143-155.

Patterson E & Scherlag BJ (2002). Anatomic and functional fast atrioventricular conduction pathway. *Journal of Cardiovascular Electrophysiology* **13**, 945-949.

Paul DL, Ebihara L, Takemoto LJ, Swenson KI & Goodenough DA (1991). Connexin46, a novel lens gap junction protein, induces voltage-gated currents in nonjunctional plasma membrane of Xenopus oocytes. *Journal of Cell Biology* **115**, 1077-1089.

Peters NS, Green CR, Poole-Wilson PA & Severs NJ (1993). Reduced content of connexin43 gap junctions in ventricular myocardium from hypertrophied and ischemic human hearts. *Circulation* **88**, 864-875.

Peters NS, Severs NJ, Rothery SM, Lincoln C, Yacoub MH & Green CR (1994). Spatiotemporal relation between gap junctions and fascia adherens junctions during postnatal development of human ventricular myocardium. *Circulation* **90**, 713-725.

Peters NS & Wit AL (1998). Myocardial architecture and ventricular arrhythmogenesis. *Circulation* **97**, 1746-1754.

Petrecca K, Amellal F, Laird DW, Cohen SA & Shrier A (1997). Sodium channel distribution within the rabbit atrioventricular node as analysed by confocal microscopy. *Journal of Physiology* **501**, 263-274.

Polak JM & Noorden SV (2002). *Introduction to Immunocytochemistry*, 3rd ed. BIOS Scientific Publishers Limited.

Racker DK & Kadish AH (2000). Proximal atrioventricular bundle, atrioventricular node, and distal atrioventricular bundle are distinct anatomic structures with unique histological characteristics and innervation. *Circulation* **101**, 1049-1059.

Rahkila P, Takala TE, Parton RG & Metsikko K (2001). Protein targeting to the plasma membrane of adult skeletal muscle fiber: an organized mosaic of functional domains. *Experimental Cell Research* **267**, 61-72.

Randall WC (1988). Differential autonomic control of SAN and AVN regions of the canine heart: structure and function. In *Progress in Clinical and Biological Research, Electrophysiology of the SInoatrial and Atrioventricular Nodes*, eds. Mazgalev TN, Dreifus LS & Michelson EL, pp. 15-31. Alan R. Liss, New York.

Rogart RB, Cribbs LL, Muglia LK, Kephart DD & Kaiser MW (1989). Molecular cloning of a putative tetrodotoxin-resistant rat heart Na+ channel isoform. *Proceedings of the National Academy of Sciences of the United States of America* **86**, 8170-8174.

Ruiz-Ceretti E & Zumino AP (1976). Action potential changes under varied $[Na^+]_0$ and $[Ca^{2+}]_0$ indicating the existence of two inward currents in cells of the rabbit atrioventricular node. *Circulation Research* **39**, 326-336.

Sanchez-Quintana D, Anderson RH, Cabrera JA, Climent V, Martin R, Farre J & Ho SY (2002). The terminal crest: morphological features relevant to electrophysiology. *Heart* **88**, 406-411.

Sanchez-Quintana D, Davies DW, Ho SY, Oslizlok P & Anderson RH (1997). Architecture of the atrial musculature in and around the triangle of Koch: its potential relevance to atrioventricular nodal reentry. *Journal of Cardiovascular Electrophysiology* **8**, 1396-1407.

Sanderson JB (1994). *Microscopical Society Handbooks 28: Biological Microtechniques* Information Press Ltd., Oxford.

Sanguinetti MC & Jurkiewicz NK (1991). Delayed rectifier outward K^+ current is composed of two currents in guinea pig atrial cells. *American Journal of Physiology* **260**, H393-H399.

Santoro B, Liu DT, Yao H, Bartsch D, Kandel ER, Siegelbaum SA & Tibbs GR (1998). Identification of a gene encoding a hyperpolarization-activated pacemaker channel of brain. *Cell* **93**, 717-729.

Schluter M, Geiger M, Siebels J, Duckeck W & Kuck KH (1991). Catheter ablation using radiofrequency current to cure symptomatic patients with tachyarrhythmias related to an accessory atrioventricular pathway. *Circulation* **84**, 1644-1661.

Schott JJ, Alshinawi C, Kyndt F, Probst V, Hoorntje TM, Hulsbeek M, Wilde AA, Escande D, Mannens MM & Le Marec H (1999). Cardiac conduction defects associate with mutations in SCN5A. *Nature Genetics* **23**, 20-21.

Schram G, Pourrier M, Melnyk P & Nattel S (2002). Differential distribution of cardiac ion channel expression as a basis for regional specialization in electrical function. *Circulation Research* **90**, 939-950.

Scott JN & Jennes L (1987). Distribution of atrial natriuretic factor in fetal rat atria and ventricles. *Cell and Tissue Research* **248**, 479-481.

Severs NJ (1990). The cardiac gap junction and intercalated disc. *International Journal of Cardiology* **26**, 137-173.

Severs NJ, Dupont E, Kaprielian RR, Yeh HI & Rothery S (1996). Gap junctions and connexins in the cardiovascular system. In *Annual of cardiac surgery 1996*, eds. Yacoub MH, Carpentier A & Pepper J, pp. 31-44. Current Science, London.

Severs NJ, Rothery S, Dupont E, Coppen SR, Yeh HI, Ko YS, Matsushita T, Kaba R & Halliday D (2001). Immunocytochemical analysis of connexin expression in the healthy and diseased cardiovascular system. *Microscopy Research and Technique* **52**, 301-322.

Shaw RM & Rudy Y (1997). Ionic mechanisms of propagation in cardiac tissue. Roles of the sodium and L-type calcium currents during reduced excitability and decreased gap junction coupling. *Circulation Research* **81**, 727-741.

Sheppard CJR & Shotton DM (1997). *Confocal Laser Scanning Microscopy*, 1st ed. BIOS Scientific Publishers Limited.

Shi W, Wymore R, Yu H, Wu J, Wymore RT, Pan Z, Robinson RB, Dixon JE, McKinnon D & Cohen IS (1999). Distribution and prevalence of hyperpolarization-activated cation channel (HCN) mRNA expression in cardiac tissues. *Circulation Research* **85**, e1-e6.

Shigeto N & Irisawa H (1974). The effect of polarization on the action potentials of the rabbit AV nodal cells. *Japanese Journal of Physiology* **24**, 605-616.

Sjöstrand FS & Andersson-Cedergren E (1960). Intercalated disks of heart muscle. In *The Structure and Function of Heart Muscle*, ed. Bourne GH, pp. 421-445. Academic Press, New York, NY.

Skeper JN (1989). An immunocytochemical study of the sinuatrial node and atrioventricular conducting system of the rat for atrial natriuretic peptide distribution. *Histochem J* **21**, 72-78.

Soares TJ, Coimbra TM, Martins AR, Pereira AG, Carnio EC, Branco LG, buquerque-Araujo WI, de NG, Favaretto AL, Gutkowska J, McCann SM & ntunes-Rodrigues J (1999). Atrial natriuretic peptide and oxytocin induce natriuresis by release of cGMP. *Proceedings of the National Academy of Sciences of the United States of America* **96**, 278-283.

Sola C, Thibault G, Haile-Meskel H, nand-Srivastava MB, Garcia R & Cantin M (1990). Atrial natriuretic factor in the vena cava and sinus node. *Journal of Histochemistry and Cytochemistry* **38**, 1123-1135.

Sousa J, Brandao L, Barreiros MC & Vagueiro MC (1994). Atrioventricular junction ablation: therapy of refractory atrial tachyarrhythmia. *Rev Port Cardiol* **13**, 389-95, 379.

Spray DC & Burt JM (1990). Structure-activity relations of the cardiac gap junction channel. *American Journal of Physiology* **258**, C195-C205.

Sung RJ, Lauer MR & Chun H (1994). Atrioventricular node reentry: current concepts and new perspectives. *Pacing and Clinical Electrophysiology* **17**, 1413-1430.

Tan HL, Bink-Boelkens MT, Bezzina CR, Viswanathan PC, Beaufort-Krol GC, van Tintelen PJ, van den Berg MP, Wilde AA & Balser JR (2001). A sodium-channel mutation causes isolated cardiac conduction disease. *Nature* **409**, 1043-1047.

Taniguchi J, Kokubun S, Noma A & Irisawa H (1981). Spontaneously active cells isolated from the sino-atrial and atrio-ventricular nodes of the rabbit heart. *Japanese Journal of Physiology* **31**, 547-558.

Tawara S (2000). *The Conduction System in the Mammalian Heart: An Anatomic-Histological Study of the Atrioventricular Bundle and the Purkinje Fibers.* Imperial College Press, Suma K, Shimada M, trans. London.

Thery C, Krivosic I & Asseman P (1994). Enzyme histochemical study of tha atrioventricular junction area. Correlation with slow and fast atrial pathways. *Archives des Maladies du Coeur et des Vaisseux* **87**, 507-513.

Toshimori H, Toshimori K, Oura C & Matsuo H (1987). Immunohistochemical study of atrial natriuretic polypeptides in the embryonic, fetal and neonatal rat heart. *Cell and Tissue Research* **248**, 627-633.

Tranum-Jensen J & Janse MJ (1982). Fine structural identification of individual cells subjected to microelectrode recording in perfused cardiac preparations. *Journal of Molecular and Cellular Cardiology* **14**, 233-247.

Truex RC & Smythe MQ (1965). Comparative morphology of the cardiac conduction tissue in animals. *Annals of the New York Academy of Sciences* **127**, 19-33.

Truex RC & Smythe MQ (1967). Reconstruction of the human atrioventricular node. *Anatomical Record* **158**, 11-19.

Truex RC, Smythe MQ & Taylor MJ (1967). Reconstruction of the human sinoatrial node. *Anatomical Record* **159**, 371-378.

Uchida F, Kasai A, Omichi C, Fujii E, Teramura S, Yasuda M & Nakano T (1998). Effect of radiofrequency catheter ablation on parasympathetic denervation: a comparison of three different ablation sites. *Pacing and Clinical Electrophysiology* **21**, 2517-2521.

Van Kempen MJ, Ten V, I, Wessels A, Oosthoek PW, Gros D, Jongsma HJ, Moorman AF & Lamers WH (1995). Differential connexin distribution accommodates cardiac function in different species. *Microscopy Research and Technique* **31**, 420-436.

Veenstra RD (1996). Size and selectivity of gap junction channels formed from different connexins. *Journal of Bioenergetics and Biomembranes* **28**, 327-337.

Veenstra RD, Wang HZ, Beyer EC & Brink PR (1994). Selective dye and ionic permeability of gap junction channels formed by connexin45. *Circulation Research* **75**, 483-490.

Verheijck EE, Van Kempen MJ, Veereschild M, Lurvink J, Jongsma HJ & Bouman LN (2001). Electrophysiological features of the mouse sinoatrial node in relation to connexin distribution. *Cardiovascular Research* **52**, 40-50.

Verheijck EE, Wessels A, Van Ginneken AC, Bourier J, Markman MW, Vermeulen JL, de Bakker JM, Lamers WH, Opthof T & Bouman LN (1998). Distribution of atrial and nodal cells within the rabbit sinoatrial node: models of sinoatrial transition. *Circulation* **97**, 1623-1631.

Verheule S, Van Kempen MJ, Postma S, Rook MB & Jongsma HJ (2001). Gap junctions in the rabbit sinoatrial node. *American Journal of Physiology* **280**, H2103-H2115.

Vozzi C, Dupont E, Coppen SR, Yeh HI & Severs NJ (1999). Chamber-related differences in connexin expression in the human heart. *Journal of Molecular and Cellular Cardiology* **31**, 991-1003.

Wainger BJ, DeGennaro M, Santoro B, Siegelbaum SA & Tibbs GR (2001). Molecular mechanism of cAMP modulation of HCN pacemaker channels. *Nature* **411**, 805-810.

Wallace RH, Scheffer IE, Barnett S, Richards M, Dibbens L, Desai RR, Lerman-Sagie T, Lev D, Mazarib A, Brand N, Ben-Zeev B, Goikhman I, Singh R, Kremmidiotis G, Gardner A, Sutherland GR, George AL, Jr., Mulley JC & Berkovic SF (2001). Neuronal sodium-channel alpha1-subunit mutations in generalized epilepsy with febrile seizures plus. *American Journal of Human Genetics* **68**, 859-865.

Wallace RH, Wang DW, Singh R, Scheffer IE, George AL, Jr., Phillips HA, Saar K, Reis A, Johnson EW, Sutherland GR, Berkovic SF & Mulley JC (1998). Febrile seizures and generalized epilepsy associated with a mutation in the Na+-channel beta1 subunit gene SCN1B. *Nature Genetics* **19**, 366-370.

Wang DW, Viswanathan PC, Balser JR, George AL, Jr. & Benson DW (2002). Clinical, genetic, and biophysical characterization of SCN5A mutations associated with atrioventricular conduction block. *Circulation* **105**, 341-346.

Wang J, Chen S & Siegelbaum SA (2001). Regulation of hyperpolarization-activated HCN channel gating and cAMP modulation due to interactions of COOH terminus and core transmembrane regions. *Journal of General Physiology* **118**, 237-250.

Watanabe Y (1981). Peculiarities of AV nodal conduction and the role of slow Na current. *Japanese Circulation Journal* **45**, 446-452.

Watanabe Y & Dreifus LS (1968). Sites of impulse formation within the atrioventricular junction of the rabbit. *Circulation Research* **22**, 717-727.

Weidmann S (1955). The effect of the cardiac membrane potential on the rapid availability of the sodium-carrying system. *Journal of Physiology* **127**, 213-224.

Wickman K & Clapham DE (1995). Ion channel regulation by G proteins. *Physiological Reviews* **75**, 865-885.

Wilders R, Jongsma HJ & Van Ginneken AC (1991). Pacemaker activity of the rabbit sinoatrial node. A comparison of mathematical models. *Biophysical Journal* **60**, 1202-1216.

Willecke K, Eiberger J, Degen J, Eckardt D, Romualdi A, Guldenagel M, Deutsch U & Sohl G (2002). Structural and functional diversity of connexin genes in the mouse and human genome. *Biological Chemistry* **383**, 725-737.

Willecke K, Heynkes R, Dahl E, Stutenkemper R, Hennemann H, Jungbluth S, Suchyna T & Nicholson BJ (1991). Mouse connexin37: cloning and functional expression of a gap junction gene highly expressed in lung. *Journal of Cell Biology* **114**, 1049-1057.

Wit AL & Cranefield PF (1977). Triggered and automatic activity in the canine coronary sinus. *Circulation Research* **41**, 434-445.

Workman AJ, Kane KA & Rankin AC (2000). Rate-dependency of action potential duration and refractoriness in isolated myocytes from the rabbit AV node and atrium. *Journal of Molecular and Cellular Cardiology* **32**, 1525-1537.

Wu J, Wu J, Olgin J, Miller JM & Zipes DP (2001). Mechanisms underlying the reentrant circuit of atrioventricular nodal reentrant tachycardia in isolated canine atrioventricular nodal preparation using optical mapping. *Circulation Research* **88**, 1189-1195.

Xie SM, Niu XL, Dong ED, Du KX & Ling FD (2004). Morphological and electrophysiological study on the inferior nodal extension and transitional cellular band in the rabbit atrioventricular junctional area. *Chinese Medical Journal (English)* **117**, 532-537.

Xue T, Marban E & Li RA (2002). Dominant-negative suppression of HCN1- and HCN2-encoded pacemaker currents by an engineered HCN1 construct: insights into structure-function relationships and multimerization. *Circulation Research* **90**, 1267-1273.

Yasui K, Liu W, Opthof T, Kada K, Lee JK, Kamiya K & Kodama I (2001). I_f current and spontaneous activity in mouse embryonic ventricular myocytes. *Circulation Research* **88**, 536-542.

Yeh HI. Vascular cell gap junctions: diversity of connexins expression in the healthy and injured artery. 1997. London University, PhD thesis.

Zhou M, Sevilla L, Vallega G, Chen P, Palacin M, Zorzano A, Pilch PF & Kandror KV (1998). Insulin-dependent protein trafficking in skeletal muscle cells. *American Journal of Physiology* **275**, E187-E196.

Zhou Y, Morais-Cabral JH, Kaufman A & MacKinnon R (2001). Chemistry of ion coordination and hydration revealed by a K^+ channel-Fab complex at 2.0 A resolution. *Nature* **414**, 43-48.

Zipes DP & Mendez C (1973). Action of manganese ions and tetrodotoxin on atrioventricular nodal transmembrane potentials in isolated rabbit hearts. *Circulation Research* **32**, 447-454

Publications

Book chapters

Boyett MR, Inada S, Yoo S, Li J, Liu J, Tellez J, Greener ID, Honjo H, Billeter R, Lei M, & Dobrzynski H (2005) Connexins in the sinoatrial and atrioventricular nodes. In *gap junctions* (in press).

Full papers

Yoo S, Fedorov VV, Xu SZ, Yamanushi TT, Jones SA, Yamamoto M, Nikolski VP, Efimov IR & Boyett MR. Localisation of Na^+ channel isoforms at the atrioventricular junction and atrioventricular node (in submit).

Abstracts

Yamanushi TT, Yoo S, Dobrzynski H, Yamamoto M & Boyett MR (2003). Regional differences in expression of neuronal Na^+ channels in rat heart. *Biophysical Journal* **84**, 216a.

Yoo S, Dobrzynski H, Yamanushi TT, Yamamoto M & Boyett MR (2005). Localization of Na^+ channel isoforms at the atrioventricular node. *Biophysical Journal* (on CD-Rom; 49th Annual Meeting).